2017

Nonlinear Instabilities in Chemical and Electrochemical Systems

Jeffrey Gordon Bell
University of Windsor

Nonlinear Instabilities in Chemical and Electrochemical Systems

By

Jeffrey Gordon Bell

A Dissertation
Submitted to the Faculty of Graduate Studies
through the Department of Chemistry and Biochemistry
in Partial Fulfillment of the Requirements for
the Degree of Doctor of Philosophy
at the University of Windsor

Windsor, Ontario, Canada

2017

Nonlinear Instabilities in Chemical and Electrochemical Systems

by

Jeffrey Bell

APPROVED BY:

_____

I. Kiss, External Examiner
St. Louis University

_____

J. Yang
Earth & Environmental Sciences

_____

J.R. Green
Department of Chemistry & Biochemistry

_____

R. Schurko
Department of Chemistry & Biochemistry

_____

J. Wang, Advisor
Department of Chemistry & Biochemistry

April 21, 2017

DECLARATION OF CO-AUTHORSHIP / PREVIOUS PUBLICATION

I. Co-Authorship Declaration

I hereby declare that this thesis incorporates material that is result of joint research with Dr. James R. Green, who collaborated on two projects, covered in Chapters 2 and 3. In all cases, the key ideas, primary contributions, and experimental designs were performed by the author, and the contribution of the co-author was primarily through performing and analyzing mass spectrometry and NMR spectrometry.

I am aware of the University of Windsor Senate Policy on Authorship and I certify that I have properly acknowledged the contribution of other researchers to my thesis, and have obtained written permission from each of the co-author(s) to include the above material(s) in my thesis.

I certify that, with the above qualification, this thesis, and the research to which it refers, is the product of my own work.

II. Declaration of Previous Publication

This thesis includes 6 original papers that have been previously published/submitted for publication in peer reviewed journals, as follows:

Thesis Chapter	Publication title/full citation	Publication status
Chapter 2	(a) Nonlinear Dynamical Behavior in the Photodecomposition of N-Bromo-1,4-Benzoquinone-4-Imine, J. G. Bell, J. R. Green, and J. Wang, J. Phys. Chem. A, 117, 4545-4550, 2013. (b) Mixed Mode and Sequential Oscillations in the Cerium-Bromate-4-Aminophenol Photoreaction, J. G. Bell and J. Wang, Chaos, 23, 033120, 2013.	(a) Published (b) Published
Chapter 3	Complex Reaction Dynamics in the Cerium - Bromate – 2-Methyl-1,4-Hydroquinone Photoreaction, J. G. Bell, J. R. Green, and J. Wang, J. Phys. Chem. A, 118, 9795-9800, 2014.	Published
Chapter 4	Complex Spatiotemporal Behavior in the Photosensitive Ferroin - Bromate – 4-Nitrophenol Reaction, J. G. Bell and J. Wang, J. Phys. Chem. A, 119, 3323-3328, 2015.	Published
Chapter 5	Current and Potential Oscillations during the Electro-Oxidation of Bromide Ions, J. G. Bell and J. Wang, J. Electroanal. Chem., 754, 133-137, 2015.	Published
Chapter 6	Nonlinear Instabilities during the Electrochemical Oxidation of Hydroxymethanesulfinate, J. G. Bell and J. Wang, Electrochim. Acta, 222, 678-684, 2016.	Published

I certify that I have obtained a written permission from the copyright owner(s) to include the above published material(s) in my thesis. I certify that the above material describes work completed during my registration as graduate student at the University of Windsor.

I declare that, to the best of my knowledge, my thesis does not infringe upon anyone's copyright nor violate any proprietary rights and that any ideas, techniques, quotations, or any other material from the work of other people included in my thesis, published or otherwise, are fully acknowledged in accordance with the standard referencing practices. Furthermore, to the extent that I have included copyrighted material that surpasses the bounds of fair dealing within the meaning of the Canada Copyright Act, I certify that I have obtained a written permission from the copyright owner(s) to include such material(s) in my thesis.

I declare that this is a true copy of my thesis, including any final revisions, as approved by my thesis committee and the Graduate Studies office, and that this thesis has not been submitted for a higher degree to any other University or Institution.

ABSTRACT

This dissertation focuses on designing and manipulating nonlinear chemical and electrochemical reactions, with the aim of discovering new behaviors as well as gaining insights into their underlying mechanisms. In Chapter 2 the nonlinear behavior of the 4-aminophenol – bromate photoreaction was investigated from two directions. First, a second autocatalytic cycle was introduced through the incorporation of the metal catalyst cerium (IV). It was found that once the autocatalytic cycles were effectively balanced, complexity in the form of mixed mode oscillations was observed in a closed reactor. This dynamic behavior was successfully simulated using a modified model, which qualitatively reproduced the experimental results. It was also found that the precipitate which forms at the onset of the reaction of 4-aminophenol with bromate, N-bromo-1,4-benzoquinone-4-imine, could form a new bromate-based photochemical oscillator.

In Chapter 3, the autocatalytic oxidation of 2-methyl-1,4-hydroquinone by acidic bromate lead to the discovery of a new photochemical oscillator. The system was found to be very sensitive to the intensity of illumination supplied, and complexity in the form of sequential oscillations was discovered using either ferroin or cerium (IV) as catalysts. Interestingly, cerium (IV) had a much more profound effect on the dynamical behavior, substantially lengthening the oscillatory period as well as being capable of inducing mixed-mode oscillations. Chapter 4 reports findings on the photosensitive 4-nitrophenol - bromate reaction. Extreme photo-inhibition was found to occur when illumination was supplied to the system whether in a stirred reactor or when being studied in a spatially extended system. Reaction diffusion experiments showed that under certain conditions long lasting complexity in the form of propagation failures took place.

In Chapter 5, oscillations in both current density and potential were observed during the electro-oxidation of bromide ions. Interestingly, mechanistic findings suggest that the oscillations occurring during the oxidation of bromide ions on a platinum electrode belong to the type of oscillator referred to as Capacitance Mediated Positive Differential Resistance oscillator, and is the first solution based system to fit this class. In Chapter 6, the electro-oxidation of two sulfur compounds was seen to display nonlinear behavior. First, the oxidation of hydroxymethanesulfinate leads to oscillations in both current and potential on platinum or gold electrodes. The formation of an inhibiting layer was seen to have a substantial influence on the systems' ability to support sustained oscillatory behavior. Electrochemical Impedance Spectroscopy showed that the oxidation of hydroxymethanesulfinate fits the class of an HN-NDR type oscillator. The oxidation of methionine only displayed nonlinear behavior on a gold surface, and only when operated under potentiostatic conditions. The oscillations were accompanied by gold dissolution and it was found that the electro-oxidation of methionine belongs to the N-NDR class.

Two novel examples of utilizing nonlinear reactions towards application-based research is shown in Chapter 7. Here, the 4-nitrophenol – bromate oscillator is used to fabricate platinum nanoparticles, exploiting the dynamic bromide ion concentration to guide the growth of the noble metal nanocrystals. As an example of using an electrochemical nonlinear reaction, the gold dissolution occurring during the oxidation of methionine was found to lead to the fabrication of a Au nanoparticle modified electrode. This modified electrode was found to be capable of simultaneously detecting both hydroquinone and pyrocatechol in solutions containing both isomers, which is a significant improvement over regular Au electrodes.

MEMORIAL

In loving memory of my father, Gordon W. Bell

1956-2005

DEDICATION

I dedicate this work first to my mother, Kimberley Bell, without whose support and encouragement this dissertation would never have been realized. Thank you for showing me not only the importance of a strong work ethic but also instilling in me the value of education.

I also dedicate this to my beautiful wife Nicole Bell. Your understanding throughout my graduate studies has been remarkable and I cannot thank you enough for accepting the late nights, the weekends and the missed outings due to Chemistry. Your support has and continues to mean everything to me, and I love you even more for it.

ACKNOWLEDGEMENTS

I would first like to thank my supervisor Dr. Jichang Wang. Over the past almost 5 years you have shown me what it means to be an independent researcher. Your open-door policy and willingness to discuss any and all ideas has been profoundly helpful throughout my graduate studies. I also want to thank you for giving me every opportunity to attend conferences as well as conduct research at Wenzhou University in China.

I would also like to thank Dr. James Green, not only for staying late and running NMR's with me, but for providing many useful insights during committee meetings. Additionally, I would like to express my gratitude to Dr. Rob Schurko for his role as a member of my committee. Your advice during my comprehensive exam as well as my research proposal was appreciated and very valuable. Apart from your role as a committee member you found a way to make proctoring and marking exams as enjoyable as possible. I also wish to express my thanks to Dr. Jianwen Yang, for serving as my outside department reader.

Finally, I would like to thank Dr. István Kiss for serving as my external examiner, and I look forward to your insights.

Throughout my entire graduate studies, I have been most thankful for the assistance afforded to me by Marlene Bezaire, Elizabeth Kickham and Catherine Wilson. You have always not only been very helpful but very friendly as well.

Lastly, I would like to thank everyone I have had the pleasure of working with in the Wang research group. Dr. Jun Li and Xuefeng Hu, you were both very welcoming to me when I first joined the group, and I especially thank you for your help at trying to prepare me for my time in China. Finally, I would like to express my gratitude to Alex

Tang for all of your help with regards to my seminar and for all of the time you spent proofreading this dissertation, it was appreciated. Also, Alex and Adit, I would be lying if I said I wouldn't miss all the thought provoking discussions, and impromptu experiments that we conducted together, it was always interesting to say the least.

TABLE OF CONTENTS

LIST OF TABLES

LIST OF FIGURES

LIST OF APPENDICES

LIST OF ABBREVIATIONS / SYMBOLS

1-D	One Dimension
^{13}C NMR	Carbon Nuclear Magnetic Resonance
^{1}H NMR	Proton Nuclear Magnetic Resonance
2-D	Two Dimensions
3-D	Three Dimensions
4-AP	4-Aminophenol
4-NP	4-Nitrophenol
APP	Analyte Pulse Perturbation
BBI	N-Bromo-1,4-Benzoquinone-4-Imine
BL	Bray-Liebhafsky
BR	Briggs-Rauscher
BZ	Belousov-Zhabotinsky
CFUR	Continuously-fed Unstirred Reactor
CMPDR	Capacitance Mediated Positive Differential Resistance
CSH	Cysteamine
CSTR	Continuous-flowed Stirred Tank Reactor

CV	Cyclic Voltammetry
ECPrOX	Electrochemical Preferential Oxidation
EDS	Energy-Dispersive X-ray Spectroscopy
EIS	Electrochemical Impedance Spectroscopy
FKN	Field - Körös - Noyes
HMBC	Heteronuclear Multiple Bond Correlation
HMS	Hydroxymethanesulfinate
HN-NDR	Hidden N-Shaped Negative Differential Resistance
HQ	Hydroquinone
IPAAm	N-isopropylacrylamide
LCST	Lower Critical Solution Temperature
LSV	Linear Sweep Voltammetry
mBQ	2-methyl-1,4-benzoquinone
mH_2Q	2-methyl-1,4-hydroquinone
MMO	Mixed Mode Oscillations
N-NDR	N-Shaped Negative Differential Resistance
NDR	Negative Differential Resistance

OKN	Orbán - Körös - Noyes
PC	Pyrocatechol
PEM	Proton Exchange Membrane
PrOX	Preferential Oxidation
RD	Reaction - Diffusion
S-NDR	S-Shaped Negative Differential Resistance
SEM	Scanning Electron Microscopy
TOF-MS	Time Of Flight Mass Spectrometry
UBO	Uncatalyzed Bromate Oscillator
UV-VIS	Ultra Violet Visible Spectroscopy

CHAPTER 1 - INTRODUCTION

1.1 Nonlinear Dynamics

There exists a common driving force behind many of the intricate and beautiful patterns seen in nature [1-3]. This driving force also manifests itself in other diverse phenomena witnessed in a variety of scientific disciplines ranging from economic trends, interacting populations, and many biologically important events such as the firing of neurons to intracellular calcium concentrations [4-8]. Although seemingly unrelated, aspects of these phenomena are all interconnected through the theory of nonlinear dynamics, making research conducted in this field applicable to a wide range of topics.

1.1.1 History

Historically speaking, a simple path toward legitimacy was not obtained in nonlinear dynamics. An initial discovery of periodic changes in current density, or periodic bursts of effervescence, was observed in 1828 by Fechner while studying the electrochemical dissolution of nickel in a nitric acid solution [9]. A second important discovery came in 1921 when Bray was studying the decomposition of hydrogen peroxide in the presence of iodate ions [10]. Later, work with Liebhafsky solidified the discovery of what is now referred to as the Bray-Liebhafsky (BL) oscillator [11]. Even though this would end up being the first homogeneous chemical oscillator, at the time its discovery was met with substantial skepticism. The skepticism stemmed from its apparent noncompliance with the 2nd law of thermodynamics: that oscillations could not occur when the system is in an equilibrium state. It was therefore assumed that the oscillatory behavior was caused through the formation of bubbles or by the presence of small particles in the solution, making it heterogeneous [12].

A significant breakthrough came through the work done by Lotka (continued by Volterra) who formulated a model, which contained autocatalysis and feedback [13-15]. Although this model was not a chemically viable mechanism (oscillations were present under all conditions), it was found to model the periodic increase and decrease in population size observed in predator/prey dynamics.

Then, work done in Russia by Boris Belousov, while studying an inorganic analog to the Krebs cycle, led to the accidental discovery of what would end up becoming the most widely studied chemical oscillator. Belousov, anticipating a monotonic color change, found that a reaction containing $KBrO_3$, citric acid, cerium sulfate, and sulfuric acid would periodically change color, from clear to yellow, while stirred. Also, it was observed that an unstirred solution would exhibit waves of yellow travelling through the solution. Although Belousov submitted his results to scientific journals, his work was not accepted, which led him to stop his pursuit [12,16].

Almost simultaneously with the work done by Belousov, Ilya Prigogine approached the idea of self-organization from a thermodynamics viewpoint. He showed that systems (chemical or biological) in far from equilibrium conditions could develop order out of chaos and self-organize. This work and other contributions to the understanding of nonequillibrium thermodynamics led to Prigogine being awarded the Nobel Prize [17,18].

In 1961 Anatol Zhabotinsky began working on and refining the work begun by Belousov. Zhabotinsky found that citric acid could be exchanged with malonic acid, and that instead of cerium; ferroin could be used to catalyze the reaction. This refinement led

to a precipitate free system, which showed visually distinct transitions between red and blue (ferroin is red in a reduced state and blue in an oxidized state) [19-21]. A major breakthrough came in 1968 through the formulation of the Brusselator mechanism, the first chemically viable model demonstrating oscillatory behavior [22]. This model, proposed by Prigogine and Lefever, was significant as it improved on the Lotka−Volterra model because oscillations and wave behavior were only observable under finite conditions.

It was the work conducted by Field, Körös and Noyes on the Belousov-Zhabotinsky reaction, which led to an elucidation of the oscillatory mechanism. This mechanism, now referred to as the FKN mechanism, was a significant contribution to the field of nonlinear chemical kinetics because it approached the problem using the same principles used to gain insights into ordinary chemical reactions [23]. The original FKN mechanism consisted of over 20 reaction steps and chemical species; however, a reduced model (with only three variable concentrations) capable of exhibiting the same dynamic phenomena was proposed in 1974. This model was aptly named the Oregonator (after the school it was researched at) and made numerical simulations of the BZ reaction much more feasible [12, 24-26].

In 1973, a new chemical oscillator was discovered which was something of a combination of the two previously known oscillators and was named after its founders Briggs and Rauscher [27]. Briggs and Rauscher found that this system, when oscillatory, gave very intense color changes, which were ideal for classroom demonstrations.

The three chemical oscillators discovered up until the 1980's were either found by chance, or designed based on combining previous systems. Chemists then set out to work on systematically designing a chemical oscillator based on the knowledge thus far obtained in the field. They devised a protocol which would be useful in designing new chemical oscillators based on (1) finding a reaction which produces a substance autocatalytically, (2) determine bistable regions in an open system, (3) add a new species which would implement negative feedback, (4) increase amount of feedback causing species to decrease the range of bistability, and (5) continue increasing feedback generating species until bistability vanishes and oscillations emerge [12]. This protocol was first successfully used in the design of the arsenite - iodate - chlorite oscillator in 1981 [28,29]. Since this discovery, many new oscillating systems have been studied and modifications to previous oscillators have also been thoroughly researched [30-40]. An important class of modified oscillator is the Uncatalyzed Bromate Oscillator (UBO), where aromatic compounds were found to oscillate in BZ type systems without the presence of any metal ion catalysts [41-45].

The field of nonlinear chemical dynamics continues to be a very active area of research with researchers attempting to design new oscillating systems as well as to gain further insights into the underlying mechanisms driving the behavior.

1.1.2 Requirements for Oscillation

Initial reluctance to accept homogeneous chemical oscillations was based on two fronts: the system was in fact inhomogeneous, and an apparent conflict with the second law of thermodynamics [12]. Perhaps the most crucial requirement allowing nonlinear behavior to occur is the necessity for the system to be maintained far from equilibrium

[46]. The explanation for this requirement can be looked at from both thermodynamic and kinetic perspectives. In terms of thermodynamics, owing to the 2nd law of thermodynamics, any creation of order (dynamic self-organization included) is accompanied by a decrease in entropy. This implies that the same system must contain an entropy producing process (dissipative process) capable of compensating for this decrease through the formation of "dissipative structures" [47]. This implies that all displays of self-organization (such as temporal oscillation or spatiotemporal pattern formation) occurring in nonequilibrium conditions are dissipative structures. Therefore, the oscillations that are occurring in a system are taking place on their way towards equilibrium [12,47].

With respect to the kinetics, there are two crucial requirements that the system must contain: (1) a nonlinearity of its dynamic characteristics and (2) the presence of feedback loops in its mechanism. The first requirement of nonlinearity implies that the reaction will not evolve in a simple linear fashion. This is realized through the presence of an autocatalytic reaction, in which a product is formed, which in turn catalyzes its own production [47,48]. The simplest representation of an autocatalytic reaction is X + Y ⇌ 2Y. Here the rate equation governing the concentration of species Y is represented by:

$$\frac{d}{dt}[Y] = k_f[X][Y] - k_r[Y]^2 \qquad [1]$$

The second requirement is that the system must contain a species capable of providing feedback in the mechanism. This feedback can either catalyze the reaction (positive feedback) or inhibit the reaction (negative feedback) [12].

1.2 Chemical Systems

Although the theory of nonlinear dynamics has been found to drive many processes or behaviors seen in geological and even biological systems, the time scales in which these processes occur often makes their direct study difficult or impossible [49,50]. Experimental designs can also prove to be outside the capabilities of traditional laboratory setups. For these reasons, the study of nonlinear dynamics using chemical systems is convenient. The ability to have control over the experimental conditions (such as initial reactant concentrations, temperature, stirring, flow rate, etc.) allows the researcher to be able to fine-tune the reaction parameters easily. Chemical systems also allow for convenient protocols for influencing the reaction through either the application of internal (e.g. chemical spiking) or external perturbations (e.g. incorporation of illumination).

1.2.1 Bray - Liebhafsky (BL) Reaction

The Bray-Liebhafsky (BL) oscillator is not only the first discovered chemical oscillator but it is also likely the simplest homogenous oscillator. Once it was accepted that the 2nd law of thermodynamics was not being violated and that heterogeneous processes were not causing the nonlinear phenomena, the BL oscillator was finally accepted and has been thoroughly studied ever since [51-55].

The BL reaction is the formation of water and oxygen through the catalytic decomposition of hydrogen peroxide (H_2O_2) in the presence of iodate and hydrogen ions.

$$(1)\ 2H_2O_2 \rightarrow 2H_2O + O_2$$

The overall reaction for the decomposition is shown in reaction (1), however the decomposition of hydrogen peroxide occurs through two separate pathways. In one pathway, hydrogen peroxide plays the role of a reducing agent (Reaction (2)), reacting with iodate ions. In the other pathway it acts as an oxidizing agent (Reaction (3)), reacting with iodine (I_2) to produce iodate.

$$(2)\ 2IO_3^- + 2H^+ + 5H_2O_2 \rightarrow I_2 + 6H_2O + 5O_2$$

$$(3)\ I_2 + 5H_2O_2 \rightarrow 2IO_3^- + 2H^+ + 4H_2O$$

A smooth, monotonic decomposition of hydrogen peroxide is observed when the rates of the two hydrogen peroxide consuming reactions are equal. However, under certain conditions, the rates of these two processes are not equal, resulting in the decomposition of hydrogen peroxide being dominated alternatively between the two pathways. This alternating dominance between the pathways leads to a non-monotonic consumption of hydrogen peroxide in which the concentrations of the intermediates produced during the reactions evolve in an oscillatory fashion [52].

1.2.2 Belousov-Zhabotinsky (BZ) Reaction

Undoubtedly the most thoroughly investigated chemical oscillator is the Belousov Zhabotinsky reaction, which essentially established the field of chemical nonlinear dynamics. Many interesting behaviors have been found studying this bromate-based oscillator (traditionally using malonic acid (MA) as the organic substrate), ranging from sustained oscillations in a batch reactor to deterministic chaos in a Continuous-flowed Stirred Tank Reactor (CSTR) [56-59]. The mechanism can be separated into 3 primary processes that are in competition with one another.

Process 1: begins with the reduction of bromate (BrO_3^-) to bromine (Br_2) by the reducing agent bromide (Br^-), through a three-step process:

$$(1)\ BrO_3^- + Br^- + 2H^+ \rightarrow HBrO_2 + HOBr$$

$$(2)\ HBrO_2 + Br^- + H^+ \rightarrow 2HOBr$$

$$(3)\ Br^- + HOBr + H^+ \rightarrow Br_2 + H_2O$$

As a result, bromate is reduced, the concentration of bromide eventually falls below a critical level $[Br^-]_{cr}$. Below this critical bromide ion concentration, Process 2 begins to overwhelm Process 1, where the bromous acid ($HBrO_2$) begins to dominate the reduction of bromate [12]. The reaction between bromous acid and bromate leads to the formation of 2 molecules of bromine dioxide radicals, one of which is subsequently reduced by Ce(III) producing 1 molecule of bromous acid.

Process 2

$$(4)\ 2HBrO_2 \rightarrow BrO_3^- + HOBr + H^+$$

$$(5)\ BrO_3^- + HBrO_2 + H^+ \rightarrow 2BrO_2^* + H_2O$$

$$(6)\ BrO_2^* + Ce(III) + H^+ \rightarrow HBrO_2 + Ce(IV)$$

Reactions (5) and (6) make up the autocatalytic sequence. Therefore, the dominant process is determined by whether $[Br^-]$ is above or below $[Br^-]_{cr}$; either Process 1 (consuming bromide ions) or Process 2 (autocatalytic oxidation of Ce(III). An important product resulting from the formation of bromine in reaction (3) of Process 1 is the formation of bromomalonic acid:

$$(7)\ MA + Br_2 \rightarrow BrMA + Br^- + H^+$$

The products of process 1 and 2 react, producing bromide ions according to Reaction 8:

$$(8)\ 2Ce(IV) + BrMA + MA \rightarrow 2Ce(III) + fBr^- + \text{other products}$$

The concurrent oxidation of the organic species in Reaction 8 reduces the cerium catalyst Ce(IV) to Ce(III), which is a gradual change since there is no autocatalysis. This process eventually causes the bromide concentration to rise above the critical level, causing the system to once again be dominated by Process 1, repeating the cycle.

1.2.3 Briggs-Rauscher (BR) Reaction

The acidic oxidation of malonic acid by iodate and hydrogen peroxide, when catalyzed by manganese(II), is perhaps the most visually appealing chemical oscillator, and is referred to as the Briggs-Rauscher (BR) oscillator. Thought of as a hybrid of the other two famous chemical oscillators (BZ and BL), the BR oscillator has been found to support various forms of complexity in an open system, as well as multiple stable states [60-64]. Investigations on the underlying mechanism by Furrow and Noyes, as well as De Kepper and Epstein, provide good insights into the nonlinear dynamical behavior [65,66]. Kim et al. found that the earlier models could be simplified to a reduced model:

$$(1)\ HOI + I^- + H^+ \rightleftharpoons I_2 + H_2O$$

$$(2)\ H^+ + HOIO + I^- \rightarrow 2HOI$$

$$(3)\ 2H^+ + IO_3^- + I^- \rightarrow HOIO + HOI$$

$$(4)\ 2HOIO \rightarrow H^+ + IO_3^- + HOI$$

$$(5)\ CH_2(COOH)_2 + I_2 \rightarrow CHI(COOH)_2 + I^- + H^+$$

$$(6)\ HOI + H_2O_2 \rightarrow I^- + O_2 + H^+ + H_2O$$

$$(7)\ H^+ + IO_3^- + HOIO \rightarrow 2HOIO + \frac{1}{2}O_2$$

The reduced model, involving seven reactions, was found to support the behavior observed experimentally [67,68]. Here molecular iodine serves a similar purpose as bromine in the BZ reaction in that it reacts with malonic acid, producing iodide ions here instead of bromide ions.

1.2.4 Closed vs. Open System

As oscillating chemical systems must be kept far from thermodynamic equilibrium, studying them in a closed or batch reactor implies that any dynamic behavior can only be transitory (i.e., only exist for a finite period of time). This implication is due to the fact that there is no exchange of chemical species with their surroundings and the effects of reactant consumption lead to an end of the oscillatory behavior and a monotonic approach to an equilibrium state [12]. Studies in a batch reactor are however the simplest experimental design for studying chemical kinetics, and many are thermally jacketed, allowing for precise control over the temperature of the solution, and minimizing the influence of external forces.

The primary method of studying a chemical oscillator in an open system is through the use of a CSTR. The main advantage of using a CSTR is that it allows for the system to be maintained sufficiently far from equilibrium in order to extend the reactivity of the system for a virtually indefinite time period. By constantly pumping in fresh

reactants and removing products, a CSTR affords convenient control over the available dynamic states of a system through the manipulation of the inflow/outflow rates of the reactants/products. The flow rate, k_0, or the average time a molecule spends in the reactor (residence time, τ), is a crucial control parameter for operating CSTRs. At low flow rates, the system is close to chemical equilibrium and is referred to as the thermodynamic branch. At high flow rates, the system is considered to be far from thermodynamic equilibrium and is commonly defined as the kinetic or flow branch [12]. As flow rate is increased from a k_0 value of 0, the system remains on the steady thermodynamic branch (i.e., composition of the system resembles the reactants), until such a value is reached that causes a jump to the stable kinetic branch (i.e., the composition of the system resembles products), showing bistability (Figure 1.1).

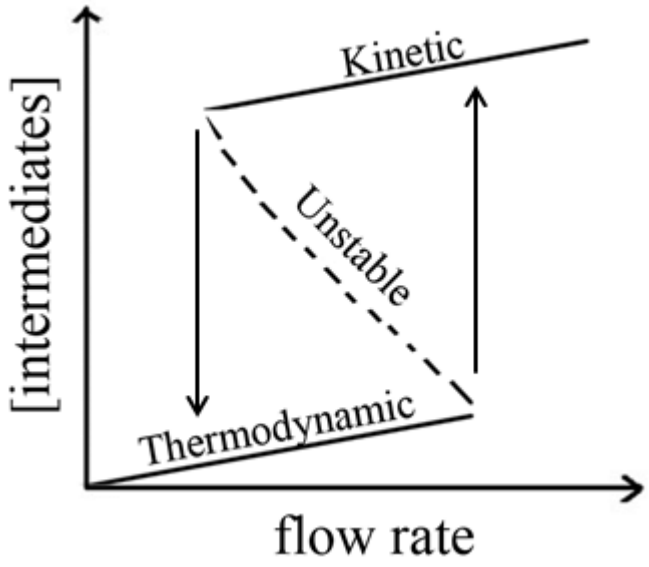

Figure 1.1 - Bistability in a CSTR using flow rate as a control parameter.

1.2.5 Complexity

Even though simple periodic oscillations are the prototypical temporal behavior associated with nonlinear chemical dynamics, various other types of more exotic oscillatory behavior have been discovered. These complex oscillations are most frequently found in open systems; however, they have also been found experimentally in batch reactors [69-74]. One type of complexity presents itself in the form of two separate and distinct bifurcation regimes, separated by a non-oscillatory quiescent period, commonly referred to as sequential oscillations. The occurrence of sequential behavior may arise through the coupling of two nonlinear feedbacks (common in oscillators catalyzed with metal redox couples) [75-77]. It has also been suggested that sequential oscillations can occur in uncatalyzed systems when an intermediate product formed during the reaction is capable of forming an autocatalytic cycle with the starting oxidant. [78,79]

Perhaps the most common form of complexity experimentally observed in chemical systems is referred to as mixed-mode oscillations (MMOs). MMOs have also been observed in laser systems and in the firing of neurons [80,81]. MMOs are characterized by a single period having a mixture of both large (L) and small (S) amplitude oscillations, researchers routinely use the L^S notation to describe them. This type of complexity largely arises through the presence of multiple time scale processes being present, where the evolution of key variables alternates between fast and slow modes [82]. Mechanisms leading to MMOs include Hopf bifurcations producing oscillations of growing amplitude or "local" mechanisms that produce small amplitude oscillations through folded nodes or singular Hopf-bifurcations [82,83].

A second type of complex oscillatory behavior observed in chemical systems and biochemical systems, as well as during the dynamic firing of neurons, is a phenomenon referred to as bursting [84-87]. Bursting is qualitatively observable through the occurrence of multiple quiescent (non-oscillatory) periods separated by "bursts" of large amplitude oscillations. These oscillations, like MMOs, can arise through the presence of multiple time scale processes [80,88].

The following two types of complexity are of significant interest to researchers as they are capable of transitioning into chaotic behavior. These so-called "routes to chaos" include (1) quasiperiodicity (torus oscillations) and (2) period doubling [89,90]. Quasiperiodicity occurs in systems that contain oscillatory behavior with two distinct and differing frequencies and has been found in many systems, such as in the electrodissolution of certain metals [91-93]. Although quasiperiodicity is rarely found in single oscillators, it is commonly found in coupled oscillatory systems, as well as in systems that are perturbed periodically by an external force [94,95]. In period doubling bifurcations, oscillations of the same amplitude do not continue periodically and the periods between oscillations of the same amplitude continually double [12]. Therefore, as the control parameter is varied, the number of oscillations per cycle would increase from $1 \rightarrow 2 \rightarrow 4 \rightarrow 8$.

1.2.6 Deterministic Chaos

As previously implied, deterministic chaos is observable in nonlinear systems and has attracted a significant amount of interest over the past few decades [57, 96-100]. Deterministic chaos is one of the central classes of dynamical behavior, along with stationary and periodic behavior, and refers to non-periodic (or aperiodic) behavior [101].

Importantly, this aperiodicity is driven by nonlinear dynamics and not by a stochastic or random event such as experimental noise. Interestingly, in a chaotic system there exists an extreme sensitivity to the initial conditions. This sensitivity can manifest in such a way that a minute concentration deviation at the onset of the reaction can cause the system to evolve in time and yield results which are significantly different than those observed for a system without this concentration deviation [102]. Lorenz, when attempting to model convection rolls in the atmosphere in order to gain knowledge into how to accurately predict weather forecasts, originally observed this extreme sensitivity [101]. He found that the solutions to his equations never settled to an equilibrium; however, they continued to vary in an aperiodic fashion. Even though the small differences in initial values resulted in extremely different (and unpredictable) results, he found that there existed a pattern to the results when plotted in three dimensional space (Figure 1.2), showing that there is an underlying beauty to the chaotic behavior [104].

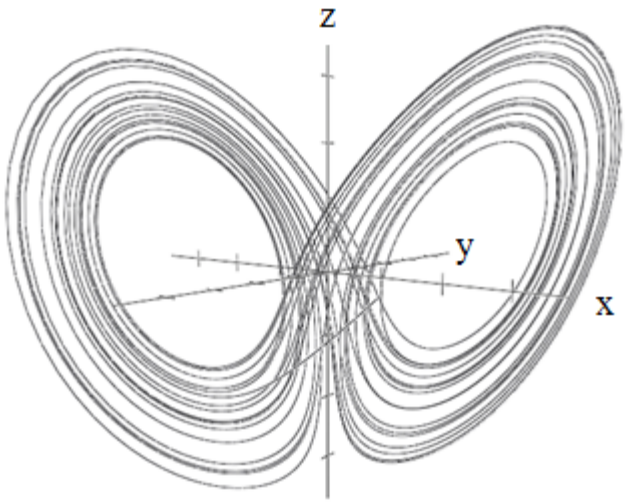

Figure 1.2 - Lorenz Attractor in a chaotic system.

The study of deterministic chaos in chemical systems is, for the large majority of the time, studied in CSTRs where steady states can be maintained while control parameters are adjusted accordingly, bringing the system through the bifurcations on a route to observing chaos. In fact, the traditional peristaltic pump CSTR was replaced with a piston pump in order to study chaos, due to the fact that the systems internal dynamics are so sensitive, a continuous inflow was preferable over periodic pulses from the peristalic pump, decreasing the stochastic nature of the CSTR [12].

1.2.7 Other Chemical Oscillators

The discovery and subsequent intense study that went into the original chemical oscillators, (BZ, BL, BR), resulted in chemists attempting to find oscillators driven by different mechanisms. This work was driven by the fact that discovering new chemical oscillators, which differ fundamentally from the previously known oscillators, could not only lead to the observation of new intricate dynamical behavior but also lead to insights regarding the exact conditions required for chemical oscillations to occur. Oxyhalogen species, which have multiple oxidation states available, were a logical choice to develop experimental methods and concomitant theoretical understandings of dynamical behavior. Apart from the traditional bromate-based BZ reaction, chemical oscillators based on oxygen, chlorite, bromite, sulfur, pH and others have been developed and have led to a wider understanding of the driving forces behind chemical nonlinear dynamics [103-110].

Another important class of chemical oscillator is a pH oscillator, where the concentration of hydrogen ions (or hydroxide ions) plays a critical role in the dynamical behavior of the system. pH oscillators offer an exciting approach with respect to

application based systems. The first pH oscillator was discovered in the mid-1980s, and since then, more than 25 different systems driven by the periodic change in hydrogen ion concentration have been reported in literature [111]. Of these systems, there are generally two classes of pH oscillators: (1) one substrate systems, and (2) two substrate systems. Both classes of pH oscillators require an oxidant such as H_2O_2, IO_4^-, IO_3^-, BrO_3^-, or BrO_2^-; however, they differ in the number of substrates included [111].

A prototypical one substrate pH oscillator is the oxidation of sodium sulfide (Na_2S) by H_2O_2 in the presence of sulfuric acid [112]. Like all one substrate systems, the oscillatory behavior in the H_2O_2 - S^{2-} system arises through competition between two distinct stoichiometries. Here, the pH oscillations are driven by an H^+ consuming process through the partial oxidation of hydrogen sulfide to sulfur (dominant at acidic pH's) and an H^+ producing process through the total oxidation of hydrogen sulfide to sulfate (at basic pH's), as shown in reactions (1) and (2) [113].

$$(1)\ HS^- + H_2O_2 + H^+ \rightarrow \frac{1}{8}S_8 + 2H_2O$$

$$(2)\ HS^- + 4H_2O_2 \rightarrow SO_4^{2-} + 4H_2O + H^+$$

The overall pH of the system determines which reaction step is dominant; thus, at acidic pHs, the partial oxidation pathway dominates, causing the gradual decrease in H^+ concentration (self - inhibitory process) until the pH becomes basic enough that the total oxidation of hydrogen sulfide to sulfate dominates (leading to the autocatalytic production of H^+). The overall model proposed by Rabai contained 6 protonation equilibria, which control the concentration of H^+ by acting as acid-base buffers as well influencing the rates of individual reaction steps, and 12 redox reactions [113].

In two substrate systems, two consecutive reactions make up the oscillatory process, where H^+ is a product in one reaction and a reactant in the other. One substrate (reductant) undergoes total oxidation, which produces H^+ in an autocatalytic fashion causing the system to become acidic, causing the consumption of H^+, increasing the pH. The second substrate primarily acts as another reductant that is only oxidized under acidic conditions [111]. An interesting two substrate system is the IO_3^- - SO_3^{2-} - $Fe(CN)_6^{4-}$ in H_2SO_4 system, which displays large amplitude oscillations (~4 pH units) as well as bistability over a wide range of experimental conditions [114].

Kovacs et al. were successful at systematically designing an organic pH oscillator (the HCHO - HSO_3^- - gluconolactone system) that does not include any redox reactions, and relies only on acid-base steps, such as base-hydrolysis and acid or base dehydration reactions [115]. Working from the knowledge that clock behavior was identified in the methylene glycol - sulfite system, they found that coupling the base catalysis of methylene glycol with hydrolysis of gluconolactone would produce sustained pH oscillations when run in an open system.

Recently, a new oscillatory system was systematically designed by Semenov et al., which coupled networks of organic reactions leading to a chemical oscillator based on thiols [116]. Using a protocol similar to the approach used to design the arsenite system in 1981, they designed a network of reactions capable of producing a substance (cysteamine, CSH) autocatalytically. Starting with cystamine and L-alanine ethyl thioester, trace amounts of CSH are produced through the reaction between the hydrolysis product of L-alanine ethyl thioester, ethanethiol, and cystamine. The autocatalytic production of 2 molecules of CSH from 1 molecule of CSH occurs through

two parallel pathways. At the onset, CSH reacts rapidly with L-alanine ethyl thioester producing two different thiols, L-alanine mercaptoethylamide and ethanethiol. Each produced thiol then independently undergoes thiolate-disulfide interchange with one of the starting materials (cystamine), yielding 1 molecule of CSH for each molecule of L-alanine mercaptoethylamide and ethanethiol. This overall process represents the positive feedback loop. Once a bistable region was identified through the use of a CSTR, an inhibiting substance needed to be added in order to establish a negative feedback loop. The negative feedback loop was implemented through the addition of acrylamide, which reacts more slowly with thiols than any other component in the system, which causes a competition between the two feedback loops. This thiol-based chemical oscillator makes an important contribution to not only chemical nonlinear dynamics, but serves as an affirmation of the protocol for designing new oscillatory systems proposed by Epstein and Pojman [12].

1.3 Reaction Diffusion Systems

The emergence of spatial patterns is a phenomenon found throughout nature ranging not only in timescale (from hours to years) but also in physical scale (from atomic to global) [117-121]. Spatial patterns can form when diffusive motion is coupled with kinetic reactivity, which can manifest itself in a wide range of pattern formations. Perhaps the first observation of this type of behavior was made by Raphael Liesegang, who noticed the formation of periodic bands of precipitation occurring when certain inorganic salts were reacted and allowed to migrate in a gel matrix [122]. Although not fully understood at the time, he recognized that the periodic banding was related to how the molecules moved in relation to one another. This led to discoveries being made where

systems having both diffusive properties and reactivity were found to have very interesting behaviors. These findings were not limited to inanimate (or simply inorganic) systems, but also found to occur in animate (living) systems as well [123-125].

The general form of the reaction diffusion equation is shown in Equation (2). This equation accounts for the two ways that a concentration can change, whether it occurs through diffusion processes, or through chemical reaction.

$$\frac{\partial c}{\partial t} = D\frac{\partial^2 c}{\partial^2 x} + R(c) \qquad [2]$$

Here, *D* represents the diffusion constant and, *R* represents the rate law for the kinetic component of the system. Reaction-diffusion (RD) processes have been thoroughly studied in chemical systems such as the BZ reaction, where interesting phenomena have been found to occur in a variety of structured media ranging from aqueous solution to gels and membranes [126-132]. An important factor when dealing with RD systems is whether the system is excitable, oscillatory or bistable.

In excitable media, there exists only one stable fixed point, which is stable to small perturbations. However, when a large enough (threshold passing) perturbation is applied, the system generates a single pulse that travels through the media, after which the system relaxes back to the initial (pre-perturbation) state. During the relaxation process, the system is in the refractory period (i.e., unresponsive to further perturbations), until the system has recovered to its initial state. In order for a second pulse to propagate through the media another perturbation must be applied. An oscillatory medium differs in that there is no excitation (perturbation) required for pulses to emerge in the media. In oscillatory media there exists an unstable fixed point, indicating that the system will not

relax back to a stable fixed point as it would in an excitable medium, thereby allowing pulses to continually develop. The third type of active media contains two stable fixed points and is referred to as bistable media. Here, starting from one of the stable fixed points, a large enough perturbation will cause the system to settle at the other stable point, without being able to return to the original state, which is referred to as front propagation [133].

The propagation of the pulse (or wave) through the medium can be understood with the chemistry of the BZ reaction. At initially high bromide ion levels the system is in a reduced state because bromide inhibits the autocatalytic oxidation of the catalyst. Once the bromide concentration decreases past a threshold level, that area of medium becomes oxidized, forming a concentration gradient with respect to the activator bromous acid. The autocatalyst then diffuses into neighboring areas, exciting the area that it diffused into, oxidizing it and thereby causing more $HBrO_2$ to be produced, which continues to diffuse and excite neighboring areas. Once the bromide ion concentration reaches a high enough level, the system reaches a reduced steady state [12]. An important consideration with respect to pulse or wave formation is how they set in spontaneously, without external perturbation. There are two possibilities that are generally accepted. The first deals with a local spontaneous concentration fluctuation that is large enough in magnitude to surpass the threshold for excitability, and the second is the presence of a catalytic site (dust particle) capable of locally changing relative concentrations through a nucleation process [12,134]. The state of the media, whether excitable, oscillatory, or bistable, plays a significant role in the types of behaviors seen when dealing with RD

systems. Another important factor is whether or not the system is studied in one-dimension (capillary tube), two-dimensions (petri dish) or three-dimensions (beaker).

1.3.1 Pattern Formation in 1-D

The simplest procedure for studying RD behavior is in a capillary tube, which is considered pseudo one-dimensional space due to the fact that the inner diameter of the tube is small enough such that the diffusion occurring can be thought of as only proceeding in one plane. The typical behavior observed in 1-D RD systems is propagating fronts, which routinely propagate at constant velocities, assuming convection induced instabilities are fully negated [12]. The velocity at which a front propagates is related to the diffusion coefficient (D) and the reaction rate coefficient (k), such that the speed of the front can be represented by the equation:

$$c = A\sqrt{Dk_{1st}} \qquad [3]$$

where A is a constant.

Although confined to a single dimension, interesting behavior can still be observed in 1-D RD systems, such as intermittent propagation failures, where a front will begin to propagate through the medium and stop; however, the preceding front will propagate fully through the medium. Interestingly, the phenomenon of intermittent propagation failures can resemble MMOs [135]. Complexity can also be observed when fronts propagating from opposite ends of the capillary tube interact [136-138].

1.3.2 Pattern Formation in 2-D

When RD systems are spatially extended into a 2nd dimension, the observed dynamical behavior becomes much richer. When a front emerges in 2-D media, it extends

outward in all directions in the form of a circle (if the speed in all directions is uniform) from the starting point (nucleation site or from external perturbation). These phenomena are commonly referred to as target patterns. Similar to the propagation of multiple fronts in 1-D media, multiple target patterns can emanate from the nucleation site [128, 139-141]. When there are multiple nucleation sites in the media, target patterns can emerge at different locations; however, when the waves interact with each other they annihilate, often leading to increased complexity in the observed patterns [12]. Unlike in 1-D media, a curvature of the wavefront may be observed in two (or three) dimensional space. This curvature can be quantitatively characterized through the wavefront's radius of curvature, which can either be positive (curved in the direction of propagation) or negative (curved in the opposite direction of propagation). Common notation denotes the radius of curvature as R and the curvature as K (equal to $1/R$). Research has shown (both experimentally and theoretically) that the velocity of the curved wavefront is dependent on the curvature [142,143], through the equation:

$$N = c + DK = c + D(\frac{1}{R}) \qquad [4]$$

where N is normal velocity of the wavefront, c is the velocity of a plane wave, and D is the diffusion coefficient of the propagator species.

In 2-D media another common pattern observed is spiral waves, which occur when a target pattern is broken by a physical disruption [128]. The broken ends of the wave can curl and continuously rotate. The phenomenon of spiral waves (and target waves) has been observed in the BZ reaction, but is also commonly found in nature. An important aspect of spiral waves is the behavior of the tip (spiral core) [144]. Spirals can

rotate rigidly, where the spiral core does not migrate, however, the spiral tip can also become destabilized and either meander or drift. In a rigidly rotating spiral, the shape of the spiral arm is fixed and remains constant [128, 145-147]. When meandering occurs, the spiral arm changes shape, and when drifting occurs, the entire spiral rotates around a moving (drifting) center of rotation [128, 148-150].

1.3.3 Pattern Formation in 3-D

Extending reaction diffusion systems into three-dimensional space is a challenging undertaking (owing to problems arising from bubble formation and/or convection), however, it offers insight into biological systems such as the human heart. For example, cardiac arrhythmia, such as ventricular fibrillation, is thought to be caused by the formation of scroll waves in cardiac tissue [151,152]. 3-D spatiotemporal behavior has been observed using various modifications of the BZ reaction and is routinely studied in gels. The extension of target waves and spiral waves into 3-D systems results in the formation of spherical waves and scroll waves respectively. Scroll waves organize around a filament, which consists of the inner edge of the scroll wave, and acts as its axis [128]. A straight scroll wave, with a linear filament can become distorted by instabilities (caused by excitability gradients, temperature gradients, etc.), leading to intricate behavior [153]. Scroll waves, similar to spiral waves, can lose their stability through meandering. This meandering instability can cause the filament to adopt a zig-zag or helical shape, due to an elongation of the filament [153,154]. Another instability is referred to as a "sproing" instability, which results in a twist along the filament [153,155].

1.3.4 Turing Patterns

Turing patterns, named after British mathematician Alan Turing, are ubiquitous in nature and are found in the patterning of zebras, tigers, fish, etc. Turing's seminal paper on morphogenesis in 1952 proposed that sets of reaction-diffusion equations could lead to spatially periodic patterns, which are independent of time, and driven by diffusion instabilities [156]. It was not until 1990 when researchers were first able to observe Turing patterns in a chemical system, which was achieved through the use of the chlorite/iodide/malonic acid (CIMA) oscillator [157]. In order for Turing patterns to emerge there are three crucial factors, the first two of which can be accomplished with a continuously fed unstirred reactor (CFUR): (1) the system must be maintained far from equilibrium and (2) only reaction and diffusion can take place (convection processes must be absent, and are negated through the use of a CFUR using gel mediums). The thirdnrequirement is that the diffusion coefficients of the activator and inhibitor must be substantially different (inhibitor diffuses quickly and the activator diffuses slowly) [158]. In the CIMA reaction iodine acts as the activator that has its diffusivity drastically reduced when starch (initially used as an indicator) is present, as iodine and starch form a reversible complex. This complex formation causes a significant difference in the diffusion rates of the activator and inhibitor, allowing spatial structures such as stripes or spots to emerge.

The BZ reaction was also found to be capable of exhibiting Turing patterns through the use of a new type of structured media, a reverse microemulsion. The system contains octane, water, and the surfactant sodium bis(2-ethylhexyl) sulfosuccinate (also known as AOT), which led to the overall naming of the BZ-AOT system. When the polar

reactants of the BZ reaction are introduced into an AOT reverse microemulsion, they separate into droplets, and act as small individually oscillating systems. The BZ reaction produces the nonpolar intermediate bromine, which also functions as an inhibitor in the BZ oscillator. This nonpolar inhibitor can enter the oil and diffuse through it, drastically altering its rate of diffusion with respect to the activator, thus allowing the emergence of Turing patterns. Interestingly, using tomographic methods, 3-D Turing patterns were observed in the BZ-AOT system, which took the form of spots, curved surfaces, hexagonally packed cylinders, as well as labyrinthine and lamellar patterns [159].

1.4 Electrochemical Systems

The study of instabilities in electrochemical systems dates back to the observation by Fechner in 1828 of spontaneous oscillatory formation of bubbles during the electrochemical dissolution of nickel in nitric acid [9]. Early on, much of the investigation of oscillatory behavior in electrochemical systems focused on metal dissolution reactions; however, in the past few decades, research has expanded greatly to include the study of small organic compounds as well as sulfur containing species [160-168]. Much focus has also been placed on the electrode being utilized in the electrochemical reaction, such as the material (platinum, gold, etc.), configuration (disk or ring), size, or number (electrode arrays) [47,169].

Electrochemistry offers a convenient protocol for studying nonlinear dynamics in that electrochemical kinetics are inherently nonlinear, and the process of applying external forces (such as a constant potential drop between two electrodes) causes the system to be pushed far from equilibrium [170].

1.4.1 Theory

In terms of electrochemical surface processes, there are four main factors affecting the observed current response during an electrochemical reaction. The first property governing the current response is mass transfer of a species from the bulk solution to the electrode surface. Secondly, the rate of electron transfer at the electrode surface also plays an important role in influencing the observed current. The third factor is whether or not chemical reactions occur on the electrode surface (before or after) the electron transfer has occurred. Lastly, other surface processes such as adsorption, desorption, or electro-deposition can directly influence the observed current during an electrochemical reaction [171]. Importantly, many of the rate constants associated with the surface processes are directly influenced by the applied potential, and the overall current (i_{tot}) flowing between the electrodes is represented by the equation of the load line [47]:

$$i_{tot} = \frac{V-E}{R_S} = \frac{V}{R_S} - \frac{E}{R_S} \quad [5]$$

Where V is the applied potential, E is the potential drop at the electrode/solution interface, and R_S is the serial resistance.

In dynamic systems, there must be a source of instability. In electrochemical systems, this instability occurs when the slope of a current / potential (i/E) graph is negative [47]. This characteristic, referred to as negative differential resistance (NDR), is a prerequisite of "true" electrochemical instabilities [172,173]. The simple representation of current is given in Equation (5); however, it does not take into account important parameters for dealing with instability, such as the double layer capacitance, C_d. Equation

(6) also takes into account the capacitive (I_c) and Faradaic (I_f) currents, as well as the electrode area (A).

$$\frac{V-E}{R_S} = I_{tot} = I_f(E) + I_c(E) = I_f(E) + C_d A \frac{dE}{dt} \quad [6]$$

Where the Faradaic current is given by Equation (7):

$$I_f = nFAk(E)c(0) \quad [7]$$

where F is the Faraday constant, A is the electrode area, k is the heterogeneous rate constant of the electron transfer (potential dependent), and c is the concentration of the electroactive species.

An electrical circuit that is equivalent to an electrochemical system is shown in Figure 1.3, where an external voltage, V, is applied between a working and reference electrode through a serial resistor, R_S. The causes of NDR arise through different factors or processes with respect to the variables in the above equations.

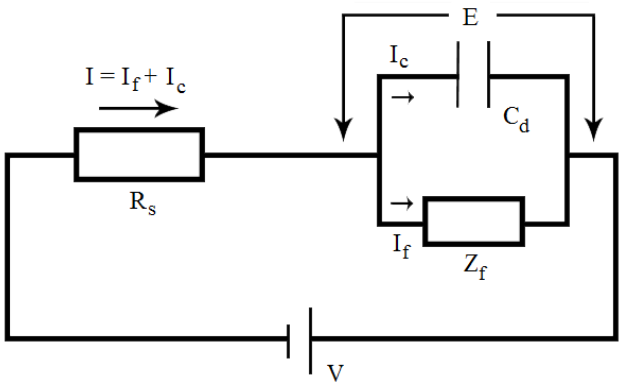

Figure 1.3 - Equivalent circuit in a dynamic system.

1.4.2 Causes of Negative Differential Resistance

Now that we recognize the significance of negative differential resistance to electrochemical oscillators, it is important to understand the underlying factors, which cause NDR to emerge in an electrochemical system. There are three principle factors leading to NDR in a system: (1) a negative dA/dE slope, (2) a negative dk(E)/dE slope, and (3) a negative di(0)/dE slope, where A represents electrode area, E represents applied potential, k represents the rate constant, and i represents the current. [47]

A negative dA/dE slope occurs when there is a decrease in the available area of the electrode surface at increased polarization (as the applied potential is increased). This decrease in active surface area occurs in a number of different situations, such as when a metal becomes passivated by an oxide layer or through the potential dependent adsorption of an inhibiting layer.

A negative dk(E)/dE slope can be caused through two different routes: (a) similar to adsorption of an inhibiting layer causing a decrease in active surface area, the potential dependent adsorption of an inhibiting layer occurs; however, it simply decreases the electron transfers rate constant, as opposed to fully cancelling it. The second route leading to a negative dk(E)/dE slope is the opposite case: (b) a potential dependent desorption of a catalyst which consequently leads to a decrease in the rate constant governing the electron transport.

The third cause of NDR (a negative di(0)/dE slope) arises when the electric potential at the reaction site is different from the electric potential in the bulk (more pronounced in electrolyte solutions with low ionic strengths).

The presence of NDR in a system which exhibits spontaneous oscillatory behavior allows the system to be classified as a truly electrochemical oscillator.

1.4.3 Types of Electrochemical Oscillators

Electrochemical systems displaying dynamic self-organization are routinely classified based on whether or not the system contains negative differential resistance (NDR). However, the location of the NDR (corresponding to a positive or negative slope in a linear sweep voltammogram (LSV)), as well as the qualitative shape of the LSV, also aid in providing a more descriptive classification of the oscillator. It has been found that there are three primary classes of electrochemical oscillators: (1) N-NDR, (2) HN-NDR, and (3) S-NDR [174]. In an N-NDR type oscillator the electrode potential, E, supplies the fast (autocatalytic) positive feedback and is an essential variable (i.e., variables which affect the oscillatory behavior when changes in their time scales are made). The oscillations occurring in such a system can be seen in current (or current density) only, and are therefore only observable under potentiostatic conditions. It is the simultaneous oscillation of the electrode potential (E = V - IR), which manifests oscillations in current. [47] A typical Nyquist diagram (obtained through EIS measurements) of an N-NDR electrochemical oscillator shows the impedance cross the imaginary axis and intersect the real impedance axis at a negative value (Figure 1.4).

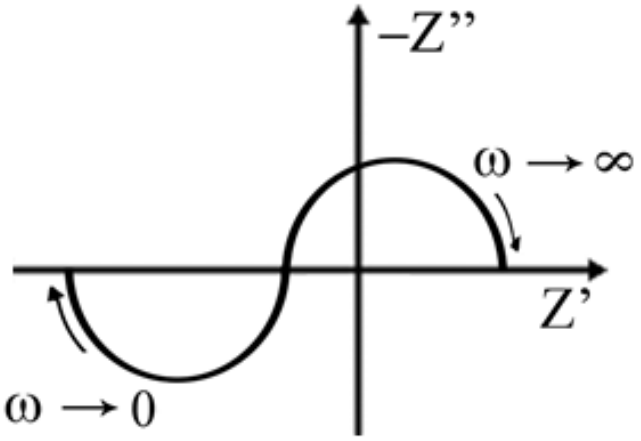

Figure 1.4 - Nyquist diagram illustrating a characteristic example of N-Shaped Negative Differential Resistance

Characteristic examples of N-NDR type oscillators are the electroreduction of $S_2O_8^{2-}$, as well as the polarographic In(III) - SCN^- oscillator [175,176].

A second type of NDR type system occurs when the region of NDR is located (hidden) on the positive slope of an LSV, referred to as an HN-NDR oscillator. HN-NDR oscillators are similar to N-NDR oscillators in that the electrode potential is responsible for the fast positive feedback [47]. However, the presence of hidden negative impedance implies that there are two potential dependent processes occurring: a fast process giving rise to negative impedance and a slow process with positive impedance. Importantly, oscillations in both current as well as potential are realized in systems that belong to the HN-NDR class. EIS measurements of HN-NDR systems show that the impedance crosses the imaginary axis before intersecting with the real negative impedance axis; however, at finite frequencies the impedance ends on the positive side (a representative diagram is shown in Figure 1.5).

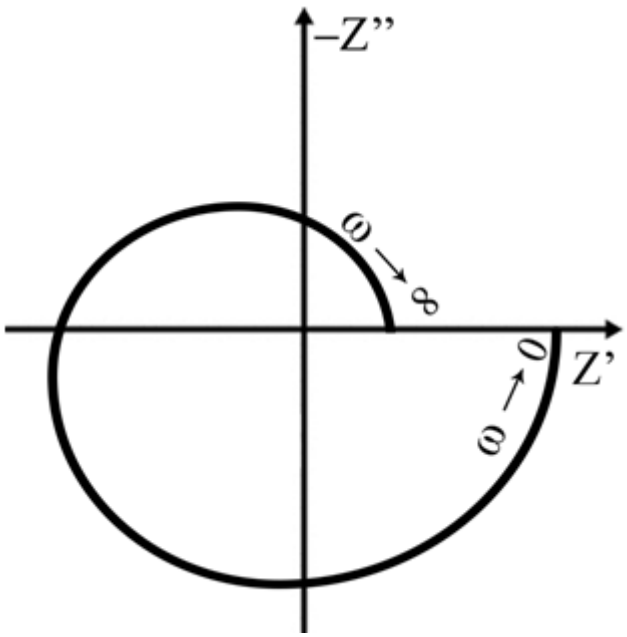

Figure 1.5 - Nyquist diagram illustrating a characteristic example of Hidden N-Shaped Negative Differential Resistance

Examples of electrochemical oscillators falling into the HN-NDR class include the oxidation of formic acid on Pt, the dissolution of nickel, and the galvanostatic reduction of IO_3^- on Ag [160, 177-179].

The third NDR based oscillator is an S-NDR (the designation S refers to the shape of its I-E curve). In an S-NDR system the electrode potential is again an essential variable; however, in this case it supplies the slow negative feedback [47]. The Nyquist diagram obtained through EIS measurements of an S-NDR type oscillator is shown in Figure 1.6. Here, the impedance intersects the real positive axis before crossing the imaginary axis and ends up intersecting with the negative real axis. The electrodeposition of Zn is an example of an electrochemical system in the class S-NDR [180,181].

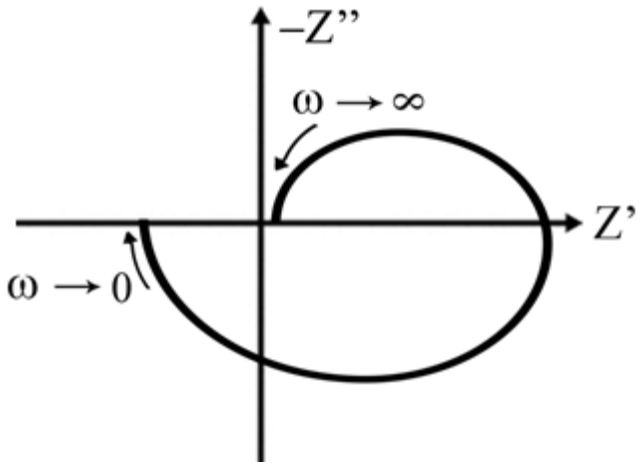

Figure 1.6 - Nyquist diagram illustrating a characteristic example of S-Shaped Negative Differential Resistance

As mentioned above, the presence of NDR is not an absolute requirement for oscillations to be observed in electrochemical systems. In fact, two other mechanisms leading to oscillations have been observed. Oscillations have been observed in systems driven by convection-induced instabilities. These instabilities arise through the formation and detachment of bubbles on the electrode surface [182]. The other non-NDR type oscillator is Capacitance Mediated Positive Differential Resistance (CMPDR) oscillator [183,184]. This CMPDR type oscillator is driven by the formation and dissolution of an inhibiting surface layer on the electrode surface. Importantly, these oscillations take place on a branch of positive differential resistance. Other features associated with this type of oscillator are that no external resistor is needed, the oscillations occur on a current plateau in an LSV, admittance spectra displays resonance behavior, and increased serial resistance causes oscillation amplitude to decrease.

1.5 Applications of Nonlinear Systems

1.5.1 Applications of Chemical Oscillators

An interesting application of chemical oscillating systems came in the field of analytical chemistry. Jimenez-Prieto et al. proposed what is known as the Analyte Pulse Perturbation (APP) technique, where a chemically oscillating system is perturbed with a milliliter amount of a target analyte and the resulting change in oscillatory amplitude or frequency is linearly proportional to the amount of analyte initially added. To formulate their technique, they ran the hydrogen peroxide and sodium thiocyanate reaction catalyzed by copper(II) in a CSTR [185]. The use of a CSTR is important in order to sustain periodic oscillations over a large timescale, allowing multiple detections to occur, without the need to set up a new oscillating reaction. Once a calibration curve is established, rapid determination of sodium thiosulfate concentrations with a relative standard deviation (RSD) of approximately 1% were achieved with sensitivity in the micro-nanomolar range. Although an interesting use of a chemical oscillator, this method is confined for strictly quantitative measurements.

Recently, Zhang et al. used a modified Briggs-Rauscher oscillating reaction to successfully identify α-ketoglutaric acid and β-ketoglutaric acid, showing that the use of chemical oscillators can be used to differentiate between certain isomers [186]. Using a tetraaza-macrocyclic complex $[NiL](ClO_4)_2$ where the ligand L in the complex was 5,7,7,12,14,14-hexamethyl-1,4,8,11-tetraazacyclotetradeca-4-11-diene, they found that in a batch reactor, the addition of α-ketoglutaric acid did not influence the oscillatory behavior. However, perturbations with β-ketoglutaric acid influenced the oscillatory dynamics by quenching the oscillations for a period of time, which was found to be

proportional to the concentration of β-ketoglutaric acid added. This inhibition was proposed to be due to a reaction between β-ketoglutaric acid and HOO^{*} radicals, forming acetone, the known oxidation product of β-ketoglutaric acid.

1.5.2 Applications of Reaction - Diffusion Systems

Stimuli-responsive polymers, also referred to as smart or intelligent polymers, are capable of responding to their environment by undergoing changes in either their chemical or physical properties [187-189]. The most common stimulus that is utilized to induce changes in stimuli-responsive polymers is temperature; however, polymers have been designed which are responsive to pH, mechanical force, electrical or magnetic fields [189]. Research into the design of smart polymers is an ongoing area of interest due to their application in drug delivery, biosensors, and artificial muscles, amongst others [187-189]. In 1996, Yoshida designed a polymer gel, which was capable of autonomously swelling and deswelling through the utilization of the Belousov-Zhabotinsky oscillating reaction [190]. A polymer was constructed consisting of N-isopropylacrylamide (IPAAm) which had ruthenium(II) tris-(2,2'-bipyridine) $(Ru(bpy)_3^{2+}$ covalently bonded to the polymer chain. IPAAm is one of the most commonly studied thermoresponsive polymers, which exhibits Lower Critical Solution Temperature (LCST) [189]. As the temperature is increased past the LCST, the IPAAm polymer chains undergo a transition from an extended coil to a compact globular conformation. The temperature that the transition occurs at can be shifted to a higher or lower temperature by copolymerizing with a component with hydrophilic or hydrophobic properties, respectively. The copolymerization of $Ru(bpy)_3^{2+}$ introduced a known catalyst of the BZ reaction to the polymer matrix [191]. When the gel was placed in a solution consisting of malonic acid,

$NaBrO_3$ and nitric acid, the reaction occurred in the gel through the catalytic function of the polymerized $Ru(bpy)_3$, resulting in redox changes of the catalyst moiety ($Ru(bpy)_3^{2+}$ ⇌ $Ru(bpy)_3^{3+}$). The change in oxidation state of the catalyst changed the swelling because when the catalyst was in the Ru(III) state, the hydrophilicity of the polymer chain increased, subsequently decreasing in the Ru(II) state. As a result of the periodic changes in the Ru(II) complex oxidation state autonomous swelling-deswelling volume changes were observed in the gel, leading to the first example of a self-oscillating polymer gel.

The use of the ruthenium complex in the design of the self-oscillating polymer offered an opportunity to externally control the swelling-deswelling process through the process of photo-irradiation. It is known that the $Ru(bpy)_3^{2+}$ catalyst has extreme photosensitivity [192-194]. This photosensitivity was found to be capable of being used as an on-off switch depending on which oxidation state the $Ru(bpy)_3^{2+}$ catalyst was in, by either causes the formation of an inhibitor (Br^-) or an activator ($HBrO_2$). The future of self-oscillating gels may lead to important contributions to drug delivery, microactuators, and sensor based devices.

1.5.3 Applications of Electrochemical Oscillators

Electrochemistry has been found to be extremely useful in many areas of chemical research such as analytical, physical, and materials chemistry. The ease in which control parameters can be fine-tuned has allowed electrochemical techniques to be utilized towards many applications (chemical/biological sensors, energy storage, etc.) [195-197]. One constant area of interest is the fabrication of nanomaterials, due largely to their optical and magnetic effects. Electrochemistry offers a convenient and efficient

method for the fabrication of nanomaterials, and nonlinear electrochemistry has also been found capable of fabricating novel nanostructures. Switzter et al. found that alternating nanolayers of copper and cuprous oxide (Cu/Cu_2O) were deposited under galvanostatic conditions from an alkaline Cu(II) lactate solution [198]. Importantly, they found that the Cu/Cu_2O layers would only be formed when the system displayed spontaneous oscillations, achieved through the application of a constant current density. Through manipulation of the frequency of oscillations and the amplitude and waveform of the oscillations (by varying pH or applied current density), they were able to fine tune the composition and resistivity of the deposited films. They proposed that only Cu_2O was deposited when the potential was at its highest during an oscillation, and that a Cu/Cu_2O composite was deposited during the period between potential spikes. Thus, through varying the pH or applied current density, they could change the frequency of the oscillations, and thereby form deposits having thicker Cu/Cu_2O composite layers. With respect to the mechanism driving the nonlinear behavior, they recognized that it could be due to periodic variations in the pH at the surface as well as the formation and dissolution of a Cu_2O/solution interface.

Another application of nonlinear electrochemistry lies in the study of fuel cells. One class of fuel cell is the Proton Exchange Membrane (PEM) fuel cell, which relies on pure H_2 as the fuel [199]. Due to the fact that on site storage of H_2 is often impractical, H_2 must be catalytically reformed from other fuel sources such as gasoline or alcohols. During this reforming process, substantial amounts of CO are often produced and remain at high levels following the water-gas-shift reaction [199,200]. One common method of reducing the amount of CO is through the use of preferential oxidation (PrOx) reactors;

however, due to the fact that oxygen must also be present in excess to reduce the CO to low enough levels, some hydrogen in the reformate is burned, reducing the overall efficiency [201]. Electrochemical methods have also been employed for the oxidation of CO, based on periodic use of an external power source. Although there is no consumption of H_2 in this method, there is an overall power consumption. Zhang and Datta showed, using a device similar to a PEM fuel cell, that an electrochemical preferential oxidation (ECPrOX) process could oxidize CO from mixture rich in H_2 without consuming any hydrogen and without the need of an external power source [202]. When operated under constant current densities in the presence of a feed stream that contains CO, oscillations in potential have been observed in PEM fuel cells. Zhang and Datta found that a higher power output was achieved when the PEM fuel cell was operated in an oscillatory state as opposed to a stable steady state. In fact, the average power density was found to be twice as high when in an oscillatory state when the PEM fuel cell was operated at 55 ^{o}C. The oscillatory dynamics are based on the following: when the surface concentration of CO increases, the anode becomes polarized to a higher potential to maintain the applied constant current. The increase in overpotential quickens the electro-oxidation of the adsorbed CO, which leads to a CO oxidation rate, which is higher than the rate of CO adsorption. This causes the overall surface coverage of CO to decline, which happens quickly past a threshold overpotential, making the oxidation of H_2 the primary reaction maintaining the current. A subsequent drop in potential occurs which allows CO adsorption to once again occur more rapidly than the oxidation of CO, which restarts the cycle. Thus, the fact that there are short bursts in potential that remove the CO from the anode surface results in a lowered time-averaged anode overpotential under oscillatory

conditions, leading to an increase in average cell voltage and power density compared to stable state (non-oscillatory) conditions.

1.6 References

[1] A. T. Winfree, *The Geometry of Biological Time*; Springer: Heidelberg, 2000.

[2] M. Orlik, *Self-Organization in Electrochemical Systems II: Spatiotemporal Patterns and Control of Chaos*; Springer, Berlin, 2012.

[3] R. J. Field, M. Burger, *Oscillations and Travelling Waves in Chemical Systems*; Wiley & Sons: New York, 1985.

[4] J. A. Scheinkman, B. LeBaron, *J. Bus.* **1989**, 62, 311-337.

[5] N.K. Vitanov, I. P. Jordanov, Z. I. Dimitrova, *Commun. Nonlinear Sci. Numer. Simulat.* **2009**, 14, 2379-2388.

[6] H. A. Braun, M. T. Huber, M. Dewald, K. Schäfer, K. Voigt, *Int. J. Bifurcation Chaos* **1998**, 8, 881-889.

[7] Y. Loewenstein, H. Sompolinsky, *Nature Neuroscience* **2003**, 6, 961-967.

[8] M. Perc, A. K. Green, C. J. Dixon, M. Marhl, *Biophys. Chem.* **2008**, 132, 33-38.

[9] M. G. T. Fechner, *J. Schweigger fur Chem. Phys.* **1828**, 53, 129-151.

[10] W. C. Bray, *J. Am. Chem. Soc.* **1921**, 43, 1262-1267.

[11] W. C. Bray, H. A. Liebhafsky, *J. Am. Chem. Soc.* **1931**, 53, 38-44.

[12] I. R. Epstein, J. A. Pojman, *An Introduction to Nonlinear Chemical Dynamics: Oscillations, Waves, Patterns, and Chaos*; Oxford University Press: Oxford, U.K., 1998.

[13] A. J. Lotka, *Proc. Natl. Acad. Sci. U.S.A.* **1920**, 6, 410-415.

[14] A. J. Lotka, *J. Am. Chem. Soc.* **1920**, 42, 1595-1599.

[15] V. Volterra, *Nature* **1926**, 118, 558-560.

[16] B. P. Belousov, *Sborkik Referatov po Radiatsionni Meditsine* **1958**, 145.

[17] I. Prigogine, *Introduction to Thermodynamics of Irreversible Processes*; Wiley, New York, 1955.

[18] G. Nicolis, I. Prigogine, *Self-Organization in Nonequilibrium Systems*; Wiley, New York, 1977.

[19] A. M. Zhabotinsky, *Biofizika,* **1964**, 9, 306-311.

[20] A. M. Zhabotinsky, *Dokl. Akad. Nauk. SSSR* **1964**, 157, 392-395.

[21] A. N. Zaikin, A. M. Zhabotinskii, *Nature* **1970**, 225**,** 535-537.

[22] I. Prigogine, R. Lefever, *J. Phys. Chem.* **1968**, 48**,** 1695-1700.

[23] R. J. Field, E. Körös, R. M. Noyes, *J. Am. Chem. Soc.* **1972**, 94**,** 8649-8664.

[24] R. J. Field, R. M. Noyes, *J. Chem. Phys.* **1974**, 60**,** 1877-1884.

[25] K. Showalter, R. M. Noyes, K. Bar-Eli, *J. Chem. Phys.* **1978**, 69**,** 2514-2524.

[26] W. Jahnke, A. T. Winfree, *Int. J. Bifurcation Chaos* **1991**, 1, 445-466.

[27] T. S. Briggs, W. C. Rauscher, *J. Chem. Ed.* **1973**, 50**,** 496.

[28] P. De Kepper, I. R. Epstein, K. Kustin, *J. Am. Chem. Soc.* **1981**, 103**,** 6121-6127.

[29] P. De Kepper, I. R. Epstein, K. Kustin, *J. Am. Chem. Soc.* **1981**, 103**,** 2133-2134.

[30] L. F. Salter, J. G. Sheppard, *Int. J. Chem. Kinet.* **1982**, 14**,** 815-821.

[31] M. Alamgir, I. R. Epstein, *J. Am. Chem. Soc.* **1983**, 105**,** 2500-2502.

[32] R. P. Rastogi, S. N. Singh, P. Chand, *Chem. Phys. Lett.* **2004**, 385**,** 403-408.

[33] P. I. Kumli, M. Burger, M. J. B. Hauser, S. C. Müller, Z. Nagy-Ungvarai, *Phys. Chem. Chem. Phys.* **2003**, 5**,** 5454-5458.

[34] S. Biswas, K. Mukherjee, D. C. Mukherjee, S. P. Moulik, *J. Phys. Chem. A* **2001**, **1**05**,** 8857-8863.

[35] M. Orbán, P. De Kepper, I. R. Epstein, *J. Am. Chem. Soc.* **1982**, 104**,** 2657-2658.

[36] M. Orbán, I. R. Epstein, *J. Phys. Chem.* **1983**, 87**,** 3212-3219.

[37] D. S. Huh, H. S. Kim, J. K. Kang, Y. J. Kim, D. H. Kim, S. H. Park, K. Yadav, J. Wang, *Chem. Phys. Lett.* **2003**, 378**,** 78-84.

[38] P. V. Lalitha, R. Ramaswamy, *React. Kinet. Catal. Lett.* **1992**, 47**,** 133-141.

[39] S. S. Lee, J. J. Jwo, *Int. J. Chem. Kinet.* **1998**, 30**,** 595-604.

[40] M. Orbán, M. Lengyel, I. R. Epstein, *J. Am. Chem. Soc.* **1991**, 113**,** 1978-1982.

[41] M. Orbán, E. Körös, *Nature* **1978**, 273**,** 371-372.

[42] M. Orbán, E. Körös, *J. Phys. Chem.* **1978**, 82**,** 1672-1674.

[43] M. Orbán, E. Körös, R. M. Noyes, *J. Phys. Chem.* **1979**, 83**,** 3056-3057.

[44] B. Zhao, J. Wang, *Chem. Phys. Lett.* **2006**, 19**,** 41-44.

[45] M. Harati, S. Amiralaei, J. R. Green, J. Wang, *Chem. Phys. Lett.* **2007**, 439**,** 337-341.

[46] P. Gray, S. K. Scott, *Chemical Oscillations and Instabilities: Nonlinear Chemical Kinetics*; Clarendon Press: Oxford, U.K., 1994.

[47] M. Orlik, *Self-Organization in Electrochemical Systems I: General Principles of Self-Organization. Temporal Instabilities*; Springer, Berlin, 2012.

[48] F. Sagués, I. R. Epstein, *Dalton Trans.* **2003**, 1201-1217.

[49] B. Drossel, P. G. Higgs, A. J. McKane, *J. Theor. Biol.* **2001**, 208**,** 91-107.

[50] P. Ortoleva, *Physica D* **1984**, 12**,** 305-320.

[51] G. Schmitz, *Phys. Chem. Chem. Phys.* **2010**, 12, 6605-6615.

[52] G. Schmitz, L. Kolar-Anić, S. Anić, T. Grozdić, V. Vukojević, *J. Phys. Chem. A* **2006**, 110, 10361-10368.

[53] F. G. Buchholtz, S. Broecker, *J. Phys. Chem. A.* **1988**, 102, 1556-1559.

[54] N. Pejić, L. Kolar-Anić, J. Maksimović, M. Janković, V. Vukojević, S. Anić, *Reac. Kinet. Mech. Cat.* **2016**, 118, 15-16.

[55] S. Kéki, G. Székely, M. T. Beck, *J. Phys. Chem. A* **2003**, 107, 73-75.

[56] L. Györgyi, R. J. Field, Z. Noszticzius, W. D. McCormick, H. L. Swinney, *J. Phys. Chem.* **1992**, 96, 1228-1233.

[57] D. Zhang, L. Györgyi, W. R. Peltier, *Chaos* **1993**, 3, 723-745.

[58] M. L. Davies, I. Schreiber, S. K. Scott, *Chem. Eng. Sci.* **2004**, 59, 139-148.

[59] M. Masia, N. Marchettini, V. Zambrano, M. Rustici, *Chem. Phys. Lett.* **2001**, 341**,** 285-291.

[60] V. K. Vanag, M. V. Alfimov, *J. Phys. Chem.* **1993**, 97, 1884-1890.

[61] N. Okazaki, I. Hanazaki, *J. Chem. Phys.* **1998**, 109, 637-642.

[62] N. Okazaki, Y. Mori, I. Hanazaki, *J. Phys. Chem.* **1996**, 100, 14941-14948.

[63] G. Szabó, A. Csavdári, L. Onel, G. Bourceanu, Z. Noszticzius, M. Wittman, *J. Phys. Chem. A* **2007**, 111, 610-612.

[64] R. Cervellati, K. Höner, S. D. Furrow, F. Mazzanti, S. Costa, *Helv. Chim. Acta* **2004**, 87, 133-155.

[65] P. De Kepper, I. R. Epstein, *J. Am. Chem. Soc.* **1982**, 104, 49-55.

[66] R. M. Noyes, S. D. Furrow, *J. Am. Chem. Soc.* **1982**, 104, 45-48.

[67] K. R. Kim, D. J. Lee, K. J. Shin, *J. Chem. Phys.* **2002**, 117, 2710-2717.

[68] K. R. Kim, K. J. Shin, D. J. Lee, *J. Chem. Phys.* **2004**, 121, 2664-2672.

[69] M. C. Guedes, R. B. Faria, *J. Phys. Chem. A* **1998**, 102, 1973-1975.

[70] Y. Chen, J. Wang, *J. Phys. Chem. A* **2005**, 109, 3950-3956.

[71] J. Wang, F. Hynne, P. G. Sørensen, K. Nielsen, *J. Phys. Chem.* **1996**, 100, 17593-17598.

[72] P. E. Strizhak, M. Menzinger, *J. Chem. Educ.* **1996**, 73, 868-873.

[73] B. R. Johnson, S. K. Scott, B. W. Thompson, *Chaos* **1997**, 7, 350-358.

[74] P. E. Strizhak, T. S. Ivashchenko, A. L. Kawczyński, *Polish J. Chem.* **1994**, 68, 2049-2055.

[75] N. Li, J. Wang, *J. Phys. Chem. A* **2009**, 113, 6297-6300.

[76] E. Körös, M. Orbán, I. Habon, *J. Phys. Chem.* **1980**, 84, 559-560.

[77] R. P. Rastogi, I. Das, A. Sharma, *J. Chem. Soc., Faraday Trans.* **1989**, 85, 2011-2019.

[78] L. Adamčiková, Z. Farbulová, P. Ševčik, A. L. Kawczyński, *J. Phys. Chem. A* **2003**, 107, 508-511.

[79] L. Adamčiková, P. Ševčik, *React. Kinet. Catal. Lett.* **1995**, 56, 137-142.

[80] M. Desroches, J. Guckenheimer, B. Krauskopf, C. Kuehn, H. M. Osinga, M. Wechselberger, *SIAM Rev.* **2012**, 54, 211-288.

[81] C. A. Del Negro, C. G. Wilson, R. J. Butera, H. Rigatto, J. C. Smith, *Biophys. J.* **2002**, 82, 206-214.

[82] M. Krupa, N. Popović, N. Kopell, *SIAM J. Appl. Dyn. Syst.* **2008**, 7, 361-420.

[83] M. Desroches, B. Krauskopf, H. M. Osinga, *Nonlinearity* **2010**, 23, 739-765.

[84] T. Haberichter, M. Marhl, R. Heinrich, *Biophys. Chem.* **2001**, 90, 17-30.

[85] A. Longtin, *Phys. Rev. E* **1997**, 55, 868-876.

[86] A. Cadena, D. Barragán, J. Ágreda, *J. Braz. Chem. Soc.* **2013**, 24, 2028-2032.

[87] A. M. Zhabotinsky, *Chaos* **1991**, 1, 379-386.

[88] M. Desroches, T. J. Kaper, M. Krupa, *Chaos* **2013**, 23, 046106.

[89] R. J. Field, L. Györgyi, *Chaos in Chemistry and Biochemistry;* World Scientific: Singapore, 1993.

[90] F. Argoul, A. Arnedo, P. Richetti, J. C. Roux, H. L. Swinney, *Acc. Chem. Res.* **1987**, 20, 436-442.

[91] O. Lev, A. Wolfberg, L. M. Piseman, *Chem. Eng. Sci.* **1988**, 43, 1339-1353.

[92] J. L. Hudson, M. R. Bassett, *Rev. Chem. Eng.* **1991**, 7, 109-170.

[93] M. Rosenblum, A. Pikovsky, *Phys. Rev. Lett.* **2007**, 98, 064101.

[94] T. Hogg, B. A. Huberman, *Phys. Rev. A* **1984**, 29, 275-281.

[95] A. Karantonis, M. Pagitsas, D. Sazou, *Chaos* **1993**, 3, 243-255.

[96] H. G. Schuster, W. Just, *Deterministic Chaos: An Introduction;* John Wiley & Sons: Weinheim, 2006.

[97] J. Qin, L. Wang, D. P. Yuan, P. Gao, B. Z. Zhang, *Phys. Rev. Lett.* **1989**, 63, 163-166.

[98] C. J. Doona, R. Blittersdorf, F. W. Schneider, *J. Phys. Chem.* **1993**, 97, 7258-7263.

[99] F. T. Arecchi, G. L. Lippi, G. P. Puccioni, J. R. Tredicce, *Opt. Commun.* **1984**, 5, 308-314.

[100] L. Györgyi, R. J. Field, *Nature* **2004**, 355, 808-810.

[101] S. H. Strogatz, *Nonlinear Dynamics and Chaos: With Applications to Physics, Biology, Chemistry, and Engineering;* Addison-Wesley: Reading, MA, 1994.

[102] R. C. Hilborn, *Am. J. Phys.* **2004**, 72, 425-427.

[103] Z. Melichová, M. Melichercík, A. Olexová, L. Treindl, *React. Kinet. Catal. Lett.* **1995**, 55, 51-57.

[104] P. Resch, R. J. Field, F. W. Schneider, M. Burger, *J. Phys. Chem.* **1989**, 93, 8181-8186.

[105] A. Nagy, A. Olexova, L. Treindl, *J. Phys. Chem.* **1991**, 95, 5809-5810.

[106] J. Masełko, I. R. Epstein, *J. Chem. Phys.* **1984**, 80, 3175-3178.

[107] K. R. Leopold, A. Haim, *Int. J. Chem. Kinet.* **1977**, 9, 83-95.

[108] M. Orbán, P. De Kepper, I. R. Epstein, K. Kustin, *Nature* **1981**, 292, 816-818.

[109] M. Orbán, I. R. Epstein, *J. Phys. Chem.* **1995**, 99, 2358-2362.

[110] D. L. Olsen, A. Scheeline, *J. Phys. Chem.* **1995**, 99, 1204-1211.

[111] M. Orbán, K. Kurin-Csörgei, I. R. Epstein, *Acc. Chem. Res.* **2015**, 48, 593-601.

[112] M. Orbán, I. R. Epstein, *J. Am. Chem. Soc.* **1985**, 391, 349-353.

[113] G. Rábai, M. Orbán, I. R. Epstein, *J. Phys. Chem.* **1992**, 96, 5414-5419.

[114] E. C. Edblom, M. Orbán, I. R. Epstein, *J. Am. Chem. Soc.* **1986**, 108, 2826-2830.

[115] K. Kovács, R. E. McIlvaine, S. K. Scott, A. F. Taylor, *J. Phys. Chem. A* **2007**, 111, 549-551.

[116] S. N. Semenov, L. J. Kraft, A. Ainla, M. Zhao, M. Baghbanzadeh, V. E. Campbell, K. Kang, J. M. Fox, G. M. Whitesides, *Nature* **2016**, 537, 656-660.

[117] B. A. Grzybowski, *Chemistry in Motion: Reaction-Diffusion Systems for Micro- and Nanotechnology*; John Wiley & Sons, United Kingdom, 2009.

[118] V. Volpert, S. Petrovskii, *Phys. Life Rev.* **2009**, 6, 267-310.

[119] S. Soh, M. Byrska, K. Kandere-Grzybowska, B. A. Grzybowski, *Angew. Chem. Int. Ed.* **2010**, 49, 4170-4198.

[120] C. H. Flather, M. Bevers, *Am. Nat.* **2002**, 159, 40-56.

[121] S. A. Gourley, N. F. Britton, *J. Math. Biol.* **1996**, 34, 297-333.

[122] R. E. Liesegang, *Naturwiss. Wochenschr.* **1896**, 11, 353.

[123] R. A. Gatenby, E. T. Gawlinski, *Cancer Res.* **1996**, 56, 5745-5753.

[124] Q. T. Ho, B. E. Verlinden, P. Verboven, S. Vandewalle, B. M. Nicolai, *J. Exp. Bot.* **2006**, 57, 4215-4224.

[125] S. Kondo, R. Asai, *Nature* **1995**, 376, 765-768.

[126] J. J. Masełko, K. Showalter, *Nature* **1989**, 339, 609-611.

[127] I. R. Epstein, I. Lengyel, S. Kádar, M. Kagan, M. Yokoyama, *Physica A* **1992**, 188, 26-33.

[128] R. Kapral, K. Showalter, *Chemical Waves and Patterns*; Kluwer Academic Publishers, Netherlands, 1995.

[129] A. M. Zhabotinsky, L. Györgyi, M. Dolnik, I. R. Epstein, *J. Phys. Chem.* **1994**, 98, 7981-7990.

[130] D. Winston, M. Arora, J. J. Masełko, V. Gáspar, K. Showalter, *Nature*, 351, 132-135.

[131] D. Haim, G. Li, Q. Ouyang, W. D. McCormick, H. L. Swinney, A. Hagberg, E. Meron, *Phys. Rev. Lett.* **1996**, 77, 190-193.

[132] K. Kurin-Csörgei, A. M. Zhabotinsky, M. Orbán, I. R. Epstein, *J. Phys. Chem.* **1996**, 100, 5393-5397.

[133] M. C. Cross, P. C. Hohenberg, *Rev. Mod. Phys.* **1993**, 65, 851-1112.

[134] A. Pagola, C. Vidal, *J. Phys. Chem.* **1987**, 91, 501-503.

[135] J. G. Bell, J. Wang, *J. Phys. Chem. A* **2015**, 119, 3323-3328.

[136] N. Manz, O. Steinbock, *Chaos* **2006**, 16, 037112.

[137] M. Harati, J. Wang, *Chaos* **2009**, 19, 023116.

[138] B. Marts, K. Martinez, A. L. Lin, *Phys. Rev. E* **2004**, 70, 056223.

[139] T. Yamaguchi, L. Kuhnert, Z. Nagy-Ungrarai, S. C. Müller, B. Hess, *J. Phys. Chem.* **1991**, 95, 5831-5837.

[140] A. E. Bugrim, M. Dolnik, A. M. Zhabotinsky, I. R. Epstein, *J. Phys. Chem.* **1996**, 100, 19017-19022.

[141] J. J. Tyson, P. C. Fife, *J. Chem. Phys.* **1980**, 73, 2224-2237.

[142] V. S. Zykov, *Biophysics* **1980**, 25, 906-911.

[143] P. Foerster, S. C. Müller, B. Hess, *Science* **1988**, 241, 685-687.

[144] O. Steinbock, V. Zykov, S. C. Müller, *Nature* **2004**, 366, 322-324.

[145] J. P. Keener, J. J. Tyson, *Physica D* **1986**, 21, 307-324.

[146] G. Biosa, S. Bastianoni, M. Rustici, *Chem. Eur. J.* **2006**, 12, 3430-3437.

[147] V. S. Zykov, *Physica D* **2009**, 238, 931-940.

[148] N. Manz, B. T. Ginn, O. Steinbock, *J. Phys. Chem. A* **2003**, 107, 11008-11012.

[149] Q. Gao, J. Li, K. Zhang, I. R. Epstein, *Chaos* **2009**, 19, 033134.

[150] H. Guo, L. Li, Q. Ouyang, J. Liu, Z. She, *J. Chem. Phys.* **2003**, 118, 5038-5044.

[151] F. Fenton, A. Karma, *Chaos* **1998**, 8, 20-47.

[152] Z. A. Jimenez, O. Steinbock, *Phys. Rev. E* **2012**, 86, 036205.

[153] D. Kupitz, M. J. B. Hauser, *Phys. Rev. E* **2012**, 86, 066208.

[154] H. Henry, V. Hakim, *Phys. Rev. Lett.* **2000**, 85, 5328-5331.

[155] C. Henze, E. Lugosi, A. T. Winfree, *Can. J. Phys.* **1990**, 68, 683-710.

[156] A. M. Turing, *Philos. Trans. Roy. Soc. London, Ser. B* **1952**, 237, 37-72.

[157] V. Castets, E. Dulos, J. Boissonade, P. De Kepper, *Phys. Rev. Lett.* **1990**, 64, 2953-2956.

[158] V. K. Vanag, I. R. Epstein, *Chaos* **2008**, 18, 026107.

[159] T. Bánsági Jr., V. K. Vanag, I. R. Epstein, *Science* **2011**, 331, 1309-1312.

[160] P. Strasser, M. Lübke, C. Eisckes, M. Eiswirth, *J. Electroanal. Chem.* **1999**, 462, 19-33.

[161] J. Lee, C. Eickes, M. Eiswirth, G. Ertl, *Electrochim. Acta* **2002**, 47, 2297-2301.

[162] A. Chen, B. Miller, *J. Phys. Chem. B* **2004**, 108, 2245-2251.

[163] L. Xu, Q. Gao, J. Feng, J. Wang, *Chem. Phys. Lett.* **2004**, 397, 265-270.

[164] G. Samjeské, M. Osawa, *Angew. Chem. Int. Ed.* **2005**, 117, 5694-5698.

[165] L. Organ, I. Z. Kiss, J. L. Hudson, *J. Phys. Chem. B* **2003**, 94, 6648-6659.

[166] S. Kariuki, H. D. Dewald, J. Thomas, R. W. Rollins, *J. Electroanal. Chem.* **2000**, 486, 175-180.

[167] Z. Du, Q. Gao, J. Feng, Y. Lu, J. Wang, *J. Phys. Chem. B* **2006**, 110, 26098-26104.

[168] J. A. O'Brien, J. T. Hinkley, S. W. Donne, *Electrochim. Acta* **2011**, 56, 4224-4230.

[169] I. Z. Kiss, Q. Lv, L. Organ, J. L. Hudson, *Phys. Chem. Chem. Phys.* **2006**, 8, 2707-2715.

[170] J. Christoph, M. Eiswirth, *Chaos* **2002**, 12, 215-230.

[171] A. J. Bard, L. R. Faulkner, *Electrochemical Methods: Fundamentals and Applications*; John Wiley & Sons, United States of America, 2001.

[172] M. T. Gorzkowski, A. Wesolowska, R. Jurczakowski, P. Ślepski, K. Darowicki, M. Orlik, *J. Solid State Electrochem.* **2011**, 15, 2311-2320.

[173] S. Nakanishi, *Self-Organized Formation of Layered Nanostructures by Oscillatory Electrodeposition,* in A. Eftekhari (Eds), *Nanostructured Materials in Electrochemistry*, Vol. 8; Wiley-VCH, New York, 2008.

[174] P. Strasser, M. Eiswirth, M. T. M. Koper, *J. Electroanal. Chem.* **1999**, 478, 50-66.

[175] L. Treindl, K. Doblhofer, K. Frischer, Z. Samec, *Electrochim. Acta* **1999**, 44, 3963-3967.

[176] R. de Levie, *Chem. J. Electroanal. Chem.* **1970**, 25, 257-273.

[177] P. Strasser, M. Eiswirth, G. Ertl, *J. Chem. Phys.* **1997**, 107, 991-1003.

[178] M. T. M. Koper, *J. Chem. Soc. Faraday Trans.* **1998**, 94, 1369-1378.

[179] O. Lev, A. Wolffberg, L. M. Piseman, M. Sheintuch, *J. Phys. Chem.* **1989**, 93, 1661-1666.

[180] I. Epelboin, M. Ksouri, E. Lejay, R. Wiart, *Electrochim. Acta* **1975**, 20, 603-605.

[181] I. Z. Kiss, Z. Kazsu, V. Gáspár, *J. Phys. Chem. A* **2005**, 109, 9521-9527.

[182] Z. L. Li, J. L. Cai, S. M. Zhou, *J. Electroanal. Chem.* **1997**, 436, 195-201.

[183] C. Zensen, K. Schönleber, F. Kemeth, K. Krischer, *J. Phys. Chem. C* **2014**, 118, 24407-24414.

[184] J. G. Bell, J. Wang, *J. Electroanal. Chem.* **2015**, 754, 133-137.

[185] R. Jiménez-Prieto, M. Silva, D. Pérez-Bendito, *Anal. Chem.* **1995**, 67, 729-734.

[186] Y. Zhang, G. Hu, J. Song, *Anal. Chem.* **2015**, 87, 10040-10046.

[187] C. de las Heras Alarcon, S. Pennadam, C. Alexander, *Chem. Soc. Rev.* **2005**, 34, 276-285.

[188] S. K. Ahn, R. M. Kasi, S. C. Kim, N. Sharma, Y. Zhou, *Soft Matter* **2008**, 4, 1151-1157.

[189] M. R. Islam, Z. Lu, X. Li, A. K. Sarker, L. Hu, P. Choi, X. Li, N. Hakobyan, M. J. Serpe, *Anal. Chim. Acta* **2013**, 789, 17-32.

[190] R. Yoshida, T. Takahashi, T. Yamaguchi, H. Ichijo, *J. Am. Chem. Soc.* **1996**, 118, 5134-5135.

[191] S. Kádár, T. Amemiya, K. Showalter, *J. Phys. Chem. A* **1997**, 101, 8200-8206.

[192] M. Jinguji, M. Ishihara, T. Nakazawa, *J. Phys. Chem.* **1992**, 96, 4279-4281.

[193] R. Yoshida, *Adv. Mater.* **2010**, 22, 3463-3483.

[194] T. Sekiguchi, Y. Mori, N. Okazaki, I. Hanazaki, *Chem. Phys. Lett.* **1994**, 219, 81-85.

[195] S. Zhang, G. Wright, Y. Yang, *Biosens. Bioelectron.* **2000**, 15, 273-282.

[196] J. R. Windmiller, J. Wang, *Electroanalysis* **2013**, 25, 29-46.

[197] R. Raccichini, A. Varzi, S. Passerini, B. Scrosati, *Nat. Mater.* **2015**, 14, 271-279.

[198] J. A. Switzer, C. J. Hung, L. Y. Huang, F. S. Miller, Y. Zhou, E. R. Raub, M. G. Shumsky, E. W. Bohannan, *J. Mater. Res.* **1998**, 13, 909-916.

[199] V. Mehta, J. S. Cooper, *J. Power Sources* **2003**, 114, 32-53.

[200] J. Zhang, R. Datta, *J. Electrochem. Soc.* **2002**, 149, A1423-A1431.

[201] F. Mariño, C. Descorme, D. Duprez, *App. Catal. B* **2004**, 54, 59-66.

[202] J. Zhang, R. Datta, *Electrochem. Solid-State Lett.* **2004**, 7, A37-A40.

CHAPTER 2 - NONLINEAR DYNAMICAL BEHAVIOR IN THE 4-AMINOPHENOL – BROMATE SYSTEM

2.1 Introduction

The study of nonlinear dynamics in chemical systems has seen substantial activity over the past few decades and remains a topic of great attention [1-10]. The autocatalytic properties of bromate oscillators, first studied by Belousov, have allowed the original parameters of the Belousov-Zhabotinsky (BZ) reaction to be expanded upon, in terms of catalyst, organic substrate, and external forces [11-20]. In 1978, Orbán and Körös published the first evidence of oscillatory behavior in an uncatalyzed system containing only H^+, BrO_3^-, and gallic acid [21]. In later work, they published a list of 23 organic substrates which were capable of exhibiting nonlinear behavior, leading to a class of bromate oscillators referred to as Uncatalyzed Bromate Oscillators (UBOs) [22]. Being the original chemical oscillator, the BZ reaction is likely the most thoroughly explored of all chemical oscillators, where the oxidation of the organic substrate by acidic bromate catalyzed by metal ions exhibits not only periodic oscillations, but under certain conditions, complex or chaotic phenomena [23-30]. One class of complex oscillations that have been uncovered in nonlinear chemical systems is mixed mode oscillations (MMOs) [31-34], which are characterized by a single period having a mixture of both large and small amplitude oscillations (described using the L^S notation).

Complex oscillations may occur, for example, through a series of period doubling bifurcations, as a result of adjusting a control parameter. Flow rate is typically investigated as the bifurcation control parameter in a chemical oscillator studied in a

continuous flow stirred tank reactor (CSTR). The continuous introduction of fresh reactants maintains the system far from equilibrium and allows the oscillatory window to be lengthened considerably, virtually indefinitely. In closed batch reactors, the gradual, but slow consumption of an initial reagent can also make such a reactant concentration act as a bifurcation parameter, leading to transient complex oscillations. Another form of complexity in batch reactors is sequential oscillations: a spontaneous onset of two oscillatory windows separated by a quiescent period [35,36]. Despite that a large number of chemical oscillators have been reported, few of them are found to support complex oscillations in a closed system [37-40].

Recent exploration of chemical oscillators has led to much research on the effects of certain external forces on nonlinear dynamics such as stirring rate, temperature, and the influence of illumination on the oscillatory phenomena [41-43]. This is partially driven by the need to gain insights into the behavior of less controllable nonlinear systems in nature, which are frequently subjected to various perturbations. A variety of phenomena that do not exist in unperturbed systems have been uncovered [44-46]. Among various means to affect reaction kinetics, light is arguably the most convenient way to implement various forms of external forcing, such as periodic or aperiodic spatiotemporal illumination [47-54]. Photochemical oscillators can loosely be separated into two groups: photocontrolled or photosensitive. A photocontrolled reaction system is dependent upon illumination in order for certain intermediates to be created, the bromate – 4-aminophenol reaction is one such photochemical oscillator where simple periodic oscillations have been found in the absence of metal catalyst [55,56]. During this photochemical reaction, these spontaneous chemical oscillations are extremely

illumination dependent. In photosensitive reactions, the illumination simply gives an alternative pathway for the formation of key intermediates.

In this study, metal catalysts Ce^{4+}/Ce^{3+} are introduced to the bromate – 4-aminophenol system to implement another autocatalytic feedback through the reaction between Ce^{3+} and bromine dioxide radicals. As shown in the following, complex oscillations emerge as a result of the competing autocatalytic processes. The variation of light intensity, as well as other reaction parameters in the cerium - bromate – 4-aminophenol photoreaction, proves to have drastic effects on the overall complexity of the oscillations. In studying the photo-decomposition of the formed intermediate N-bromo-1,4-benzoquinone-4-imine (BBI) in aqueous solution it was found that while there is no reactivity in the absence of light, under illumination the dissolution of BBI exhibits an autocatalytic excursion. When sodium bromate is introduced to the BBI photo-decomposition, spontaneous oscillations occur, forming a new photocontrolled oscillator. The results provide new insights into the reaction mechanism of the bromate – 4-aminophenol oscillations.

2.2 Experimental Procedures

All reactions were carried out in a thermal-jacketed 50 mL glass beaker (ChemGlass). The reaction temperature was held constant at 25.0 ± 0.1 ^{o}C by a circulating water bath (Thermo NesLab RTE 7). The volume for every reaction was held constant at 30.0 mL. The reaction solution was stirred with a magnetic stirring bar driven by a magnetic stirrer (Fischer Isotemp), in order to ensure homogeneity. Reactions were monitored with a platinum electrode coupled with a $Hg|Hg_2SO_4|K_2SO_4$ reference electrode (Radiometer Analytical, XR200 and M231 Pt-9) filled with a saturated K_2SO_4

solution. A Teflon cap was used on top of the thermal-jacketed beaker in order to hold the electrodes. All measurements were recorded through a pH/potential meter (Radiometer PHM220) connected to a computer through a PowerLab/4SP data logger. The source of illumination was a 150 W halogen bulb (Fisher Scientific, model DLS-100HD).

Stock solutions of analytical grade sodium bromate ($NaBrO_3$, Aldrich, 99%), 0.1 M, sodium bromide (NaBr, Aldrich, 99%) 0.1 M, sulfuric acid (Aldrich 95-98%), 6.0 M, and $Ce(SO_4)_2$ (Aldrich) 0.003 M were prepared with double-distilled water. The 4-aminophenol (Aldrich, 98+%) was directly dissolved in the reaction mixture. N-bromo-1,4-benzoquinone-4-imine was prepared in our lab through the reaction between sodium bromate and 4-aminophenol in 1.7 M H_2SO_4 solution, in which the N-bromo-1,4-benzoquinone-4-imine was collected through filtration techniques and dried thoroughly. The purity of the product was analyzed with ^1H NMR spectroscopy and thin layer chromatography. To avoid the decomposition of N-bromo-1,4-benzoquinone-4-imine, it was prepared immediately prior to its use in the reaction.

All NMR studies were performed on a Bruker Avance 500 MHz spectrometer, and the samples were dissolved in deuterated chloroform (Cambridge Isotope Laboratories, 99.8%). Mass spectrometry measurements were performed using a 1200-L single quadrupole MS (Varian) through a direct insertion probe, and using a Waters XEVO GS-XF Time-Of-Flight, with samples introduced via an Atmospheric Solids Analysis probe. Numerical simulations were run using Berkeley Madonna 9.0 software. The simulations were performed by integrating a set of differential equations obtained through application of the law of mass action on the reaction equations.

2.3 Results and Discussion

2.3.1 Experimental Results: Cerium – Bromate – 4-Aminophenol Photoreaction

Systematically changing the concentration of sulfuric acid (Figure 2.1) greatly affects the complexity of the system. At the onset of the reaction the solution grows viscous with the formation of precipitate, N-bromo-1,4-benzoquinone-4-imine (BBI). As the reaction continues, the yellow precipitate dissolves, accompanied by the gradual decrease of the Pt potential. The sharp potential spike marks the complete dissolution of the precipitate, at which point the solution remains yellow, but transparent. After the potential spike, there is another induction time before the potential begins to fluctuate periodically, leading to spontaneous chemical oscillations. As is evident, the induction time increases as the concentration of sulfuric acid decreases from 1.0 M in (a) to 0.4 M in (d). When the system is more acidic the frequency and number of oscillations increases. At 0.8 M and 0.6 M H_2SO_4 (time series (b) and (c)) similar complex oscillations occur, where one large amplitude peak is preceded by a number of small amplitude oscillations, which are characteristics of mixed-mode oscillations (MMO). This indicates that the system has the ability to show complexity over a broader range in acid. As seen in the inset of time series (c), these complex mixed-mode oscillations range from $L^S = 1^3$ to 1^1 and then transform into simple periodic oscillations. The inset also shows that oscillations with gradually increasing amplitude emerge after a long stable interval. The MMOs then last for two hours before the transition into simple oscillations occurs, after which the redox potential remains at a low level, indicative of the reduced cerium state.

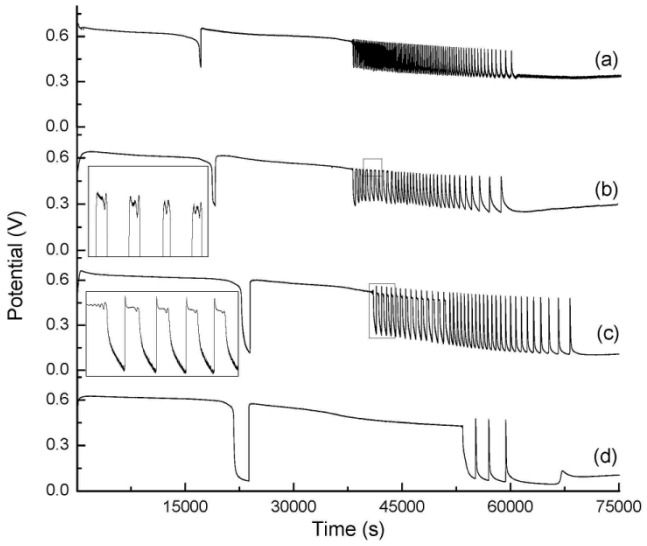

Figure 2.1 - Time series of the cerium catalyzed bromate – 4-aminophenol reaction carried out at different initial sulfuric acid concentrations: (a) 1.0 M, (b) 0.80 M, (c) 0.60M, and (d) 0.40 M. Other reaction conditions were [4-AP] = 0.025 M, [$NaBrO_3$] = 0.06 M, and [Ce(IV)] = 3.0 x 10^{-5} M.

As is intuitive in Figure 2.2, variation in the concentration of 4-aminophenol (4-AP) can have a great influence on the oscillatory dynamics of the system. The other reaction conditions are kept constant at 0.06 M $NaBrO_3$, 0.80 M H_2SO_4, and 3.0 x 10^{-5} M Ce^{4+}. Both the frequency and overall number of oscillations increased significantly as the 4-AP concentration was decreased from (a) 0.035 M to (e) 0.020 M. The amount of time required for the complete dissolution of the bromobenzoquinone imine and the corresponding redox potential spike decreases slightly as the concentration of 4-AP is decreased, presumably due to less amount of BBI precipitate formed at low 4-AP concentrations. The induction time of those transient oscillations can be seen to decrease with decreasing concentrations of 4-AP. Complex mixed-mode oscillations occur with a

4-AP concentration between 0.025 M and 0.030 M (see inset). Irregular variation in the oscillation frequency can also be seen in time series (b).

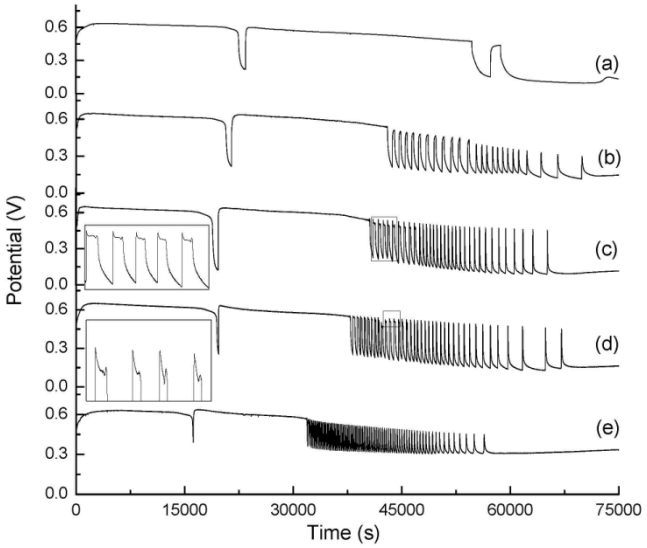

Figure 2.2 - Time series of the cerium catalyzed bromate – 4-aminophenol reaction carried out at different 4-aminophenol concentrations: (a) 0.035 M, (b) 0.030 M, (c) 0.0275 M, (d) 0.025 M, and (e) 0.020 M. Other reaction conditions were $[NaBrO_3]$ = 0.06 M, $[H_2SO_4]$ = 0.80 M, and [Ce(IV)] = 3.0 x 10^{-5} M.

Figure 2.3 presents time series illustrating how changing the bromate concentration affects the reaction dynamics of the system. Long lasting simple periodic oscillations with a high frequency were found when the concentration of bromate was 0.070 M (Figure 2.3a). The induction time of those spontaneous oscillations is shorter at high concentrations of bromate. At 0.060 M bromate, complex mixed-mode oscillations occur at the beginning of the oscillatory window. Fewer complex oscillations were found at a bromate concentration of 0.050 M, and a marked difference between the amplitude of the complex and the simple oscillations was observed. A 20% difference in the bromate concentration (from 0.050 to 0.060 M) can be seen to drastically alter the nonlinear

behavior indicating that the system is extremely sensitive to the amount of bromate. At the low bromate concentration of 0.045 M, no complex oscillations occurred and only three, low frequency oscillations with decreasing amplitude arose.

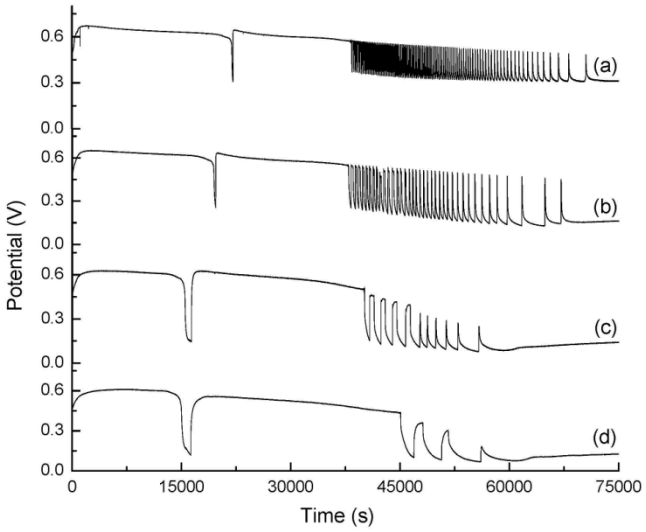

Figure 2.3 - Time series of the cerium catalyzed bromate – 4-aminophenol reaction carried out at different initial bromate concentrations: (a) 0.070 M, (b) 0.060 M, (c) 0.050 M, and (d) 0.045 M. Other reaction conditions were [4-AP] = 0.025 M, $[H_2SO_4]$ = 0.80 M, and [Ce(IV)] = 3.0 x 10^{-5} M.

The effect of changing the concentration of cerium is shown in Figure 2.4. The most noticeable difference in altering the cerium concentration is the effect it has on the induction time. Decreasing the concentration of cerium from 4.5 x 10^{-5} M (Figure 2.4a) to 1.5 x 10^{-5} M (Figure 2.4e) causes the induction time to increase from just over 3.5 h to slightly less than 9.5 h. The number of oscillations together with the frequency of oscillations can also be seen to decrease as the concentration of Ce^{4+} is decreased, indicating that the catalyst plays a crucial role in the onset of chemical oscillations.

Meanwhile, the complex oscillation pattern in time series (c) also looks quite different from the MMO seen earlier as shown in Figure 2.1c.

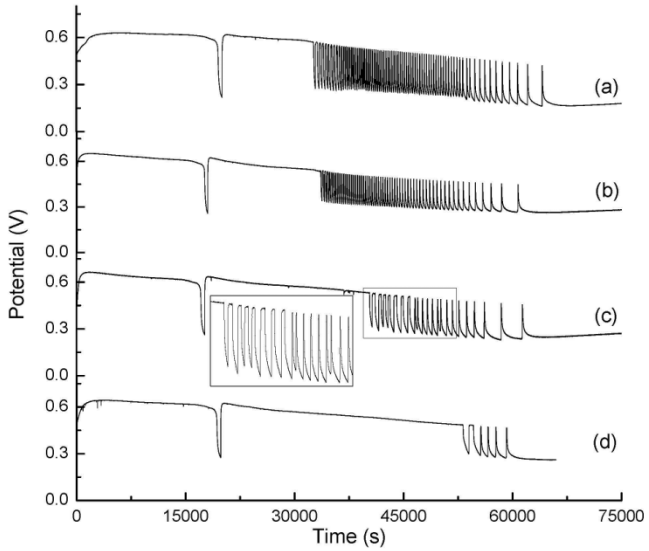

Figure 2.4 - Time series of the cerium catalyzed bromate – 4-aminophenol reaction carried out at different initial cerium concentrations: (a) 4.5 x 10^{-5} M, (b) 3.75 x 10^{-5} M, (c) 2.25 x 10^{-5} M, and (d) 1.5 x 10^{-5} M. Other reaction conditions were [4-AP] = 0.025 M, $[H_2SO_4]$ = 0.80 M, and $[NaBrO_3]$ = 0.060 M.

Figure 2.5 is a phase diagram representing the concentration of 4-AP and sulfuric acid concentration plane, where (×) represents conditions under which the system displays transient complex oscillations, and the filled squares (■) represent conditions where complex oscillations are not present. Upon increasing the amount of 4-AP in the reaction solution, an increase in the amount of sulfuric acid is needed for the system to develop complex oscillations. The diagonal strip shaped parameter domain implies that the ratio between 4-AP and H_2SO_4 is more important than the actual concentrations

themselves. Notably, the complex oscillation pattern varies within the above parameter domain.

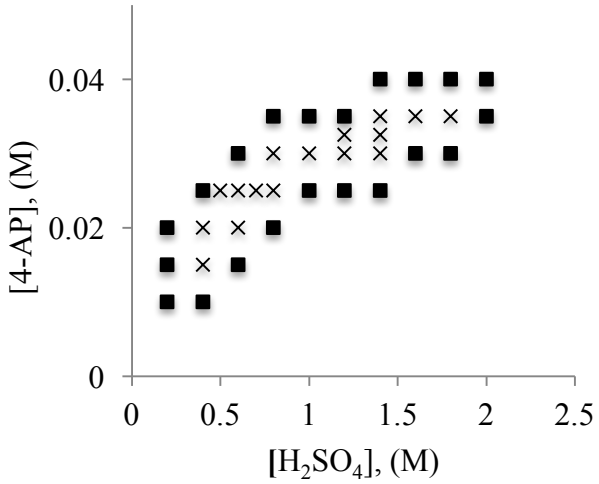

Figure 2.5 - Phase diagram presenting the region of complex oscillatory behavior in the concentration of 4-AP and H_2SO_4 concentration plane. (×) Represents conditions under which the system displays transient complex oscillations and the filled square (■) denotes conditions where complex oscillations were absent. The [$NaBrO_3$] and [Ce(IV)] were held constant at 0.06 M and 3.0 x 10^{-5} M respectively.

Two representative examples are presented in Figure 2.6, where in time series (a) MMO evolve into another complex mode that resembles period-doubled oscillations. Figure 2.6b presents mixed mode oscillations ranging from 1^5 to 1^2 before transitioning into simple oscillations.

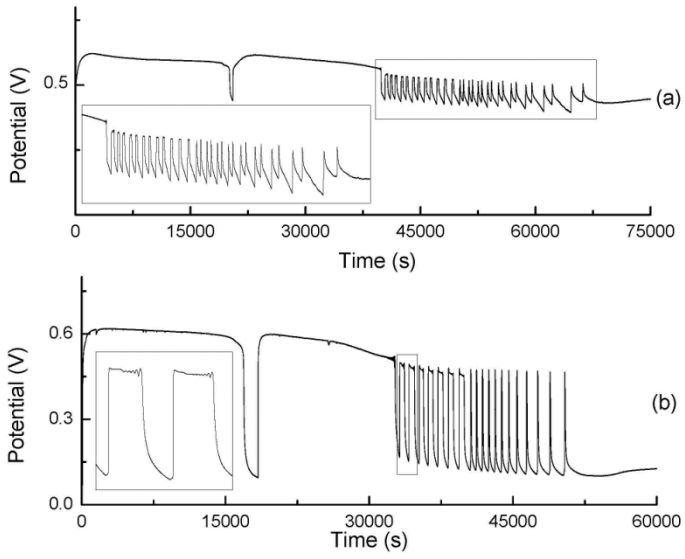

Figure 2.6 - Time series illustrating rich nonlinear dynamics at boundary regions in the 4-AP and H_2SO_4 concentration plane: (a) 0.03 M 4-AP and 1.2 M H_2SO_4, (b) 0.02 M 4-AP and 0.04 M H_2SO_4. Other reaction conditions were [$NaBrO_3$] = 0.06 M and [Ce(IV)] = 3.0 x 10^{-5} M.

In Figure 2.7, the intensity of the illumination was varied, which showed arguably the greatest influence on the nonlinear behavior of the system. At a very high intensity of illumination (468 mW/cm^2 in (a)), the dissolution of the precipitate occurs very rapidly, after approximately 40 min. No spontaneous oscillations were observed here, despite that the Pt potential varied continuously over the span of 24 h. At an intensity of 135 mW/cm^2 (Figure 2.7b), the dissolution of the precipitate can be seen to occur in a little over 2 h followed by an induction time of 4 h before spontaneous oscillations emerge. Only the first oscillation shows any hint of complexity as the remaining oscillations are simple. When the intensity is decreased further to 65 mW/cm^2, apart from the prolonged time for the dissolution of the precipitate, the induction time of those high frequency oscillations also becomes significantly longer, taking eleven and a half hours. At this intensity, a new

form of complexity arises: there are two oscillation peaks at the point the precipitate dissolved. Together with the following long series of high frequency oscillations, the system forms the behavior of sequential oscillations. In the absence of illumination, the potential remains constant and no oscillations occur even though 4-AP completely dissolves (Figure 2.7e), as does the bromobenzoquinone imine, over a span of 24 h. The dramatic impact of illumination on the overall kinetics of the system is likely due to the photochemical reduction of benzoquinone and the excitation of bromine molecules.

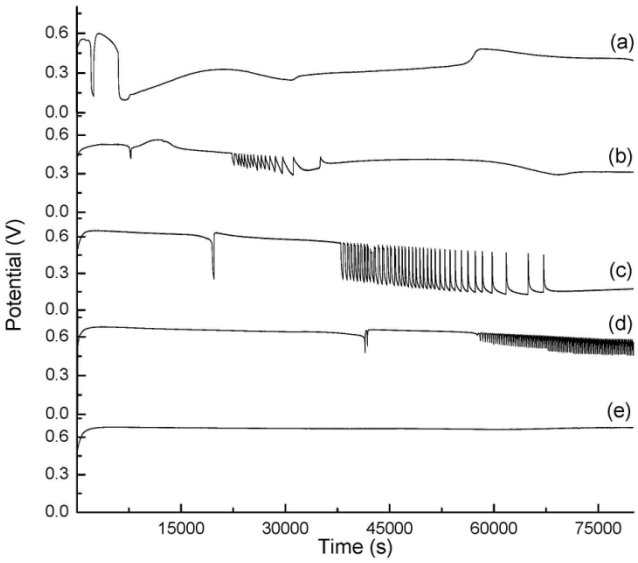

Figure 2.7 - Time series of the cerium catalyzed bromate – 4-aminophenol reaction carried out at different light intensities: (a) 468 mW/cm^2, (b) 135 mW/cm^2, (c) 105 mW/cm^2, (d) 65 mW/cm^2, and (e) 0 mW/cm^2. Other reaction conditions were [4-AP] = 0.025 M, [$NaBrO_3$] = 0.06 M, [H_2SO_4] = 0.80 M, and [Ce(IV)] = 3.0 x 10^{-5} M.

Figure 2.8 further illustrates the dependence of the system to the presence of illumination and shows the effect that immediate removal of illumination has on the reaction kinetics. The abrupt removal of light when the oscillating system is in an

oxidized state, high potential, does not completely quench the reaction but does decrease both the amplitude and frequency of oscillations. When the illumination was returned to the system, the frequency and amplitude returned to the pre-perturbation levels. Removing the illumination when the system is in a reduced state, low potential, the same effect of reduced amplitude and frequency of the oscillations emerged, which switched back to pre-perturbation levels once illumination was restored. Increasing the intensity of the illumination, whether at the top or bottom of an oscillation, results in a drastic decrease in potential followed by an increase and non-oscillatory evolution. Spontaneous oscillations only re-emerge after the intensity is reduced.

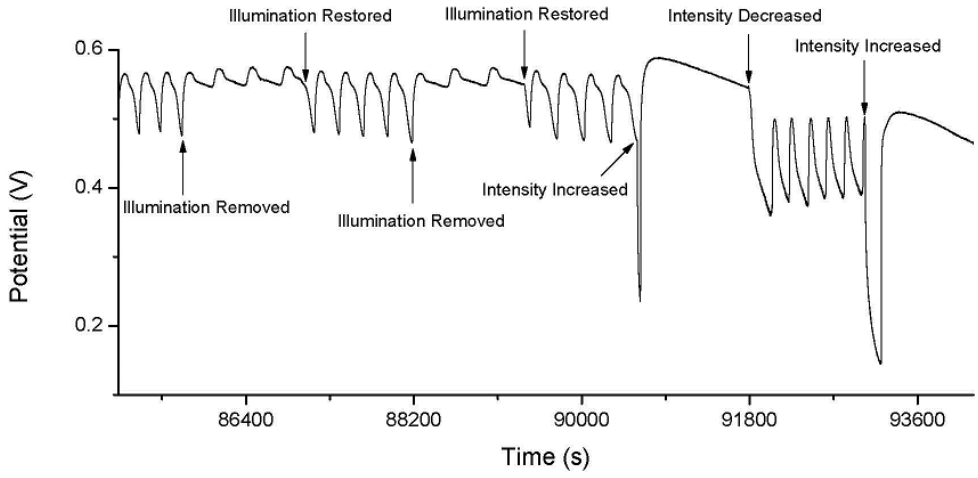

Figure 2.8 - Time series illustrating the photosensitive nature of the cerium catalyzed bromate – 4-aminophenol reaction. The reaction conditions are: [4-AP] = 0.025 M, $[NaBrO_3]$ = 0.06 M, $[H_2SO_4]$ = 0.80 M, [Ce(IV)] = 3.0 x 10^{-5} M, and light intensity = 65 mW/cm^2.

2.3.2 Numerical Simulations: Cerium - Bromate – 4-Aminophenol Photoreaction

To understand whether the above transient complex oscillations arise from the coupling of two autocatalytic cycles, i.e., reaction between bromine dioxide radicals and Ce^{3+} and between bromine dioxide radicals and 4-AP and derivatives from 4-AP, numerical simulations were carried out. While the full mechanism of the bromate – 4-AP reaction remains to be deciphered, earlier mechanistic studies have demonstrated the autocatalytic oxidation of 4-AP by acidic bromate, which led to a major product 1,4-benzoquinone [56]. Such information led us to adopt a general model (OKN) developed by Orbán, Körös and Noyes for uncatalyzed bromate-aromatic oscillators [57], modified to include reactions involving Ce^{4+}/Ce^{3+} as well as the photoreduction of 1,4-benzoquinone to 1,4-hydroquinone [11,30,54]. The original OKN model consists of 16 reaction steps, 10 of which have been utilized in our simulation. As listed in Table 2.1, reaction steps (R13-R16) incorporated processes from the cerium redox pair. The photochemical reduction of benzoquinone, a major component after dissolution of the bromobenzoquinone imine, to hydroquinone is represented by a single reaction step (R12), in which the rate constant is affected by the intensity of illumination supplied to the system. In this model listed in Table 2.1, there are 16 reaction steps and 12 variables, BrO_3^-, Br^-, $HBrO_2$, HOBr, BrO_2*, Ce(III), Ce(IV), H^+, $HAr(OH)_2$, HAr(OH)O*, $BrAr(OH)_2$, $HArO_2$, where $HAr(OH)_2$ is hydroquinone, HAr(OH)O* is semiquinone, $BrAr(OH)_2$ is brominated hydroquinone, and $HArO_2$ is benzoquinone. The simulations were performed by integrating a set of differential equations obtained through application of the law of mass action on the reaction equations. Rate constants used in the simulations are listed in Table 2.1.

Table 2.1 Model employed for simulating transient complex oscillations

	Reaction	Rate Constants* $k_{forward}$	$k_{reverse}$	Ref.
R1	$BrO_3^- + Br^- + 2H^+ \leftrightarrow HBrO_2 + HOBr$	0.1	100	44
R2	$HBrO_2 + Br^- + H^+ \rightarrow 2HOBr$	1.5×10^9		44
R3	$BrO_3^- + HBrO_2 + H^+ \leftrightarrow 2BrO_2^* + H_2O$	650	2×10^7	44
R4	$BrO_2^* + HAr(OH)_2 \rightarrow HBrO_2 + HAr(OH)O^*$	900		44
R5	$BrO_2^* + HAr(OH)O^* \rightarrow HArO_2 + HBrO_2$	1000		44
R6	$2HBrO_2 \rightarrow BrO_3^- + HOBr + H^+$	4×10^7		44
R7	$HOBr + HArOHO^* \rightarrow Br^- + HArO_2 + H_2O$	1.5×10^5		44
R8	$HOBr + Br^- + H^+ \leftrightarrow Br_2 + H_2O$	9.5×10^9	$110\ s^{-1}$	44
R9	$Br_2 + HAr(OH)_2 \rightarrow BrAr(OH)_2 + Br^- + H^+$	700		44
R10	$HOBr + HAr(OH)_2 \rightarrow BrAr(OH)_2 + H_2O$	25		44
R11	$HAr(OH)_2 + HArO_2 \leftrightarrow 2HAr(OH)O^*$	0.022	4×10^4	44
R12	$2HArO_2 + H_2O + hv \rightarrow HAr(OH)_2 +$ other products	1×10^4		35
R13	$Ce(III) + BrO_2^* + H^+ \rightarrow Ce(IV) + HBrO_2 + H_2O$	1.4×10^5		20
R14	$Ce(IV) + BrAr(OH)_2 \rightarrow Ce(III) + Br^- + HArO_2 + H^+$	1×10^4		46
R15	$Ce(IV) + HAr(OH)_2 \rightarrow Ce(III) + HAr(OH)O^* + H^+$	100		45
R16	$Ce(IV) + HAr(OH)O^* \rightarrow Ce(III) + HArO_2 + H^+$	1×10^4		45

*Rate constants have the units ($M^{-1}\ s^{-1}$) unless otherwise stated and their values have been adjusted in this study in order to obtain the behavior shown in Figure 9.

Simple periodic oscillations can be seen in the time series in Figure 2.9a, which was calculated with an initial concentration of Ce^{4+} of 0.0 M, i.e., without coupled autocatalytic cycles. Initial concentrations of other reactants are 0.06 M $NaBrO_3$, 0.8 M H_2SO_4, and 0.025 M $HAr(OH)_2$, which are the same as experimental values, except that hydroquinone is used in place of 4-AP. Transient complex oscillations of the form 1^1 emerged when the Ce^{4+} concentration was set to 1.317×10^{-5} M in Figure 2.9b. The complexity of the oscillation was enhanced further as the Ce^{4+} concentration was increased to 3.0×10^{-5} M (Figure 2.9c). Consistent with what was seen experimentally, as Ce^{4+} concentration became too high, complex oscillations disappeared. The above simulation results provide strong support that the observed complex oscillations might arise from the coupling of two nonlinear feedbacks and, importantly, show that there

exists an optimal coupling strength for the emergence of complex oscillations. During our simulations, it was noticed that the reaction between hydroquinone and bromine dioxide radicals had significant influences on the reaction behavior, in which a slow reaction would favor the complex oscillations. In the modeling, varying the initial reactant concentrations resulted in period doubling and dynamically more complex mixed-mode oscillations, predicting that very rich nonlinear dynamical behavior could be achieved through coupling two autocatalytic cycles.

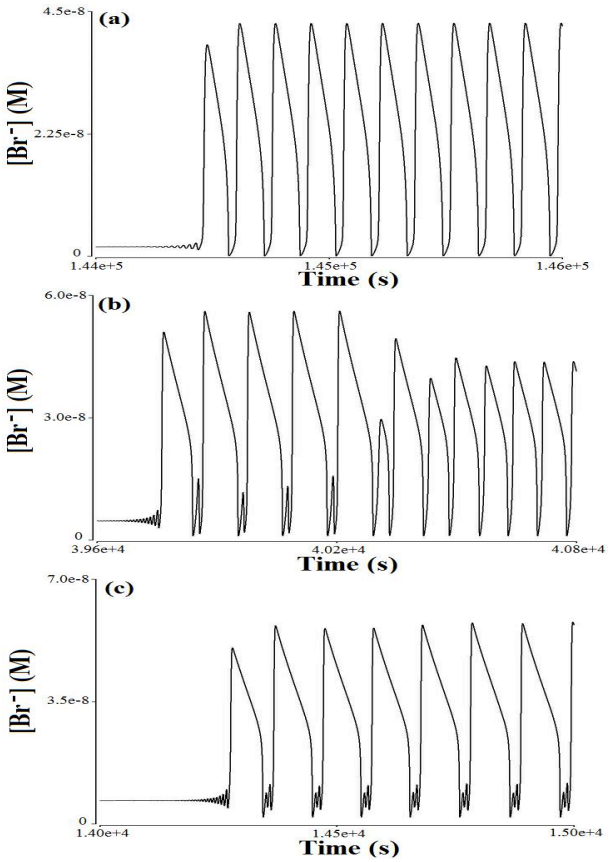

Figure 2.9 - Time series showing the emergence of complex oscillations through the coupling of two autocatalytic cycles. It is calculated with the model proposed in Table I. (a) $[Ce(IV)]_0 = 0.0$ M, (b) $[Ce(IV)]_0 = 1.137 \times 10^{-5}$ M, and (c) $[Ce(IV)]_0 = 3.0 \times 10^{-5}$ M. $[HAr(OH)_2] = 0.025$ M, $[NaBrO_3]_0 = 0.06$ M, $[H_2SO_4]_0 = 0.8$ M, and $[Br^-]_0 = 1 \times 10^{-7}$ M.

2.3.3 Temporal Kinetics: Bromate – N-Bromo-1,4-Benzoquinone-4-Imine Reaction

In order to gain further insights into the mechanism driving the bromate – 4-AP oscillatory behavior, the precipitate that forms at the onset of the reaction, N-bromo-1,4-benzoquinone-4-imine (BBI) was collected. It was found that BBI is relatively stable in water. For instance, when 3.0 x 10^{-4} mole of BBI is mixed with 30.0 mL of water, there is no visible decrease in the amount of solid after 24 h, while the water shows only a very light yellow color. When the BBI and water mixture is exposed to light, however, the solution turns yellow rapidly, indicating a photoassisted dissolution/reaction. Figure 2.10 presents two time series illustrating the critical influence of an acidic environment on the photoreaction of BBI. In Figure 2.10a, when the photodecomposition of BBI was studied in a neutral solution, the Pt potential gradually increased over the first 90 min and then remained at an elevated level throughout the reaction. The reaction solution became light orange with very little of the BBI dissolving. In an acidic environment, the photodecomposition of BBI began to occur within 15 min where the Pt potential can be seen to drastically decrease from its initial high level to a very low level, exhibiting the kinetic feature of autocatalytic reactions. The solution became a dark orange color as the reaction proceeds and all of the BBI was photodecomposed. ^{1}H NMR measurements, taken after all of the BBI had dissolved, show the presence of 1,4-benzoquinone at a spectral resonance of δ = 6.80, indicating that the BBI - photoreaction led to the production of 1,4-benzoquinone. This conclusion is further supported by characterization with Electron Impact (EI) mass spectrometry (*m/e* = 108). The formation of 1,4-benzoquinone leads us to speculate that introducing bromate into the photodecomposition of BBI may form a new photocontrolled chemical oscillator.

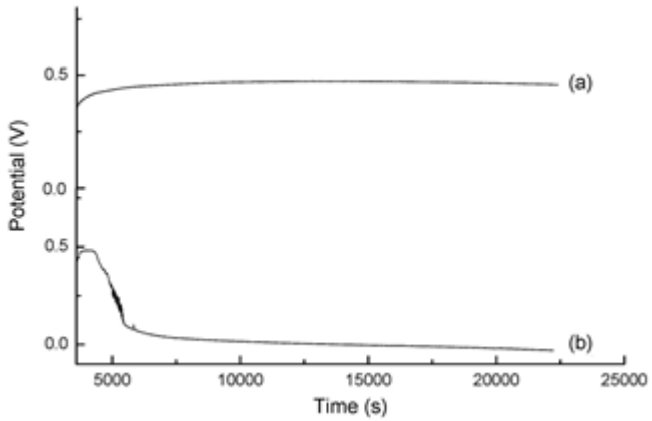

Figure 2.10 - Time series showing the photodecomposition of 9.41 x 10^{-3} M N-bromo-1,4-benzoquinone-4-imine in (a) neutral solution and (b) 1.7 M H_2SO_4. Intensity of illumination was 468 mW/cm^2.

Figure 2.11a presents a time series under concentrations of bromate (0.040 M), BBI (9.41 x 10^{-3} M), and sulfuric acid (1.7 M). The solution immediately becomes yellow upon the addition of BBI and grows viscous after bromate is added and the photoreaction proceeds. The sharp spike in potential marks the complete dissolution of the BBI, at which point the solution remains yellow but transparent. The potential reaches a maximum and slowly decreases until spontaneous oscillations occur. The oscillations continue for several cycles, which stop at the low potential, at which point the color of the solution remains yellow.

Figure 2.11b presents time series proving the photocontrolled nature of this new bromate oscillator. It shows that when illumination is removed from the reaction system while oscillations are occurring, they stop abruptly and the potential reaches a stable non-oscillatory state. However, when illumination is reintroduced to the system, oscillations reemerge. Notably, removing the illumination at opposite phases of the oscillation caused

different responses of the system, where turning off the illumination at the bottom of an oscillation causes the system to return to the high potential immediately, followed by a decrease to the stable potential. The magnitude of the oscillation is also influenced by the intensity of the illumination involved; in fact, there is a threshold intensity that must be reached in order for oscillations to occur. Notably, both the oscillation waveform and the long induction time are reproducible, despite their great sensitivity to illumination.

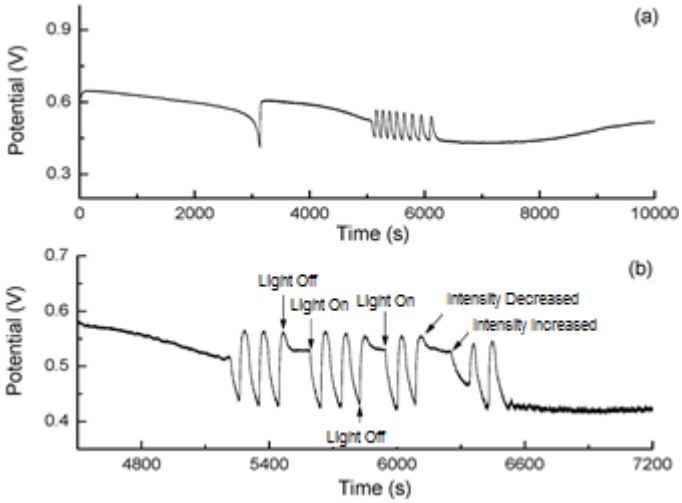

Figure 2.11 - (a) Time series of the bromate – BBI reaction and (b) Time series illustrating the photocontrolled nature of the uncatalyzed bromate – BBI reaction. Reaction conditions are $[NaBrO_3]$ = 0.04 M, $[H_2SO_4]$ = 1.7 M, and [BBI] = 9.41 x 10^{-3} M.

Figure 2.12 illustrates the effect of changing the concentration of bromate while holding the amount of BBI (9.41 x 10^{-3} M), and sulfuric acid (1.7 M) constant. It can be seen that the concentration of bromate is a critical parameter influencing the nonlinear reaction kinetics. At low concentrations of bromate, not enough oxidant is present to oxidize the BBI resulting in a Pt potential that decreases and is unable to spike, and the

solution becomes a murky yellow/orange color. An increased concentration of bromate shows a spike in potential, and an induction time followed by a drastic drop in potential with no oscillations. As the concentration of bromate is increased further, to 0.030 M, five oscillations are present. When the bromate concentration is increased to 0.040 M, the number of oscillations increased; however, the amplitude of the oscillations decreased. This decrease in amplitude became more obvious at 0.050 M bromate. The number of oscillations can also be seen to decrease as the concentration of bromate is increased and at 0.060 M, the potential remains high after the potential spike, and the solution becomes transparent with a yellow tint.

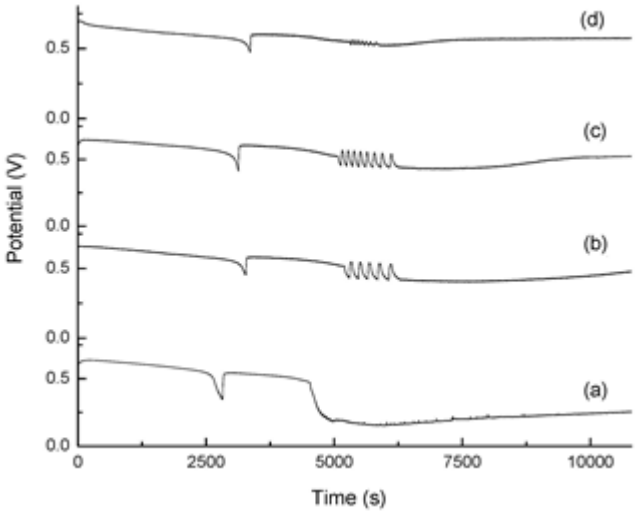

Figure 2.12 - Time series of the bromate – BBI reaction carried out at different bromate concentrations: (a) 0.02 M, (b) 0.03 M, (c) 0.04 M, and (d) 0.05 M. Other reaction conditions were $[H_2SO_4]$ = 1.7 M and [BBI] = 9.41 x 10^{-3} M.

Figure 2.13 is a time series showing the effect of changing the concentration of BBI while holding the concentration of bromate (0.040 M) and sulfuric acid (1.7 M) constant. Adding 0.105 g of BBI (0.0188M) to the 30.0 mL reaction vessel gives full

dissolution; however, adding more BBI effectively saturates the solution leaving a film of undissolved powder in the system. Spontaneous oscillations are still present in such saturated system, although the exact concentration of BBI is unknown. As such, there is no upper boundary to the concentration of BBI.

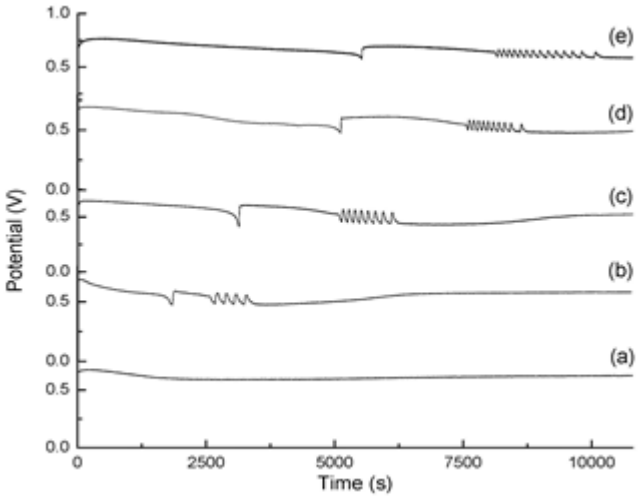

Figure 2.13 - Time series of the bromate – BBI reaction carried out at different BBI concentrations: (a) 3.14 x 10^{-3} M, (b) 6.28 x 10^{-3} M, (c) 9.41 x 10^{-3} M, (d) 1.25 x 10^{-2} M, and (e) 1.88 x 10^{-2} M. Other reaction conditions were [$NaBrO_3$] = 0.04 M and [H_2SO_4] = 1.7 M.

For this reason, the phase diagrams in Figure 2.14 and Figure 2.16 show no upper limit in the concentration of the BBI. Below the concentration of BBI required for oscillations the solution does not become murky at the onset of the reaction and as the reactant dissolves the solution becomes transparent with a slight yellow color. The potential undergoes a gradual decrease until the potential stabilizes. As the concentration of BBI is increased, the amount of time for the potential spike to occur increases, which is reasonable due to an increased amount of reactant; the induction time also increases.

Figure 2.14 is a phase diagram in the concentration of BBI and bromate concentration plane, where the filled triangles (▲) indicate the conditions under which the system displays spontaneous oscillations.

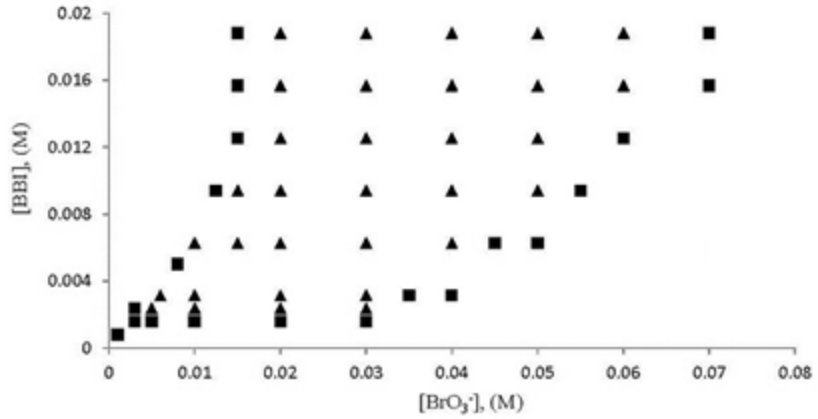

Figure 2.14 - Phase diagram illustrating regions of oscillatory phenomenon in the BBI and bromate concentration space. Conditions that displayed spontaneous oscillations are denoted by ▲.

Figure 2.15 illustrates the effect of changing the concentration of sulfuric acid while holding the amount of BBI (9.41 x 10^{-3} M), and bromate (0.040 M) constant. Immediately it is obvious that the range of H^+ which allows for oscillations to occur is much larger than the range for BrO_3^-. The H_2SO_4 serves simply as a source of H^+ needed to ensure that the pH is kept low enough for the autocatalytic cycle to continue. Below the concentration of sulfuric acid that produces oscillations a sharp potential decrease is observed, but unlike being below the lower limit in bromate concentration (where the sharp decline occurs quickly), the potential remains stable for over 90 min. The most notable difference between the time series in Figure 2.12 and Figure 2.15 is apparent at the extreme cases. High acid concentrations have their spike early, whereas cases with

high bromate concentrations undergo the potential spike after remaining at a stable potential for a prolonged period.

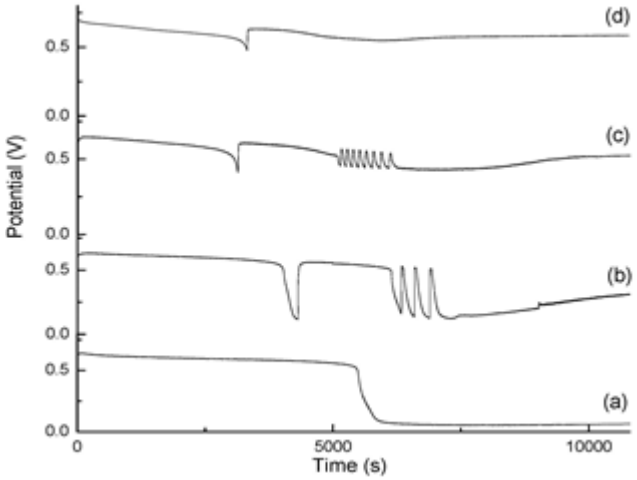

Figure 2.15 - Time series of the bromate – BBI reaction carried out at different sulfuric acid concentrations: (a) 0.4 M, (b) 1.0 M, (c) 1.7 M, and (d) 2.2 M. Other reaction conditions were $[NaBrO_3]$ = 0.04 M and [BBI] = 9.41 x 10^{-3} M.

Figure 2.16 is a phase diagram in the BBI and H_2SO_4 concentration plane, where the filled triangle (▲) indicates the conditions under which the system displays spontaneous oscillations. Notably, a large concentration range of sulfuric acid was capable of supporting the occurrence of spontaneous oscillatory behavior depending on the initial concentration of BBI.

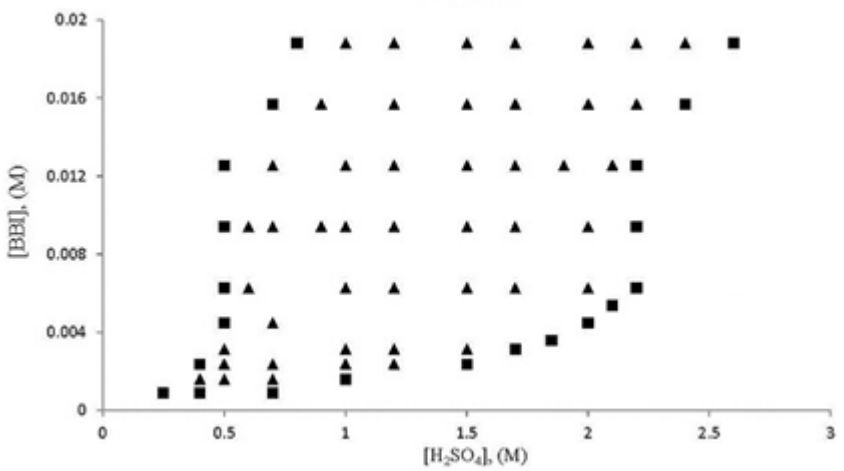

Figure 2.16 - Phase diagram illustrating regions of oscillatory phenomenon in the BBI and sulfuric acid concentration space. Conditions that displayed spontaneous oscillations are denoted by ▲.

2.3.4 Mechanistic Study: Bromate – N-Bromo-1,4-Benzoquinone-4-Imine Reaction

A study of the compounds involved in the system was undertaken using multiple characterization techniques in order to gain insights into the underlying mechanism responsible for the oscillatory behavior. Figure 2.17 presents three ^{1}H NMR spectra recorded in $CDCl_3$ solvent taken at key intervals as the reaction progressed. Figure 2.17a spectrum was taken after all of the BBI had dissolved, but prior to the occurrence of spontaneous oscillations. The spectral resonance of $\delta = 6.80$ indicates the presence of 1,4-benzoquinone and was confirmed by the $\delta = 136.6$ and 187.3 resonances in the ^{13}C NMR spectrum of a more concentrated sample. Figure 2.17b shows the ^{1}H NMR spectrum of the composition of the reaction solution during the oscillatory window. As can be seen the component giving resonances at $\delta = 6.97$ and 7.02 with a distinct AB coupling pattern (AB quartet, $J = 10.5$ Hz), which was only present in minute quantities before oscillations occurred, has increased at the expense of 1,4-benzoquinone. Finally, in Figure 2.17c,

after the oscillatory window had ceased, the component at δ = 6.97 and 7.02 has grown significantly at the expense of 1,4-benzoquinone.

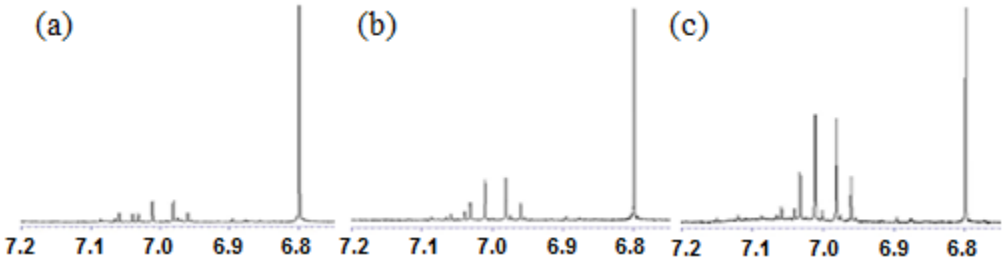

Figure 2.17 - ^{1}H NMR spectra at three unique points in the reaction: (a) after potential spike and before oscillations (b) during the oscillatory window and (c) after the oscillations have occurred.

Further spectroscopic experiments were conducted in order to establish a reasonable candidate for the identity of this new compound. This compound is of limited thermal stability, which has precluded chromatographic purification or crystallization. Nevertheless, the ^{13}C NMR spectrum of more highly concentrated samples displayed resonances at δ = 69.0, 94.6, 135.3, 137.7, 182.3, and 189.2. The HMBC spectrum (Figure 2.18) of the same sample showed correlations of both the δ = 69.0 and 189.2 ^{13}C resonances with the δ = 6.97 ^{1}H resonance.

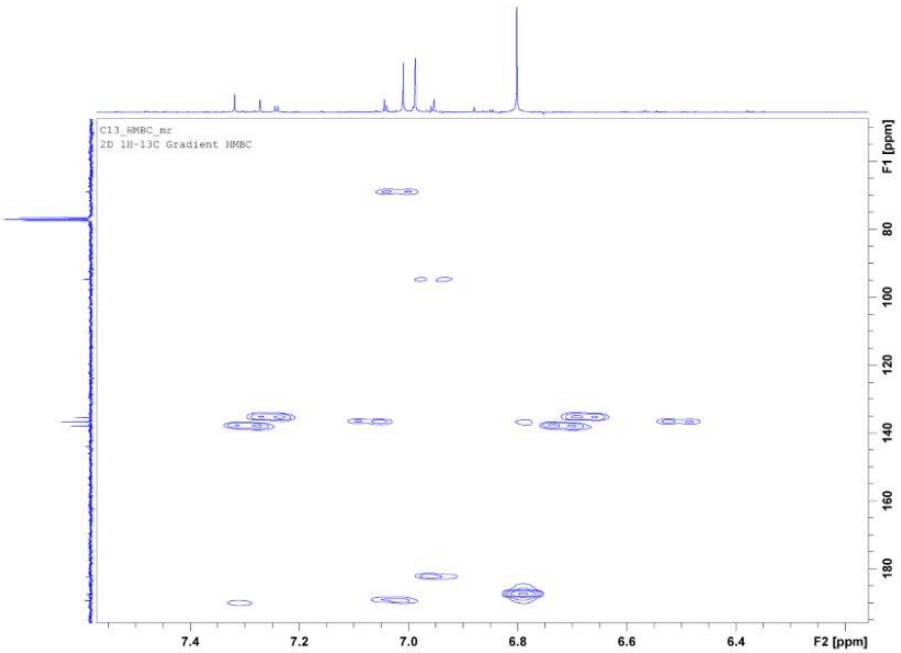

Figure 2.18 - Heteronuclear Multiple Bond Correlation (HMBC) spectrum of sample taken after oscillations had occurred.

Finally, electrospray-TOF mass spectrometry (negative ion mode) gives an intense set of ions at m/e = 345, 347, 349, and 351, with a characteristic isotope pattern of a tribrominated compound. Given the propensity for negative ion electrospray MS to give prominent $(M + H)^-$ ions [41 BBI], this is strongly suggestive of a compound with a $C_6H_3Br_3O_2$ molecular formula. In light of this evidence, it is our working hypothesis that this new compound is 3,4,4-tribromo-2-hydroxycyclohexa-2,5-dienone (Figure 2.19).

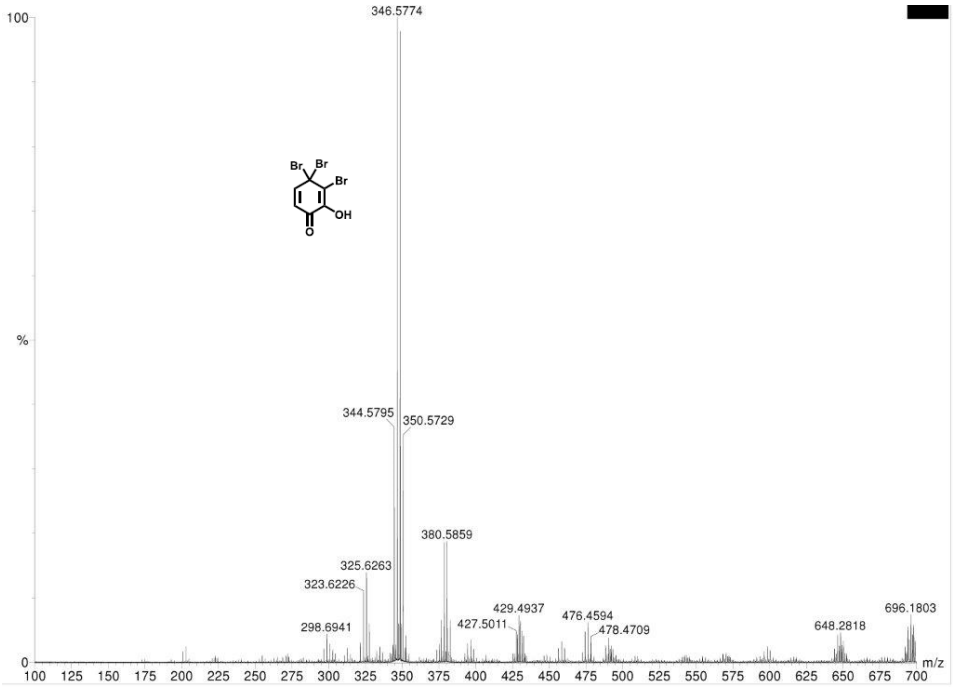

Figure 2.19 - Electrospray-TOF mass spectrometry spectrum and proposed reaction intermediate 3,4,4-tribromo-2-hydroxycyclohexa-2,5-dienone.

2.4 Conclusions

This work reported a study of nonlinear dynamics in the cerium catalyzed bromate – 4-aminophenol photochemical oscillator and observed complex behavior in the form of mixed-mode, period doubling and sequential oscillations. The intensity of illumination applied to the system was seen to greatly affect the induction time and the overall oscillatory dynamics. The system was also found to be sensitive to the initial concentrations of bromate, cerium, sulfuric acid, and 4-AP. A phase diagram in the sulfuric acid and 4-AP concentration space shows that mixed-mode oscillations emerge in a narrow concentration region and have a significant dependence on the ratio of the two reactants as opposed to their absolute concentrations. Previous research on the uncatalyzed bromate – 4-AP photochemical oscillations did not display any richer

dynamical behavior than periodic transient oscillations [56], suggesting that the coupling of the catalyst to the photochemical oscillating reaction is responsible for the emergence of the complexity.

Interplay between the concentration of cerium and the intensity of the illumination was found to be an important factor in the emergence of complex oscillations. Specifically, as concentrations of the catalyst were increased to a level which was too high to allow the complexity to form, an increase in light intensity counteracted the domination of the catalysts' autocatalytic cycle through enhancing the formation of 1,4-hydroquinone that competes with Ce^{3+} for bromine dioxide radicals and revived the complex behavior. The formation of 1,4-benzoquinone in this system was confirmed by NMR and GC/MS spectroscopic analysis. As was observed experimentally, the emergence of complex oscillations due to the addition of cerium and transitions from simple to complex and then to simple oscillations could be reproduced numerically using a model that was developed based on general mechanisms proposed for bromate-aromatic compounds reactions.

This study also led to the discovery of a new photochemical oscillator through the isolation of the precipitate formed during the reaction of bromate and 4-AP. When reacted with acidic bromate, in the presence of illumination, N-bromo-1,4-benzoquinone-4-imine was found to support spontaneous oscillations. The extreme sensitivity of the system to the intensity of the illumination was apparent through the manipulation of the oscillatory window by both abruptly removing and reintroducing the illumination, or by decreasing and then increasing the intensity of the illumination. The system was also found to be sensitive to the concentrations of bromate, sulfuric acid, and BBI. Changing

the concentrations of the reactants not only had an effect on the number of oscillations but also the amplitude of the oscillations as well as the induction time. Spectroscopic measurements indicate that N-bromo-1,4-benzoquinone-4-imine is transformed into 1,4-benzoquinone preceding the onset of spontaneous oscillations, leading to a major product assigned as 3,4,4-tribromo-2-hydroxycyclohexa-2,5-dienone.

2.5 References

[1] R. J. Field, M. Burger, *Oscillations and Travelling Waves in Chemical Systems*; Wiley & Sons: New York, 1985.

[2] I. R. Epstein, J. A. Pojman, *An Introduction to Nonlinear Chemical Dynamics: Oscillations, Waves, Patterns, and Chaos*; Oxford University Press: Oxford, U.K., 1998.

[3] P. Gray, S. K. Scott, *Chemical Oscillations and Instabilities: Nonlinear Chemical Kinetics*; Clarendon Press: Oxford, U.K., 1994.

[4] S. K. Scott, *Oscillations, Waves, and Chaos in Chemical Kinetics*; Oxford University Press: Oxford, U.K., 1994.

[5] F. Sagués, I. R. Epstein, *Dalton Trans.* **2003**, 1201-1217.

[6] E. Szabo, L. Adamčiková, P. Ševčik, *J. Phys. Chem. A* **2011**, 115, 6518-6524.

[7] T. Yamaguchi, L. Kuhnert, Zs. Nagy-Ungrarai, S. C. Müller, B. Hess, *J. Phys. Chem.* **1991**, 95, 5831-5837.

[8] Z. Nosziticzius, *J. Am. Chem. Soc.* **1979**, 101, 3660-3663.

[9] Q. Gao, J. Wang, *Chem. Phys. Lett.* **2004**, 391, 349-353.

[10] R. M. Noyes, S. D. Furrow, *J. Am. Chem. Soc.* **1982**, 104, 45-48.

[11] I. Szalai, K. Kurin-Csörgei, I. R. Epstein, M. Orbán, *J. Phys. Chem. A* **2003**, 107, 10074-10081.

[12] A. K. Dutt, S. C. Müller, *J. Chem. Phys.* **1996**, 104, 583-586.

[13] M. Burger, E. Körös, *J. Phys. Chem.* **1980**, 84, 496-500.

[14] A. M. Zhabotinsky, F. Buchholtz, A. B. Kiyatkin, I. R. Epstein, *J. Phys. Chem.* **1993**, 97, 7578-7584.

[15] N. B. Ganaie, M. A. Nath, G. M. Peerzada, *Kinet. Catal.* **2010**, 51, 25-30.

[16] L. Adamčiková, R. Bielik, P. Ševčik, *Collect. Czech. Chem. Commun.* **2004**, 69, 1553-1565.

[17] S. Kadar, T. Amemiya, K. Showalter, *J. Phys. Chem. A* **1997**, 101, 8200-8206.

[18] R. Ramaswamy, P. V. Lalitha, *Int. J. Chem. Kinet.* **1993**, 25, 457-468.

[19] R. K. Srivastava, Y. Mori, I. Hanazaki, *Chem. Phys. Lett.* **1992**, 190, 279-284.

[20] M. Harati, J. R. Green, B. F. T. Cooper, J. Wang, *Chem. Phys. Lett.* **2009**, 113, 6548-6551.

[21] M. Orbán, E. Körös, *Nature* **1978**, 273**,** 371-372.

[22] M. Orbán, E. Körös, *J. Phys. Chem.* **1978**, 82**,** 1672-1674.

[23] S. R. Pullela, D. Cristancho, P. He, D. Luo, K. R. Hall, Z. Cheng, *Phys. Chem. Chem. Phys.* **2009**, 11**,** 4236-4243.

[24] I. R. Epstein, J. A. Pojman, O. Steinbock, *Chaos* **2006**, 16**,** 037101.

[25] E. Yu. Kalishin, M. M. Goncharenko, V. A. Khavrus', P. E. Strizhak, *Kinet. Catal.* **2002**, 43**,** 256-268.

[26] P. E. Strizhak, A. L. Kawczyński, *J. Phys. Chem.* **1995**, 99**,** 10830-10833.

[27] J. L. Hudson, J. C. Mankin, *J. Chem. Phys.* **1981**, 74**,** 6171-6177.

[28] R. A. Schmitz, K. R. Graziani, J. L. Hudson, *J. Chem. Phys.* **1977**, 67**,** 3040-3044.

[29] R. H. Simoyi, A. Wolf, H. L. Swinney, *Phys. Rev. Lett.* **1982**, 49**,** 245-248.

[30] L. Györgyi, R. J. Field, *Nature* **1992**, 355**,** 808-810.

[31] M. Rachwalksa, A. L. Kawczyński, *J. Phys. Chem. A* **1999**, 103**,** 3455-3457.

[32] J. Liu, S. K. Scott, *J. Chem. Soc. Faraday Trans.* **1991**, 87**,** 2135-2140.

[33] A. Z. Ivanović-Šašić, V. M. Marković, S. R. Anić, Lj. Z. Kolar-Anić, Ž. D. Čupić, *Phys. Chem. Chem. Phys.* **2011**, 13**,** 20162-20171.

[34] D. Bakeš, L. Schreiberová, I. Schreiber, M. J. B. Hauser, *Chaos* **2008**, **1**8**,** 015102.

[35] J. Li, J. Wang, *Phys. Chem. Chem. Phys.* **2011**, 13**,** 15539-15545.

[36] L. Adamčiková, P. Ševčik, *React. Kinet. Catal. Lett.* **1995**, 56**,** 137-142.

[37] P. Ruoff, R. M. Noyes, *J. Chem. Phys.* **1986**, 84**,** 1413-1423.

[38] J. Wang, P. G. Sørensen, F. Hynne, *J. Phys. Chem.* **1994**, 98**,** 725-727.

[39] J. Wang, F. Hynne, P. G. Sørensen, K. Nielsen, *J. Phys. Chem.* **1996**, 100**,** 17593-17598.

[40] B. R. Johnson, S. K. Scott, B. W. Thompson, *Chaos* **1997**, 7**,** 350-358.

[41] J. Wang, *Chem. Phys. Lett.* **2001**, 339**,** 357-361.

[42] O. Steinbock, V. S. Zykov, S. C. Müller, *Nature* **1993**, 366**,** 322-324.

[43] C. Hemming, R. Kapral, *Chaos* **200**, 10**,** 720-730.

[44] K. Pelle, M. Wittmann, Z. Noszticzius, *J. Phys. Chem. A* **2003**, 107**,** 2039-2047.

[45] K. Sriram, M. S. Gopinathan, *React. Kinet. Catal. Lett.* **2003**, 79**,** 341-349.

[46] F. Rossi, R. Lombardo, L. Sciascia, C. Sbriziolo, M. L. T. Liveri, *J. Phys. Chem. B* **2008**, 112**,** 7244-7250.

[47] B. Borderia, D. Lavabre, J. C. Micheau, J. P. Laplante, *J. Phys. Chem.* **1992**, 96**,** 2953-2961.

[48] A. Kaminaga, I. Hanazaki, *Chem. Phys. Lett.* **1997**, 278**,** 16-20.

[49] D. S. Huh, H. S. Kim, J. K. Kang, Y. J. Kim, D. H. Kim, S. H. Park, K. Yadav, J. Wang, *Chem. Phys. Lett.* **2003**, **3**78**,** 78-84.

[50] V. K. Vanag, I. R. Epstein, *Chaos* **2008**, 18**,** 026107.

[51] T. Sakurai, E. Mihaliuk, F. Chirila, K. Showalter, *Science* **2002**, 296**,** 2009-2012.

[52] J. Wang, K. Yadav, B. Zhao, Q. Y. Gao, D. S. Huh, *J. Chem. Phys.* **2004**, 121**,** 10138-10144.

[53] J. Li, J. Wang, *J. Phys. Chem. A* **2012**, 116**,** 8130-8137.

[54] B. Zhao, J. Wang, *Chem. Phys. Lett.* **2006**, 430**,** 41-44.

[55] J. G. Bell, J. R. Green, J. Wang, *J. Phys. Chem. A* **2013**, 117**,** 4545-4550.

[56] M. Harati, S. Amiralaei, J. R. Green, J. Wang, *Chem. Phys. Lett.* **2007**, 439**,** 337-341.

[57] M. Orbán, E. Körös, R. M. Noyes, *J. Phys. Chem.* **1979**, 83**,** 3056-3057.

CHAPTER 3 - COMPLEX REACTION DYNAMICS IN THE CATALYZED BROMATE – 2-METHYL-1,4-HYDROQUINONE PHOTOREACTION

3.1 Introduction

The compound 1,4-hydroquinone is capable of being autocatalytically oxidized by acidic bromate, forming benzoquinone [1], which in turn can be photoreduced to reform hydroquinone in aqueous solutions and thus create a benzoquinone-hydroquinone cycle [2,3]. Chemical oscillations have recently been uncovered in the bromate – 2-methyl-1,4-benzoquinone (mBQ) photoreaction [4]. However, no attempt was made to study the effect that addition of one-electron redox couples would have on the above nonlinear system. Introduction of metal catalysts such as ferroin or cerium ions to the reaction have the ability to generate a second autocatalytic cycle through their reactions with bromine dioxide [5-8]. Körös and co-workers have reported that spontaneous oscillations could be revived in the uncatalyzed bromate-aromatic compound oscillators upon the introduction of one-electron redox couples [9], suggesting that a nonlinear system consisting of multiple oscillatory subunits might be conveniently constructed by introducing metal ions into bromate-aromatic compound oscillators.

Exploration into the intricate nature of those coupled or perturbed nonlinear chemical systems has grown substantially over the past two decades and continues to be an area of active research [10-16]. Existing reports have shown that the presence of coupled autocatalytic cycles could lead to the observation of various complex chemical oscillations such as bursting, period-doubling, chaos, etc. [17-20]. Because

photosensitivity offers a convenient approach for implementing various temporal and spatiotemporal couplings and perturbations, the incorporation of illumination into nonlinear chemical dynamics has seen much study in the past two decades [21-28].

In this study, the 2-methyl-1,4-hydroquinone (mH_2Q) photoreaction was investigated with and without the presence of the one-electron redox couples Ce^{4+}/Ce^{3+} and $Fe(phen)_3^{3+}/Fe(phen)_3^{2+}$. As shown in the following, depending on the concentration of the catalyst, different complex oscillations were seen to emerge in this photo-controlled oscillatory system. When catalyzed by cerium, as the initial reactants are consumed in time, the studied chemical system gradually evolves through mixed-mode oscillations (MMOs), which are characterized by a single period that contains a large amplitude and one or more small amplitude oscillations (L^S notation) [29-34]. Under suitable conditions, sequential oscillations, which feature the coexistence of two or more isolated oscillatory regimes, were also observed in this closed reaction system. Although sequential oscillation may occur through coupling of two nonlinear feedbacks, earlier studies also have suggested that his may occur if an intermediate product formed during the reaction can form an oscillator with the starting oxidant [35,36]. To shed light on such a question, mechanistic studies using ^1H NMR spectroscopy and ultra-violet-visible (UV-VIS) spectroscopic techniques were performed to measure intermediate species formed in this bromate – Based photochemical oscillator.

3.2 Experimental Procedure

All reactions were carried out in a 50 mL thermal-jacketed glass beaker (ChemGlass) in which the reaction temperature was sustained at 25.0 ± 0.1 ^oC by a circulating water bath (Thermo NesLab RTE 7). A 30.0 mL volume was used for every

reaction. To obtain a homogenous system the reaction solution was stirred with a magnetic stir bar, driven by a magnetic stirrer (Fisher Isotemp) at approximately 1000 rpm. Reactions were monitored with a platinum electrode coupled with a $Hg|Hg_2SO_4|K_2SO_4$ reference electrode (Radiometer Analytical, XR200 and M231Pt-9) filled with a saturated K_2SO_4 solution, which were held in place by a Teflon cap placed on top of the thermal-jacketed beaker. All reaction profiles were recorded through a pH-potential meter (Radiometer PHM220) connected to a computer through an e-Corder 201 data logger (eDAQ company). The source of illumination was a 150 W halogen light (Fisher Scientific, Model DLS-100HD) with a continuous variable light level and was placed at a distance of 60 mm from the reaction beaker. The intensity of illumination was measured with an optical power meter (Model 1815-C, Newport).

All ^1H NMR spectroscopic studies were performed using a Bruker Avance 500 MHz spectrometer, and the samples were dissolved in deuterated chloroform (Cambridge Isotope Laboratories, 99.8%). All electrochemical experiments were performed at room temperature (22 ± 2 ^oC) with a CHI760D electrochemical workstation (CHInstrument, USA). A conventional three-electrode system was used. Mass spectrometry measurements were performed using a Waters XEVO GS-XF TOF, with samples introduced via an ASAP probe. Absorption spectroscopic investigations were performed using a UV-visible spectrophotometer (Ocean Optics, 2000 USB), where a quartz cuvette (HELLMA) with a 10.0 mm light path was placed in a CUV sample holder. The cuvette was stirred continuously with a small magnetic stir bar. Illumination was supplied with a halogen lamp with the assistance of an optic fiber that was placed directly above the cuvette. Stock solutions of analytical grade sodium bromate ($NaBrO_3$, Aldrich, 99%), 0.6

M; sulfuric acid (H_2SO_4, Aldrich 95-98%), 6.0 M; cerium (IV) ($Ce(SO_4)_2$, Aldrich), 0.01 M, and ferroin (prepared from calculated amounts of $FeSO_4$ and 1,10-phenanthroline, Aldrich, 99%), 0.03M, were prepared with double-distilled water. The 2-methyl-1,4-hydroquinone ($C_7H_8O_2$, Aldrich, 98+%) was directly dissolved in the reaction mixture.

3.3 Results and Discussion

3.3.1 Kinetic Behavior

Figure 3.1 presents transient oscillatory behavior in the bromate – mH_2Q system. After a brief induction time, there is a redox potential spike, which signals the autocatalytic oxidation of mH_2Q to mBQ.

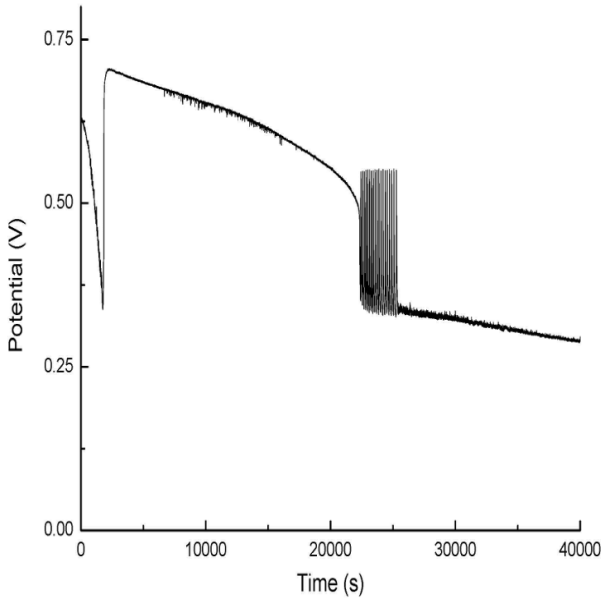

Figure 3.1 - Chemical oscillations in the bromate – mH_2Q photoreaction. Reaction conditions were: [mH_2Q] = 0.075 M, [H_2SO_4] = 1.5 M, [$NaBrO_3$] = 0.1 M, and a light intensity of 200 mW/cm^2.

Following the drastic potential spike, the redox potential gradually decreases for

nearly 5 h. During the potential decrease the solution transitions to a yellow color, which persists throughout the reaction until gradually fading. Such a decrease in the redox potential will diminish or be significantly slowed when the applied illumination intensity is reduced suggesting that such a process is related to the photoreduction of mBQ. Later, a group of spontaneous oscillations emerge, suggesting that the bromate – mH_2Q photoreaction forms a chemical oscillator. There was no evidence of periodic color change while the oscillations were occurring. Notably, illumination is absolutely crucial in this system as removal of illumination during the oscillations causes the system to return to a nonreactive state. Despite our extensive effort of varying reaction parameters such as the concentration of each reagent, only transient simple oscillations were obtained in the uncatalyzed bromate – mH_2Q photoreaction.

The effect of introducing cerium (IV) to the bromate – mH_2Q photoreaction is significant, as can be seen in Figure 3.2. At a cerium concentration of 8.3×10^{-5} M (Figure 3.2a), sequential oscillations were present with a quiescent period of approximately 5 h. Notably, the second set of high-frequency oscillations lasted over 11 h. Increasing the concentration of cerium proved to increase the number of oscillations in both oscillatory windows while decreasing the time interval between them. Complexity at the end of the reaction in the form of mixed-mode oscillations, arose at a cerium concentration of 2.5×10^{-4} M (Figure 3.2c). In Figure 3.2f, when the concentration of cerium was 5.0×10^{-4} M, the two oscillatory windows converge, giving rise to a single oscillatory window with aperiodicity emerging near the end of the oscillatory window. Here, the variation of cerium concentration was performed with initial reactant concentrations of $[mH_2Q] = 0.075$ M, $[NaBrO_3] = 0.1$ M, and $[H_2SO_4] = 1.3$ M. The

supplied light intensity is 80 mW/cm^2, which allowed for a slow evolution of the system. The addition of cerium introduces the following reaction:

$$(1)\ Ce(III) + BrO_2^* + H^+ \rightarrow Ce(IV) + HBrO_2$$

in which the bromine dioxide radicals that were also autocatalytically generated and consumed in the uncatalyzed bromate – mH_2Q reaction implement the desired coupling. Note that couplings may also take place through the reaction between Ce(IV) and the organic reductants, such as:

$$(2)\ 2Ce(IV) + mH_2Q \rightarrow 2Ce(III) + mBQ + 2H^+$$

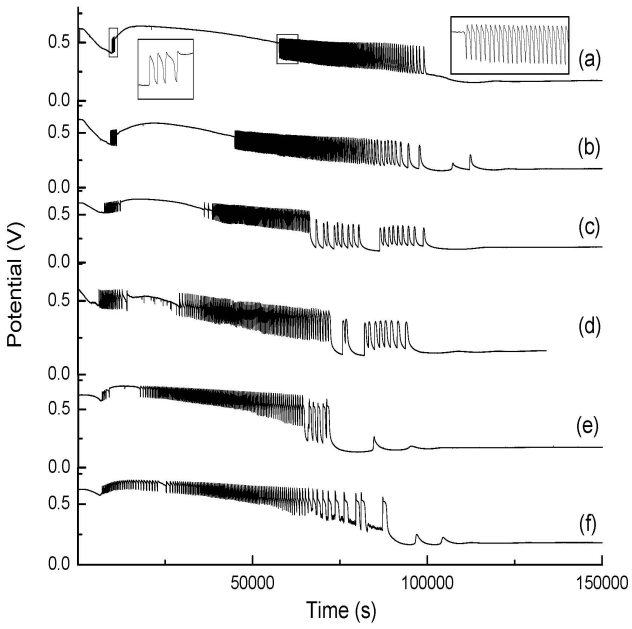

Figure 3.2 - Time series of the cerium - bromate – mH_2Q photoreaction carried out at different initial cerium concentrations: (a) 8.3 x 10^{-5} M, (b) 1.7 x 10^{-4} M, (c) 2.5 x 10^{-4} M, (d) 3.3 x 10^{-4} M, (e) 4.2 x 10^{-4} M, and (f) 5.0 x 10^{-4} M. Other reaction conditions were: [mH_2Q] = 0.075 M, [H_2SO_4] = 1.3 M, [$NaBrO_3$] = 0.1 M, and a light intensity of 80 mW/cm^2.

In the cerium - bromate – mH_2Q system, at a sulfuric acid concentration of 1.0 M (Figure 3.3a), only one long-lasting sequence of oscillations occurs. In Figure 3.3b, increasing the acid concentration to 1.1 M causes two oscillatory windows to form with a brief quiescent period. At the end of the oscillatory window, mixed-mode oscillations occur and a transition from 1^3 to 1^1 can be seen. An increase in H_2SO_4 concentration, from 1.2 M to 1.5 M (panels c and d in Figure 3.3, respectively) gives an increase in the quiescent time period between oscillatory windows as well as mixed-mode oscillations.

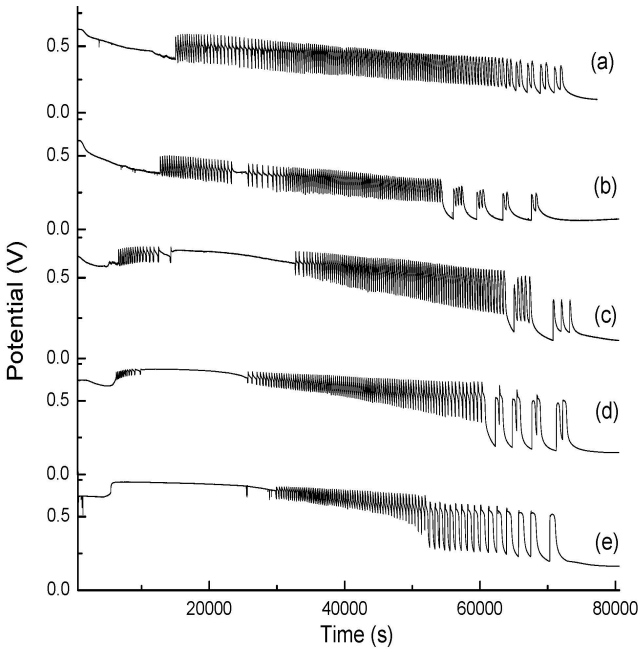

Figure 3.3 - Time series of the cerium - bromate – mH_2Q photoreaction carried out at different initial sulfuric acid concentrations: (a) 1.0 M, (b) 1.1 M, (c) 1.2 M, (d) 1.5 M, and (e) 1.8 M. Other reaction conditions were: $[mH_2Q] = 0.075$ M, $[Ce(IV)] = 3.3 \times 10^{-4}$ M, $[BrO_3^-] = 0.1$ M, and a light intensity of 80 mW/cm^2.

At an even higher acid concentration of 1.8 M, the primary set of oscillations is no longer present and two distinct oscillatory frequencies emerge in the second window. This time

series highlights that variation in the concentration of sulfuric acid had a profound influence on the mH_2Q system catalyzed by cerium.

Changing the concentration of mH_2Q also had a significant impact. The quiescent period between oscillations decreased when the concentration of mH_2Q was increased, and at 0.12 M, the two oscillatory windows merged into a single regime. Mixed mode oscillations were present between 0.09 and 0.065 M mH_2Q when the other reactant concentrations were $[H_2SO_4]$ = 1.0 M, $[NaBrO_3]$ = 0.1 M, and [Ce(IV)] = 3.3 x 10^{-4} M. When the concentration of bromate was varied, sequential oscillations were present between 0.09 and 0.12 M bromate, and the two oscillatory regimes were seen to merge at 0.08 M.

A drastic shortening of the overall oscillatory window was observed when the illumination was decreased from 250 mW/cm^2 to 20 mW/cm^2 (Figure 3.4). When 250 mW/cm^2 illumination is supplied to the reaction, only high-frequency oscillations occur (Figure 3.4a). Two separate oscillatory windows emerge when the intensity has been decreased to 150 mW/cm^2 (Figure 3.4b), and mixed-mode oscillations occur during the second oscillatory window when the intensity is further decreased to 80 mW/cm^2 (Figure 3.4c). Further decreasing the intensity eliminates the first set of oscillations, and the induction time increases with decreasing intensity. At 40 mW/cm^2, oscillations occur after a lengthy induction time of approximately 13 h and last for about 25 h (Figure 3.4e). An induction time of about 30 h occurs at an intensity of just 20 mW/cm^2 (Figure 3.4f), but the system maintains oscillations for over 55 h.

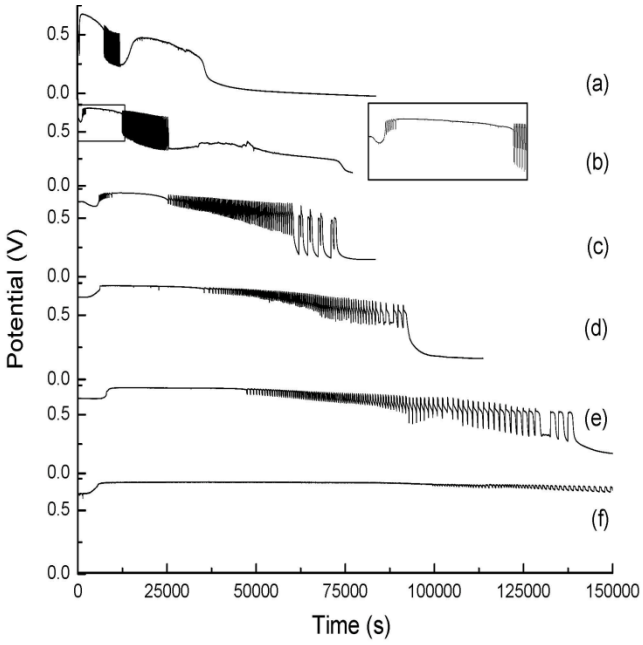

Figure 3.4 - Time series of the cerium - bromate – mH_2Q photoreaction carried out at different initial light intensities: (a) 250 mW/cm^2, (b) 150 mW/cm^2, (c) 80 mW/cm^2, (d) 65 mW/cm^2, (e) 40 mW/cm^2, and (f) 20 mW/cm^2. Other reaction conditions were: $[mH_2Q]$ = 0.075 M, $[H_2SO_4]$ = 1.5 M, [Ce(IV)] = 3.3 x 10^{-4} M, and $[BrO_3^-]$ = 0.1 M

The addition of ferroin to this oscillating reaction introduces a second autocatalytic cycle through the interaction of ferroin with bromine dioxide radicals:

$$(3)\ Fe(phen)_3^{2+} + BrO_2^* + H^+ \rightarrow Fe(phen)_3^{3+} + HBrO_2$$

$$(4)\ 2Fe(phen)_3^{3+} + mH_2Q \rightarrow 2Fe(phen)_3^{2+} + mBQ$$

Figure 3.5 shows the effect of changing the concentration of ferroin while holding other initial reactants constant at: $[mH_2Q]$ = 0.05 M, $[NaBrO_3]$ = 0.1 M, and $[H_2SO_4]$ = 1.0 M. At a catalyst concentration of 1.0 x 10^{-3} M (Figure 3.5c) two oscillatory windows

are present, the first having 3 oscillations and the second with 39 with a hint of aperiodicity.

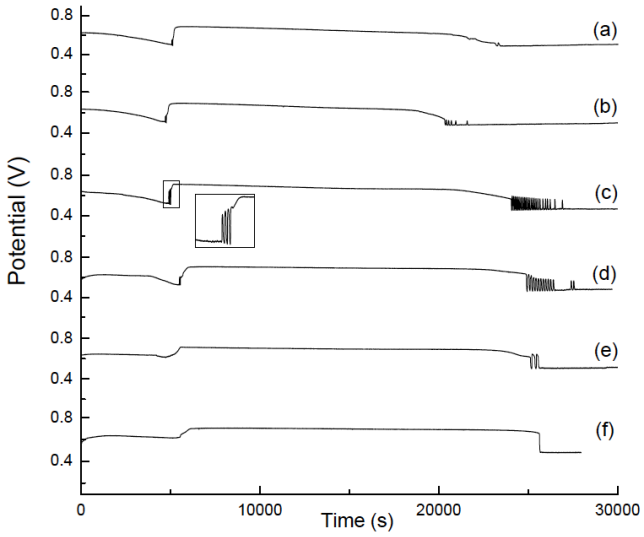

Figure 3.5 - Time series of the ferroin-catalyzed bromate – mH_2Q photoreaction carried out at different initial ferroin concentrations: (a) 1.0 x 10^{-4} M, (b) 6.0 x 10^{-4} M, (c) 1.0 x 10^{-3} M, (d) 2.5 x 10^{-3} M, (e) 3.25 x 10^{-3} M, and (f) 3.75 x 10^{-3} M. Other reaction conditions were: $[mH_2Q]$ = 0.050 M, $[H_2SO_4]$ = 1.0 M, $[BrO_3^-]$ = 0.1 M, and a light intensity of 200 mW/cm^2.

The first set of oscillations is accompanied by a color change from turquoise to green, which is not the prototypical color change associated with use of the ferroin indicator (red in a reduced state and blue in an oxidized state), and suggests that a slight modification of the ferroin complex has occurred. The second set of oscillations is also accompanied by a color change; however, the change is barely noticeable in that the solution changes in the shade of yellow, turning slightly orange. As the concentration of ferroin is increased to 2.5 x 10^{-3} M (Figure 3.5d) the number of oscillations decrease in both windows and a further increase eliminates the first set of oscillations altogether.

When the concentration is decreased to 1.0 x 10^{-4} M in Figure 3.5a only 2 oscillations occur in the primary window, and the secondary set vanish completely. Overall, the Ce^{4+}/Ce^{3+} redox couple proved to have a greater influence on the system resulting in longer lasting oscillations with higher frequencies, as well as displaying complexity in the form of mixed mode oscillations.

Variation in the concentration of sulfuric acid has a profound influence on the ferroin – bromate – mH_2Q photoreaction as shown in Figure 3.6. Sequential oscillations were observed at concentrations of H_2SO_4 between 0.9 and 1.0 M (Figure 3.6b and 3.6c), with other reactant concentrations of mH_2Q = 0.05 M, $Fe(phen)_3^{2+}$ = 0.001 M, and $NaBrO_3$ = 0.1 M. Below 0.9 M sulfuric acid no oscillations were present, and above 1.0 M only the primary set of oscillations occurred.

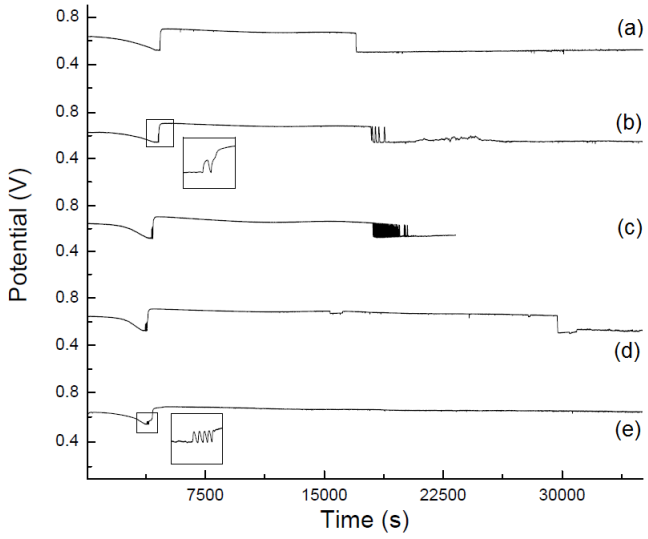

Figure 3.6 - Time series of the ferroin-catalyzed bromate – mH_2Q photoreaction carried out at different initial H_2SO_4 concentrations: (a) 0.8 M, (b) 0.9 M, (c) 1.0 M, (d) 1.1 M, and (e) 1.2 M. Other reaction conditions were: $[mH_2Q]$ = 0.050 M, $[Fe(phen)_3^{2+}]$ = 1.0 x 10^{-3} M, $[BrO_3^-]$ = 0.1 M, and a light intensity of 200 mW/cm^2.

In Figure 3.7 the effect of changing the concentration of mH_2Q from 0.03 M to 0.07 M while catalyzed by ferroin is illustrated. At the low mH_2Q concentration of 0.03 M (Figure 3.7a) the Pt potential remains fairly level throughout the reaction with no oscillations. Increasing the mH_2Q to 0.04 M (Figure 3.7b) allows for spontaneous oscillations to occur in the primary window, and between 0.0425 M and 0.06 M sequential oscillations are present, with an increasing quiescent time as the concentration increases. A further increase to 0.07 M mH_2Q, Figure 3.7f, causes the secondary oscillations to be absent, and at 0.08 M, neither oscillatory window was visible.

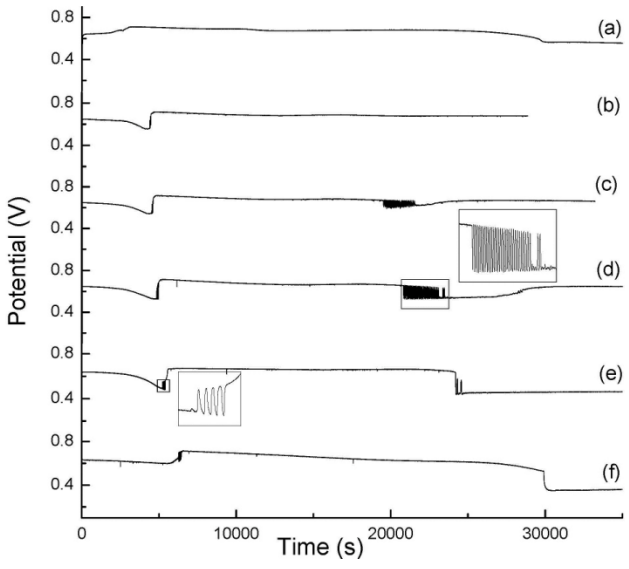

Figure 3.7 - Time series of the ferroin-catalyzed bromate – mH_2Q photoreaction carried out at different initial mH_2Q concentrations: (a) 0.03 M, (b) 0.04 M, (c) 0.0425 M, (d) 0.045 M, (e) 0.06 M, and (f) 0.07 M. Other reaction conditions were: $[H_2SO_4]$ = 1.0 M, $[Fe(phen)_3^{2+}]$ = 1.0 x 10^{-3} M, $[BrO_3^-]$ = 0.1 M, and a light intensity of 200 mW/cm^2.

Figure 3.8 illustrates the result of changing the bromate concentration on the nonlinear kinetics in the ferroin-catalyzed mH_2Q photoreaction. In Figure 3.8a, at 0.07 M

bromate, there is not enough oxidant present to drive the autocatalytic cycle and no oscillations occur. Sequential oscillations occur between 0.08 M (Figure 3.8b) and 0.105 M bromate (Figure 3.8d) when the initial reactant concentrations are 0.05 M mH_2Q, 1.0 M H_2SO_4, and 0.001 M $Fe(phen)_3^{2+}$. In Figure 3.8e when the amount of oxidant is increased to 0.11 M only the primary set of oscillations arise, and a further increase to 0.12 M prevents any oscillatory behavior at all.

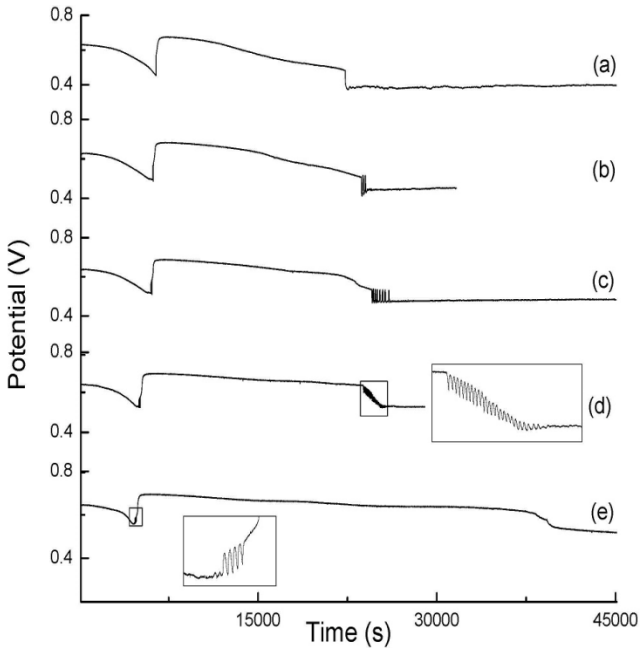

Figure 3.8 - Time series of the ferroin-catalyzed bromate – mH_2Q photoreaction carried out at different initial bromate concentrations: (a) 0.07 M, (b) 0.08 M, (c) 0.09 M, (d) 0.105 M, and (e) 0.11 M. Other reaction conditions were: $[H_2SO_4]$ = 1.0 M, $[Fe(phen)_3^{2+}]$ = 1.0 x 10^{-3} M, $[mH_2Q]$ = 0.050 M, and a light intensity of 200 mW/cm^2.

An intensity of 200 mW/cm^2 was found to be ideal, with respect to number of oscillations as well as complexity, in the ferroin-catalyzed system. Altering the intensity of the supplied illumination proved to have a significant effect on the ferroin - catalyzed

methyl-hydroquinone reaction system. Figure 3.9 shows the time series for the ferroin-catalyzed system when the intensity of illumination is varied from 0 mW/cm^2 (unilluminated) in 3.9a to 250 mW/cm^2 in 3.9f.

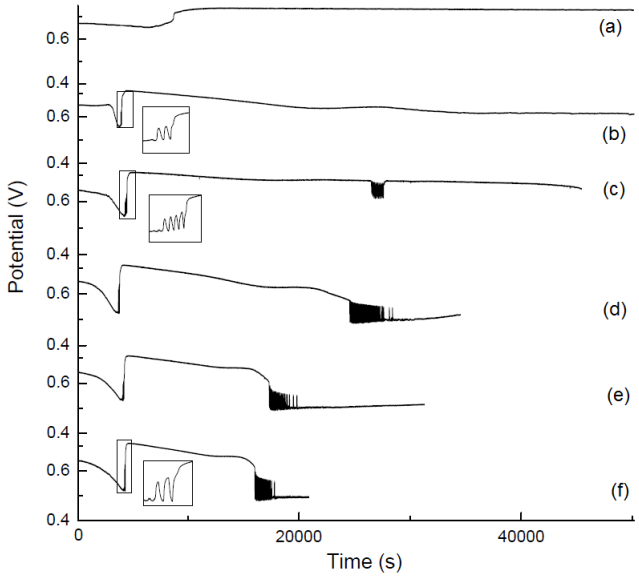

Figure 3.9 - Time series of the ferroin-catalyzed bromate – mH_2Q photoreaction carried out at different initial light intensities: (a) 0 mW/cm^2, (b) 150 mW/cm^2, (c) 175 mW/cm^2, (d) 200 mW/cm^2, (e) 225 mW/cm^2, and 250 mW/cm^2. Other reaction conditions were: [mH_2Q] = 0.050 M, [H_2SO_4] = 1.0 M, [$Fe(phen)_3^{2+}$] = 1.0 x 10^{-3} M, and [BrO_3^-] = 0.1 M.

As can be seen in Figure 3.9a when there is no illumination supplied to the system there is no reactivity and after the potential increase (indicating the oxidation of mH_2Q to mBQ) the potential remains stable for the entirety of the reaction. Increasing the light intensity to 150 mW/cm^2 (Figure 3.9b) resulted in the initial set of oscillations to emerge, however, no sequential behavior was observed. At an intensity of 175 mW/cm^2 sequential oscillations occurred with a lengthy quiescent period between the two oscillatory regimes where the second set of oscillations began approximately 8 hours into the reaction time.

Increasing the intensity up to 250 mW/cm^2 (Figure 3.9f) was shown to decrease the quiescent time drastically, allowing the second set of oscillations to begin just after four hours of reaction time. The induction time of the primary set of oscillations was influenced much less significantly when the illumination was varied, compared to the second set, suggesting that the oscillations occurring during the second set are much more sensitive to illumination.

3.3.2 Mechanistic Characterization

Compositions of the reaction solution were analyzed shortly after the potential spike seen in Figure 3.1, where the formation of mBQ (δ = 6.77, ½ AB, J = 10.5 Hz; 6.73 doublet of ½ AB, J = 2.5, 10.5 Hz; 6.62, doublet of quartets, J = 2.5 Hz, 1.6 Hz; 2.05, A = 3, doublet, J = 1.6 Hz) was confirmed using ^{1}H NMR spectroscopy (Figure 3.10).

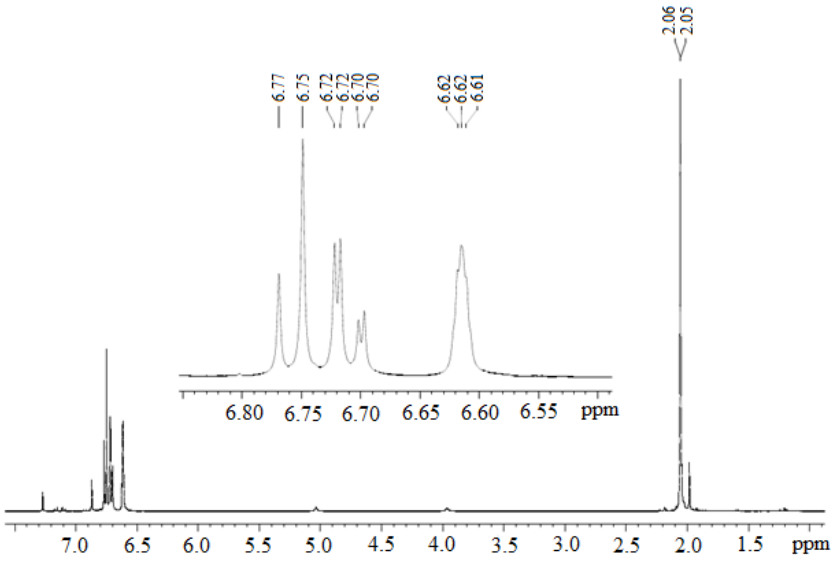

Figure 3.10 - ^{1}H NMR spectrum illustrating the formation of 2-methyl-1,4-benzoquinone before oscillations begin. The reaction conditions were: [mH_2Q] = 0.075 M, [H_2SO_4] = 1.5 M, [BrO_3^-] = 0.1 M and a light intensity of 200 mW/cm^2.

Another compound was found to emerge before spontaneous oscillations take place and remain throughout the reaction giving spectral resonances of δ = 7.11 and 7.17 with a distinct AB coupling pattern (J = 10.8 Hz) and δ = 2.03 (singlet, A = 3), indicative of a 2,3-disubstituted benzoquinone, of which 2-bromo-3-methyl-benzoquinone is the most likely candidate (Figure 3.11).

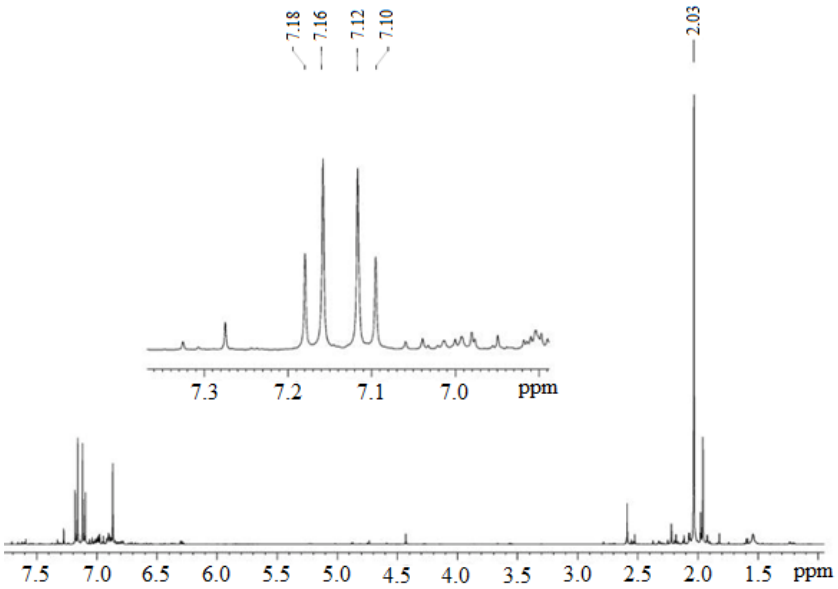

Figure 3.11 - ^{1}H NMR spectrum showing the formation of a product with a distinct AB coupling pattern indicative of a 2,3-disubstituted benzoquinone, of which 2-bromo-3-methyl-1,4-benzoquinone is the most likely candidate. The reaction conditions were: [mH_2Q] = 0.075 M, [H_2SO_4] = 1.5 M, [BrO_3^-] = 0.1 M and a light intensity of 200 mW/cm^2. This spectrum was taken after oscillations had ceased.

Bromine is an important intermediate in bromate based chemical reactions and plays a critical role in modulating the concentration of bromide ions, which are known as the inhibitor of bromate – Based chemical oscillators. The reaction between bromine and mH_2Q was studied here using UV-visible spectroscopy. The reaction was first examined

while illuminated. In Figure 3.12, absorption spectrum (i) is of 0.001 M mH_2Q before illumination was present and (ii) was collected after 600 s of illumination; no observable change in the mH_2Q peak at 290 nm was observed. Once bromine (Br_2) was introduced to the system, the peak associated with mH_2Q (290 nm) immediately disappears and a peak indicative of the presence of mBQ appears at 259 nm (spectrum (iii)). Spectrum (iv) was collected 600 s after the introduction of bromine, where the absorbance of mH_2Q again begins to grow. This observation is consistent with an earlier report that mBQ can be photoreduced to mH_2Q [37].

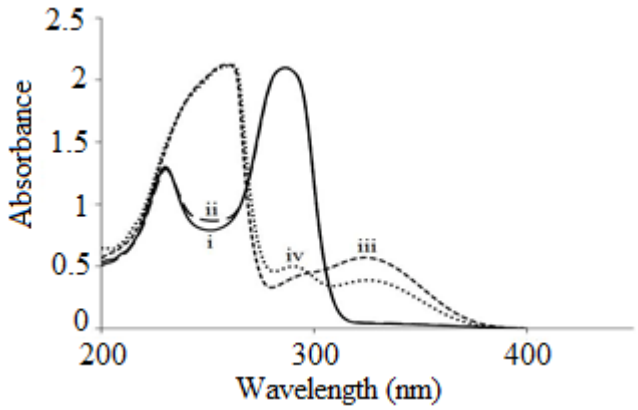

Figure 3.12 - Absorption spectra of the illuminated mH_2Q - bromine reaction. The absorption spectrum (i) shows mH_2Q at t = 0, (ii) t = 600 seconds, (iii) 15 seconds after the addition of bromine, (iv) 600 seconds after the addition of bromine. The concentration of mH_2Q is 0.001 M.

^1H NMR spectroscopy of the reaction solution was conducted in order to determine the products, i.e., whether bromination and oxidation occurred concurrently. However, no evidence of bromination of the organic substrate was found in addition to mH_2Q and mBQ ^1H NMR spectral resonances of δ = 6.98, s, 1H; 6.74, ½ AB, J = 10.1

Hz, 1H; 6.73, ½ AB, J = 10.1 Hz, 1H; and 1.96, s, 3H are identical with earlier reports for the chemical shifts of 2-hydroxy-3-methyl-1,4-benzoquinone, [38,39] the product from the photoreduction of mBQ which does not participate in the autocatalytic cycle. The above process can be described by Scheme 1:

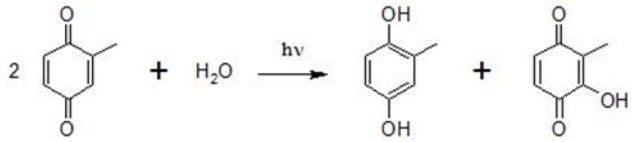

Scheme 3.1 - Photochemical reduction of 2-methyl-1,4-benzoquinone leads to the formation of 2-methyl-1,4-hydroquinone and 2-hydroxy-3-methyl-1,4-benzoquinone

Next, the experiment was performed without illumination. Spectrum (i) in Figure 3.13 shows the absorbance of mH_2Q before bromine was added, and spectrum (ii) was 15 s after the addition of bromine.

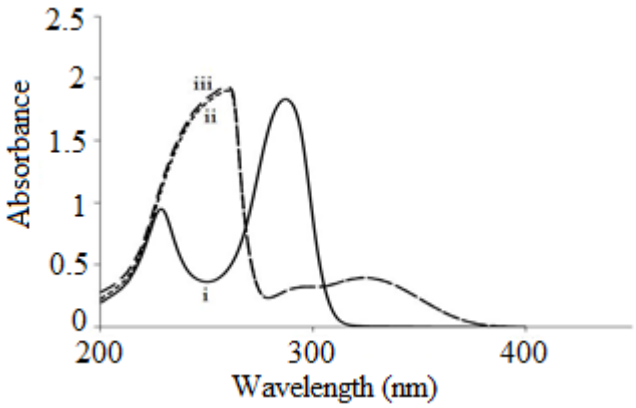

Figure 3.13 - Absorption spectra of the unilluminated mH_2Q - bromine reaction. The absorption spectrum (i) shows mH_2Q before the addition of bromine, (ii) 15 seconds after the addition of bromine, and (iii) 600 seconds after the addition of bromine. The concentration of mH_2Q is 0.001 M.

As can be seen, the conversion of mH_2Q is not illumination-dependent. Spectrum (iii) was collected 600 s after the addition of bromine, which essentially overlaps with spectrum (ii). Therefore, the main difference caused by the lack of illumination in the mH_2Q - bromine reaction is the absence of the photoconversion from mBQ to mH_2Q. The reaction between bromine and mBQ was also studied under both illuminated and nonilluminated conditions; however, no formation of brominated mH_2Q or brominated mBQ was found after 45 min of reaction time.

To further examine the photoreduction of mBQ, absorption spectra of 0.001 M mBQ solution under constant illumination were acquired (Figure 3.14)

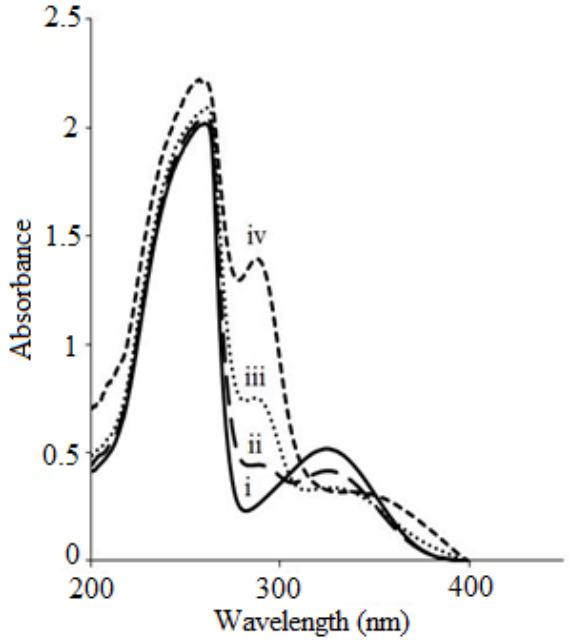

Figure 3.14 - Absorption spectrum showing the photoreduction of mBQ to mH_2Q under 35 mW/cm^2 intensity of illumination: (i) before illumination, (ii) after 300 s illumination, (iii) after 1200 s illumination and (iv) after 3600s illumination. The concentration of mBQ is 0.001 M.

Spectrum (i) was collected at the start of the experiment, where two absorption peaks were seen at 259 and 325 nm. This result provides support that the new peaks seen in Figures 3.12 and 3.13 are from mBQ. As can be seen in spectrum (ii), the absorption at approximately 290 nm, representative of mH_2Q, begins to grow after 300 s of illumination time. After 1200 s (spectrum (iii)) the mH_2Q peak has grown even more (see spectrum (iv)). ^1H NMR spectroscopic analysis showed that the resulting product mixture was composed of mBQ, mH_2Q, and 2-hydroxy-3-methyl-1,4-benzoquinone, in agreement with Scheme 3.1.

3.4 Conclusions

The one electron redox couples Ce^{4+}/Ce^{3+} and $Fe(phen)_3^{3+}/Fe(phen)_3^{2+}$ were introduced to the bromate – mH_2Q photochemical reaction in order to study coupled autocatalytic cycles. Two bifurcation regimes were found to exist when the two autocatalytic cycles were effectively balanced which was achieved through manipulation of the individual reaction parameters. Cerium proved to exhibit the most prevalent effect on the system and was capable of lengthening the oscillatory window substantially as opposed to either the uncatalyzed or ferroin catalyzed systems. Mixed-mode oscillations were also present when cerium was utilized. The sensitivity of the system to illumination was significant as removal of illumination during an oscillatory regime completely quenched the reactivity. Analysis with ^1H NMR spectroscopy indicates that the presence of the methyl group prevents bromination during the mH_2Q - bromine reaction. However, 2-bromo-3-methyl-1,4-hydroquinone was detected with ^1H NMR spectroscopic analysis during the bromate – mH_2Q photoreaction.

3.5 References

[1] I. Szalai, E. Körös, *J. Phys. Chem. A* **1998**, 102, 6892-6897.

[2] H. Görner, *J. Phys. Chem. A* **2003**, 107, 11587-11595.

[3] N. Li, J. Wang, *J. Phys. Chem. A* **2009**, 113, 6297-6300.

[4] T. Amemiya, J. Wang, *J. Phys. Chem. A* **2010**, 114, 13347-13352.

[5] R. J. Field, E. Körös, R. M. Noyes, *J. Am. Chem. Soc.* **1972**, 94, 8649-8664.

[6] P. E. Strizhak, A. L. Kawczyński, *J. Phys. Chem.* **1995**, 99, 10830-10833.

[7] C. Luengviriya, J. Luengviriya, M. Sutthiopad, P. Porjai, B. Tomapatanaget, S. C. Müller, *Chem. Phys. Lett.* **2013**, 561, 170-174.

[8] T. Bánsági, M. Leda, M. Toiya, A. M. Zhabotinsky, I. R. Epstein, *J. Phys. Chem. A* **2009**, 113, 5644-5648.

[9] E. Körös, M. Orbán, I. Habon, *J. Phys. Chem.* **1980**, 84, 559-560.

[10] I. R. Epstein, J. A. Pojman, *An Introduction to Nonlinear Chemical Dynamics: Oscillations, Waves, Patterns, and Chaos*; Oxford University Press: Oxford, U.K., 1998.

[11] R. J. Field, M. Burger, *Oscillations and Travelling Waves in Chemical Systems*; Wiley & Sons: New York, 1985.

[12] K. Blaha, J. Lehnert, A. Keane, T. Dahms, P. Hoevel, E. Schoell, J. L. Hudson, *Phys. Rev. E: Stat., Nonlinear, Soft Matter Phys.* **2013**, 88, 062915.

[13] O. Pesek, L. Schreiberová, I. Schreiber, *Phys. Chem. Chem. Phys.* **2011**, 13, 9849-9856.

[14] F. Sagués, I. R. Epstein, *Dalton Trans.* **2003**, 1201-1217.

[15] F. Rossi, R. Lombardo, L. Sciascia, C. Sbriziolo, M. L. T. Liveri, *J. Phys. Chem. B* **2008**, 112, 7244-7250.

[16] O. Steinbock, V. S. Zykov, S. C. Müller, *Nature* **1993**, 366, 322-324.

[17] D. Bakeš, L. Schreiberová, I. Schreiber, M. J. B. Hauser *Chaos* **2008**, 18, 015102.

[18] M. Dolnik, A. S. Banks, I. R. Epstein, *J. Phys. Chem. A* **1997**, 101, 5148-5154.

[19] F. Rossi, M. A. Budroni, N. Marchettini, L. Cutietta, M. Rustici, M. L. T. Liveri, *Chem. Phys. Lett.* **2009**, 480, 322-326.

[20] R. J. Field, L. Györgyi, *Chaos in Chemistry and Biochemistry;* World Scientific: Singapore, 1993.

[21] J. G. Bell, J. R. Green, J. Wang, *J. Phys. Chem. A* **2013**, 117, 4545-4550.

[22] J. G. Bell, J. Wang, *Chaos* **2013**, 23, 033120.

[23] I. Berenstein, L. Yang, M. Dolnik, A. M. Zhabotinsky, I. R. Epstein, *J. Phys. Chem. A* **2005**, 109, 5382-5387.

[24] M. Harati, S. Amiralaei, J. R. Green, J. Wang, *J. Photochem. Photobiol. A* **2008**, 198, 92-97.

[25] J. Li, J. Wang, *J. Phys. Chem. A* **2012**, 116, 8130-8137.

[26] B. Zhao, J. Wang, *J. Photochem. Photobiol. A* **2007**, 192, 204-210.

[27] B. Zhao, J. Wang, *Chem. Phys. Lett*. **2006**, 430, 41-44.

[28] T. Amemiya, J. Wang, *Acta Phys.-Chim. Sin.* **2010**, 26, 99-109.

[29] B. R. Johnson, S. K. Scott, B. W. Thompson, *Chaos* **1997**, 7, 350-358.

[30] A. Gragnani, *Int. J. Bifurcation Chaos Appl. Sci. Eng.* **2006**, 16, 579-588.

[31] J. Wang, P. G. Sørensen, F. Hynne, *J. Phys. Chem.* **1994**, 98, 725-727.

[32] P. Ruoff, R. M. Noyes, *J. Chem. Phys.* **1986**, 84, 1413-1423.

[33] K. Sriram, M. S. Gopinathan, *React. Kinet. Catal. Lett.* **2003**, 79, 341-349.

[34] M. C. Guedes, R. B. Faria, *J. Phys. Chem.* **1998**, 102, 1973-1975.

[35] L. Adamčiková, Z. Farbulová, P. Ševčik, A. L. Kawczyński, *J. Phys. Chem. A* **2003**, 107, 501-511.

[36] M. Rachwalska, *Z. Naturforsch. A: Phys. Sci.* **2007**, 62, 41-55.

[37] D. Gan, M. Jia, P. P. Vaughan, D. E. Falvey, N. V. Blough, *J. Phys. Chem. A* **2008**, 112, 2803-2812.

[38] A. Rashid, G. Read, *J. Chem. Soc. C* **1967**, 1323-1325.

[39] J. C. Sheehan, Y. S. Lo, *J. Med. Chem.* **1974**, 17, 371-372.

CHAPTER 4 - COMPLEX SPATIOTEMPORAL BEHAVIOR IN THE PHOTOSENSITIVE FERROIN – BROMATE – 4-NITROPHENOL REACTION

4.1 Introduction

Over the past four decades the theory of nonlinear dynamics has been incorporated into a diverse array of scientific disciplines ranging from computer science to molecular biology [1-4]. The study of nonlinear chemical dynamics continues to be an area of significant interest [5-8]. Chemical oscillators such as the Belousov-Zhabotinsky (BZ) reaction rely on autocatalytic processes to establish the necessary nonlinear feedback for the development of spontaneous temporal oscillations [9]. A host of organic substrates have been found capable of reacting with acidic bromate to form bromate-based chemical oscillators [10-12]. Among these, aromatic compounds have seen increasing use due to the lack of the formation of gas molecules, which is a desired property when the system is employed to explore pattern formation in reaction-diffusion media. The reaction of phenol with acidic bromate, for example, has been found to give rich dynamical behavior, and derivatives of phenol such as 4-aminophenol, 1,4-dihydroxybenzene, 1,4-benzoquinone, and 1,4-cyclohexanedione have also been found to oscillate, although some of these require the presence of external illumination [13-17].

The occurrence and evolution of chemical waves, such as propagating fronts, target patterns, and spirals in reaction-diffusion media, have been found to mimic spatiotemporal phenomena observed in nature such as animal patterning [18-28]. Chemical wave activity, when studied in capillary tubes, has been found capable of

exhibiting a variety of interesting interactions such as repelling fronts or nonannihilation collisions [29-31]. Because illumination can be conveniently implemented in various forms as a means of external control or perturbation, photosensitive chemical systems are attractive models for studying nonlinear behavior [32-35]. A modulation in reactivity by illumination may be observed in the form of longer lasting oscillatory windows or in a complexity emerging when only simple oscillations are present in an unperturbed system, whereas a decrease in reactivity can be as significant as a complete quenching of the oscillatory behavior.

The oxidation of 4-nitrophenol (4-NP) by bromate has been studied by Nair and co-workers [36]. They reported in 1981 that chemical oscillations could be seen in the bromate oxidation of 4-NP in an unstirred batch reactor, but noted that the oscillations would be fully quenched if the system was made homogeneous through stirring. The inability of supporting temporal oscillations has made this ferroin – bromate – 4-NP system less appealing and there have been no further reports on this system since the 1981 paper. In contrast to the earlier report, in this study we found that long lasting chemical oscillations could exist in the well-stirred ferroin – bromate – 4-NP system. The success was achieved through our extensive exploration of the uncatalyzed bromate – 4-NP reaction, in which spontaneous oscillations were observed over broad concentration ranges. A study of propagating fronts in a one-dimensional ferroin – bromate – 4-NP reaction-diffusion medium unveiled long lasting wave activity with various complex behaviors. Interestingly, a strong effect of light on the reaction behavior was also observed in both stirred and reaction-diffusion media, making this low-cost reaction

system a potential model for investigating perturbed nonlinear dynamics. Preliminary mechanistic studies were also carried out in this report.

4.2 Experimental Procedure

Spatiotemporal behavior was investigated at room temperature (22.0 ± 1 ^{o}C) by injecting the reaction solution into a glass capillary tube, which has an inner diameter of 1.8 mm. The capillary tube is horizontally placed on a flat table. We have also carried out experiments with a 0.9 mm diameter capillary tube, and the same behavior was obtained there. The evolution of the spatially extended medium was monitored with a charge coupled device (CCD) camera equipped with a zoom lens. The CCD camera was connected to a personal computer running a frame grabber program (Matrox Imaging Library). Temporal kinetics were investigated in a thermal-jacketed 50 mL glass beaker (ChemGlass). A circulating water bath (Thermo NesLab RTE 7) held the reaction temperature constant at 25.0 ± 0.1 ^{o}C. The reaction solution was held constant at 30.0 mL and was stirred continuously with a magnetic stirring bar driven by a magnetic stirrer (Fisher Isotemp) to ensure homogeneity. All ^{1}H NMR studies were performed using a Bruker Avance 500 MHz spectrometer and the samples were dissolved in deuterated chloroform (Cambridge Isotope Laboratories, 99.8%).

Stock solutions of analytical grade sodium bromate ($NaBrO_3$, Aldrich, 99%), 0.1 M and sulfuric acid (Aldrich, 95-98%), 6.0 M were prepared with double-distilled water. The 4-nitrophenol (Aldrich, 98+%) was directly dissolved in the reaction mixture. A Teflon cap was placed on top of the thermal-jacketed beaker to hold the electrodes. Reactions were monitored with a platinum electrode coupled with a $Hg|Hg_2SO_4|K_2SO_4$ reference electrode (Radiometer Analytical, XR200 and M231 Pt-9) filled with a

saturated K_2SO_4 solution, and the electrode potential was recorded through a pH/potential meter (Radiometer PHM220) connected to a computer through a PowerLab/4SP data logger. The illumination source was a 150 W halogen light (Fischer Scientific, Model DLS-100HD) with a continuous variable light level. The intensity of the illumination was measured with an optical power meter (Model 1815-C, Newport).

4.3 Results and Discussion

4.3.1 Temporal Reaction Kinetics

Figure 4.1 shows a typical time series illustrating the reaction dynamics of the well-stirred bromate – 4-nitrophenol reaction measured with a platinum electrode. At the onset of the reaction the potential can be seen to slightly increase and subsequently decrease before a drastic drop in potential occurs, which is then followed by the occurrence of spontaneous oscillations. Under these conditions, 0.01 M 4-NP, 1.0 M H_2SO_4, and 0.03 M BrO_3^-, the oscillatory window lasts for approximately 14 hours and over 40 oscillations occur.

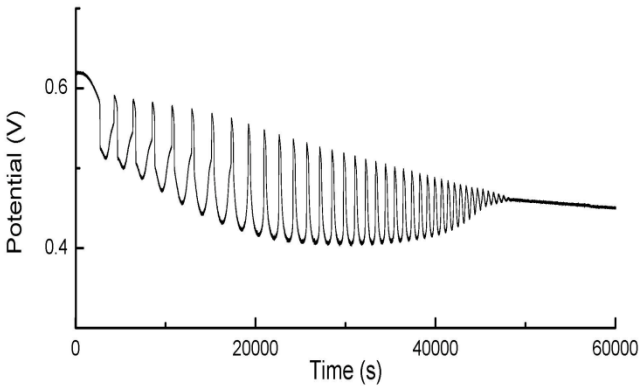

Figure 4.1 - Time series showing chemical oscillations in the bromate – 4-NP reaction. Reaction conditions were: [4-NP] = 0.010 M, [H_2SO_4] = 1.0 M, and [$NaBrO_3$] = 0.03 M.

The amplitude of the oscillations increases before decreasing as the reaction proceeds, and the frequency of the oscillations appears to increase monotonically. The color of the reaction mixture gradually changes from colorless to pale yellow (at the onset of the oscillatory window) as the reaction progresses. No periodic color change was seen in this uncatalyzed system, and there was no visible precipitation formed. Figure 4.2 shows the effect of changing the concentration of 4-NP. Decreasing the 4-NP concentration from 0.03 M in Figure 4.2a to 0.01 M in Figure 4.2d leads to an overall decrease in the amplitude of the oscillations, but an increase in the oscillatory frequency.

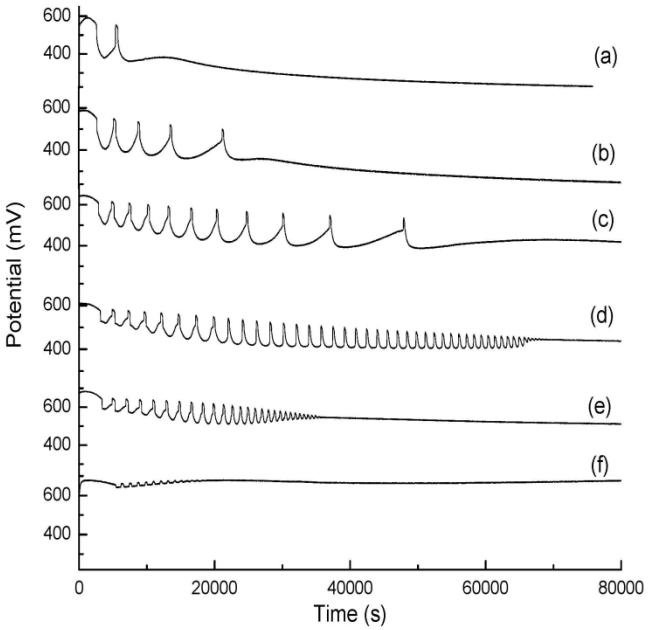

Figure 4.2 - Time series of the bromate – 4-NP reaction carried out at different initial 4-NP concentrations: (a) 0.030 M, (b) 0.020 M, (c) 0.0125 M, (d) 0.010 M, (e) 0.0075 M, and (f) 0.00075 M. Other reaction conditions were $[NaBrO_3]$ = 0.03 M and $[H_2SO_4]$ = 1.0 M.

For 4-NP below 0.0075 M (Figure 4.2e), the number of oscillations, amplitude, and the oscillatory time period begin to decrease. This trend continues, as evidenced in Figure 4.2f, where the amplitude is very small. A further decrease of 4-NP causes the oscillations to vanish.

In Figure 4.3 the concentration of bromate is varied from 0.05 M (Figure 4.3a) to 0.01 M (Figure 4.3f). As the bromate concentration was decreased from 0.05 to 0.03 M, the bromate – 4-NP system exhibited increasing numbers of oscillations, where the frequency of oscillations remained similar. Further lowering the bromate concentration led to a significant decrease in both the frequency and number of oscillations. When the concentration of bromate was decreased to 0.01 M, the oscillations ceased to emerge.

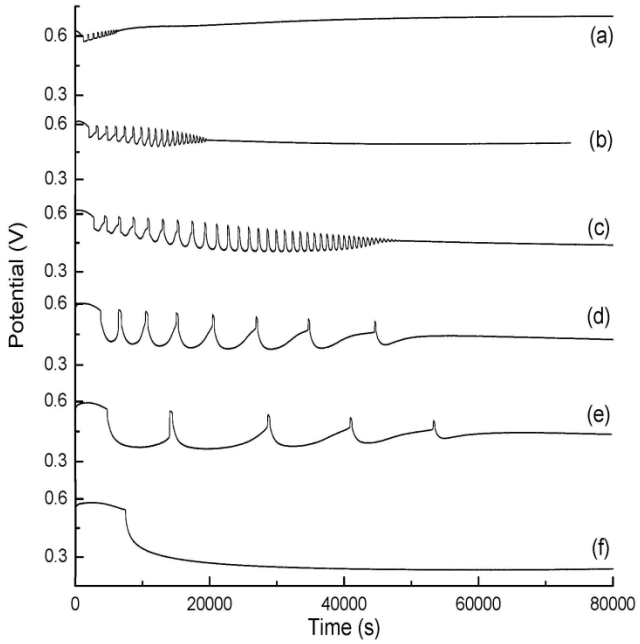

Figure 4.3 - Time series of the bromate – 4-NP reaction carried out at different initial bromate concentrations: (a) 0.05 M, (b) 0.04 M, (c) 0.03 M, (d) 0.02 M, (e) 0.015 M, and (f) 0.01 M. Other reaction conditions were $[H_2SO_4]$ = 1.0 M and [4-NP] = 0.010 M.

Variation in the concentration of sulfuric acid, while holding the concentration of 4-NP and bromate at 0.01 M and 0.03 M respectively, can be seen to have a significant influence on the reaction behavior (Figure 4.4).

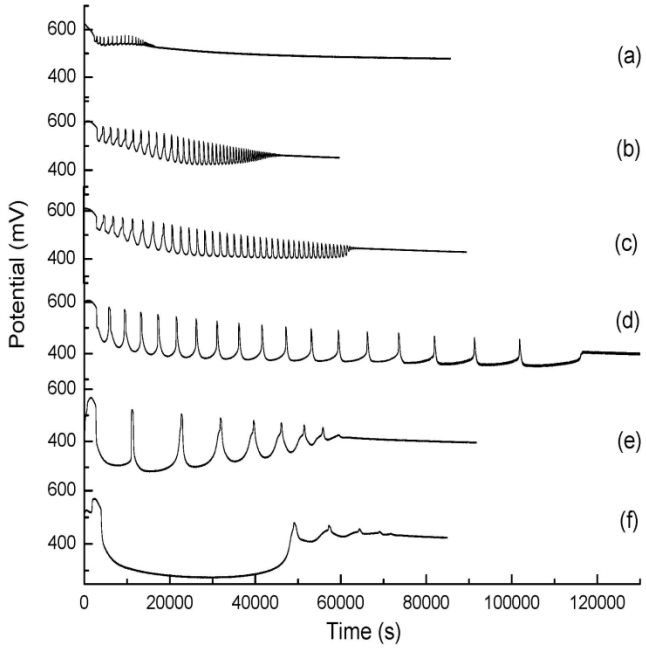

Figure 4.4 - Time series of the bromate – 4-NP reaction carried out at different initial sulfuric acid concentrations: (a) 2.0 M, (b) 1.2 M, (c) 1.0 M, (d) 0.60 M, (e) 0.20 M, and (f) 0.10 M. Other reaction conditions were [4-NP] = 0.01 M and [$NaBrO_3$] = 0.03 M.

Decreasing the concentration of sulfuric acid from 2.0 M (Figure 4.4a) to 0.1 M (Figure 4.4f) leads to a drastic increase in the induction time of those spontaneous oscillations. As the acid concentration decreases, the amplitude of the oscillations increases while their frequency decreases. At a sulfuric acid concentration of 0.6 M, 17 oscillations occur over a span of approximately 30 hours before reaching a stable state, an extremely long time for an uncatalyzed bromate oscillator to remain oscillatory. Figure 4.5 is a phase diagram in the 4-NP and sulfuric acid concentration plane, where the

regime filled with solid triangles (▲) represents conditions at which the system exhibits spontaneous oscillations. Notably, very minute amounts of 4-NP (3.0 x 10^{-5} M) are needed for the system to exhibit spontaneous oscillations, whereas the sulfuric acid concentration can be adjusted over a range from 0.025 M to 2.2 M. This plot demonstrates that very broad concentration ranges of 4-NP and sulfuric acid are capable of supporting the occurrence of chemical oscillations.

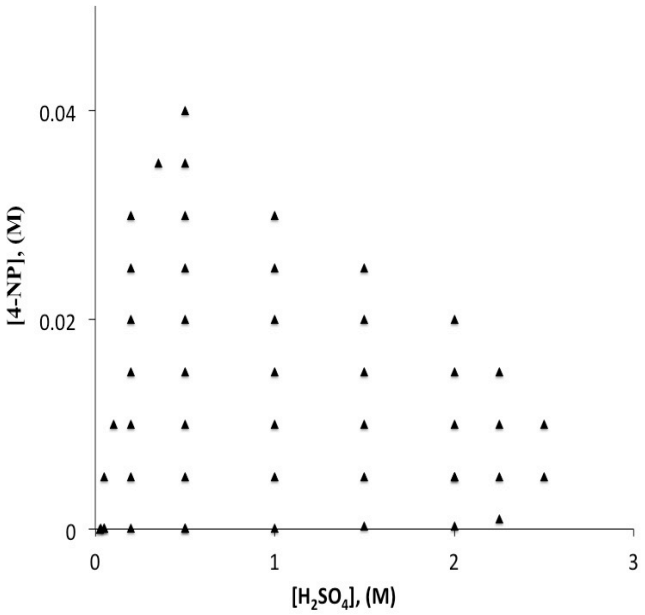

Figure 4.5 - Phase diagram illustrating regions of oscillatory phenomenon in the 4-NP and sulfuric acid concentration plane, where the filled triangle (▲) represents conditions that exhibit spontaneous oscillations. Bromate concentration is held constant at 0.03 M.

In Figure 4.6, the photosensitivity of the bromate 4-NP oscillator was investigated. For comparison, Figure 4.6a presents an unilluminated system to display the prototypical behavior. In Figure 4.6b, at a light intensity of 25 mW/cm^2 there is a dramatic transition in the frequency of oscillations in the middle of the oscillatory window, as opposed to the gradual increase of the oscillation frequency seen in the

unilluminated system. This change became more apparent as the illumination intensity was increased. Increasing the intensity from 25 to 400 mW/cm^2 (Figure 4.6f) appears to have completely eliminated those high frequency oscillations. Clearly, the introduction of illumination can greatly alter the waveform of the corresponding oscillations, depending upon the light intensity supplied.

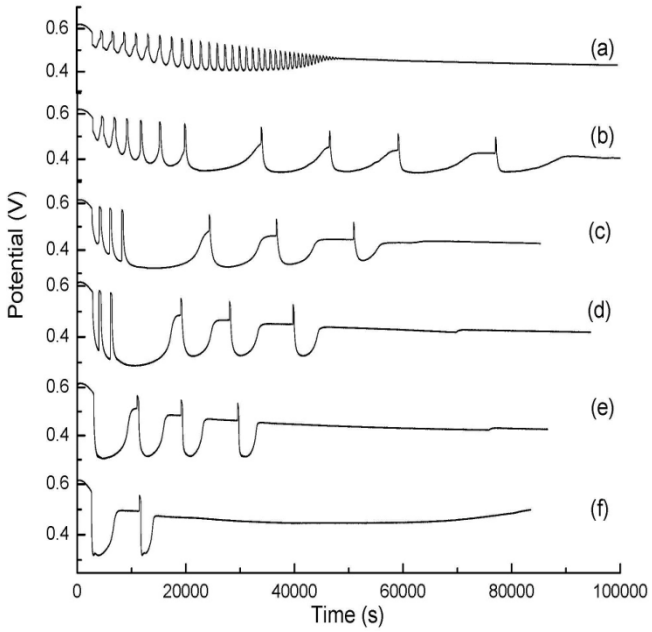

Figure 4.6 - Time series illustrating the effect of light on the bromate – 4-NP system: (a) 0, (b) 25, (c) 50, (d) 100, (e) 200, and (f) 400 mW/cm^2. Other reaction conditions were: $[H_2SO_4]$ = 1.0 M, [4-NP] = 0.010 M, and $[NaBrO_3]$ = 0.03 M.

To gain insight into the intermediates and final products of the bromate – 4-NP oscillatory reaction, ^{1}H NMR spectroscopy measurements were performed. A reaction containing 0.01 M 4-NP, 1.0 M sulfuric acid, and 0.03 M bromate was stopped after 5 h, approximately halfway through the oscillatory window, and was extracted twice with diethyl ether. After the diethyl ether solution was concentrated under reduced pressure, an

^{1}H NMR sample was prepared with deuterated chloroform. The ^{1}H NMR spectrum indicated the presence of a small amount of starting material (doublets at 6.91 and 8.16 ppm) as well as 1,4-benzoquinone (singlet at 6.80 ppm). The spectrum also showed that bromination occurred on both 1,4-benzoquinone and 4-NP, yielding 2-bromo-1,4-benzoquinone (doublet of doublets at 6.85, doublet at 6.98, and the small doublet at 7.32 ppm), 2,6-dibromo-1,4-benzoquinone (singlet at 7.34 ppm), 2-bromo-4-nitrophenol (doublet at 7.12, small doublet at 8.44, and partially obscured doublet of doublets under the 8.15 ppm peaks). The presence of mono- and dibrominated 4-NP suggests that bromination occurs fairly easily in the studied system. A speculative pathway forming 1,4-benzoquinone in proposed in Scheme 4.1, where the starting material reacts with bromine dioxide radicals. This reaction oxidizes the phenolic group, leading to destabilization of the aromatic ring, which results in the indirect formation of 1,4-benzoquinone through the autocatalytic step.

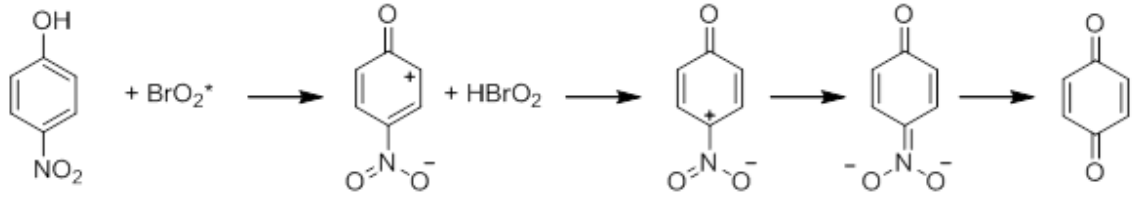

Scheme 4.1 - Proposed scheme for the formation of 1,4-benzoquinone in the bromate – 4-NP reaction.

To gain further insight into the bromination of 4-NP, the reaction with bromine and 4-NP was investigated using UV-VIS spectroscopy (Figure 4.7). Two absorbance peaks were present in a 0.001 M 4-NP and 1.0 M sulfuric acid solution (~240 nm and ~ 310 nm). Upon the reaction of bromine with 4-NP there is a drastic increase in the peak at

240 nm while the peak at 310 nm decreased; these results strongly suggest that a reaction has occurred.

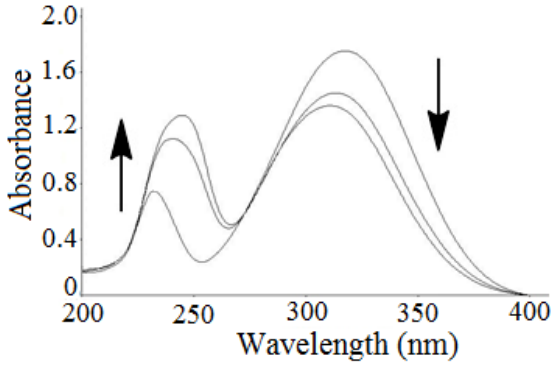

Figure 4.7 - UV-VIS spectrum showing the reaction between bromine and 4-NP in 1.0 M sulfuric acid. Addition of bromine causes 4-NP absorbance peak at 240 nm to increase and the peak at 310 decreases.

To achieve periodic color change for the study of spatiotemporal behavior, metal catalyst ferroin was introduced to the above bromate – 4-NP reaction. Note that the presence of ferroin implements a second autocatalytic cycle through the reaction between ferroin and bromine dioxide radicals. As a result, dramatic effects on the nonlinear phenomenon may occur. In Figure 4.8 at a ferroin concentration of 1.0×10^{-6} M, low frequency oscillations emerged. Both the frequency and the total number of oscillations were reduced greatly, when being compared with the time series of the ferroin-free system listed in Figure 4.8a.

Increasing the concentration of ferroin to 1.0×10^{-4} M (Figure 4.8c), however, led to high frequency oscillations lasting over 10 h. At 1.0×10^{-3} M ferroin (Figure 4.8d) low frequency oscillations emerged that lasted approximately 7 h. The subtle influences of ferroin may arise from the fact that there are coupled autocatalytic cycles in the ferroin –

bromate – 4-NP system. Notably in Figure 3.8d the oscillation frequency appears to modulate, as opposed to gradual change seen in most of the closed reaction systems [5,6]. When the concentration of ferroin was increased, red precipitates were found to form in the stirred system, which stopped us from examining the kinetics at higher ferroin concentrations.

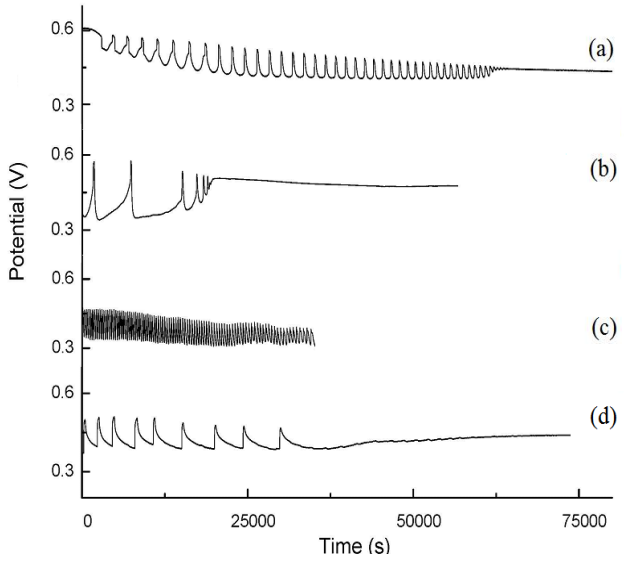

Figure 4.8 - Time series of the ferroin catalyzed bromate – 4-NP reaction at different ferroin concentrations: (a) 0, (b) 1.0 x 10^{-6} M, (c) 1.0 x 10^{-4} M, and (d) 1.0 x 10^{-3} M. Other reaction conditions were [H_2SO_4] = 1.0 M, [4-NP] = 0.010 M, and [$NaBrO_3$] = 0.030 M.

4.3.2 Spatiotemporal Behavior

Spatiotemporal behavior of the ferroin – bromate – 4-NP system in a pseudo-one-dimensional configuration was investigated as described below. Pictures of the capillary tube were taken every 15 s and later a space-time plot was generated by taking one horizontal cut through the center of the capillary tube and sequentially arranging these

one-dimensional images. In Figure 4.9 the horizontal axes represent space and the vertical axes represent time. Bright and dark gray levels correspond to the oxidized and reduced states of the ferroin/ferriin complex, respectively. As can be seen here, pulses are formed at both boundaries, propagating inward; however, after a few pulses wave activity at the left boundary evolved to the state where only every other pulse could propagate fully through the medium to collide with the one formed at the opposite end of the tube. This intermittent propagation failure phenomenon resembles the 1^1 mixed mode oscillations in homogenous systems. The 1^1 patterns can be seen to repeat in Figure 4.9 for more than 2 h. Meanwhile, pulses formed at the right boundary also exhibited some sort of complexity due to an unsteady propagation rate.

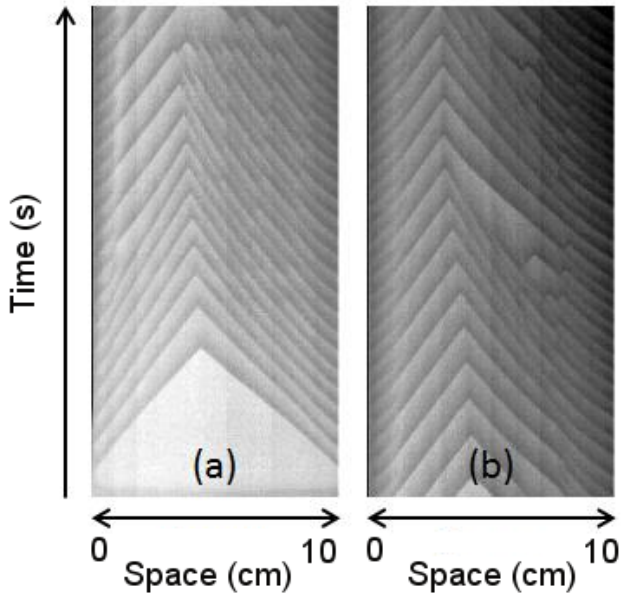

Figure 4.9 - Space-time plot of propagating wave trains in the ferroin – bromate – 4-NP reaction. Reaction conditions were $[H_2SO_4]$ = 1.3 M, [4-NP] = 0.011 M, $[NaBrO_3]$ = 0.036 M, and [ferroin] = 2.7 x 10^{-3} M. The time scale presented is (a) 0-4455 s and (b) 4455-8910 s.

Panel (b) in Figure 4.9 indicates that wave activity may also emerge at other regimes in the tube, leading to rich interactions. Notably, wave trains observed here could last for more than 20 h, which is long enough to make this closed system suitable for studying interactions between intrinsic dynamics and various external perturbations. The identical reaction was carried out with the ends of the capillary tube sealed and the same phenomenon was observed, suggesting that the intermittent propagation failure behavior is not due to the influence of air/oxygen at the boundaries.

The effect of sulfuric acid concentration on the above spatiotemporal behavior was examined (Figure 4.10). At a sulfuric acid concentration of 1.0 M (Figure 4.10a), during the initial reaction stage, pulses that fail to fully propagate alternate with a pulse that is able to propagate through the medium, showing the pattern 1^1 (1 failure, 1 success). As the reaction progresses, the frequency of the propagation failure begins to decrease, where three pulses fully propagate before one failure and then four fully propagating pulses precede the propagation failure, exhibiting 1^3 and 1^4 behaviors. In Figure 4.10b, an increase in the sulfuric acid concentration to 1.4 M increases the observed complexity. Here, four propagation failures occur before the first fully propagating pulse emerges, after which the pattern 1^1 persists until a series of 1^3 behavior, which transitions into the pattern 1^1 that lasts for several hours. In Figure 4.10c, at a sulfuric acid concentration of 1.6 M a different form of complexity arises as the reaction proceeds. The observed curvature in all three conditions indicates that pulses do not propagate at a constant speed as normally seen with chemical waves. Such a property may potentially result in even more complex spatiotemporal behavior.

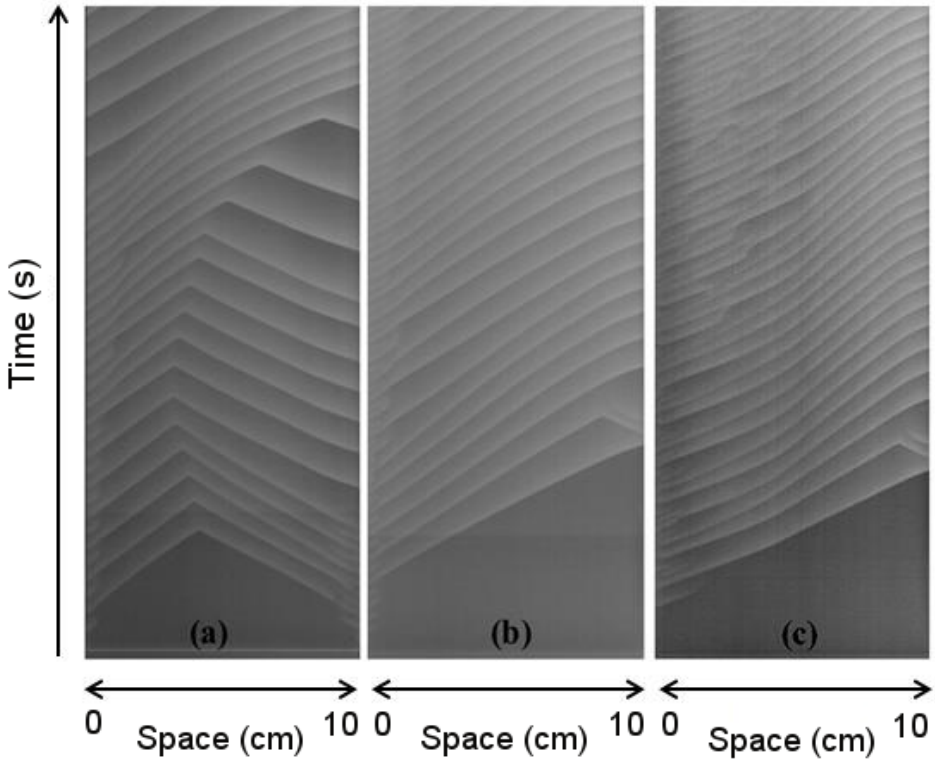

Figure 4.10 - Space-time plot of propagating wave trains in the ferroin – bromate – 4-NP reaction carried out at different sulfuric acid concentrations: (a) 1.0 M, (b) 1.4 M, and (c) 1.6 M. Other reaction conditions were [4-NP] = 0.009 M, [$NaBrO_3$] = 0.027 M, and [ferroin] = 2.7 x 10^{-3} M. The amount of time elapsed in each panel is 13500 s.

Figure 4.11 shows the effect of light on the reaction-diffusion behavior, where a 60 s pulse of illumination was supplied to the center of the capillary tube (ca. 3 cm). It effectively quenched the wave activity and drove that area to a reduced state. Upon the removal of light, the medium was able to regain its activity to support wave propagation. This preliminary test demonstrates the feasibility of manipulating the 4-NP reaction-diffusion system with light, although the catalyst ferroin does not have great photosensitivity.

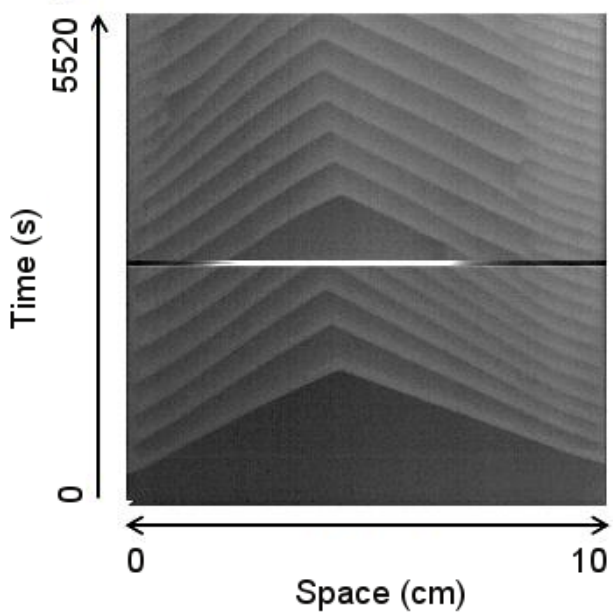

Figure 4.11 - Space-time plot showing the photosensitivity of the wave activity. Reaction conditions were [4-NP] = 0.011 M, [$NaBrO_3$] = 0.036 M, [H_2SO_4] = 1.0 M, and [ferroin] = 2.7 x 10^{-3} M. Illumination was applied for 60 s (the bright strip in the image).

Interestingly, when the wave behavior was investigated in a vertically, as opposed to horizontally, positioned capillary tube, red precipitates were formed (Figure 4.12) at the same ferroin concentration used in Figures 4.9 and 4.10, presumably through a buoyancy-driven aggregation process.

Figure 4.12 shows the evolution of the formation of the precipitate as the reaction proceeded in the capillary tube. In Figure 4.12a, there are no precipitates observable after 3000 s reaction time; however, at 10800 s, (Figure 4.12b) the presence of precipitate is obvious. Importantly there is virtually no change in the amount/appearance of the precipitate as the reaction continues to progress to 6 h (Figure 4.12c).

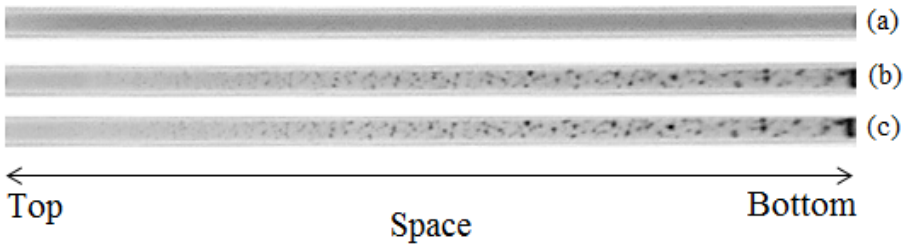

4.12 - CCD snapshots of the capillary tube showing the formation of precipitation after (a) 3000 s, (b) 10800 s, and (c) 19000 s.

Variation in the local kinetics due to the formation of precipitates caused wave pulses to preferentially develop at the bottom end of the tube, while intermittent propagation failure phenomena could still be seen, as shown in Figure 4.13.

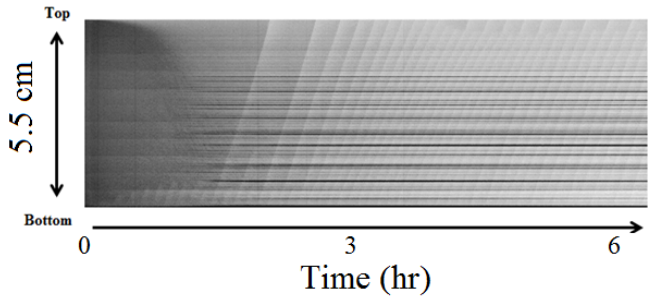

Figure 4.13 - Space-time plot showing the formation of precipitation in the capillary tube when the capillary tube was placed in a vertical orientation.

4.4 Conclusions

This exploration leads to the conclusion that the bromate – 4-NP reaction supports spontaneous oscillations over a broad concentration window, in which low frequency oscillations can last longer than 12 h. In complement to the earlier report [36] here we show that the ferroin – bromate – 4-NP reaction also supports long lasting temporal oscillations. However, depending on the ferroin concentration, the oscillation frequency

can be reduced to a very low value, which is in great contrast to oscillations seen in other ferroin-catalyzed bromate oscillators. Overall, ferroin has a very subtle influence on the nonlinear behavior, presumably due to the implementation of a second autocatalytic cycle. Complexity in the form of intermittent propagation failure was observed in the reaction-diffusion media. Preliminary exploration illustrates that the complexity exhibits a strong response to variation of the sulfuric acid concentration. Consistent with the observation that those long-lived spontaneous oscillations in the bromate 4-NP system were inhibited by external illumination, an inhibitory effect of light on wave activity was also seen.

The long lasting oscillation window (>12 h) in both stirred and reaction-diffusion media makes this bromate oscillator an attractive chemical system for use in investigating perturbed nonlinear dynamics; in particular, this system has great photosensitivity. For those applications, developing a realistic chemical model is necessary. So far, through ^{1}H NMR spectroscopic measurements key components of this reaction system were determined to be 1,4-benzoquinone, 2-bromo-1,4-benzoquinone, and 2-bromo-4-nitrophenol.

4.5 References

[1] S.H. Strogatz, *Nature* **2001**, 410, 268-276.

[2] D. A. Hsieh, *J. Finance* **1991**, 46, 1839-1877.

[3] J. Mørk, B. Tromborg, J. Mark, *IEEE J. Quantum Electron.* **1992**, 28, 93-108.

[4] V. Volpert, S. Petrovskii, *Phys. Life. Rev*. **2009**, 6, 267-310.

[5] S. K. Scott, *Oscillations, Waves, and Chaos in Chemical Kinetics*; Oxford University Press: Oxford, U.K., 1994.

[6] I. R. Epstein, J. A. Pojman, *An Introduction to Nonlinear Chemical Dynamics: Oscillations, Waves, Patterns, and Chaos*; Oxford University Press: Oxford, U.K., 1998.

[7] R. J. Field, M. Burger, *Oscillations and Travelling Waves in Chemical Systems*; Wiley & Sons: New York, 1985.

[8] V. Petrov, Q. Ouyang, H. L. Swinney, *Nature* **1997**, 388, 655-657.

[9] R. J. Field, E. Körös, R. M. Noyes, *J. Am. Chem. Soc.* **1972**, 94, 8649-8664.

[10] M. Orbán, E. Körös, *React. Kinet. Catal. Lett.* **1978**, 8**,** 273-276.

[11] V. L. Farage, D. Janjic, *Chem. Phys. Lett.* **1982**, 88, 301-304.

[12] L. C. Silva, R. B. Faria, Chem. Phys. Lett. 2007, 440, 79-82.

[13] L. Adamčiková, Z. Farbulová, P. Ševčik, *New J. Chem.* **2001**, 25, 487-490.

[14] T. Amemiya, J. Wang, *J. Phys. Chem. A* **2010**, 114, 13347-13352.

[15] B. Zhao, J. Wang, *Chem. Phys. Lett*. **2006**, 430, 41-44.

[16] J. G. Bell, J. R. Green, J. Wang, *J. Phys. Chem. A* **2013**, 117, 4545-4550.

[17] I. Szalai, K. Kurin-Csörgei, I. R. Epstein, M. Orbán, *J. Phys. Chem. A* **2003**, 107, 10074-10081.

[18] A. Schrader, M. Braune, H. Engel, *Phys. Rev. E* **1995**, 52, 98-108.

[19] A. T. Winfree, *Science* **1973**, 181, 937-939.

[20] A. E. Bugrim, M. Dolnik, A. M. Zhabotinsky, I. R. Epstein, *J. Phys. Chem.* **1996**, 100, 19017-19022.

[21] A. P. Steinberg, I. R. Epstein, M. Dolnik, *J. Phys. Chem. A* **2014**, 118, 2393-2400.

[22] P. Dähmlow, M. J. B. Hauser, *Phys. Rev. E* **2013**, 88, 062923.

[23] Z. Nagy-Ungvarai, S. C. Müller, B. Hess, *Chem. Phys. Lett.* **1989**, 156, 433-437.

[24] D. Horváth, A. Tóth, *J. Chem. Phys*. **1998**, 108, 1447-1451.

[25] A. Tóth, B. Veisz, D. Horváth, *J. Phys. Chem. A* **1998**, 79, 5157-5159.

[26] J. D. Murray, *Sci. Am*. **1988**, 258, 80-87.

[27] H. Ke, Z. Zhang, O. Steinbock, *J. Phys. Chem. A* **2014**, 118, 6819-6826.

[28] K. Kurin-Csörgei, I. Szalai, E. Körös, *React. Kinet. Catal. Lett.* **1995**, 54, 217-224.

[29] B. Marts, K. Martinez, A. L. Lin, *Phys. Rev. E* **2004**, 70, 056223.

[30] N. Manz, O. Steinbock, *Chaos* **2006**, 16, 037112.

[31] M. Harati, J. Wang, *Chaos* **2009**, 19, 023116.

[32] D. S. Huh, Y. L. Kim, H. S. Kim, J. K. Kang, J. Wang, *Phys. Chem. Chem. Phys.* **2003**, 5, 3188-3192.

[33] O. Steinbock, V. S. Zykov, S. C. Müller, *Nature* **1993**, 366, 322-324.

[34] J. Wang, *Chem. Phys. Lett.* **2001**, 339, 357-361.

[35] T. Sakurai, E. Mihaliuk, F. Chirila, K. Showalter, *Science* **2002**, 296, 2009-2012.

[36] P. K. R. Nair, A. Mittal, K. Srinivasulu, *React. Kinet. Catal. Lett.* **1981**, 16, 399-402.

CHAPTER 5 - CURRENT AND POTENTIAL OSCILLATIONS DURING THE ELECTRO-OXIDATION OF BROMIDE IONS

5.1 Introduction

Electrochemical oxidation of bromide ions on platinum electrodes has recently been thoroughly researched due to their potential applications in the construction of a new class of energy storage devices [1-3]. Recent reports, for example, have indicated that the recombination of hydrogen, H_2, and bromine, in a fuel cell allows for up to 90% of the chemical energy stored in the reactants to be converted to electricity, which is much higher than that associated with the state of the art H_2/air fuel cells, for which the conversion can only reach about 50% [3,4]. Investigations undertaken by Conway and co-workers have led to the suggestion that the recombination of bromine radicals is the rate determining step in the formation of bromine ($2Br^* \rightarrow Br_2$) [1]. Other possible reaction steps from the most recent report on bromide electro-oxidation include [3]:

$$(1)\ Br^- \rightarrow Br^* + e^-$$

$$(2)\ Br^- \rightarrow Br^{(1-\delta)} + \delta e^-$$

$$(3)\ Br^* + Br^- \rightarrow Br_2 + e^-$$

$$(4)\ Br^- + Br_2 \rightleftharpoons Br_3^-$$

Despite the earlier investigation on its electrochemical kinetics, there is no report on nonlinear instabilities during the oxidation of bromide ions on polycrystalline Pt electrodes. On the other hand, the importance of bromide ions in chemical and electrochemical oscillations is well documented [5-10]. For example, oscillations have

been observed during the electro-dissolution of gold in an electrolyte solution containing bromide ions [9]. The introduction of bromide ions to a solution of hydrogen peroxide and sulfuric acid has also been found to induce chaotic behavior when being studied on a platinum electrode [10]. Overall, nonlinear behavior in electrochemical systems has been a subject that constantly attracts intense attention [11-19]. The first reported instance of nonlinear dynamics in electrochemistry can be dated back to 1828 [20], and since then, electrochemical oscillations have been found during the dissolution of certain metals such as iron, copper, and nickel, the oxidation of H_2 on platinum, the oxidation of sulfur containing compounds such as thiosulfate, and the oxidation of small organic molecules such as methanol [21-29].

Thorough investigation has led to the classification of electrochemical oscillations into four types on the basis of the systems' Electrochemical Impedance Spectroscopic (EIS) results [30]. Of the four categories, the three most prevalent classes of electrochemical oscillators are those having N-Shaped Negative Differential Resistance (N-NDR), S-Shaped Negative Differential Resistance (S-NDR), and Hidden N-Shaped Differential Resistance (HN-NDR). An important feature of those NDR systems is that there exists a negative Faradic resistance where the double layer potential becomes an essential variable in the oscillation mechanism [31]. Oscillatory phenomena can also occur when convection assumes the role of the essential parameter through the process of replenishing the diffusion layer with the electroactive species [32]. Very recently, Zensen and co-workers demonstrated with two- and three-variable models the possibility of capacitance mediated positive differential resistance oscillators, in which the formation and dissolution of inhibiting surface layers played a key role [33]. Through systematic

exploration, this study uncovered the fact that the electro-oxidation of bromide ions could undergo both potential and current oscillations under a positive differential resistance and without an external resistor, pointing to the possibility of being a capacitance-mediated electrochemical oscillator. Under high applied potentials (> 1.5 V), the current oscillates above a limiting current and is accompanied with vigorous bubble formation, suggesting that the observed oscillations are likely driven by convection processes [32].

5.2 Experimental Procedures

All the electrochemical experiments were performed on a CHI660D Instrument (CHI Instruments, US). Polycrystalline platinum electrodes with a diameter of 2.0 mm (CHI Instruments) were applied as working electrodes. The counter electrode was a platinum film (3 mm x 5 mm, Shanghai Ruosull Technology Co., LTD) and a saturated calomel electrode (SCE) was applied as the reference electrode. All the potential values reported in this study are versus SCE. Before each experiment the working electrode was polished with fine alumina powder (0.05μm), rinsed with double distilled water, cleaned by an ultrasonic cleaner (Branson 1510, USA) for 10 min, and again rinsed with double distilled water.

All reactions were carried out in a custom built thermal-jacketed electrochemical cell with 5 multi-purpose ports. The three electrodes were placed in the traditional triangle configuration and all electrochemical experiments were performed at room temperature (22.0 ± 1 ^{o}C). Stock solutions of sulfuric acid (Aldrich, 95-98%), 6.0 M, were prepared with double distilled water and the sodium bromide (NaBr, Aldrich, 98 + %) and potassium sulfate (K_2SO_4, ACP Chemicals) was directly dissolved in the reaction mixture. Reaction solution volumes were held constant at 60.0 mL. Electrochemical

impedance spectroscopy (EIS) experiments were measured in the frequency range of 100 kHz to 0.001 Hz.

5.3 Results and Discussion

5.3.1 Nonlinear Kinetics

Figure 5.1a is a linear sweep voltammogram (LSV) of 0.075 M bromide in a 0.75 M H_2SO_4 solution conducted at a scan rate of 1.0 mV/s. It shows that following the onset of bromide oxidation at around 0.8 V, oscillations in the current take place on an otherwise fairly flat branch. When the potential is increased to above 1.5 V, the current density resumes its increase, but in an oscillatory fashion.

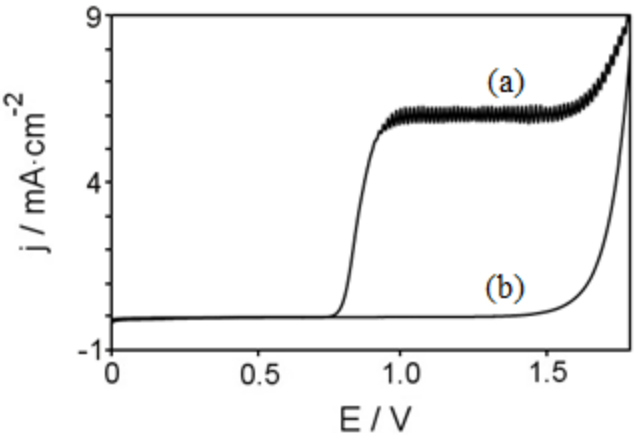

Figure 5.1 - Linear sweep voltammogram (LSV) of the solution consisting of (a) 0.075 M NaBr and 0.75 M H_2SO_4 and (b) 0.75 M H_2SO_4.

Meanwhile, small bubbles begin to form at the working electrode, suggesting that this second positive branch is increasingly dominated by the oxidation of hydroxide ions. To examine the relative influence that oxygen formation would have on the oxidation of bromide ions, Figure 5.1b shows the LSV of 0.75 M sulfuric acid without the presence of

bromide ions, where the current density begins to increase sharply, accompanied with bubble formation, once the potential reaches approximately 1.5 V.

Results in Figure 5.1 suggest that convection processes are negligible at low potentials, but may play a very important role in the observed nonlinear kinetics at the potential above 1.5 V. At a high potential of 1.75 V, irregular oscillations are observed which begin at a current value that is above the limiting current of bromide oxidation. The presence of visible bubbles on the working electrode supports the notion that convection induced by bubble formation and detachment plays an important role in those current oscillations, where the irregularity is likely due to the non-uniform formation of bubbles. As suggested in an earlier report [32], at the minimum peak current of the oscillations, oxygen gas evolution becomes prominent, while at the maximum peak currents of the oscillations, gas evolution is repressed by the oxidation of Br^- ions that are replenished through the convection induced by the gas evolution. If the system is exposed to a constant agitation with a strength that is equal or larger than that induced by the oxygen evolution, the oscillations will stop and the current stabilizes at a state where only the bromide ions are oxidized (i.e., the oxidation of OH^- is negligible) [32]. Our experiments conducted with a rotating disk electrode confirm the above scenario.

Figure 5.2 presents a series of potentiostatic experiments conducted at the low potential range where the effect of convection is considered negligible. At the applied potential of 0.84 V, no oscillations take place and the current density remains near 0. When the applied potential is increased to 0.85 V in time series (b), oscillations emerge after a brief induction period. A further increase to 0.95 V shows oscillations occurring without an induction time, where the oscillation frequency is 0.042 Hz. The time series

(d) shows current oscillations at the applied potential of 1.15 V, where the oscillation frequency increases slightly to 0.05 Hz. Notably, for the applied potential between 1.0 V and 1.5 V, the current was found to oscillate around a plateau in an LSV (see Figure 5.1a)). This is one of the features associated with a capacitance mediated electrochemical oscillator [33]. No external resistor is required in the above current oscillations, which is another property associated with the capacitance-mediated electrochemical oscillator.

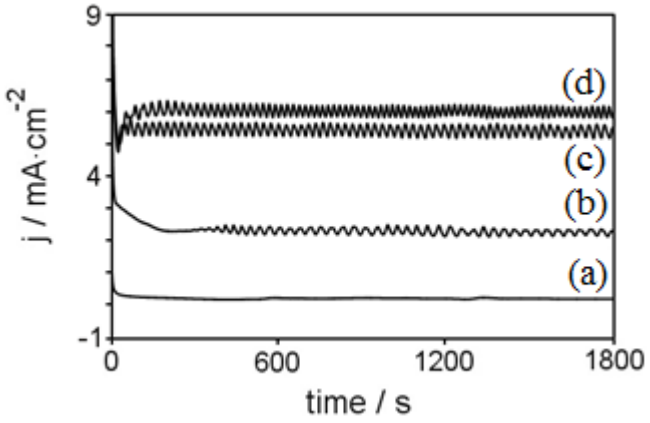

Figure 5.2 - Potentiostatic experiments performed with applied potentials of (a) 0.84 V, (b) 0.85 V, (c) 0.95 V, and (d) 1.15 V (vs. SCE). Other reaction conditions were: [NaBr] = 0.075 M and [H_2SO_4] = 0.75 M.

Electrochemical Impedance Spectroscopy (EIS) measurements have been found very useful in the classification of the type of electrochemical oscillator [30]. Here, the electro-oxidation of bromide ions exhibits oscillations even without the presence of external resistance, which restricts us to conduct the impedance measurements at the potentials studied in Figure 5.2. Figure 5.3 shows EIS obtained at an applied potential of 0.84 V with the applied perturbation of 0.0008 sin(ωt)V. There is a semicircle, reflecting the charge transfer resistance, and Warburg diffusion impedance. Notably, at the low

frequency range, while remaining in the positive range, the impedance showed some fluctuation, presumably because the system is just outside of the oscillatory regime and is therefore sensitive to external perturbation/noise.

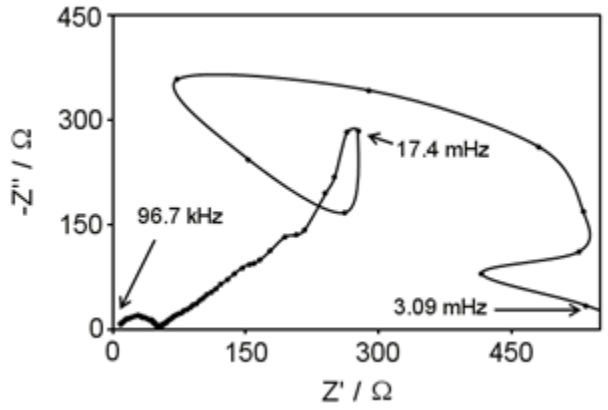

Figure 5.3 - Electrochemical Impedance spectrum performed at 0.84 V. The perturbation amplitude is 0.8 mV and a frequency range of 100 kHz to 1.0 mHz.

The admittance spectrum in Figure 5.4 shows a small resonance peak at a frequency of 0.014 Hz, which is close to the frequency of current oscillations seen at 0.85 V (0.025 Hz).

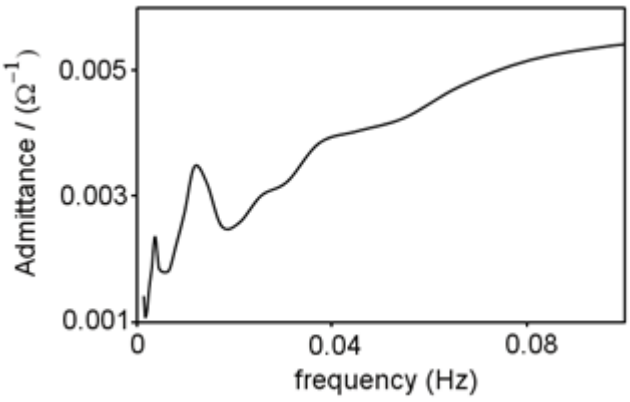

Figure 5.4 - Admittance spectrum performed at 0.84 V with a frequency range of 100 kHz to 1.0 mHz and the perturbation amplitude is 0.8 mV.

It is useful to point out that time series in Figure 5.2 indicate that the frequency of oscillations decreases as the applied potential moves closer to the bifurcation point. The resonance behavior is also affected by its distance from the bifurcation point. Such a feature is consistent with the simulations performed by Zensen et al. [33]. This admittance spectrum, together with the two features mentioned above, suggests that at the low potential range (0.85 V to 1.4 V) the oxidation of bromide is likely a capacitance mediated positive differential resistance oscillator.

To make further comparisons with the behavior of capacitance-mediated positive differential resistance oscillators, external resistors of various resistances were introduced to monitor their influence on the system. Figure 5.5 shows that the oscillation amplitude is decreased through increasing the magnitude of the external resistor.

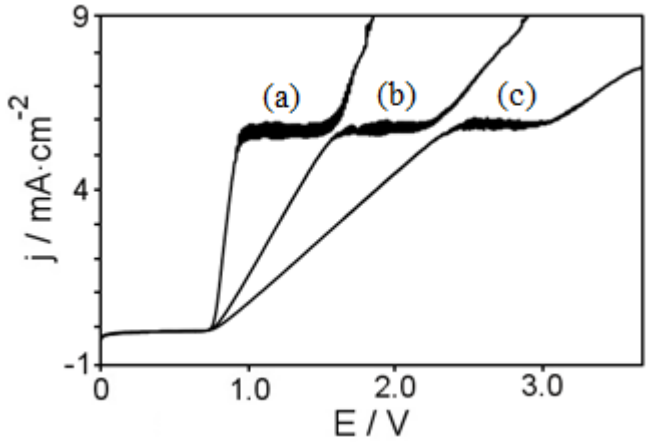

Figure 5.5 - Linear sweep voltammograms showing the effect of external resistance on the electro-oxidation of 0.075 M NaBr in 0.75 M H_2SO_4, performed at a scan rate of 1 mV/s. The resistors used were (a) 220 Ω, (b) 3900 Ω, (c) 8200 Ω.

Such a trend is, again, the same as that seen in the modeling of capacitance-mediated electrochemical oscillators [33]. Another notable difference in Figure 5.5 is a change in the slope of the positive branch of the oxidation peak during an LSV, shifting the oscillations to a higher potential range.

Using the applied current density as a control parameter, a linear galvanostatic sweep was performed at a scan rate of 1.0 x 10^{-5} mA/s. The shape of the galvanostatic linear voltammogram in Figure 5.6 shows that an excursion occurs at approximately 5.6 mA/cm^2, causing a jump from below 1.0 V (oxidation of Br^-) to above 1.5 V (oxygen production).

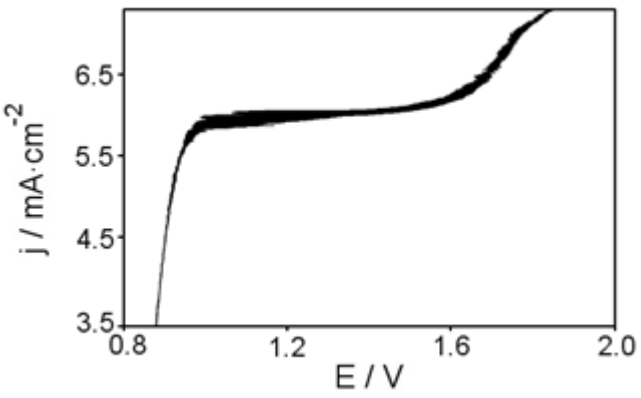

Figure 5.6 - Galvanodynamic experiment performed between 3.5 and 7.5 mA/cm^2 at a scan rate of 1.0 x 10^{-5} mA/cm^2. Reaction conditions were [NaBr] = 0.075 M and [H_2SO_4] = 0.75 M.

Figure 5.7 presents time series conducted at different constant currents. For the current above 5.7 mA/cm^2, potential oscillations occur in a range between 1.5 and 1.7 V (time series d) and begin to fluctuate aperiodically as the applied current increases. Time series (a to c) illustrate that when the applied current was between 1.6 mA/cm^2 and 4.5

mA/cm^2, sustained potential oscillations occurred between approximately 0.83 and 0.90 V.

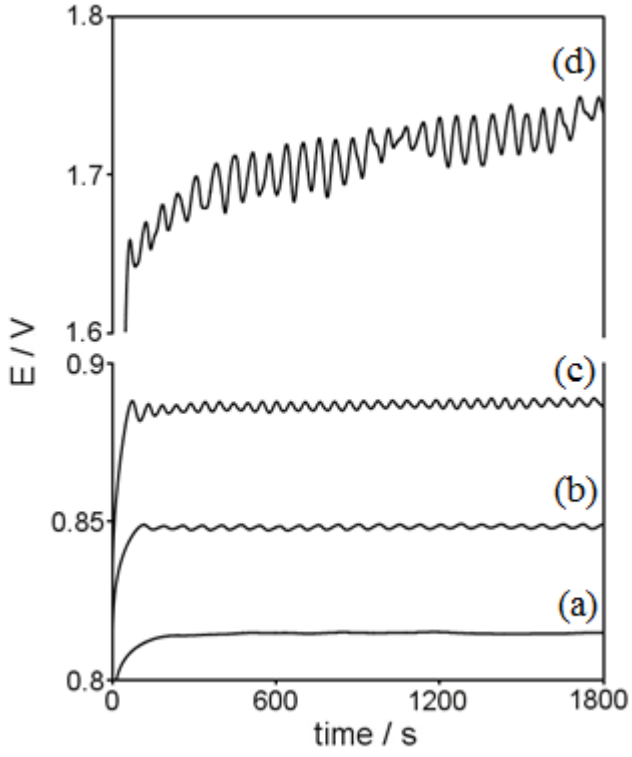

Figure 5.7 - Time series under galvanostatic conditions: (a) 0.3, (b) 1.6, (c) 3.8, and (d) 6.1 mA/cm^2. Other reaction conditions were: [NaBr] = 0.075 M and [H_2SO_4] = 0.75 M.

Figure 5.8 shows the effect of bromide concentration on the current oscillations. As can be seen in Figure 5.8a, at a bromide concentration of 0.012 M no oscillations occur. Once the concentration was increased to 0.025 M (Figure 5.8b), small amplitude oscillations in the current emerge after a brief induction period. A further increase to 0.05 M (Figure 5.8c) causes a decrease in the induction period and an increase in the amplitude and frequency of the oscillations. As can be seen in the time series (e) at a concentration of 0.125 M, the oscillations have a much higher frequency and an irregular

oscillation pattern. A yellow stream is visible, emanating from the working electrode at further increased concentrations of bromide, which is indicative of a high concentration of bromine being formed. A general trend in increased frequency with increase bromide concentration was observed here.

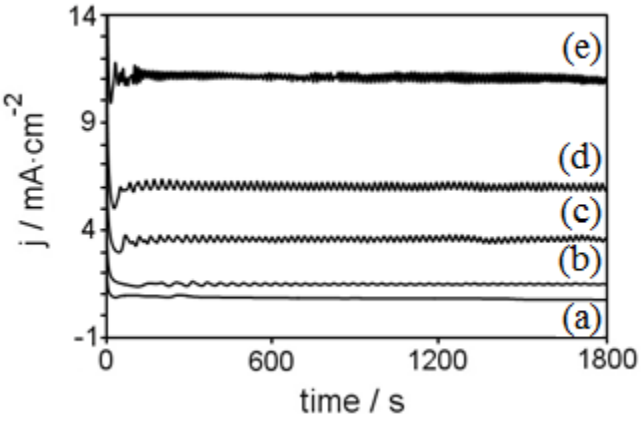

Figure 5.8 - Time series showing the effect that varying the concentration of NaBr has on the reaction behavior under potentiostatic conditions. The reaction solutions are: (a) 0.0125 M, (b) 0.025 M, (c) 0.05 M, (d) 0.075 M, and (e) 0.125 M. The concentration of H_2SO_4 was constant at 0.75 M and the applied potential was 1.2 V (vs. SCE)

In the absence of supporting electrolyte, only transient oscillations were observed, which lasted longer as the NaBr concentration was increased. There are more than 20 peaks in a 0.2 M NaBr solution (Figure 5.9d), as opposed to only 2 peaks in a 0.05 M NaBr solution (Figure 5.9a). A trend of increased oscillatory frequency when the concentration of bromide was increased was observed, which is similar to the result shown in Figure 5.8. The transitory nature of the oscillations may have been due to the absence of an inhibitory effect from such as supporting anions occupying the active sites. This speculation is supported by the fact that at the same bromide concentration the

oxidation current density is a lot higher in the absence of supporting electrolyte than that in the presence of H_2SO_4.

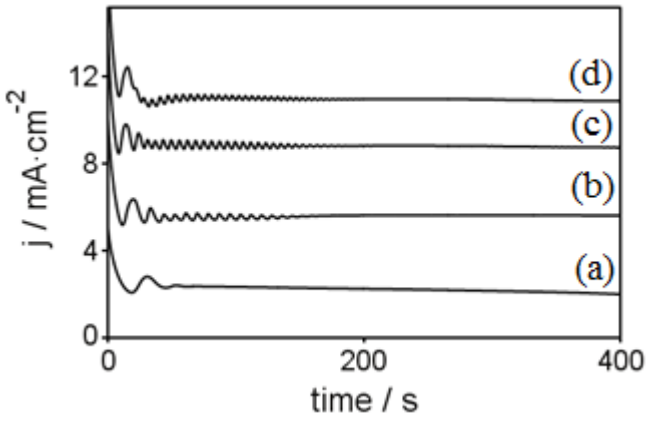

Figure 5.9 - Time series showing the effect that varying the concentration of NaBr without the presence of any supporting electrolyte has on the reaction behavior under potentiostatic conditions (the applied potential = 1.2 V). The [NaBr] was (a) 0.05 M, (b) 0.1 M, (c) 0.15 M, and (d) 0.2 M.

Figure 5.10 shows the effect of the supporting electrolyte H_2SO_4 on the nonlinear behavior, in which sustained periodic oscillations were present between 0.2 and 1.0 M H_2SO_4 (time series (b) and (c)). For H_2SO_4 concentration above 1.0 M the oscillations became irregular, however, the current density of the system remains within the region under which periodic oscillations were observed. Other supporting electrolytes such as potassium sulfate were used. Using 0.2 M K_2SO_4 was found to have nearly the same outcome as using 0.2 M H_2SO_4 supporting electrolyte, suggesting that pH of the solution does not play an essential role in the observation of nonlinear instability.

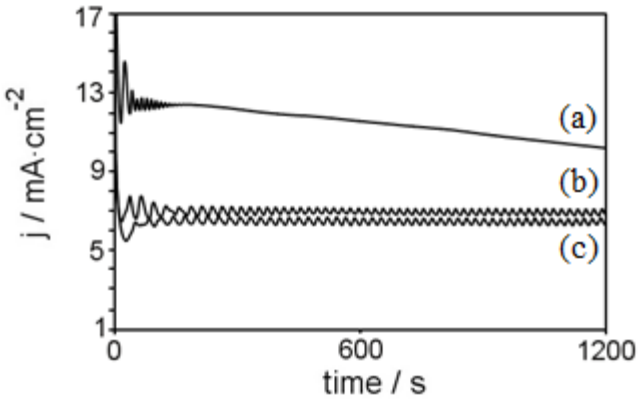

Figure 5.10 - Potentiostatic experiments at an applied potential of 1.2 V (vs. SCE) showing the effect influence of the supporting electrolyte by varying the concentration of sulfuric acid: (a) 0 M, (b) 0.3 M and (c) 0.75 M. The concentration of NaBr was 0.075 M.

Figure 5.11 presents cyclic voltammograms (CVs) of the three solutions investigated in Figure 5.10. There are noticeable changes in the CVs, including the peak potential. Variation in the peak potential as well as the limiting current is likely responsible for the transformation to transient oscillations seen in Figure 5.10.

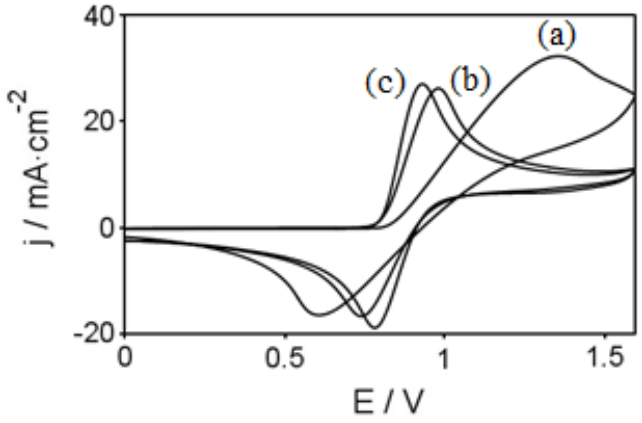

Figure 5.11 - Cyclic voltammograms at a scan rate of 100 mV/s of 0.075 M NaBr dissolved in (a) 0, (b) 0.1 M, and (c) 0.3 M H_2SO_4.

The decrease of the solution resistance from 300 Ω (a) to 5 Ω (c) is also likely playing an important role here, although oscillations have been seen over a broad resistance range.

5.3.1 Mechanistic Discussion

In this system it is necessary to separetly analyze the oscillations occurring in current density and those occurring in potential. For the current oscillations occurring between the applied potentials of 0.85 V and 1.4 V, the electro-oxidation of bromide ions likely belongs to the class of electrochemical oscillators known as capacitance-mediated positive differential resistance oscillators, which relies on the formation and dissolution of inhibiting surface layers. Here, the inhibiting layer (capacitor) is established through tribromide complexes (Br_3^-), where its formation and dissolution is described as $Br_2 + Br^- \rightleftharpoons Br_3^-$ [2,3]. The anodic current J_{ox} is proportional to $(U - \Delta\varphi_{sl})$, where U equals $\Delta\varphi_{dl}$ (double layer potential) in the absence of ohmic series resistance and $\Delta\varphi_{sl}$ is the potential drop of the inhibiting solution layer Br_3^-. When J_{ox} increases, the capacitance of the inhibiting solution layer Br_3^- (C_{sl}) increases, which results in the decrease of $\Delta\varphi_{sl}$. Consequently, the term $(U - \Delta\varphi_{sl})$ increases, which subsequently leads to the increase of J_{ox}. Therefore, a positive feedback loop is established through $\Delta\varphi_{sl}$. As discussed by Zensen and co-workers [33], this positive feedback loop requires a positive differential resistance of the current-potential curve J_{ox} $(U - \Delta\varphi_{sl})$. The formation of tribromide complexes, meanwhile, causes a decrease of reactant ion Br^-, implementing a negative feedback on J_{ox}.

Oscillations in potential occurring under galvanostatic conditions were seen to occur in two regions as shown in Figure 5.6, between 0.83 and 0.9 V (current below limiting current) and above 1.6 V (current above limiting current). For the oscillations

occurring while the applied current is below the limiting current the feedback is implemented by the reaction between the anodic oxidation product Br_2 and reactant Br^-, which causes the accelerated decrease of Br^- concentration (i.e. faster than the consumption by anodic oxidation). It consequently forces the potential to increase in order to maintain the current density (i.e., generating a positive feedback). When the potential increases to the point where the anodic reaction becomes limited by the diffusion-transportation of Br^- ions, Br_2 production is slowed down and the dissociation of Br_3^- overwhelms its formation, making a positive contribution to the increase of Br^- concentration. As a result, the required potential for maintaining the current decreases.

Above the limiting current, when the oscillations in potential occur above 1.6 V, the observation of bubble formation and detachment suggests that those oscillations may be accounted for on the basis of convection-driven feedbacks [32], where as a current larger than the limiting current (stationary) is imposed, the surface concentration of Br^- ions depletes to zero due to the limited supply rate by diffusion. This depletion implements a negative feedback. Meanwhile, the potential moves to the higher side of the plateau with the decrease of the Br^- surface concentration until oxygen evolution takes place to keep up the applied current. Because growth, detachment, and movement of bubbles produce a forced convection that replenishes the surface concentration Br^- ions, oxygen evolution is thus repressed and the potential drops again [32]. Li and co-workers have demonstrated that convection-enhanced mass transportation can induce oscillatory behavior in both current and potential. In the system studied here mass transportation of Br^- affects the formation of the inhibitory layer, Br_3^-. The thickness of the inhibitory layer has been reported to be an important quantity in the capacitance-mediated

electrochemical oscillator [33]. To examine such a factor, rotating disk experiments were undertaken in Figure 5.12 to determine if oscillations persist when the diffusion layer was decreased through forced convection. It was found that rotation speeds of just 50 rpm were capable of quenching the oscillatory behavior. This confirms that the diffusion layer plays an important role in the current and potential oscillations seen here.

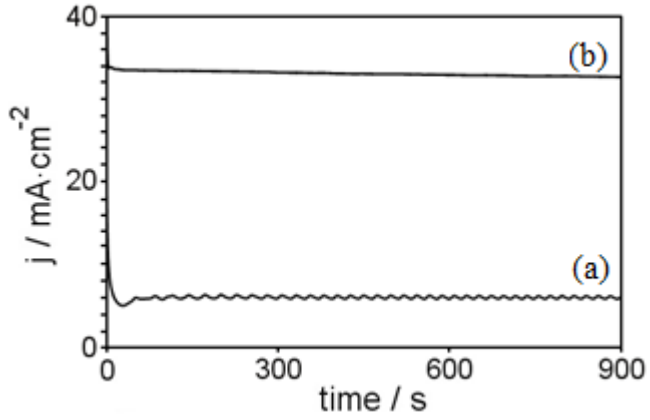

Figure 5.12 - Potentiostatic experiments performed with a Pt rotating disk electrode with various rotation speeds: (a) 0 rpm and (b) 50 rpm. Reaction conditions were [NaBr] = 0.075 M and [H_2SO_4] = 0.75 M, and the applied potential was 1.0 V (vs. SCE).

5.4 Conclusions

Bromide ions have been known to have great effects on the nonlinear behavior of a number of electrochemical reactions; however, there was no report on the nonlinear instabilities of their own. This research illustrates that electro-oxidation of bromide ions at a Pt electrode could undergo sustained oscillations in both current and potential over a broad bromide concentration range. The supporting electrolytes can be sulfuric acid, potassium sulfate, or potassium nitrate, suggesting that pH of the solution does not play an essential role in the observed oscillations. Under galvanostatic conditions two regions

of oscillatory behavior emerged, which correspond, respectively, to the peak oxidation potentials of bromide and hydroxide ions. Oscillations seen on the second positive differential resistance branch are likely governed by convection driven processes, as supported by the vigorous bubble formation at the electrode.

Current oscillations observed at the low potential range between 0.85 and 1.5 V, however, have several features associated with a capacitance-mediated positive differential resistance oscillator [33,34], which include (1) taking place at a current plateau in an LSV, (2) occurring without an external resistor, (3) having a decreased amplitude with the increase of external resistance, (4) occurring on a positive differential resistance branch, and (5) demonstrating resonance behavior in the admittance spectra. In our experiments, current oscillations are seen in both the forward and reverse CV scans. In this system, the formation and dissolution of tribromide complexes are proposed to be responsible for the capacitance-mediated nonlinear instability.

5.5 References

[1] B. E. Conway, Y. Phillips, S. Qian, *J. Chem. Soc. Faraday Trans.* **1995**, 91, 283-293.

[2] P. K. Adanuvor, R. E. White, *J. Electrochem. Soc.* **1987**, 134, 1450-1454.

[3] J. Xu, N. S. Georgescu, D. A. Scherson, *J. Electrochem. Soc.* **2014**, 161, H392-H398.

[4] V. Livshits, A. Ulus, E. Peled, *Electrochem. Commun*. **2006**, 8, 1358-1362.

[5] R. M. Noyes, *J. Am. Chem. Soc.* **1980**, 102, 4644-4649.

[6] M. Orbán, P. De Kepper, I. R. Epstein, *J. Am. Chem. Soc.* **1982**, 104, 2657-2658.

[7] R. H. Simoyi, I. R. Epstein, *J. Phys. Chem.* **1987**, 91, 5124-5128.

[8] J. Li, J. Wang, *Phys. Chem. Chem. Phys.* **2011**, 13, 15539-15545.

[9] J. Zheng, W. Huang, S. Chen, Z. Niu, Z. Li, *Electrochem. Commun.* **2006**, 8, 600-604.

[10] Y. Mukouyama, M. Kikuchi, H. Okamoto, *J. Solid State Electrochem.* **2005**, 9, 290-295.

[11] M. Orlik, *Self-Organization in Electrochemical Systems I: General Principles of Self-Organization. Temporal Instabilities*; Springer, Berlin, 2012.

[12] K. Krischer, *Nonlinear Dynamics in Electrochemical Systems,* in R.C. Alkire, D. M. Kolb (Eds), *Advances in Electrochemical Science and Engineering*, Vol. 8; Wiley-VCH, New York, 2003.

[13] I. Z. Kiss, T. Nagy, V. Gaspar, *Dynamical Instabilities in Electrochemical Processes,* in V. V. Kharton (Ed), *Solid State Electrochemistry II: Electrodes, Interfaces, and Ceramic Membranes*, Vol. 1; Wiley-VCH, New York, 2011.

[14] M. T. M. Koper, J. H. Sluyters, *J. Electroanal. Chem.* **1994**, 371, 149-159.

[15] I. Z. Kiss, W. Wang, J. L. Hudson, *Phys. Chem. Chem. Phys.* **2000**, 2, 3847-3854.

[16] M. T. M. Koper, *Electrochim. Acta* **1992**, 37, 1771-1778.

[17] R. Nagao, I. R. Epstein, E. R. Gonzalez, H. Varela, *J. Phys. Chem. A* **2008**, 112, 4617-4624.

[18] J. L. Hudson, T. T. Tsotsis, *Chem. Eng. Sci.* **1994**, 49, 1493-1572.

[19] Y. Mukoutama, S. Nakanishi, H. Konishi, Y. Ikeshima, Y. Nakato, *J. Phys. Chem. B* **2001**, 105, 10905-10911.

[20] M. G. T. Fechner, *J. Schweigger fur Chem. Phys.* **1828**, 53, 129-151.

[21] J. J. Podesta, R. C. V. Piatti, A. J. Arvia, *J. Electrochim. Soc.* **1979**, 8, 1363-1367.

[22] Z. H. Gu, J. Chen, T. Z. Fahidy, *Electrochim. Acta* **1992**, 37, 2637-2644.

[23] O. Lev, M. Sheintuch, L. M. Piseman, C. Yarnitzkyt, *Nature* **1988**, 336, 458-459.

[24] H. Varela, K. Krischer, *Catal. Today* **2001**, 70, 411-425.

[25] J. A. O'Brien, J. T. Hinkley, S. W. Donne, *Electrochim. Acta* **2011**, 56, 4224-4230.

[26] Z. Du, Q. Gao, J. Feng, Y. Lu, J. Wang, *J. Phys. Chem. B* **2006**, 110, 26098-26104.

[27] W. Bi, Y. He, M. F. Cabral, H. Varela, J. Yang, R. Jiang, Q. Gao, *Electrochim. Acta* **2014**, 133, 308-315.

[28] P. Strasser, M. Lubke, F. Raspel, M. Eiswirth, G. Ertl, *J. Chem. Phys.* **1997**, 107, 979-990.

[29] J. Lee, C. Eickes, M. Eiswirth, G. Ertl, *Electrochim. Acta* **2002**, 47, 2297-2301.

[30] P. Strasser, M. Eiswirth, M. T. M. Koper, *J. Electroanal. Chem.* **1999**, 478, 50-66.

[31] K. Krischer, *Principles of Temporal and Spatial Pattern Formation in Electrochemical Systems,* in B. E. Conway, J. O. M. Bockris, R. White (Eds), *Modern Aspects of Electrochemistry*, Vol. 32; Plenum, New York, 1999.

[32] Z. L. Li, J. L. Cai, S. M. Zhou, *J. Electroanal. Chem.* **1997**, 436, 195-201.

[33] C. Zensen, K. Schonleber, F. Kemeth, K. Krischer, *J. Phys. Chem. C* **2014**, 118, 24407-24414.

[34] F. Ozanam, N. Blanchard, J. N. Chazalviel, *Electrochim. Acta* **1993**, 38, 1627-1630.

CHAPTER 6 - ELECTROCHEMICAL OSCILLATIONS DURING THE OXIDATION OF IMPORTANT SULFUR CONTAINING SPECIES

6.1 Introduction

Dynamic instabilities in electrochemical reactions have been a topic of great interest ever since the first report of oscillating current in an electrochemical cell in 1828 [1-4]. Oscillations in electrochemical systems have been uncovered during the oxidation or reduction of various organic and inorganic substances as well as during the corrosion of various metals [5-13]. For example, the dissolutions of vanadium, iron, copper, nickel, and cobalt (amongst others) have been found to lead to oscillatory behavior [14-20]. In corrosion-driven nonlinear electrochemical systems, upon an increasing applied potential, the system goes through three distinct regions, which become visible on polarization curves. Firstly, the current increases as the metal is oxidized in the active region; the abrupt decrease in current at the Flade potential is caused by the onset of the passive region; finally, at sufficiently high applied potentials, the passive layer is destroyed due to the formation of oxygen bubbles caused by the oxidation of hydroxide ions [2]. The passivation of the electrode causes the presence of negative differential resistance (NDR), which is a prerequisite for an electrochemical system's classification as an electrochemical oscillator [21,22]. Electrochemical oscillators are classified differently depending on the location of their NDR, whether it is hidden on a positive slope (HN-NDR) or whether it is on a negative branch (N-NDR). Koper described a method for determining the presence of NDR through the use of Electrochemical Impedance Spectroscopy (EIS), through the plotting of Nyquist diagrams [23,24]. In systems that contain NDR the double layer potential (φ_{dl}) acts as an essential variable (autocatalytic in

the case of N-Shaped plots or acting as the slow variable in S-Shaped plots) occurring at regions of negative Faradic resistance [25]. The oscillations in these types of systems arise through the presence of a positive feedback loop (supplied through the NDR) and a negative feedback loop (surface coverage of a potential dependent adsorbed species or surface concentration of an electroactive species) [23,25]. Nyquist diagrams have been useful in locating regions of NDR in various systems such as ethanol, formaldehyde, H_2, formic acid, and others [5,26-32].

Sulfur-containing compounds have very important functions in a variety of areas ranging from industrial applications to biochemical processes [33-36]. In fact, much attention in nonlinear electrochemical systems focuses on sulfur compounds due to potential access through oxidation/reduction to reach multiple oxidation states, leading to rich dynamical behavior being observed in sulfur based electrochemical systems, such as thiosulfate, thiourea, and hydrogen sulfide [37-42]. Temporal oscillations have been reported in systems utilizing sulfur compounds, and various interesting spatial patterns have been observed in reaction diffusion experiments [43-46]. In this study the electrochemical oxidation of two important sulfur-based compounds were investigated.

Firstly, the compound hydroxymethanesulfinate (HMS) was chosen, as it is an important sulfur based reducing agent and has been used in the reduction of vat dyes, in anticancer formulations as an antioxidant stabilizer, and in emulsion polymerization experiments as a redox initiator [47-49]. Earlier studies have shown that the decomposition of HMS may occur in parallel with main reactions, resulting in the conspicuous consumption of the reagent in the industrial process. Polenov and coworkers have developed a kinetic model for the decomposition of HMS in aqueous solution [50].

The investigation of its electrochemical reaction behavior shall provide useful insights into the chemical stabilities. The fact that HMS contains a hydroxyl group as well as a sulfur atom also makes this kinetic study particularly interesting due to the fact that very rich nonlinear phenomena have recently been observed during the oxidation and bromination of aromatic compounds containing hydroxyl functional groups [51-53]. As shown in the following, oscillations in both potential and current density are observed at Pt and Au electrodes. Notably, the oxidation products of HMS show strong interactions with Au, leading to severe pitting of the Au surface.

Methionine is one of two sulfur-containing proteinogenic α-amino acids (cysteine being the other) and is crucial to many biological functions such as its important role as an initiator in protein synthesis [54]. In biological systems, its oxidation also plays an important role in protein stability and can lead to biological damage depending on the nature of the oxidant involved [55]. Apart from biology, methionine has been found to form Self-Assembled Monolayers (SAMs) on gold surfaces [56], suggesting that a study of its oxidation on a gold electrode could provide insights into not only relevant biochemical processes, but could also lead to useful information to material chemists researching applications of methionine - gold SAMs. This study reports on the discovery of electrochemical oscillations during the oxidation of methionine on a gold electrode. Dissolution of the gold electrode was found to occur, and likely plays a significant role in the nonlinear behavior.

6.2 Experimental Procedures

The electrochemical experiments were performed on a Voltalab PGZ100 system (Radiometer Analytical, USA) and CHI 660D/760E (CHI Instruments, Texas, US). Polycrystalline platinum and gold electrodes with diameters of 2.0 mm (CHI Instruments) were applied as working electrodes. The counter electrode was a platinum film (Shanghai Ruosull Technology Co., LTD) and a saturated calomel electrode (SCE) was applied as the reference electrode. Before each experiment the working electrode was polished with consecutively finer grades of alumina powder, rinsed with double distilled water, cleaned by an ultrasonic cleaner (Branson 1510, USA) for 10 minutes, and again rinsed with double distilled water. The three electrodes were placed in the traditional triangle configuration and all electrochemical experiments were performed at room temperature ($22 \pm 2\ ^{o}C$).

Reagents sodium hydroxymethanesulfinate ($CH_3NaO_3S \cdot 2H_2O$, 98+%), l-methionine ($C_5H_{11}NO_2S$, 98+%), potassium ferricyanide ($K_3Fe(CN)_6$, 99%) and potassium chloride (KCl, 99+%) were purchased from Sigma Aldrich. All reactions investigating HMS contained 0.2 M sodium hydroxymethanesulfinate (with no additional supporting electrolyte), unless otherwise stated. All reactions investigating methionine contained 0.05 M l-methionine in 0.1 M KCl, unless otherwise stated. Reaction volumes were held constant at 60.0 mL, and all experiments were performed under ambient conditions (no purging with inert gases). Electrochemical impedance spectroscopy experiments were measured in the frequency range of 100 kHz to 34 mHz (unless otherwise stated) with an amplitude of 5 mV and 12 points per frequency decade were collected. Scanning electron microscopy (SEM) and energy-dispersive X-ray

spectroscopy (EDS) were performed with a Quanta 200 FEG microscope (FEI, Inc.). Mass Spectrometry measurements were taken on a Micromass LCT - electrospray ionization time-of-flight mass spectrometer. Images were also taken with a charge coupled device (CCD) camera equipped with a zoom lens.

6.3 Results and Discussion

6.3.1 Oxidation Behavior of Hydroxymethanesulfinate on a Au Electrode

Figure 6.1 shows the chemical structure of hydroxymethanesulfinate (HMS).

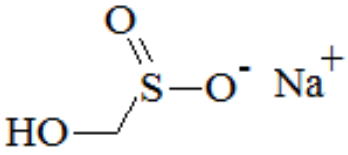

Figure 6.1 - Chemical Structure of sodium hydroxymethanesulfinate

Figure 6.2 shows a linear sweep voltammogram (LSV) at a scan rate of 0.5 mV/s. Using such a low scan rate allows one to mimic potentiostatic conditions where the applied potential can be considered a control parameter, gaining information on the various dynamic regimes of the system. Here, oscillations with a high frequency emerged at around 0.8 V (vs. SCE electrode) and existed over a large potential range (0.8 - 2.0 V). At even higher potentials, vigorous bubble formation was seen, indicating that the oxidation of hydroxide ions became significant under those conditions.

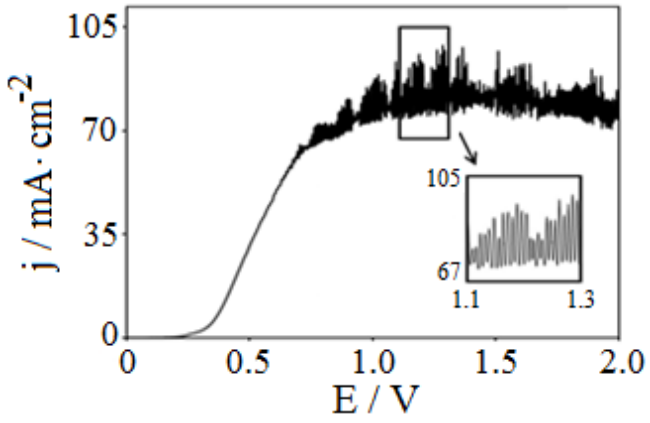

Figure 6.2 - Linear sweep voltammogram performed with a scan rate of 0.5 mV/s, in a solution of 0.2 M HMS. Experiment was performed on a gold working electrode

Figure 6.3 shows a current ramp experiment performed between 47 and 70 mA/cm^2 at a scan rate of 3.2 x10^{-3} mA/cm^2/s. As can be seen here, high frequency potential oscillations occur, which grow in amplitude as the current is increased.

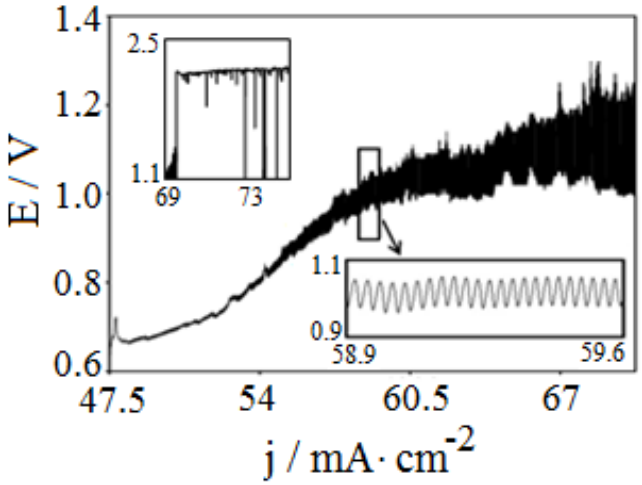

Figure 6.3 - A current ramp experiment between 47 mA/cm^2 and 70 mA/cm^2 mA at a scan rate of 1.0 x 10^{-4} mA/s, in a solution of 0.2 M HMS. Experiment performed on a gold working electrode.

Past 70 mA/cm^2, large bubbles may form on the working electrode, which causes an immediate jump in the potential to approximately 2.2 V, which then returns to the low potential once the bubble bursts, as shown in the inset in Figure 6.3

The effect of altering the applied potential on the electrochemical oscillations is shown in Figure 6.4. At a constant external potential of 0.9 V (Figure 6.4a) the current density can be seen to decrease while oscillations of a moderate frequency persist for approximately 10 min before low frequency, low amplitude oscillations emerge. When the potential was increased to 1.0 V (Figure 6.4b), the current density again decreased at the onset of the reaction reaching a stable current density after approximately 5 min. The amplitude and frequency of the oscillations had increased in comparison to the results of Figure 6.4a. Complex behavior in the form of quasi-periodic oscillations was found to emerge when the applied potential was between 1.2 V and 1.3 V (Figure 6.4d and Figure 6.4e). At these potentials there was no decrease in current density at the onset of the reaction, and increasing the external potential caused an increase in the mean current density around which the system oscillated. A further increase in the potential to 1.5 V caused the current density to again decrease where low frequency, small amplitude simple oscillations were observed.

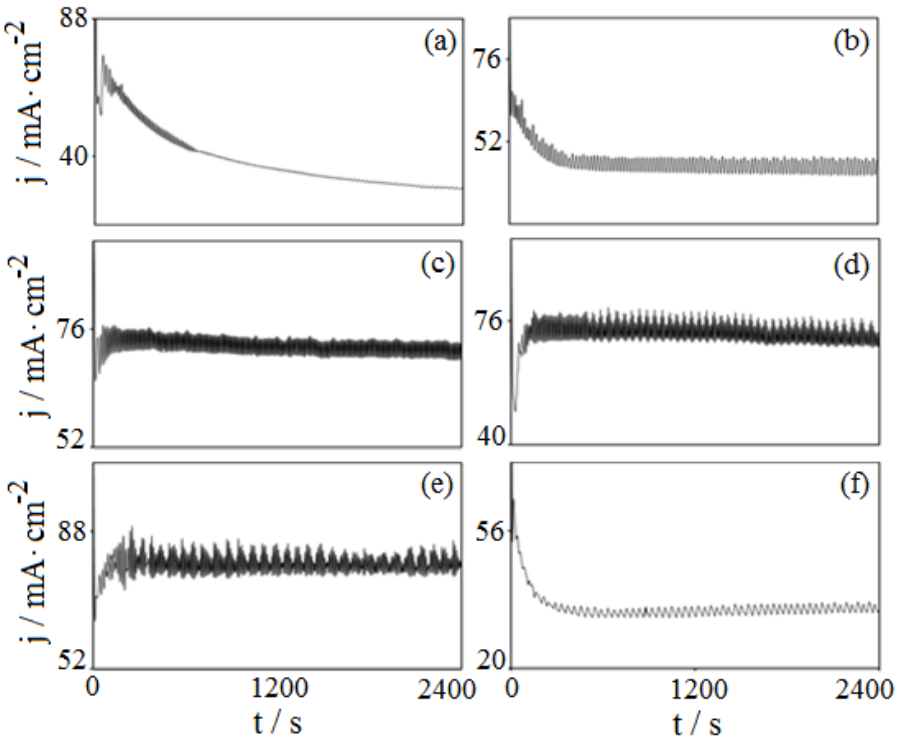

Figure 6.4 - Time series showing the effect that varying the applied potential has on the reaction behavior of a 0.2 M HMS solution. The applied voltages are: (a) 0.9 V, (b) 1.0 V, (c) 1.1 V, (d) 1.2 V, (e) 1.3 V, and (f) 1.5 V (vs. SCE). A gold working electrode was employed.

The above observed oscillations are not transitory and could last for several hours, but become irregular as the time period increased. The frequency of the oscillations seen under potentiostatic conditions on gold were seen to range from 43 mHz at an applied potential of 1.0 V, which increased to 95 mHz at applied potentials of 1.2 and 1.3 V, before decreasing to 25 mHz at 1.5 V. According to literature, nonlinear behavior of sulfur compounds electrochemically oxidized on a gold surface has only been observed once [38], for the oxidation of thiosulfate. Bi et al. found that the frequency of oscillations under potentiostatic conditions was significantly higher than that found in

this study, where frequencies of 200 and 360 mHz were found for simple oscillations, and increased to as high as 480 mHz during complex behavior. Figure 6.5 shows galvanostatic experiments performed at different applied current densities, the results of which are consistent with the current ramp results shown in Figure 6.3.

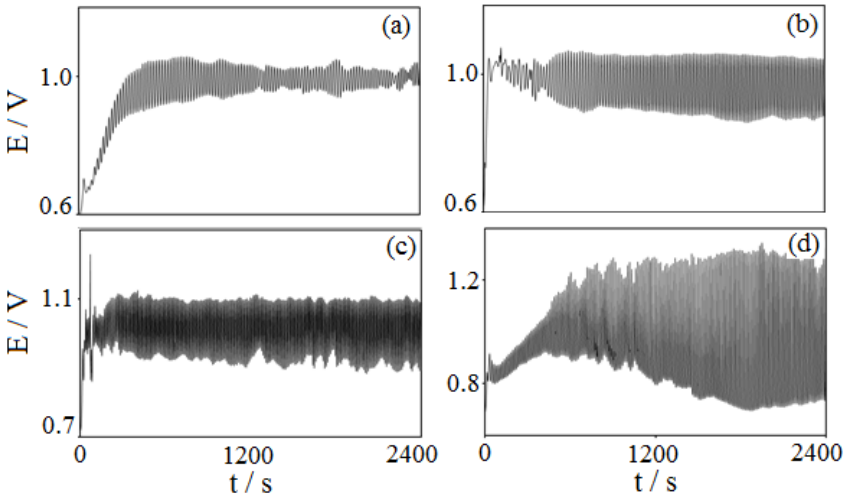

Figure 6.5 - Time series showing the effect that varying the applied current has on the reaction behavior of a 0.2 M HMS solution. The applied currents are: (a) 51 mA/cm^2, (b) 54 mA/cm^2, (c) 64 mA/cm^2, and (d) 70 mA/cm^2. A gold working electrode was employed.

At an applied current density of 51 mA/cm^2 the potential rises from approximately 0.7 V to 1.0 V while oscillating. Increasing the current density to 54 mA/cm^2 (Figure 6.5b) the frequency and amplitude of the oscillations increase substantially, as does the amount of time required for the system to reach its stable oscillatory potential. In Figure 6.5c very high frequency oscillations occur between 0.9 and 1.1 V with some variation in the waveform, again, which resembled quasi-periodic oscillations. When the applied current density is increased further to 70 mA/cm^2 very

high amplitude potential oscillations emerge which reach maximum amplitude of about 0.6 V.

Varying the concentration of HMS was found to have a substantial effect on the nonlinear behavior (Figure 6.6), in which experiments were run under potentiostatic conditions with the applied potential of 1.0 V. At 0.4 M HMS (Figure 6.6a) irregular oscillations emerge, which become more regular when the concentration was decreased to 0.3 M (Figure 6.6b). Stable oscillations occurred at both 0.2 M and 0.1 M (Figures 6.6c and 6.6d); however, a brief induction time was observed before oscillations emerged at the HMS concentration of 0.1 M. An obvious trend in decreasing current density with decreasing HMS concentration can be observed in Figure 6.6. At an HMS concentration of 0.05 M, no oscillations were found.

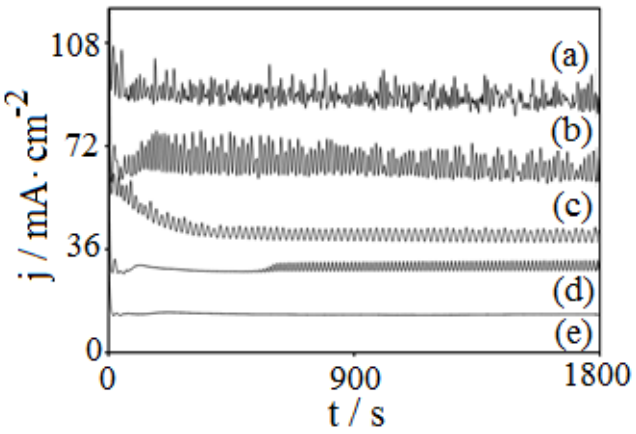

Figure 6.6 - Time series showing the effect that varying the concentration of HMS has on the reaction behavior under a potentiostatic condition (1.0 V vs. SCE). The reaction solutions are: (a) 0.4 M, (b) 0.3 M, (c) 0.2 M, (d) 0.1 M, and (e) 0.05 M. A gold working electrode was employed.

As that was confirmed through mass spectrometry, thiosulfate is one of the products formed during the electro-oxidation of HMS. Thiosulfate is a disproportionation product of dithionite, one of the precursor compounds (together with formaldehyde), which are used to form HMS. Compounds such as thiosulfate, thiourea, and sulfite have been reported as being capable of causing Au dissolution under certain conditions [57-59]. Thiosulfate is capable of forming a complex with gold in aqueous solutions according to: $Au + 2S_2O_3^{2-} \rightarrow Au(S_2O_3)_2^{3-} + e^-$. The gold-thiosulfate complex is soluble and leads to the dissolution of the gold electrode [57]. To shed light on this issue, CCD images of the Au electrode prior to the electrochemical reaction and after multiple long time scale reactions (cleaned ultrasonically after each reaction) are presented respectively in Figure 6.7a and Figure 6.7b, which clearly demonstrate the occurrence of pitting on the Au electrode.

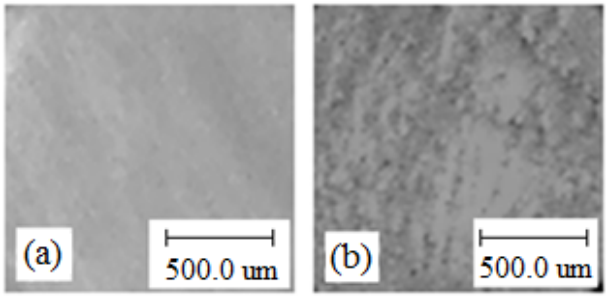

Figure 6.7 - (a) CCD image of gold electrode before electrochemical reaction in 0.2 M HMS solution and (b) CCD image of gold electrode after multiple electrochemical reactions showing pitting on the surface.

Careful examination showed that a black film formed on the gold electrode at the applied potentials above 1.0 V when the experiments were run for an extended period of time. Figure 6.8a and 6.8b show scanning electron microscopy (SEM) images of the film,

which formed on the Au electrode. The film appears to have a very porous structure, and cavities are present, which are likely caused due to the continuous dissolution of the thus-formed Au-sulfur complexes. Energy-dispersive X-ray spectroscopy (EDS) results of the corresponding film (see Figure 6.8c) indicate the presence of sulfur as well as oxygen in the film. The carbon element in the EDS comes from the conductive tape used for the sample preparation. To understand the importance of Au dissolution (i.e., the formation of Au complexes) in the above-observed rich nonlinear behavior, electro-oxidation of HMS was also performed on a Pt surface in this study.

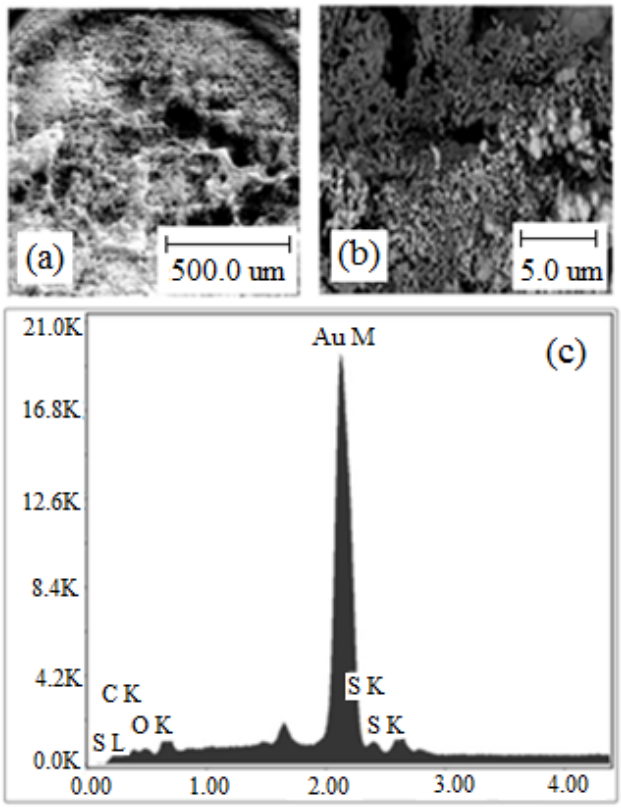

Figure 6.8 - (a) and (b) SEM images of the black film which formed on the gold surface and (c) EDS spectrum of the porous black film.

6.3.2 Oxidation Behavior of Hydroxymethanesulfinate on a Pt Electrode

Figure 6.9a shows an LSV performed at a scan rate of 0.5 mV/s, where there are low frequency fluctuations in the response current in two regions: between 0.6 and 1.0 V and above 1.6 V. Potentiostatic experiments were subsequently conducted in and around the two dynamically unstable regions. At a potential of 0.6 V, short-lived irregularities in the current density were observed (Figure 6.9b(i)). Increasing the potential to 0.65 V caused approximately 10 oscillations to occur (see Figure 6.9b(ii)) and a further increase to 0.7 V increased the number of oscillations and the length of the oscillatory window (Figure 6.9b(iii)).

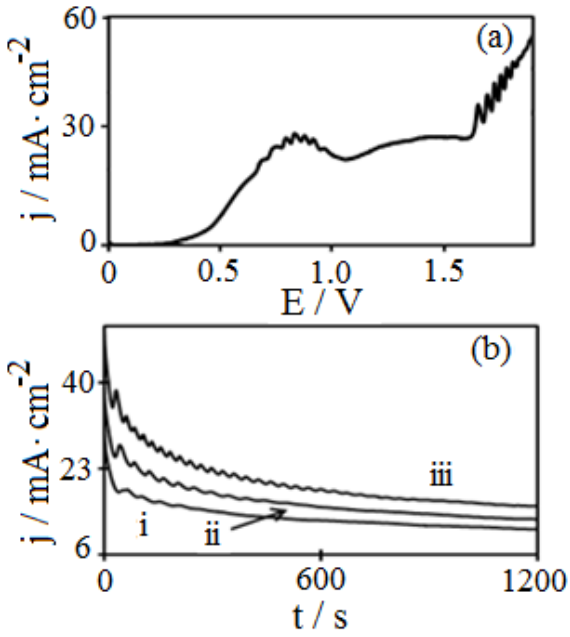

Figure 6.9 - (a) Linear sweep voltammogram 0.2 M HMS solution performed with a scan rate of 0.5 mV/s. (b) Potentiostatic experiments at applied potentials (i) 0.6 V, (ii) 0.65 V, and (iii) 0.7 V (vs. SCE). A platinum working electrode was employed.

Further increases in potential to above 0.8 V, however, caused the oscillations to vanish. Notably, on the platinum surface, the observed oscillations are always transitory and all attempts to achieve long lasting stable oscillations under the potentiostatic conditions were unsuccessful. No oscillations were present with the applied potentials ranging from 1.5 - 1.9 V, which correspond to the second oscillatory regime observed in Figure 6.9a. The frequencies of the transient oscillations ranged from 13 mHz at 0.6 V to 33 mHz at 0.7 V. Unlike gold, nonlinear phenomena have been extensively studied on platinum, allowing for a more thorough comparison of the behavior of HMS on Pt to other sulfur based systems. Interestingly, the electro-oxidation of thiosulfate on platinum was found to have a much lower oscillatory frequency (6.5 - 18 mHz) [39] than was observed when oxidized on a gold surface, which is the same phenomenon found in this study. Other compounds such as sulfur dioxide [42] had higher frequency oscillations under potentiostatic conditions (60.90 - 64.39 mHz), and the electrochemical oxidation of thiourea on platinum [41] produced oscillations with frequencies between 50 and 70 mHz.

Figure 6.10 presents several galvanostatic experiments at the Pt electrode. In order to avoid overlap in the time series, the time series labeled (a) has been shifted down by 0.1 V and the time series labeled (e) has been shifted upward by 0.1 V. At an applied current of 12.7 mA/cm^2 (time series (a)) transient small amplitude oscillations emerged between 0.6 and 0.7 V. Increasing the current density from 14.3 to 15.3 mA/cm^2 (time series (b) and (c)) shows oscillations in potential beginning around 0.7 V and lasting until approximately 0.9 V, before a potential spike occurred after which no oscillations emerged. At 15.9 mA/cm^2, after a few oscillations the potential spiked and stable large

amplitude low frequency oscillations began. A further increase to 19.1 mA/cm^2 caused a similar rapid increase in potential, after which stable oscillations were developed with smaller amplitude and higher frequency than those obtained at 15.9 mA/cm^2. No bubble formation was observed on the platinum electrode when the potential was oscillating at such a high potential. In contrast to the behavior under potentiostatic conditions, stable oscillations were found to emerge under the galvanostatic conditions, which occurred in the second oscillatory region seen in Figure 6.9a.

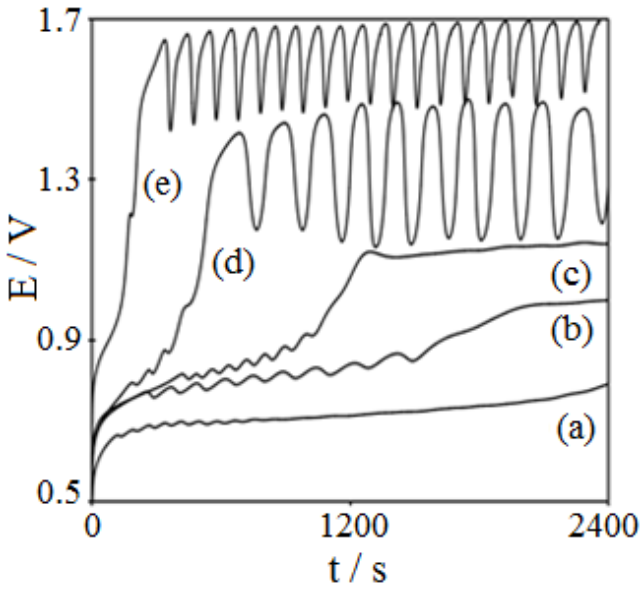

Figure 6.10 - Time series showing the effect that varying the applied current density has on the reaction behavior of a 0.2 M HMS solution. The applied currents are: (a) 12.7 mA/cm^2, (b) 14.3 mA/cm^2, (c) 15.3 mA/cm^2, (d) 15.9 mA/cm^2, and (e) 19.1 mA/cm^2. A platinum working electrode was employed.

Analysis of the Pt electrode with a CCD camera prior and after the electrochemical oxidation of HMS does not show the occurrence of pitting. However, characterizations of the Pt electrode with SEM (Figure 6.11a) and EDS (Figure 6.11b) illustrate that the oxidation of HMS has resulted in the partial coverage of the Pt surface by sulfur compounds.

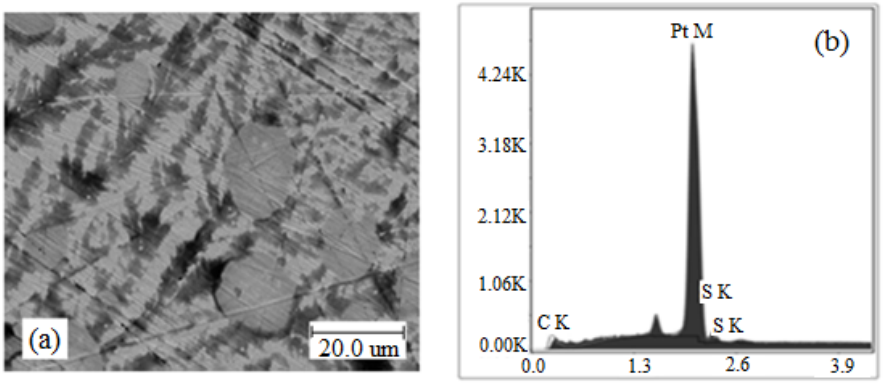

Figure 6.11 - (a) SEM image showing the presence of a film on the Pt surface, (b) EDS spectrum of formed film on Pt electrode which indicates the film contains sulfur.

The formation of a film on the Pt electrode was further confirmed by electrochemical impedance spectroscopy (EIS) in Figure 6.12, which shows the behavior in a 2 mM ferricyanide solution of (a) a bare Pt electrode, (b) a Pt electrode having been used for 100 s and (c) a Pt electrode having been used for 1200 s at 1.0 V in an HMS solution.

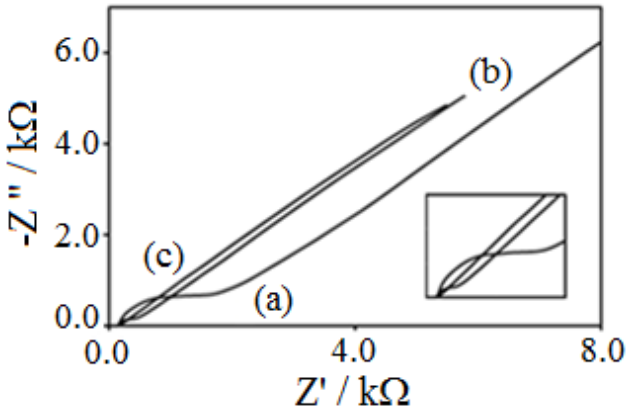

Figure 6.12 - EIS spectrum of (a) a bare Pt electrode, (b) Pt electrode used for 100 s in a HMS oxidation and (c) Pt electrode used for 1200 s in a HMS oxidation reaction.

As can be seen, the behavior of the bare Pt electrode showed a semicircle and straight line, however, the Pt electrode used for 100 s demonstrated a significantly smaller semicircle, and the electrode used for 1200 s (Figure 6.12c) showed virtually no semicircle. The above results provide strong evidence that the Pt electrode has been covered by the oxidation products of HMS, leading to the passivation of the active surface and the development of negative differential resistance in the system. Under galvanostatic conditions, however, the lowered surface activity due to the partial coverage would force the system to adjust to a higher potential value in order to maintain the constant current. This in turn might become powerful enough to oxidize/remove the deposition layer. Then, the revived surface activity should lead the system to return to a low potential in order to ensure the constant current. As such, sustained oscillations in the potential were developed. As shown in Figure 6.13, the deposit can be electrochemically dissolved at the applied potentials where electrochemical oscillations have been observed.

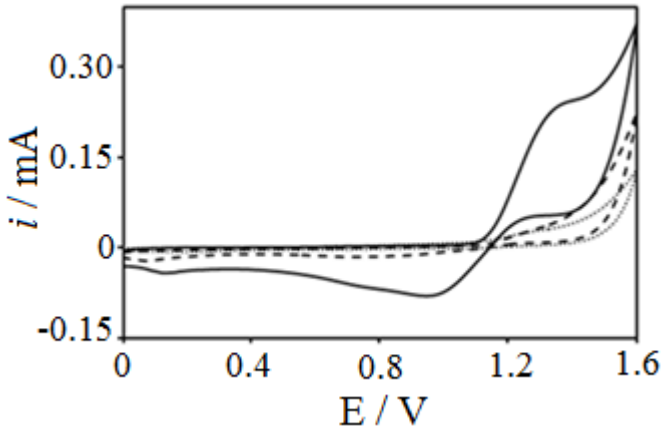

Figure 6.13 - Cyclic voltammograms conducted at a scan rate of 100 mV/s in a 0.1 M KCl solution with three Pt electrodes: (dotted line) bare Pt electrode, (solid line) Pt electrode covered with sulfur compounds deposit (see Figure 6.11a) and (dashed line) the coated Pt electrode that has been subjected to 100 s oxidation at 1.4 V in 0.1 M KCl. The results illustrate that sulfur compounds deposit can be electrochemically dissolved.

As suggested by Koper et al., EIS measurements are an effective tool for gaining further insights into the type of electrochemical oscillator. EIS measurements at 0.8 V show both a semicircle and a straight line, which indicates that the charge transfer process was driven by mass transportation of reactant from the solution bulk to the electrode surface. The fact that transient oscillations could be obtained at the Pt surface under those potentials may be attributed to the gradual modification of the Pt surface by deposition of the electro-oxidation products of HMS. Increasing the applied potential to 1.0 V, the EIS intersects with the imaginary axis as can be seen in Figure 6.14, which is indicative of the presence of hidden negative differential resistance in the oxidation of HMS.

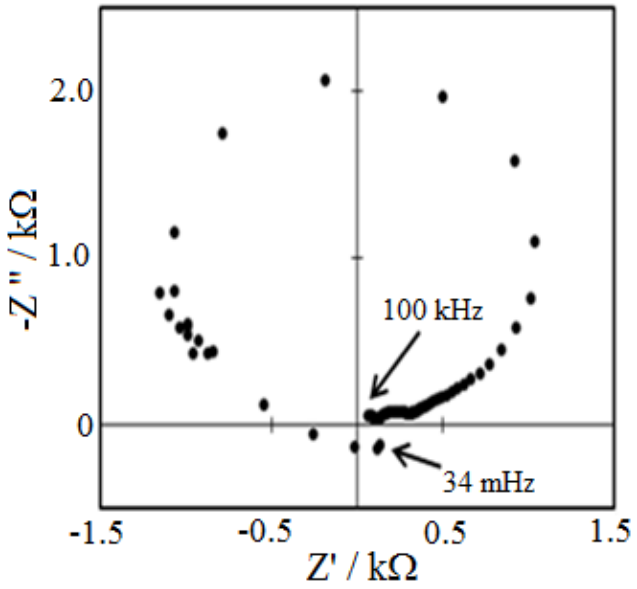

Figure 6.14 - EIS spectrum performed at a platinum working electrode showing the crossing of the imaginary axis. It was performed at an applied potential of 1.0 V (vs. SCE).

Therefore, the type of electrochemical oscillator shall fit HN-NDR. The presence of oscillations in both current and potential also lends support to the classification of the HMS electrochemical oscillator as an HN-NDR oscillator [23,24].

In order to gain insight into the reaction mechanism, mass spectrometry measurements were carried out. Prior to analysis, the HMS solution was oxidized for 12 h under potentiostatic conditions at 1.0 V. The sample was diluted 5:1500 with LC-MS water and then a 5 µL aliquot of this dilution was further diluted with approximately 1000 µL 50:50 H_2O:CH_3CN before measurements were conducted. The analysis indicated the presence of thiosulfate ($S_2O_3^{2-}$), bisulfate (HSO_4^-) and sulfite (SO_3^{2-}). The presence of thiosulfate gives strong support for $S_2O_3^{2-}$ being responsible for the observed phenomenon of gold dissolution. In addition to the three reagents being proposed here,

the mass spectra also contain peaks with higher *m/e* numbers such as 233.25, 325.18, etc., which we have not been able to determine.

6.3.3 Oxidation Behavior of L-Methionine

Whereas HMS was an important industrial sulfur based compound, methionine (shown schematically in Figure 6.15) is a biologically important sulfur based compound.

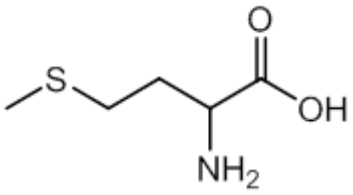

Figure 6.15 - Chemical structure of methionine

In Figure 6.16, a linear sweep voltammetry (LSV) experiment was performed at different scan rates. At 100 mV/s there is an oxidation peak centered at approximately 1.1 V. The oxidation peak becomes more broad as the scan rate is decreased to 25 mV/s (Figure 6.16b) and at a scan rate of 1.0 mV/s (Figure 6.16c) oscillations in current density become observable on the oxidation peak and disappear during the abrupt decrease in anodic current. Scanning at such a slow scan rate as 1.0 mV/s utilizes the applied potential as a control parameter taking the system through various dynamical regimes. Importantly, the shape of the linear voltammogram at 1.0 mV/s exhibits the classic N-shape, which is suggestive of the presence of negative differential resistance (NDR). The presence of the negative branch in the LSV at sufficiently slow scan rate is strongly suggestive that the negative branch is caused by negative differential resistance as opposed to limited mass transportation of analyte from the electrode surface.

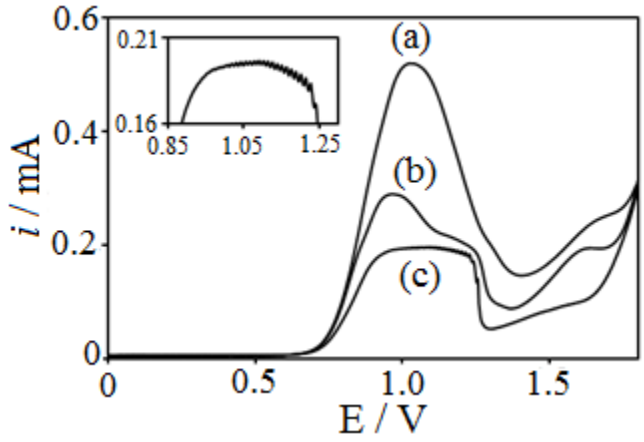

Figure 6.16 - Linear sweep voltammogram at scan rates of: (a) 100 mV/s, (b) 25 mV/s, and (c) 1.0 mV/s in a solution of 0.05 M methionine and 0.1 M KCl.

In order to confirm that the system indeed possesses NDR, electrochemical impedance measurements were conducted at various potentials along the positive and negative branches seen in Figure 6.16. Along the positive slope, from 0.6 V to 0.9 V there is no evidence of any hidden NDR (HN-NDR) properties, as a semicircle and a line were found at high and low frequencies respectively. This indicates that both electron transfer processes as well as mass transportation (diffusion) of the reactant from the bulk solution to the electrode surface are important. In the regions where oscillations were observed, approximately 1.0 V - 1.2 V the EIS spectra were expectedly unstable, however, once EIS measurements were taken at potentials on the negative branch the EIS became stable. Figure 6.17 shows an EIS spectrum conducted at 1.25 V, which shows the impedance crossing the imaginary axis and intersecting with the negative axis before intersecting again at -2000 Ω.

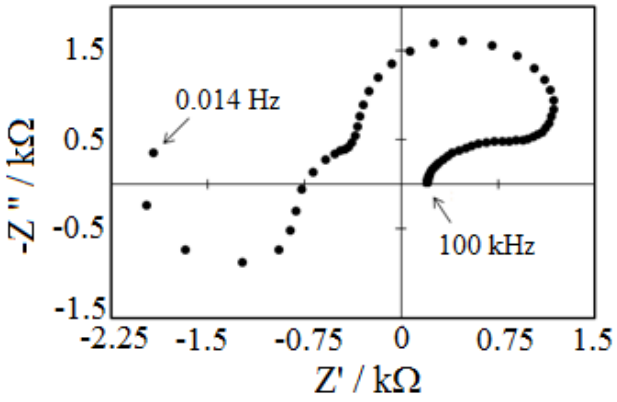

Figure 6.17 - Electrochemical Impedance spectrum (EIS) at an applied potential of 1.25 V in a solution consisting of 0.05 M methionine and 0.1 M KCl.

These results clearly indicate that the system possesses NDR on the negative branch and together with the classic n-shape curve obtained during slow scan LSV experiments this new electrochemical oscillator falls into the N-NDR class.

In N-NDR type oscillators the double layer potential $Ø_{DL}$ acts as an essential variable driving the oscillatory behavior. During the electrochemical oxidation of methionine in potassium chloride, there is gold dissolution occurring, as evidenced by visible pitting on the Au surface. Gold dissolution has been found to occur through the electrochemical oxidation of sulfur containing species, but has also been observed in solutions containing halogens such as bromide ions [60]. The oxidation of methionine was also conducted on a platinum electrode, which showed no evidence of NDR or of dissolution of platinum. Figure 6.18 shows an LSV of a 0.1 M KCl solution without (Figure 6.18a) and with (Figure 6.18b) the presence of methionine.

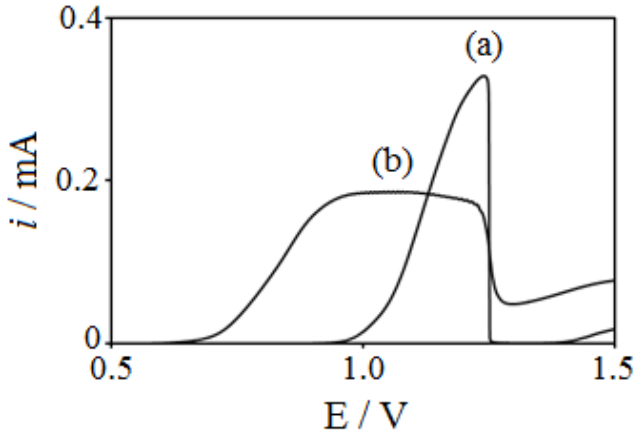

Figure 6.18 - Linear sweep voltammogram at a scan rate of 1.0 mV/s in a solution of 0.1 M KCl with a methionine concentration of (a) 0.0 M and (b) 0.05 M.

As can be seen, the presence of methionine drastically changes the shape of the LSV, however, the negative differential resistance is present in the solution containing just 0.1 M KCl. Notably, the shape of the LSV resembles an LSV for a system in which activation/passivation of the electrode surface is occurring, and the drastic decrease in current density corresponds to the Flade potential (here 1.25 V). This result indicates that passivation of the Au surface in the presence of chloride ions occurs, however, oscillations seen in Figure 6.18b cease to exist once this potential is surpassed. The LSV in Figure 6.18 suggest that there is a competition occurring at the electrode surface. The oxidation of methionine can be seen to begin at approximately 0.7 V whereas the oxidation of the gold electrode occurs at approximately 0.9 V. The flat methionine "oxidation peak" overlaps with the region where gold is being actively oxidized, which suggests that the oxidation of gold is playing a role in the oxidation kinetics of methionine, leading to oscillatory behavior. This implies that the interactions between methionine and gold, more particularly the strong interactions between sulfur and gold

are likely responsible for the nonlinear behavior. The NDR (positive feedback) here is likely caused by the decrease in active surface area caused by the passivation of the electrode area through the adsorption of methionine or methionine oxidation products on the gold surface. The negative feedback would then be driven by the surface concentration of methionine. To gain insights into the possible oxidation products high-resolution mass spectrometry analysis was conducted. These results indicated that the electrochemical oxidation of methionine ($C_5H_{11}NO_2S$) results in the formation of the compounds methionine sulfoxide, (*m/e* 165, $C_5H_{11}NO_3S$), as well as methionine sulfone (*m/e* 181, $C_5H_{11}NO_4S$). The formation of methionine sulfoxide and methionine sulfone corresponds to consecutive two-electron oxidation processes, as shown in Scheme 6.1.

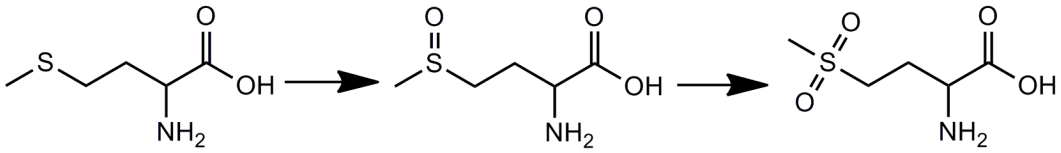

Scheme 6.1 - Oxidation pathway for the electrochemical oxidation of methionine.

Figure 6.19 shows potentiostatic experiments demonstrating the effect that changing the applied potential has on the methionine system and interestingly no external resistance is required to maintain the oscillatory behavior. In Figure 6.19a, at an applied constant potential of 0.8 V, there are very small amplitude damped oscillations before the system remains stable (non-oscillatory) for the duration of the reaction. Once the applied potential is increased to 1.0 V simple oscillations can be seen to emerge. Increasing the potential to 1.1 V and 1.2 V (Figure 6.19c and 6.19d) simple oscillations occur and once the applied potential is 1.3 V (Figure 6.19e) oscillations no longer exist. The frequency of

the oscillations does not change between 1.0 V and 1.2 V and is approximately 90 mHz; however, the amplitude of the oscillations can be seen to increase as the potential is increased from 1.0 V to 1.2 V.

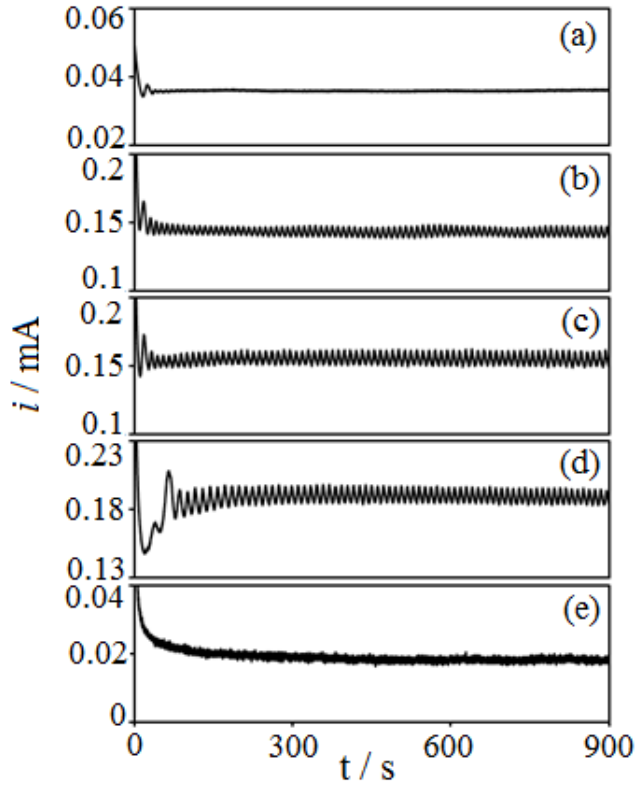

Figure 6.19 - Potentiostatic experiments performed with applied potentials of (a) 0.80 V, (b) 1.0 V, (c) 1.1 V, (d) 1.2 V, and (e) 1.3 V. Other reaction conditions were: [methionine] = 0.05 M and [KCl] = 0.1 M with no external resistance.

It should be noted that theoretically systems which fall into the classification of an N-NDR type electrochemical oscillator require the incorporation of external resistance, of a magnitude matching the resistance where the first intersection with the negative axis in an EIS spectrum occurs, in order to sustain oscillatory behavior. The occurrence of oscillations in this system without external resistance is likely due to the fact that the

concentration of supporting electrolyte is sufficiently low, such that the solution resistance overcomes the necessity for the inclusion of external resistance. To test this theory, a solution of methionine containing 1.0 M KCl (ten times the original supporting electrolyte concentration) was studied with EIS, which similarly to 0.1 M KCl solutions, showed the presence of NDR. The solution resistance was found to be 22 Ω, and the impedance was found to cross the negative axis at approximately -330 Ω. An LSV of the methionine oxidation in 1.0 M KCl is shown in Figure 6.20 with and without the presence of external resistance, dashed line and solid line respectively. As can be seen, no oscillations in current emerge at this concentration of supporting electrolyte when no external resistance is incorporated. However, once an appropriate resistor was utilized to compensate for the shift in solution resistance, the oscillatory regime emerged.

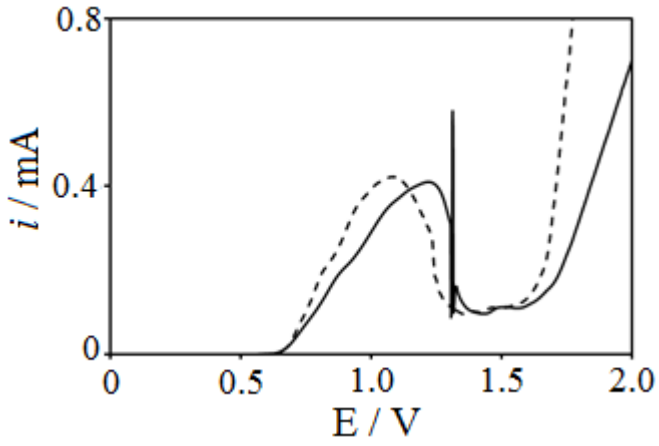

Figure 6.20 - Linear sweep voltammogram in a solution of 0.05 M methionine and 1.0 M KCl without external resistance (dashed line) and with an external resistor of magnitude 330 Ω (solid line).

Figure 6.21 shows a time series of the methionine oxidation in 1.0 M KCl with and without the presence of an external resistor of magnitude 330 Ω (under potentiostatic

conditions). As can be seen, oscillations in current are absent without the external resistor in series (dotted line), however, once the resistor is in series, stable oscillations emerge, giving more evidence that this new methionine electrochemical oscillator falls into the N-NDR class.

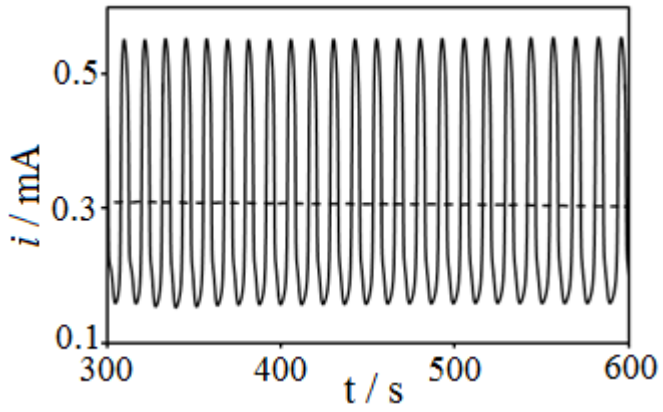

Figure 6.21 - Potentiostatic experiments conducted at 1.25 V without external resistance (dashed line) and with an external resistor of magnitude 330 Ω.

6.4 Conclusions

Electrochemically oxidizing hydroxymethanesulfinate was found to exhibit very different behaviors on Au and Pt surfaces. Long lasting, high frequency oscillations in both potential and current density were observed on a gold electrode, as opposed to only transient oscillations in current observed on a platinum electrode. As evidenced by SEM measurements, the oxidation of HMS (on both Pt and Au) led to the formation of a sulfur-based deposit on the electrode, which reduced the active surface area of the electrode. Such a passivation process resulted in a negative differential resistance, a necessary condition for the occurrence of electrochemical oscillations. This deposit can be electrochemically dissolved at the applied potentials where electrochemical

oscillations have been observed. The passivation-depassivation of working electrodes causes the observed oscillatory behavior in the studied system.

The gradual dissolution of Au due to its etching by sulfur compounds formed during the oxidation of HMS provides another feedback to the nonlinear oxidation of HMS, leading to both sustained oscillatory behavior as well as complex oscillations such as quasi-periodic oscillations. Mass spectrometry measurements illustrate the production of thiosulfate ($S_2O_3^{2-}$), bisulfate (HSO_4^-) and sulfite (SO_3^{2-}) in the solution. EIS measurements indicate that the oxidation of HMS has a hidden negative differential resistance, placing this new electrochemical oscillator in the category of HN-NDR. Overall, the observed nonlinear behavior was found to be very sensitive to varying experimental parameters, including the applied potential, applied current density as well as the solution concentration. The pitting of the Au electrode during the oscillatory process offers an interesting and perhaps nonlinear dynamical approach to generate an Au surface with different morphologies, which could have great potential applications in electrochemical analysis.

The electrochemical oxidation of methionine on a gold electrode led to the discovery of a new electrochemical oscillator, which fits the classification of an N-NDR type. Oscillations in current were found to occur with and without the presence of external resistance depending on the overall solution resistance. During the oxidation process pitting was found to occur on the Au surface caused by the dissolution of the electrode by methionine and methionine oxidation products (the oxidation products methionine sulfoxide as well as methionine sulfone were both identified using high-resolution mass spectrometry). The presence of regions of NDR on a Au surface and not

on a Pt surface is due to the strong affinity of sulfur compounds with Au, which leads to the dissolution and passivation of the electrode surface.

6.5 References

[1] M. G. T. Fechner, *J. Schweigger fur Chem. Phys.* **1828**, 53, 129-151.

[2] M. Orlik, *Self-Organization in Electrochemical Systems I: General Principles of Self-Organization. Temporal Instabilities*; Springer, Berlin, 2012.

[3] I. Z. Kiss, T. Nagy, V. Gáspár, *Dynamical Instabilities in Electrochemical Processes,* in V. V. Kharton (Eds), *Solid State Electrochemistry II: Electrodes, Interfaces, and Ceramic Membranes,* Vol. 1, Wiley-VCH, New York, 20011.

[4] K. Krischer, *Nonlinear Dynamics in Electrochemical Systems,* in R.C. Alkire, D. M. Kolb (Eds), *Advances in Electrochemical Science and Engineering*, Vol. 8; Wiley-VCH, New York, 2003.

[5] J. Lee, C. Eickes, M. Eiswirth, G. Ertl, *Electrochim. Acta* **2002**, 47, 2297-2301.

[6] N. Fetner, J. L. Hudson, *J. Phys. Chem.* **1990**, 94, 6506-6509.

[7] S. Kariuki, H. D. Dewald, J. Thomas, R. W. Rollins, *J. Electroanal. Chem.* **2000**, 486, 175-180.

[8] P. Strasser, M. Lübke, C. Eisckes, M. Eiswirth, *J. Electroanal. Chem.* **1999**, 462, 19-33.

[9] J. G. Bell, J. Wang, *J. Electroanal. Chem.* **2015**, 754, 133-137.

[10] G. Samjeské, M. Osawa, *Angew. Chem. Int. Ed.* **2005**, 117, 5694-5698.

[11] M. R. Basset, J. L. Hudson, *J. Phys. Chem.* **1988**, 92, 6963-6966.

[12] L. Organ, I. Z. Kiss, J. L. Hudson, *J. Phys. Chem. B* **2003**, 94, 6648-6659.

[13] Z. H. Gu, J. Chen, T. Z. Fahidy, *Electrochim. Acta* **1992**, 37, 2637-2644.

[14] I. Z. Kiss, V. Gáspár, *J. Phys. Chem. A* **1997**, 101, 8668-8674.

[15] J. J. Podestá, R. C. Piatti, A. J. Arvia, *J. Electrochem. Soc.* **1979**, 126, 1363-1367.

[16] D. Sazou, K. Michael, M. Pagitsas, *Electrochim. Acta* **2014**, 119, 175-183.

[17] V. Alonzo, A. Darchen, E. Le Fur, J. Y Pivan, *Electrochim. Acta* **2006**, 51, 1990-1995.

[18] O. Lev, M. Sheintuch, L. M. Piseman, Ch. Yarnitzkyt, *Nature* **1988**, 336, 458-459.

[19] D. Sazou, M. Pagitsas, *Electrochim. Acta* **1993**, 38, 835-845.

[20] F. N. Albahadily, M. Schell, *J. Chem. Phys.* **1988**, 88, 4312-4319.

[21] M. T. Gorzkowski, A. Wesolowska, R. Jurczakowski, P. Ślepski, K. Darowicki, M. Orlik, *J. Solid State Electrochem.* **2011**, 15, 2311-2320.

[22] S. Nakanishi, *Self-Organized Formation of Layered Nanostructures by Oscillatory Electrodeposition,* in A. Eftekhari (Eds), *Nanostructured Materials in Electrochemistry*, Vol. 8; Wiley-VCH, New York, 2008.

[23] P. Strasser, M. Eiswirth, M. T. M. Koper, *J. Electroanal. Chem.* **1999**, 478, 50-66.

[24] A. Bonnefont, R. Morschl, P. Bauer, K. Krischer, *Electrochim. Acta* **2009**, 55, 410-415.

[25] K. Krischer, *Principles of Temporal and Spatial Pattern Formation in Electrochemical Systems,* in B. E. Conway, J. O. M. Bockris, R. White (Eds), *Modern Aspects of Electrochemistry*, Vol. 32; Plenum, New York, 1999.

[26] L. Han, H. Ju, Y. Xu, *Int. J. Hydrogen Energy* **2012**, 37, 15156-15163.

[27] W. Wolfe, M. Lubke, M. T. M. Koper, K. Krischer, M. Eiswirth, G. Ertl, *J. Electroanal. Chem.* **1995**, 399, 185-196.

[28] F. Seland, R. Tunold, D. A. Harrington, *Electrochim. Acta* **2008**, 53, 6851-6864.

[29] E. Sitta, M. A. Nascimento, H. Varela, *Phys. Chem. Chem. Phys.* **2014**, 118, 15195-15206.

[30] V. Vedharathinam, G. G. Botte, *J. Phys. Chem. C* **1992**, 37, 21806-21812.

[31] M. Hromadová, L. Pospíšil, R. Sokolová, N. Fanelli, *Electrochim. Acta* **2009**, 54, 4991-4996.

[32] Y. Mukouyama, S. Nakanishi, T. Chiba, K. Murakoshi, Y. Nakato, *J. Phys. Chem. B* **2001**, 105, 7246-7253.

[33] M. G. Aylmore, D. M. Muir, *Miner. Eng.* **2001**, 14, 135-174.

[34] W. H. Wang, O. Rusin, X. Y. Xu, K. K. Kim, J. O. Escobedo, S. O. Fakayode, K. A. Fletcher, M. Lowry, C. M. Showalter, C. M. Lawrence, F. R. Fronczek, I. M. Warner, R. M. Strongin, *J. Am. Chem. Soc.* **2005**, 127, 15949-15958.

[35] M. Gutscher, A. L. Pauleau, L. Marty, T. Branch, G. H. Wabnitz, Y. Samstag, A. J. Meyer, T. P. Dick, *Nat. Methods* **2008**, 5, 553-559.

[36] A. H. Hall, R. Dart, G. Bogdan, *Ann. Emerg. Med.* **2007**, 49, 806-813.

[37] A. Chen, B. Miller, *J. Phys. Chem. B* **2004**, 108, 2245-2251.

[38] W. Bi, Y. He, M. F. Cabral, H. Varela, J. Yang, R. Jiang, Q. Gao, *Electrochim. Acta* **2014**, 133, 308-315.

[39] Z. Du, Q. Gao, J. Feng, Y. Lu, J. Wang, *J. Phys. Chem. B* **2006**, 110, 26098-26104.

[40] Y. Jia, Y. Zhao, Y. He, C. Pan, C. Ji, W. Bi, Q. Gao, *J. Phys. Chem. C* **2015**, 119, 24837-24843.

[41] L. Xu, Q. Gao, J. Feng, J. Wang, *Chem. Phys. Lett.* **2004**, 397, 265-270.

[42] J. A. O'Brien, J. T. Hinkley, S. W. Donne, *Electrochim. Acta* **2011**, 56, 4224-4230.

[43] G. Rábai, M. Orbán, I. R. Epstein, *J. Phys. Chem.* **1992**, 96, 5414-5419.

[44] P. De Kepper, I. R. Epstein, K. Kustin, M. Orbán, *J. Phys. Chem.* **1982**, 86, 170-171.

[45] Z. Wang, Q. Gao, C. Pan, Y. Zhao, A. K. Horváth, *Inorg. Chem.* **2012**, 51, 12062-12064.

[46] L. Shi, J. Liu, N. Li, J. Gao, *J. Solution Chem.* **2013**, 42, 1207-1220.

[47] S. V. Makarov, C. Mundoma, S. A. Svarovsky, X. Shi, P. M. Gannett, R. H. Simoyi, *Arch. Biochem. Biophys.* **1999**, 367, 289-296.

[48] M. N. Nassar, M. J. Reff, S. N. Aghankar, US Patent 5, 508, 268.

[49] Y. V. Polenov, V. A. Pushkina, V. V. Budanov, O. S. Khilinskaya, *Russ. J. Appl. Chem.* **2001**, 74, 1301-1304.

[50] Y. V. Polenov, V. A. Pushkina, E. V. Egorova, A. N. Labutin, R. L. Khalizov, *Kinet. Catal.* **2002**, 43, 465-468.

[51] J. G. Bell, J. Wang, *Chaos* **2013**, 23, 033120.

[52] N. Li, J. Wang, *J. Phys. Chem. A* **2008**, 112, 6281-6284.

[53] J. G. Bell, J. Wang, *J. Phys. Chem. A* **2015**, 119, 3323-3328.

[54] M. Kozak, *Microbiol Rev.* **1983**, 47, 1-455.

[55] A. Drazic, J. Winter, *Biochimica et Biophysica Acta* **2014**, 1844, 1367-1382.

[56] V. Humblot, F. Tielens, N. B. Lugue, H. Hampartsoumian, C. Methivier, C. Pradier, *Langmuir* **2014**, 30, 203-212.

[57] A. G. Zelinsky, O. N. Novgorodtseva, *Hydrometallurgy* **2013**, 138, 79-83.

[58] A. G. Zelinsky, *Electrochim. Acta* **2015**, 154, 315-320.

[59] L. Chai, M. Okido, W. Wei, *Hydrometallurgy* **1999**, 53, 255-266.

[60] J. Zheng, W. Huang, S. Chen, Z. Niu, Z. Li, *Electrochem. Commun.* **2006**, 8, 600-604.

CHAPTER 7 - APPLICATION OF NONLINEAR DYNAMICS TO THE FABRICATION OF NANOMATERIALS

7.1 Introduction

A significant amount of research has been conducted in the field of materials science towards the fabrication of nanomaterials with distinct morphologies [1-6]. A major motivation behind the control of morphology with respect to nanoparticles is driven by the desire to fine tune their properties [7-10]. Various methods have been utilized for the formation of different nanoparticle shapes, such as triangles, tubes, stars, etc. One common method is the incorporation of a reductant such as ascorbic acid or citrate, which may also act as a capping agent, inhibiting the growth of the nanoparticle [11-13]. The introduction of halides has also been found to play a role in tuning the morphology of nanoparticles by preferentially adsorbing to certain facets [14-18]. Of course, new methods of reproducibly fabricating nanoparticles represent a major area of active research. The field of nonlinear chemical dynamics may prove to be very effective for enhancing the rational design of nanoparticles with fixed sizes and novel morphologies.

The application of nonlinear dynamics to materials science has been a topic of interest for chemists who wish to exploit the inherent instabilities in these systems. One example of using nonlinear behavior in materials science is the polymerization of acrylonitrile in a solution containing acidic bromate, malonic acid, and cerium (Belousov-Zhabotinsky reaction) [19-21]. It was found that the polymerization only occurs in the oscillatory regime and that bromine dioxide was responsible for the periodic

termination and polymerization processes. Switzer et al. found that multilayers of Cu/Cu_2O could form during electrodeposition experiments, which were accompanied by spontaneous oscillations of the electrode potential [22]. Interestingly, they also found that the composition of the formed layer was dependent on the oscillating electrode potential. Electrodeposited layers, through their ability to modify the activity of electrode surfaces, have great potential to be applied in the field of electroanalysis. In fact, modified electrodes have been fabricated through the use of conductive polymers, graphene, metal nanoparticles, nanotubes and other similar materials for the purpose of selectively and sensitively detecting target analytes in solution [23-30]. However, to the best of our knowledge, no electrodes that have been fabricated under oscillatory regimes have been applied for the detection of analytes in solution.

This chapter explores the novel use of two separate nonlinear systems for the fabrication of nanomaterials. Through the use of the bromate – 4-nitrophenol chemical oscillator [31], platinum nanocubes were synthesized by introducing platinum chloride to the oscillating reaction. The second nonlinear system utilized was the methionine electrochemical oscillator, in which dissolution of the gold electrode was found to play a significant role in the nonlinear behavior and led to the coating of the counter electrode with gold nanoparticles. As a test case, this gold nanoparticle modified electrode was used for the oxidation of hydroquinone and pyrocatechol in solution, showing excellent catalytic behavior and yielding a good peak-to-peak separation of the two isomers during differential pulse voltammetry (DPV) experiments.

7.2 Experimental Procedures

7.2.1 Bromate – 4-Nitrophenol Oscillator - Pt Nanocubes

Kinetics were investigated in a thermal-jacketed 50 mL glass beaker. A circulating water bath (THX-2005, Ningbo Tianheng Instrument Factory) held the reaction temperature constant at 25.0 ± 0.1 ^{o}C. The reaction solution was held constant at 30.0 mL and was stirred continuously with a magnetic stirring bar driven by a magnetic stirrer (MS-H-PRO, Daxingxing Experimental Instrument (Beijing) Co.) to ensure homogeneity. Stock solutions of sodium bromate ($NaBrO_3$, Shanghai Aladdin Biochemical Technology Co., Ltd, GR Grade), 0.1 M and sulfuric acid (H_2SO_4, Zhejiang Zhongxing Chemical Reagent Co., Ltd, AR Grade), 6.0 M were prepared with doubly distilled water (Elix5-Milli-Q, Millipore (US)). The 4-nitrophenol ($C_6H_5NO_3$, Shanghai McLean Biochemical Technology Co., Ltd, GC Grade) was directly dissolved in the reaction mixture. The platinum chloride ($PtCl_2$, Shanghai Aladdin Biochemical Technology Co., Ltd, AR Grade) was either directly added to the reaction or dispersed using an ultrasonic bath (Kunshan City Ultrasound Instrument Co., Ltd.). Ethanol (Anhui Ante Foods Co., Ltd., AR Grade) and acetone (Zhejiang Zhongxing Chemical Reagent Co., Ltd, AR Grade) were used in conjunction with a centrifuge (KQ-300DB, Shanghai Anting Scientific Instrument Co., Ltd.) for collecting products after reactions had finished. A Teflon cap was placed on top of the thermal-jacketed beaker to hold the electrodes. Reactions were monitored with a platinum electrode (Pt005, Tiangin Adaheng Sheng Technology Co., Ltd) coupled with a $Hg|Hg_2SO_4|K_2SO_4$ reference electrode (R0401,Tiangin Adaheng Sheng Technology Co., Ltd) filled with a saturated K_2SO_4

solution. Scanning Electron Microscopy (SEM) measurements were conducted on a Nova Nanosem 200 (FEI, US) system.

7.2.2 Methionine Electrochemical Oscillator - Au Nanoparticles

Electrochemical experiments were performed on a Voltalab PGZ100 system (Radiometer Analytical, USA) and CHI 760E (CHI Instruments, Texas, US). Polycrystalline gold or platinum electrodes with diameters of 2.0 mm (CHI Instruments) were applied as working electrodes. The counter electrode was a platinum wire (PT99WIRE0508, KITCO) and a saturated calomel electrode (SCE) was applied as the reference electrode. Before each experiment, the working electrode was polished with consecutively finer grades of alumina powder, rinsed with doubly distilled water, cleaned by an ultrasonic cleaner (Branson 1510, USA) for 10 minutes, and again rinsed with double distilled water. The three electrodes were placed in the traditional triangle configuration and all electrochemical experiments were performed at room temperature ($22 \pm 2\ ^{o}C$).

Reagents L-methionine ($C_5H_{11}NO_2S$, 98+%), potassium chloride (KCl, 99+%), hydroquinone ($C_6H_6O_2$, 99%), pyrocatechol ($C_6H_6O_2$, 99%) and potassium ferricyanide ($K_3Fe(CN)_6$, 99%) were purchased from Sigma Aldrich. All reactions contained 0.05 M L-methionine in 0.1 M KCl, unless otherwise stated. Reaction volumes were held constant at 60.0 mL, and all experiments were performed under ambient conditions (no purging with inert gases). Electrochemical impedance spectroscopy experiments were measured in the frequency range of 100 kHz to 0.1 mHz (unless otherwise stated) with an amplitude of 5 mV and 12 points per frequency decade were collected. Scanning electron microscopy (SEM) and energy-dispersive X-ray spectroscopy (EDS) were performed

with a Quanta 200 FEG microscope (FEI, Inc.). The parameters used in differential pulse voltammetry (DPV) experiments were 10 mV increments, 50 mV pulse amplitude, 200 ms pulse width and 500 ms pulse period.

7.3 Results and Discussion

7.3.1 Fabrication of Pt Nanocubes with Chemical Oscillator

The bromate – 4-nitrophenol chemical oscillator was studied in Chapter 4 and shown to exhibit long lasting and relatively low frequency chemical oscillations. Being a bromate based system, periodic changes in the concentration of bromide ion are occurring. This changing bromide ion concentration offers a dynamic protocol for introducing halogens towards the manipulation of nanoparticle morphology. Traditionally, reductants such as ascorbic acid or citrate are used to reduce metal ions during nanoparticle synthesis [11,12], implying that if the bromate – 4-nitrophenol oscillator could potentially be used towards Pt nanoparticle fabrication, 4-NP (or a formed intermediate) must be able to reduce platinum ions. Figure 7.1 shows a time series of the reaction between 4-NP and platinum chloride. The arrow in Figure 7.1 indicates the moment that 0.015 mmol of $PtCl_2$ was added to a 0.01 M 4-NP solution in 1.0 M sulfuric acid. As can be seen, a drastic spike in the potential was observed, followed by a gradual leveling off at approximately 0.45 V.

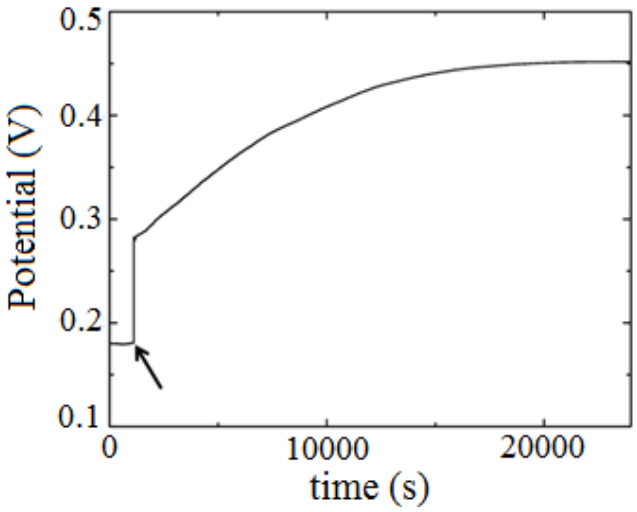

Figure 7.1 - Time series of the reaction between $PtCl_2$ and 4-nitrophenol. 0.015 mmol $PtCl_2$ was added to the solution at the arrow. Other reaction conditions were: [4-NP] = 0.01 M and $[H_2SO_4]$ = 1.0 M.

Even though the change in potential is suggestive of a reaction occurring, Scanning Electron Microscopy (SEM) measurements were conducted on the $PtCl_2$ before and after the reaction in the acidic 4-NP solution. Figure 7.2a shows an SEM of the $PtCl_2$ that was dissolved in ethanol and Figure 7.2b shows the solid product of the reaction of $PtCl_2$ with 4-NP collected after 5 h. Here a distinct change in morphology was observed, as the product of the reaction demonstrated a tubular morphology implying the reduction might have occurred. Transmission Electron Microscopy (TEM) measurements confirmed the formation of Pt.

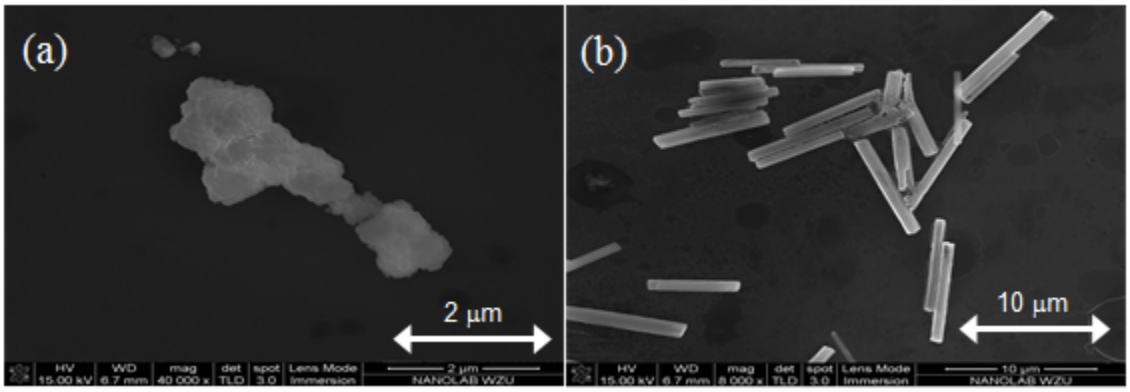

Figure 7.2 - SEM images of (a) unreacted $PtCl_2$ and (b) the product of the reaction between $PtCl_2$ and 4-nitrophenol after 5 h reaction time. Reaction conditions for (b) were: [4-NP] = 0.01 M, $[H_2SO_4]$ = 1.0 M, and $[PtCl_2]$ = 0.015 mmol.

Figure 7.3 shows a time series illustrating the influence that the addition of 0.015 mmol $PtCl_2$ at the onset of the reaction had on the kinetics of the bromate – 4-NP oscillator. A prototypical time series is shown in Figure 7.3i, where the incorporation of $PtCl_2$ causes a decrease in the oscillatory window as well as the number of oscillations (Figure 7.3ii). This phenomenon was expected as some of the 4-NP was consumed through its reaction with $PtCl_2$ and therefore unable to participate (directly or indirectly) in the autocatalytic cycle.

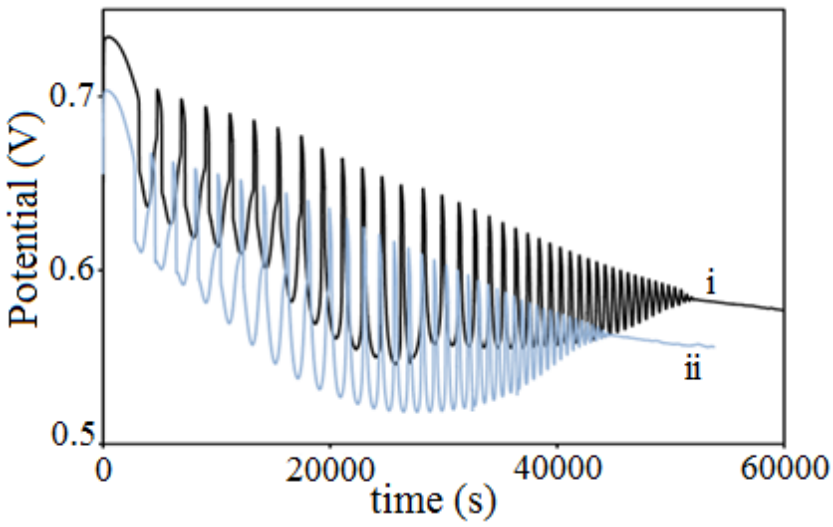

Figure 7.3 - Time series showing the effect of $PtCl_2$ on the kinetics of the bromate – 4-nitrophenol oscillator. Reaction conditions were: [4-NP] = 0.01 M, $[H_2SO_4]$ = 1.0 M, $[NaBrO_3]$ = 0.03 M. (i) $[PtCl_2]$ = 0.0 mmol and (ii) $[PtCl_2]$ = 0.015 mmol.

SEM measurements of the solid products collected after the $PtCl_2$ was in the oscillatory reaction showed that the bromate – 4-NP oscillator, after a 3 h reaction time, had resulted in the formation of platinum nanocubes as seen in Figure 7.4a and Figure 7.4b. Comparing with the tubular structure seen in the $PtCl_2$ - 4-NP reaction, this result provides proof of concept evidence that bromate-based chemical oscillators have the ability to manipulate and direct the formation of nanoparticles with distinct morphologies. The preferential adsorption of bromide ions on a particular facet of the platinum crystals has likely controlled the growth of the nanoparticle leading to the preferential formation of platinum nanocubes in this system.

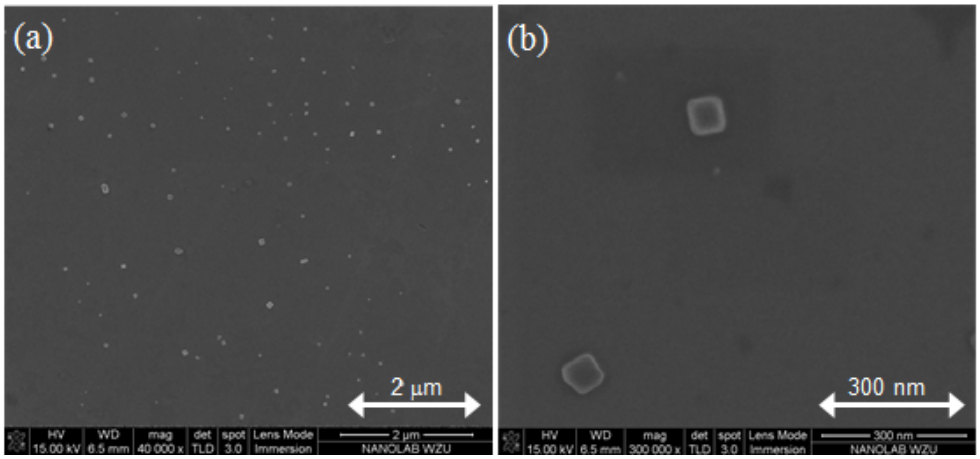

Figure 7.4 - SEM images showing the formation of Pt nanocubes through the incorporation of $PtCl_2$ in the bromate – 4-nitrophenol oscillator. Reaction conditions were: [4-NP] = 0.01 M, $[H_2SO_4]$ = 1.0 M, $[NaBrO_3]$ = 0.03 M and $[PtCl_2]$ = 0.015 mmol. Samples were collected after 3 h reaction time.

Varying the initial reaction conditions, as well as the reaction time, both had a minimal effect on the morphology of the formed nanocubes. Figure 7.5 shows the effect that different reaction times had on the Pt nanoparticles.

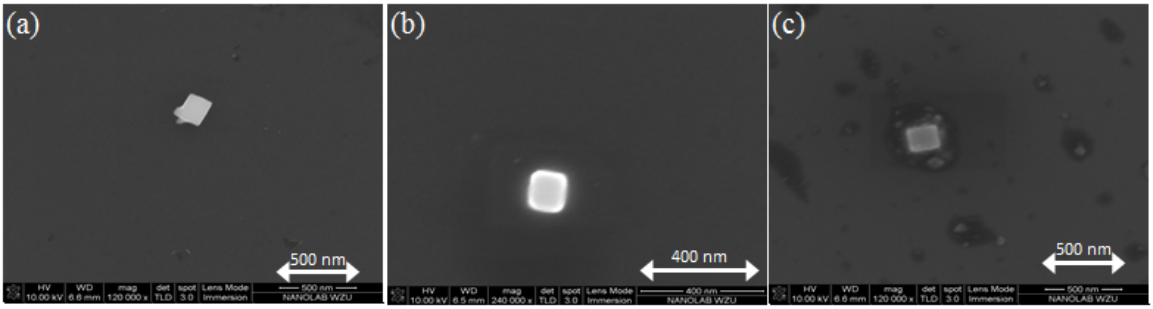

Figure 7.5 - SEM images showing the influence of reaction time on the formation of Pt nanocubes. Conditions were: [4-NP] = 0.01 M, $[H_2SO_4]$ = 1.0 M, $[NaBrO_3]$ = 0.03 M and $[PtCl_2]$ = 0.015 mmol. Samples were collected after (a) 2 h, (b) 6 h, and (c) 12 h.

7.3.2 Fabrication of Au Nanoparticles with an Electrochemical Oscillator

The phenomenon of electrochemical oscillations during the oxidation of methionine on a gold working electrode was discussed in Chapter 6. As mentioned, during the electro-oxidation of methionine on a gold surface, gold dissolution occurs, causing significant pitting on the electrode surface. The dissolution is likely driven by the formation of a sulfur-Au complex, which becomes soluble in solution. Once the dissolution has occurred, the sulfur-gold complexes migrate toward the platinum counter electrode and when operated under potentiostatic conditions, which exhibited nonlinear behavior, the sulfur-gold particles get reduced and become capable of coating the Pt counter electrode. Scanning Electron Microscopy (SEM) of the Pt counter wire after potentiostatic oxidation of methionine for 6 h showed that nanoparticles with consistent size and shape were deposited (Figure 7.6).

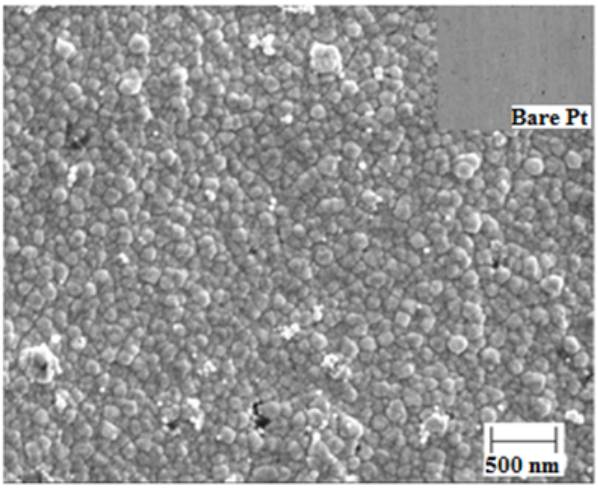

Figure 7.6 - SEM image showing the as-deposited Au nanoparticles occurring during the electro-oxidation of methionine. Reaction conditions were: [methionine] = 0.05 M and [KCl] = 0.1 M. Deposition occurred during a 6 h potentiostatic experiment conducted at 1.0 V (vs. SCE).

In Figure 7.7 energy-dispersive X-ray spectroscopy (EDS) measurements confirmed that the as-deposited nanoparticles consisted of Au.

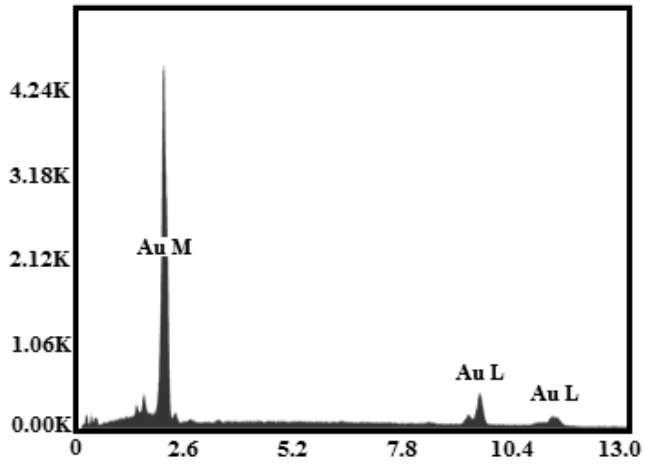

Figure 7.7 - EDS measurement of the deposited Au nanoparticles shown in Figure 7.6.

To further characterize the modified electrode, EIS measurements were conducted in a 2 mM $K_3Fe(CN)_6$ solution. When a bare gold electrode was used (Figure 7.8i), there was a small semi-circle followed by a straight line. Figure 7.8ii and 7.8iii show the difference between the unmodified Pt wire electrode (7.8ii) and the modified electrode (7.8iii). As can be seen, there is a distinct difference between the Au-nanoparticle modified Pt electrode and either the bare Au or bare Pt, indicating that the modified electrode has different properties compared to either unmodified surface.

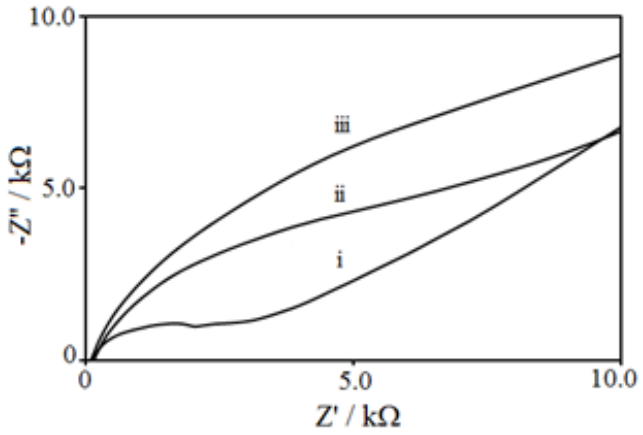

Figure 7.8 - Electrochemical Impedance Spectroscopic (EIS) Spectrum of (i) bare Au electrode, (b) bare Pt electrode and (c) Pt wire modified with gold nanoparticles. Experiments were conducted in a 2 mM Ferricyanide and 0.1 M KCl solution, at an applied potential of 0.25 V.

As a case study, this Au-nanoparticle modified electrode, fabricated through the nonlinear dynamical reaction, was applied towards the detection of the isomers hydroquinone (HQ) and pyrocatechol (PC). Hydroquinone and pyrocatechol are two important toxicological compounds that often coexist in environmental samples; hence, the ability to detect both isomers in solution at low concentrations could have a mojor impact on environmental research. Figure 7.9 shows the DPV (Differential Pulse Voltammogram) of a solution consisting of 2000 μM HQ and 2000 μM PC in 0.1 M KCl. Neither the bare Au (dashed line) nor the bare Pt (dotted line) electrodes are capable of detecting both HQ and PC simultaneously, showing the presence of an unresolved single peak. However, once the Au-nanoparticle modified electrode was used (solid line), the two isomers become individually detectable (HQ at approximately 0.05 V and PC at 0.11 V).

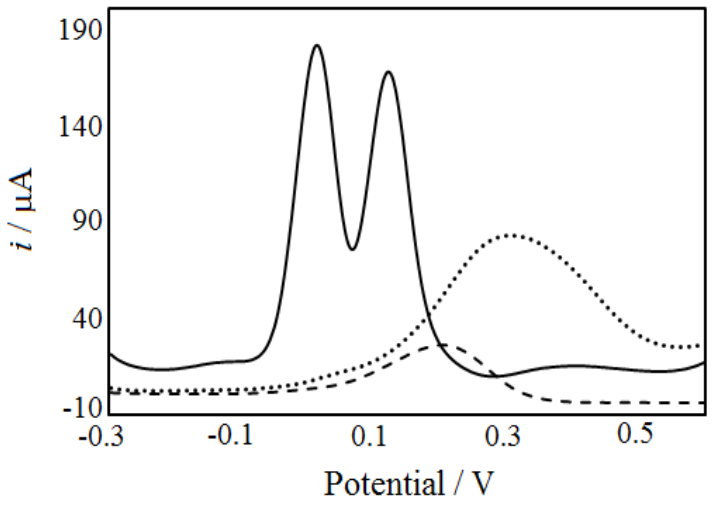

Figure 7.9 - Differential Pulse Voltammogram (DPV) measurements of a 2000 μM hydroquinone (HQ) and 2000 μM pyrocatechol (PC) solution on a: bare Pt wire electrode (dotted line) a bare Au electrode (dashed line) a Pt wire electrode modified with gold nanoparticles (solid line). The solution also contained 0.1 M KCl.

The ability to differentiate the two isomers is likely due to their differing degrees of interaction with the Au-nanoparticle modified surface. Also, in comparison to the bare electrodes, the modified electrode shows excellent catalytic properties for the oxidation of HQ and PC.

7.4 Conclusions

This research provides encouraging results and preliminary support for the use of nonlinear systems for the fabrication of nanomaterials. Through the use of a chemical oscillator, the bromate – 4-nitrophenol system, platinum nanoparticles with distinct morphologies were formed. Although the only observed morphology came in the form of nanocubes, this protocol offers a dynamic approach of introducing halides into reactions aimed at directing the growth of nanomaterials. This research also demonstrates the first

example of fabricating an electrochemical sensor using the dynamic regime of a nonlinear electrochemical oscillator. In order to harness the nonlinear dynamical behavior occurring during the electrochemical oxidation of methionine towards an application in electroanalysis a thorough exploration of the system was reported in Chapter 6. During the oscillatory reaction the dissolved gold was found to migrate and coat the Pt counter electrode with Au-nanoparticles, which was confirmed by SEM and EDS measurements. Successfully, this modified electrode was applied to the electroanalysis of HQ and PC coexisting in solution. DPV experiments were able to simultaneously differentiate between the two isomers.

7.5 References

[1] W. Niu, Y. A. A. Chua, W. Zhang, H. Huang, X. Lu, *J. Am. Chem. Soc.* **2015**, 137, 10460-10463.

[2] H. L. Wu, H. R. Tsai, Y. T. Hung, K. U. Lao, C. W. Liao, P. J. Chung, J. S. Huang, I. C. Chen, M. H. Huang, *Inorg. Chem.* **2011**, 50, 8106-8111.

[3] L. Vayssieres, *Adv. Mater.* **2003**, 15, 464-466.

[4] B. Nikoobakht, M. A. El-Sayed, *Chem. Mater.* **2003**, 15, 1957-1962.

[5] H. Wang, D. W. Brandl, F. Le, P. Nordlander, N. J. Halas, *Nano Lett.* **2006**, 6, 827-832..

[6] S. Cho, S. H. Jung, K. H. Lee, *J. Phys. Chem. C* **2008**, 112, 12769-12776.

[7] Y. Xia, N. J. Halas, *MRS Bull.* **2005**, 30, 338-348.

[8] E. C. Cho, C. M. Cobley, M. Rycenga, Y. Xia, *J. Mater. Chem.* **2009**, 19, 6317-6320.

[9] J. Wang, F. Ren, R. Yi, G. Qiu, X. Liu, *J. Alloys Compd.* **2009**, 479, 791-796.

[10] L. Zhang, H. Wang, *ACS Nano* **2011**, 5, 3257-3267.

[11] L. Guo, C. J. Murphy, *J. Mater. Chem.* **2004**, 14, 735-738.

[12] X. Dong, X. Ji, H. Wu, L. Zhao, J. Li, W. Yang, *J. Phys. Chem. C* **2009**, 16, 6573-6576.

[13] L. Guo, C. J. Murphy, *Nano Lett.* **2003**, 2, 231-234.

[14] J. S. DuChene, W. Niu, J. M. Abendroth, Q. Sun, W. Zhao, F. Huo, W. D. Wei, *Chem. Mater.* **2013**, 25, 1392-1399.

[15] B. T. Sneed, M. C. Golden, Y. Liu, H. K. Lee, I. Andoni, A. P. Young, G. McMahon, N. Erdman, M. Shibata, X. Y. Ling, C. K. Tsung, *Surf. Sci.* **2016**, 648, 307-312.

[16] M. H. Huang, P. H. Lin, *Adv. Funct. Mater.* **2012**, 22, 14-24.

[17] T. H. Ha, H. J. Koo, B. H. Chung, *J. Phys. Chem. C* **2007**, 111, 1123-1130.

[18] W. Niu, G. Xu, *Nano Today* **2011**, 6, 265-285.

[19] M. Orlik, *J. Solid State Electrochem.* **2009**, 13, 245-261.

[20] J. A. Pojman, D. C. Leard, W. W. West, *J. Am. Chem. Soc.* **1992**, 114, 8298-8299.

[21] R. P. Washington, W. W. West, G. P. Misra, J. A. Pojman, *J. Am. Chem. Soc.* **1999**, 121, 7373-7380.

[22] J. A. Switzer, C. J. Hung, L. Y. Huang, F. S. Miller, Y. Zhou, E. R. Raub, M. G. Shumsky, E. W. Bohannan, *J. Mater. Res.* **1998**, 13, 909-916.

[23] M. Gerard, A. Chaubey, B. D. Malhotra, *Biosens. Bioelectron.* **2002**, 17, 345-359.

[24] M. Ates, *Mater. Sci. Eng. C* **2013**, 33, 1853-1859.

[25] C. Janáky, C. Visy, *Anal. Bioanal. Chem.* **2013**, 405, 3489-3511.

[26] W. Lei, W. Si, Y. Xu, Z. Gu, Q. Hao, *Microchim. Acta* **2014**, 181, 707-722.

[27] S. N. Kim, J. F. Rusling, F. Papadimitrakopoulos, *Adv. Mater.* **2007**, 19, 3214-3228.

[28] Y. Kim, S. Song, Y. J. Kang, Y. Yang, R. K. Mahajan, J. S. Kim, H. Kim, *Biosens. Bioelectron.* **2010**, 25, 2366-2369.

[29] X. Luo, A. Morrin, A. J. Killard, M. R. Smyth, *Electroanalysis* **2006**, 18, 319-326.

[30] G. Inzelt, *Conducting Polymers: A New Era in Electrochemistry*; Springer, Heidelberg, 2012.

[31] J. G. Bell, J. Wang, *J. Phys. Chem. A* **2015**, 119, 3323-3328.

CHAPTER 8 - CONCLUSIONS AND PERSPECTIVES

8.1 Conclusions

The research presented in this thesis focused on finding new chemical and electrochemical nonlinear systems and gaining insights into their reaction mechanisms. In Chapter 2, the bromate – 4-aminophenol photochemical oscillator was investigated from two viewpoints, in order to gain insight into the underlying mechanisms driving the nonlinear behavior. Firstly, the redox catalyst cerium was introduced in order to implement coupled autocatalytic feedbacks. Here, mixed-mode and sequential oscillations emerged making it one of the few chemical systems known to support complex behavior in a batch reactor [1]. The complex behavior showed a strong dependence on the intensity of illumination supplied to the system. Removal of illumination during an oscillatory window affected both the frequency and amplitude of the oscillation but did not fully extinguish them, indicating that the cerium - bromate – 4-aminophenol oscillator was photosensitive, rather than photo-controlled. A moderate light intensity allowed for a slow evolution of the system, which proved critical for the emergence of transient complex oscillations. Kinetic simulations provided strong support that transient complex oscillations observed experimentally arise from the coupling of two autocatalytic cycles.

Second, a subset of the 4-aminophenol oscillator was studied by isolating the formed precipitate N-bromo-1,4-benzoquinone-4-imine. Interestingly, the photodecomposition of N-bromo-1,4-benzoquinone in an acidic media exhibited the nonlinear kinetic feature of an autocatalytic excursion. During the photodecomposition process the N-bromo-1,4-benzoquinone-4-imine is converted into 1,4-benzoquinone, as

was confirmed with ^{1}H NMR and mass spectrometry. When bromate was introduced to the studied system, transient spontaneous oscillations were uncovered, forming a new photochemical oscillator [2]. The system's sensitivity to the intensity of the illumination was great as decreases below a threshold value completely quenched the reactivity. Electrospray-TOF mass spectrometry and ^{13}C NMR spectra suggest that 3,4,4-tribromo-2-hydroxycyclohexa-2,5-dienone is a major product in the system. The insights gained while studying the N-bromo-1,4-benzoquinone-4-imine system led to important mechanistic information with respect to the bromate – 4-aminophenol oscillator, and suggested a strong importance on the formation of 1,4-benzoquinone in both the 4-aminophenol and N-bromo-1,4-benzoquinone oscillators.

In Chapter 3, the bromate – 2-methyl-1,4-hydroquinone oscillator was studied. Based on previous knowledge regarding the formation of 1,4-benzoquinone in the 4-aminophenol oscillator, the influence of a functional group on the reduction product of 1,4-benzoquinone was investigated. Spectroscopic investigation showed the oxidation of 2-methyl-1,4-hydroquinone by bromine molecules and the photoreduction of 2-methyl-1,4-benzoquinone reforming 2-methyl-1,4-hydroquinone in aqueous media. ^{1}H NMR measurements suggest that the presence of the methyl group hinders the bromination of the organic substrate. The concurrent photoreduction of 2-methyl-1,4-benzoquinone and oxidation of 2-methyl-1,4-hydroquinone by bromate derivatives lead to spontaneous oscillations in a closed reaction system [3]. A substantial lengthening of the oscillatory window and a dramatic increase in the complexity of the reaction behavior arose upon the addition of ferroin or cerium (IV) ions to the bromate – 2-methyl-1,4-hydroquinone system. Sequential oscillations were observed through the addition of each metal catalyst

and mixed-mode oscillations were present in the cerium - catalyzed reaction. A strong dependence of the complexity of the reaction behavior on the intensity of illumination supplied was observed.

In order to gain further insights into 1,4-disubstituted aromatic oscillators, which contain hydroxyl functionalities, 4-nitrophenol was investigated in Chapter 4. Systematic investigation found that the bromate – 4-nitrophenol reaction could undergo spontaneous oscillations under very broad reaction conditions [4]. Similar to the bromate – 4-aminophenol oscillator, the presence of 1,4-benzoquinone was identified in the bromate – 4-nitrophenol oscillator. However, the incorporation of illumination was not required in order for the bromate – 4-nitrophenol system to support oscillations. The addition of ferroin has subtle influences on the nonlinear behavior, in which the frequency and total number of oscillations were greatly reduced at a low or high ferroin concentration as opposed to the significant increase at a moderate ferroin concentration. Temporal oscillations with a modulating frequency were observed in the ferroin – bromate – 4-nitrophenol system. In a capillary tube the ferroin – bromate – 4-nitrophenol reaction generated propagating wave trains with various complex behaviors such as period-doubled intermittent propagation failure. Overall, the behavior of the 4-nitrophenol system differed greatly to the other.

Owing to the significant role of bromide ions in bromate based chemical oscillators, an electrochemical study of bromide ions in acidic media was undertaken in Chapter 5 to gain insights into its oxidation process, which could provide useful information applicable to bromate oscillators. Interestingly, the electrochemical oxidation of bromide ions led to the observation of both current and potential oscillations [5].

Under galvanostatic conditions the electrode potential was seen to oscillate around two narrow regions, 0.9 V and 1.6 V. Sustained current oscillations at the high potentials were accompanied with bubble formation and are often irregular, implicating that their development may be attributed with convection-driven processes. At the low potentials, the current oscillations exhibit several features associated with a capacitance mediated electrochemical oscillator, such as (1) taking place around a current plateau in a cyclic voltammogram, (2) occurring without the need of an external resistor, (3) showing a decrease in amplitude with the increase of external resistance, (4) emerging on a branch of positive differential resistance, and (5) having resonance behavior in an admittance spectra. The reversible formation and dissolution of tribromide complexes (Br_3^-) from the reaction between bromide (Br^-) and its electro-oxidation product bromine (Br_2) was proposed to have played an important role in this system.

After achieving success with hydroxyl containing compounds in nonlinear chemical systems and gaining insight into the oxidation of bromide ions electrochemically, the compound hydroxymethanesulfinate was investigated electrochemically in Chapter 6. Consisting of not only a hydroxyl group, but also a sulfur compound, which can potentially give access to multiple oxidation states, the electro-oxidation of hydroxymethanesulfinate was an ideal candidate to display rich dynamical behavior. The oxidation of hydroxymethanesulfinate was conducted on both platinum and gold electrodes. On a platinum surface, the oscillatory behavior was transient when operated under potentiostatic conditions; however, sustained oscillations in potential were observed under galvanostatic conditions [6]. Scanning Electron Microscopic (SEM) measurements showed that the platinum electrode was coated with sulfur deposits, which

were capable of being oxidized at high potentials, leading to the sustained oscillatory behavior seen under galvanostatic conditions. Interestingly, SEM measurements show that the electro-oxidation process caused significant pitting of the gold electrodes. The continuous dissolution of the gold surface is likely to have played an important role in the sustained simple and complex oscillatory behaviors in both current density and potential. Electrochemical Impedance Spectroscopy (EIS) results indicate that the oxidation of hydroxymethanesulfinate possesses a hidden negative differential resistance, implying that this new electrochemical oscillator belongs to the HN-NDR class. Mass spectrometry analysis of the reaction solution suggests the formation of thiosulfate, a reagent which is likely responsible for the observed gold dissolution occurring during the electro-oxidation of hydroxymethanesulfinate.

To gain further insights into the oxidation of sulfur containing compounds the biologically important amino acid methionine was also investigated in Chapter 6. On a gold electrode negative differential resistance was observed through the use of EIS. The presence of negative differential resistance allowed this new oscillator to be classified as an N-NDR type. Under the potentiostatic conditions at which the system exhibits oscillatory behavior the process of gold dissolution occurs, which is likely due to the strong interactions of sulfur compounds and gold. Spectroscopic studies of the methionine reaction mixture after electrochemical oxidation were able to identify methionine sulfoxide and methionine sulfone as the major oxidation products.

8.2 Perspectives

In depth study of the mechanisms behind these chemical and electrochemical systems will provide insight not only into their driving forces but also into the most

effective ways to control and manipulate their behavior. One interesting way to potentially manipulate photochemical oscillators is through the use of a shutter. Incorporating a shutter with open and close intervals that can be externally controlled provides a direct way to perturb and manipulate the photochemical reactivity of oscillatory systems. The 4-aminophenol system discussed in Chapter 2 of this dissertation would be an ideal candidate to begin such a perturbation study. The extreme photosensitivity exhibited by the 4-aminophenol oscillator could lead to very rich nonlinear behavior through periodically perturbing the system with illumination. This may also lead to an interesting method of studying the influence of various light intensities or wavelengths on synchronization and entrainment of the reactivity of the system with the period of the perturbation.

With respect to the utilization of a chemical oscillator towards the selective control of nanoparticle morphology, more work is needed. Experiments in this dissertation have shown that the bromate based 4-nitrophenol oscillator is capable of directing the formation of platinum nanocubes; however, no other morphology was observed. This could be due to the fact, that at least on gold, relatively high concentrations of bromide ions are needed (> 1 mM) to have a noticeable influence on the surface morphology [7,8]. Due to the fact that the overall bromide ion concentration in bromate based oscillators is quite low (10^{-6} - 10^{-8} M) and that the overall concentration change occurring during an individual oscillation cycle is also low, bromate-based oscillators may not be the most efficient towards this endeavor. Research has shown that iodide ions can also influence nanoparticle morphology and can do so at lower concentrations in comparison to the concentration of bromide ions often required [7,8].

Fortunately, this suggests that the Briggs-Rauscher oscillator, which undergoes periodic oscillation in the concentration of the iodide ion can potentially be utilized as a dynamic fabrication method aimed at manipulating the morphology of nanoparticles [9].

As reported in Chapter 5, oscillations occurring during the electro-oxidation of bromide ions were found to fit the mechanism of a Capacitance Mediated Positive Differential Resistance oscillator, in which the formation and dissolution of an inhibiting layer was crucial for the nonlinear behavior. In this system the inhibiting layer is the tribromide species, Br_3^-, whose formation occurs through the reaction between the oxidation product bromine and bromide ions according to the reaction: $Br_2 + Br^- \leftrightarrow Br_3^-$. This important reaction step offers the opportunity to manipulate the formation of the inhibitory layer through introducing a second compound which is easily brominated which may lead to dynamically much richer phenomenon than was seen in the bromide system alone. Preliminary experiments were conducted with the traditional Belousov-Zhabotinsky reactant, malonic acid, with the goal of influencing the production of the Br_3^- complex through inhibiting its formation to an extent that the system would evolve into complex behavior as opposed to simple periodic oscillations. A noticeable change in the oscillatory behavior was not seen, however, other compounds could potentially be used, such as 1,4-cyclohexanedione. 1,4-cyclohexanedione has demonstrated oscillatory behavior during its oxidation with bromate, and a key intermediate in the overall mechanism driving the oscillatory behavior is 2-bromo-1,4-cyclohexanedione [10].

Another exciting opportunity for the use of nonlinear dynamics is through the use of electrochemical oscillators towards the constructive manipulation of electrode surfaces. An example was shown in Chapter 7 showing how dissolution of a gold

electrode can lead to the fabrication of a gold nanoparticle modified electrode. Electrochemical oscillators, which undergo passivation/dissolution processes, offer a potentially nonlinear protocol for the modification of the electrode surface with distinct morphologies. Through altering the experimental parameters such as applied potential or current can lead to a variation in not only oscillatory frequency but the amplitude as well. These changes in frequency or amplitude have been directly related to thickness of deposited films and could potentially lead to different morphologies of the electrode surface in corrosion driven reactions [11]. For example, the corrosion of copper in various media has been studied and rich dynamical behavior has been observed [12-14]. Copper nanoparticles as well as nanotubes have also been utilized in various electroanalytical experiments towards the detection of glucose, with differing sensitivities [15-17]. Therefore, research conducted towards modifying the morphology of copper electrodes through nonlinear processes could potentially lead to the fabrication of affordable and sensitive electrodes useful for the detection of glucose.

8.3 References

[1] J. G. Bell, J. Wang, *Chaos* **2013**, 23, 033120.

[2] J. G. Bell, J. R. Green, J. Wang, *J. Phys. Chem. A* **2013**, 117**,** 4545-4550.

[3] J. G. Bell, J. R. Green, J. Wang, *J. Phys. Chem. A* **2014**, 118, 9795-9800.

[4] J. G. Bell, J. Wang, *J. Phys. Chem. A* **2015**, 119, 3323-3328.

[5] J. G. Bell, J. Wang, *J. Electroanal. Chem.* **2015**, 754, 133-137.

[6] J. G. Bell, J. Wang, *Electrochim. Acta* **2016**, 222, 678-684.

[7] T. H. Ha, H. J. Koo, B. H. Chung, *J. Phys. Chem. C* **2007**, 111, 1123-1130.

[8] J. S. DuChene, W. Niu, J. M. Abendroth, Q. Sun, W. Zhao, F. Huo, W. D. Wei, *Chem. Mater.* **2013**, 25, 1392-1399.

[9] P. De Kepper, I. R. Epstein, *J. Am. Chem. Soc.* **1982**, 104**,** 49-55.

[10] I. Szalai, E. Körös, *J. Phys. Chem. A* **1998**, 102**,** 6892-6897.

[11] J. A. Switzer, C. J. Hung, L. Y. Huang, F. S. Miller, Y. Zhou, E. R. Raub, M. G. Shumsky, E. W. Bohannan, *J. Mater. Res.* **1998**, 13, 909-916.

[12] M. Orlik, *Self-Organization in Electrochemical Systems I: General Principles of Self-Organization. Temporal Instabilities*; Springer, Berlin, 2012.

[13] A. L. Kawczyński, M. Przansnyski, B. Baranowski, *J. Electroanal. Chem.* **1984**, 179**,** 285-288.

[14] G. Inzelt, *J. Electroanal. Chem.* **1993**, 348**,** 465-471.

[15] C. Batchelor-McAuley, G. G. Wildgoose, R. G. Compton, L. Shao, M. L. H. Green, *Sens. Actuators, B* **2008**, 132**,** 356-360.

[16] J. Luo, H. Zhang, S. Jiang, J. Jiang, X. Liu, *Microchim. Acta* **2012**, 177**,** 485-490.

[17] X. Chen, G. Wu, Z. Cai, M. Oyama, X. Chen, *Microchim. Acta* **2014**, 181**,** 689-705.

APPENDICES

Appendix A - Code of Simulation for Table 2.1

```
METHOD ROSENBROCK (STIFF)

STARTTIME = 0
STOPTIME = 80000
DTMIN = 1.OE-8
DTMAX = 0.1
DTOUT = 0
TOLERANCE = 0.001

{ 1:    BrO3 + Br + 2H < - - > HBrO2 + HOBr }
        RXN1 = K1f*BrO3*Br*H^2 - K1r*HBrO2*HOBr
        K1f = 0.1
        K1r = 100
        INIT Br = 1.0e-7
        INIT BrO3 = 0.06
        INIT H = 0.8
        INIT HBrO2 = 0
        INIT HOBr = 0

        d/dt(Br) = -RXN1 - RXN2 + RXN7 - RXN8 + RXN9 - RXN14
        d/dt(BrO3) = -RXN1 - RXN3 + RXN6
        d/dt(H) = -2*RXN1 - RXN2 - RXN3 + RXN6 - RXN8 + RXN9 - RXN13 + RXN14 +
        RXN15 + RXN16
```

d/dt(HBrO2) = +RXN1 - RXN2 - RXN3 + RXN4 + RXN5 - 2*RXN6 + RXN13

d/dt(HOBr) = +RXN1 + 2*RXN2 + RXN6 - RXN7 - RXN8 - RXN10

{ 2: HBrO2 + Br + H < - - > 2HOBr }

RXN2 = K2f*HBrO2*Br*H - K2r*HOBr^2

K2f = 1.5e+09

{ 3: BrO3 + HBrO2 + H < - - > 2BrO2 + H2O }

RXN3 = K3f*BrO3*HBrO2*H - K3r*BrO2^2*H2O

K3f = 600

K3r = 2e+07

INIT BrO2 = 0

INIT H2O = 55

d/dt(BrO2) = 2*RXN3 - RXN4 - RXN5 - RXN13

d/dt(H2O) = RXN3 + RXN7 + RXN8 + RXN10 - RXN12 + RXN13

{ 4: BrO2 + HArOH2 < - -> HBrO2 + HArOHO }

RXN4 = K4f*BrO2*HArOH2 - K4r*HBrO2*HArOHO

K4f = 900

K4r = 0

INIT HArOH2 = 0.025

INIT HArOHO = 0

d/dt(HArOH2) = -RXN4 - RXN9 - RXN10 - RXN11 + RXN12 - RXN15

d/dt(HArOHO) = RXN4 - RXN5 - RXN7 + 2*RXN11 + RXN15 - RXN16

{ 5: BrO2 + HArOHO < - - > HArO2 + HBrO2 }

RXN5 = K5f*BrO2*HArOHO - K5r*HArO2*HBrO2

K5f = 1000

K5r = 0

d/dt(HArO2) = RXN5 + RXN7 - RXN11 - 2*RXN12 + RXN14 + RXN16

{ 6: 2HBrO2 < - - > BrO3 + HOBr + H }

RXN6 = K6f*HBrO2^2 - K6r*BrO3*HOBr*H

K6f = 4e+07

K6r = 0

{ 7: HOBr + HArOHO < - - > Br + HArO2 + H2O }

RXN7 = K7f*HOBr*HArOHO - K7r*Br*HArO2*H2O

K7f = 150000

K7r = 0

{ 8: HOBr + Br + H < - -> Br2 + H2O }

RXN8 = K8f*HOBr*Br*H - K8r*Br2*H2O

K8f = 9.5e+09

K8r = 110

INIT Br2 = 0

d/dt(Br2) = RXN8 - RXN9

{ 9: Br2 + HArOH2 < - - > BrArOH2 + Br + H }

RXN9 = K9f*Br2*HArOH2 - K9r*BrArOH2*Br*H

K9f = 700

K9r = 0

INIT BrArOH2 = 0

d/dt(BrArOH2) = RXN9 + RXN10 - RXN14

{ 10: HOBr + HArOH2 < - - > BrArOH2 + H2O }

RXN10 = K10f*HOBr*HArOH2 - K10r*BrArOH2*H2O

K10f = 25

K10r = 0

{ 11: HArOH2 + HArO2 < - - > 2HArOHO }

RXN11 = K11f*HArOH2*HArO2 - K11r*HArOHO^2

K11f = 0.022

K11r = 40000

{ 12: 2HArO2 + H2O < - - > HArOH2 }

RXN12 = K12f*HArO2^2*H2O - K12r*HArOH2

K12f = 10000

K12r = 0

{ 13: CeIII + BrO2 + H < - - > CeIV + HBrO2 + H2O }

RXN13 = K13f*CeIII*BrO2*H - K13r*CeIV*HBrO2*H2O

K13f = 140000

K13r = 0

INIT CeIII = 0

INIT CeIV = 0.00003

d/dt(CeIII) = -RXN13 + RXN14 + RXN15 + RXN16

d/dt(CeIV) = RXN13 - RXN14 - RXN15 - RXN16

{ 14: CeIV + BrArOH2 < - - > CeIII + Br + HArO2 + H }

RXN14 = K14f*CeIV*BrArOH2 - K14r*CeIII*Br*HArO2*H

K14f = 10000

K14r = 0

{ 15: CeIV + HArOH2 < - - > CeIII + HArOHO + H }

RXN15 = K15f*CeIV*HArOH2 - K15r*CeIII*HArOHO*H

K15f = 100

K15r = 0

{ 16: CeIV + HArOHO < - - > CeIII + HArO2 + H }

RXN16 = K16f*CeIV*HArOHO - K16r*CeIII*HArO2*H

K16f = 10000

K16r = 0

Appendix B - Copyright Release for J. Phys. Chem. A

Copyright Clearance Center RightsLink®

Home | Account Info | Help

ACS Publications Most Trusted. Most Cited. Most Read.

Title:	Nonlinear Dynamical Behavior in the Photodecomposition of N-Bromo-1,4-Benzoquinone-4-Imine
Author:	Jeffrey G. Bell, James R. Green, Jichang Wang
Publication:	The Journal of Physical Chemistry A
Publisher:	American Chemical Society
Date:	Jun 1, 2013

Logged in as: Jeffrey Bell

LOGOUT

Copyright © 2013, American Chemical Society

PERMISSION/LICENSE IS GRANTED FOR YOUR ORDER AT NO CHARGE

This type of permission/license, instead of the standard Terms & Conditions, is sent to you because no fee is being charged for your order. Please note the following:

- Permission is granted for your request in both print and electronic formats, and translations.
- If figures and/or tables were requested, they may be adapted or used in part.
- Please print this page for your records and send a copy of it to your publisher/graduate school.
- Appropriate credit for the requested material should be given as follows: "Reprinted (adapted) with permission from (COMPLETE REFERENCE CITATION). Copyright (YEAR) American Chemical Society." Insert appropriate information in place of the capitalized words.
- One-time permission is granted only for the use specified in your request. No additional uses are granted (such as derivative works or other editions). For any other uses, please submit a new request.

BACK | CLOSE WINDOW

Copyright © 2017 Copyright Clearance Center, Inc. All Rights Reserved. Privacy statement. Terms and Conditions.
Comments? We would like to hear from you. E-mail us at customercare@copyright.com

Appendix C - Copyright Release for Chaos

AIP PUBLISHING LLC LICENSE
TERMS AND CONDITIONS

Jan 27, 2017

This Agreement between Jeffrey G Bell ("You") and AIP Publishing LLC ("AIP Publishing LLC") consists of your license details and the terms and conditions provided by AIP Publishing LLC and Copyright Clearance Center.

License Number	4037141482536
License date	Jan 27, 2017
Licensed Content Publisher	AIP Publishing LLC
Licensed Content Publication	Chaos
Licensed Content Title	Mixed mode and sequential oscillations in the cerium-bromate-4-aminophenol photoreaction
Licensed Content Author	
Licensed Content Date	Sep 1, 2013
Licensed Content Volume Number	23
Licensed Content Issue Number	3
Type of Use	Thesis/Dissertation
Requestor type	Author (original article)
Format	Print and electronic
Portion	Excerpt (> 800 words)
Will you be translating?	No
Title of your thesis / dissertation	Nonlinear Dynamical Behavior in Chemical and Electrochemical Systems
Expected completion date	Apr 2017
Estimated size (number of pages)	200
Requestor Location	

Billing Type	
Billing Address	

Total 0.00 CAD

Terms and Conditions

AIP Publishing LLC -- Terms and Conditions: Permissions Uses

AIP Publishing hereby grants to you the non-exclusive right and license to use and/or distribute the Material according to the use specified in your order, on a one-time basis, for the specified term, with a maximum distribution equal to the number that you have ordered. Any links or other content accompanying the Material are not the subject of this license.

1. You agree to include the following copyright and permission notice with the reproduction of the Material:"Reprinted from [FULL CITATION], with the permission of AIP Publishing." For an article, the credit line and permission notice must be printed on the first page of the article or book chapter. For photographs, covers, or tables, the notice may appear with the Material, in a footnote, or in the reference list.
2. If you have licensed reuse of a figure, photograph, cover, or table, it is your responsibility to ensure that the material is original to AIP Publishing and does not contain the copyright of another entity, and that the copyright notice of the figure, photograph, cover, or table does not indicate that it was reprinted by AIP Publishing, with permission, from another source. Under no circumstances does AIP Publishing purport or intend to grant permission to reuse material to which it does not hold appropriate rights.
   You may not alter or modify the Material in any manner. You may translate the Material into another language only if you have licensed translation rights. You may not use the Material for promotional purposes.
3. The foregoing license shall not take effect unless and until AIP Publishing or its agent, Copyright Clearance Center, receives the Payment in accordance with Copyright Clearance Center Billing and Payment Terms and Conditions, which are incorporated herein by reference.
4. AIP Publishing or Copyright Clearance Center may, within two business days of granting this license, revoke the license for any reason whatsoever, with a full refund payable to you. Should you violate the terms of this license at any time, AIP Publishing, or Copyright Clearance Center may revoke the license with no refund to you. Notice of such revocation will be made using the contact information provided by you. Failure to receive such notice will not nullify the revocation.
5. AIP Publishing makes no representations or warranties with respect to the Material. You agree to indemnify and hold harmless AIP Publishing, and their officers, directors, employees or agents from and against any and all claims arising out of your use of the Material other than as specifically authorized herein.
6. The permission granted herein is personal to you and is not transferable or assignable without the prior written permission of AIP Publishing. This license may not be amended except in a writing signed by the party to be charged.
7. If purchase orders, acknowledgments or check endorsements are issued on any forms containing terms and conditions which are inconsistent with these provisions, such inconsistent terms and conditions shall be of no force and effect. This document, including the CCC Billing and Payment Terms and Conditions, shall be the entire agreement between the parties relating to the subject matter hereof.

This Agreement shall be governed by and construed in accordance with the laws of the State of New York. Both parties hereby submit to the jurisdiction of the courts of New York County for purposes of resolving any disputes that may arise hereunder.

V1.1

Questions? customercare@copyright.com or +1-855-239-3415 (toll free in the US) or +1-978-646-2777.

Appendix D - Copyright Release for J. Electroanal. Chem

ELSEVIER LICENSE
TERMS AND CONDITIONS

Jan 27, 2017

This Agreement between Jeffrey G Bell ("You") and Elsevier ("Elsevier") consists of your license details and the terms and conditions provided by Elsevier and Copyright Clearance Center.

License Number	4037141174713
License date	Jan 27, 2017
Licensed Content Publisher	Elsevier
Licensed Content Publication	Journal of Electroanalytical Chemistry
Licensed Content Title	Current and potential oscillations during the electro-oxidation of bromide ions
Licensed Content Author	Jeffrey G. Bell,Jichang Wang
Licensed Content Date	1 October 2015
Licensed Content Volume Number	754
Licensed Content Issue Number	n/a
Licensed Content Pages	5
Start Page	133
End Page	137
Type of Use	reuse in a thesis/dissertation
Portion	full article
Format	both print and electronic
Are you the author of this Elsevier article?	Yes
Will you be translating?	No
Order reference number	
Title of your thesis/dissertation	Nonlinear Dynamical Behavior in Chemical and Electrochemical Systems
Expected completion date	Apr 2017
Estimated size (number of pages)	200
Elsevier VAT number	GB 494 6272 12
Requestor Location	

Total 0.00 CAD

Terms and Conditions

INTRODUCTION

1. The publisher for this copyrighted material is Elsevier. By clicking "accept" in connection with completing this licensing transaction, you agree that the following terms and conditions apply to this transaction (along with the Billing and Payment terms and conditions established by Copyright Clearance Center, Inc. ("CCC"), at the time that you opened your Rightslink account and that are available at any time at http://myaccount.copyright.com).

GENERAL TERMS

2. Elsevier hereby grants you permission to reproduce the aforementioned material subject to the terms and conditions indicated.
3. Acknowledgement: If any part of the material to be used (for example, figures) has appeared in our publication with credit or acknowledgement to another source, permission must also be sought from that source. If such permission is not obtained then that material may not be included in your publication/copies. Suitable acknowledgement to the source must be made, either as a footnote or in a reference list at the end of your publication, as follows:
"Reprinted from Publication title, Vol /edition number, Author(s), Title of article / title of chapter, Pages No., Copyright (Year), with permission from Elsevier [OR APPLICABLE SOCIETY COPYRIGHT OWNER]." Also Lancet special credit - "Reprinted from The Lancet, Vol. number, Author(s), Title of article, Pages No., Copyright (Year), with permission from Elsevier."
4. Reproduction of this material is confined to the purpose and/or media for which permission is hereby given.
5. Altering/Modifying Material: Not Permitted. However figures and illustrations may be altered/adapted minimally to serve your work. Any other abbreviations, additions, deletions and/or any other alterations shall be made only with prior written authorization of Elsevier Ltd. (Please contact Elsevier at permissions@elsevier.com). No modifications can be made to any Lancet figures/tables and they must be reproduced in full.
6. If the permission fee for the requested use of our material is waived in this instance, please be advised that your future requests for Elsevier materials may attract a fee.
7. Reservation of Rights: Publisher reserves all rights not specifically granted in the combination of (i) the license details provided by you and accepted in the course of this licensing transaction, (ii) these terms and conditions and (iii) CCC's Billing and Payment terms and conditions.
8. License Contingent Upon Payment: While you may exercise the rights licensed immediately upon issuance of the license at the end of the licensing process for the transaction, provided that you have disclosed complete and accurate details of your proposed use, no license is finally effective unless and until full payment is received from you (either by publisher or by CCC) as provided in CCC's Billing and Payment terms and conditions. If full payment is not received on a timely basis, then any license preliminarily granted shall be deemed automatically revoked and shall be void as if never granted. Further, in the event that you breach any of these terms and conditions or any of CCC's Billing and Payment terms and conditions, the license is automatically revoked and shall be void as if never granted. Use of materials as described in a revoked license, as well as any use of the materials beyond the scope of an unrevoked license, may constitute copyright infringement and publisher reserves the right to take any and all action to protect its copyright in the materials.
9. Warranties: Publisher makes no representations or warranties with respect to the licensed

material.
10. Indemnity: You hereby indemnify and agree to hold harmless publisher and CCC, and their respective officers, directors, employees and agents, from and against any and all claims arising out of your use of the licensed material other than as specifically authorized pursuant to this license.
11. No Transfer of License: This license is personal to you and may not be sublicensed, assigned, or transferred by you to any other person without publisher's written permission.
12. No Amendment Except in Writing: This license may not be amended except in a writing signed by both parties (or, in the case of publisher, by CCC on publisher's behalf).
13. Objection to Contrary Terms: Publisher hereby objects to any terms contained in any purchase order, acknowledgment, check endorsement or other writing prepared by you, which terms are inconsistent with these terms and conditions or CCC's Billing and Payment terms and conditions. These terms and conditions, together with CCC's Billing and Payment terms and conditions (which are incorporated herein), comprise the entire agreement between you and publisher (and CCC) concerning this licensing transaction. In the event of any conflict between your obligations established by these terms and conditions and those established by CCC's Billing and Payment terms and conditions, these terms and conditions shall control.
14. Revocation: Elsevier or Copyright Clearance Center may deny the permissions described in this License at their sole discretion, for any reason or no reason, with a full refund payable to you. Notice of such denial will be made using the contact information provided by you. Failure to receive such notice will not alter or invalidate the denial. In no event will Elsevier or Copyright Clearance Center be responsible or liable for any costs, expenses or damage incurred by you as a result of a denial of your permission request, other than a refund of the amount(s) paid by you to Elsevier and/or Copyright Clearance Center for denied permissions.

LIMITED LICENSE

The following terms and conditions apply only to specific license types:
15. **Translation**: This permission is granted for non-exclusive world **English** rights only unless your license was granted for translation rights. If you licensed translation rights you may only translate this content into the languages you requested. A professional translator must perform all translations and reproduce the content word for word preserving the integrity of the article.
16. **Posting licensed content on any Website**: The following terms and conditions apply as follows: Licensing material from an Elsevier journal: All content posted to the web site must maintain the copyright information line on the bottom of each image; A hyper-text must be included to the Homepage of the journal from which you are licensing at http://www.sciencedirect.com/science/journal/xxxxx or the Elsevier homepage for books at http://www.elsevier.com; Central Storage: This license does not include permission for a scanned version of the material to be stored in a central repository such as that provided by Heron/XanEdu.
Licensing material from an Elsevier book: A hyper-text link must be included to the Elsevier homepage at http://www.elsevier.com . All content posted to the web site must maintain the copyright information line on the bottom of each image.

Posting licensed content on Electronic reserve: In addition to the above the following clauses are applicable: The web site must be password-protected and made available only to bona fide students registered on a relevant course. This permission is granted for 1 year only. You may obtain a new license for future website posting.
17. **For journal authors:** the following clauses are applicable in addition to the above:
Preprints:

A preprint is an author's own write-up of research results and analysis, it has not been peer-reviewed, nor has it had any other value added to it by a publisher (such as formatting, copyright, technical enhancement etc.).
Authors can share their preprints anywhere at any time. Preprints should not be added to or enhanced in any way in order to appear more like, or to substitute for, the final versions of articles however authors can update their preprints on arXiv or RePEc with their Accepted Author Manuscript (see below).
If accepted for publication, we encourage authors to link from the preprint to their formal publication via its DOI. Millions of researchers have access to the formal publications on ScienceDirect, and so links will help users to find, access, cite and use the best available version. Please note that Cell Press, The Lancet and some society-owned have different preprint policies. Information on these policies is available on the journal homepage.
Accepted Author Manuscripts: An accepted author manuscript is the manuscript of an article that has been accepted for publication and which typically includes author-incorporated changes suggested during submission, peer review and editor-author communications.
Authors can share their accepted author manuscript:

- immediately
  - via their non-commercial person homepage or blog
  - by updating a preprint in arXiv or RePEc with the accepted manuscript
  - via their research institute or institutional repository for internal institutional uses or as part of an invitation-only research collaboration work-group
  - directly by providing copies to their students or to research collaborators for their personal use
  - for private scholarly sharing as part of an invitation-only work group on commercial sites with which Elsevier has an agreement
- after the embargo period
  - via non-commercial hosting platforms such as their institutional repository
  - via commercial sites with which Elsevier has an agreement

In all cases accepted manuscripts should:

- link to the formal publication via its DOI
- bear a CC-BY-NC-ND license - this is easy to do
- if aggregated with other manuscripts, for example in a repository or other site, be shared in alignment with our hosting policy not be added to or enhanced in any way to appear more like, or to substitute for, the published journal article.

Published journal article (JPA): A published journal article (PJA) is the definitive final record of published research that appears or will appear in the journal and embodies all value-adding publishing activities including peer review co-ordination, copy-editing, formatting, (if relevant) pagination and online enrichment.
Policies for sharing publishing journal articles differ for subscription and gold open access articles:
Subscription Articles: If you are an author, please share a link to your article rather than the full-text. Millions of researchers have access to the formal publications on ScienceDirect, and so links will help your users to find, access, cite, and use the best available version.
Theses and dissertations which contain embedded PJAs as part of the formal submission can be posted publicly by the awarding institution with DOI links back to the formal publications on ScienceDirect.

If you are affiliated with a library that subscribes to ScienceDirect you have additional private sharing rights for others' research accessed under that agreement. This includes use for classroom teaching and internal training at the institution (including use in course packs and courseware programs), and inclusion of the article for grant funding purposes.
Gold Open Access Articles: May be shared according to the author-selected end-user license and should contain a CrossMark logo, the end user license, and a DOI link to the formal publication on ScienceDirect.
Please refer to Elsevier's posting policy for further information.
18. **For book authors** the following clauses are applicable in addition to the above:
Authors are permitted to place a brief summary of their work online only. You are not allowed to download and post the published electronic version of your chapter, nor may you scan the printed edition to create an electronic version. **Posting to a repository:** Authors are permitted to post a summary of their chapter only in their institution's repository.
19. **Thesis/Dissertation**: If your license is for use in a thesis/dissertation your thesis may be submitted to your institution in either print or electronic form. Should your thesis be published commercially, please reapply for permission. These requirements include permission for the Library and Archives of Canada to supply single copies, on demand, of the complete thesis and include permission for Proquest/UMI to supply single copies, on demand, of the complete thesis. Should your thesis be published commercially, please reapply for permission. Theses and dissertations which contain embedded PJAs as part of the formal submission can be posted publicly by the awarding institution with DOI links back to the formal publications on ScienceDirect.

Elsevier Open Access Terms and Conditions
You can publish open access with Elsevier in hundreds of open access journals or in nearly 2000 established subscription journals that support open access publishing. Permitted third party re-use of these open access articles is defined by the author's choice of Creative Commons user license. See our open access license policy for more information.
Terms & Conditions applicable to all Open Access articles published with Elsevier:
Any reuse of the article must not represent the author as endorsing the adaptation of the article nor should the article be modified in such a way as to damage the author's honour or reputation. If any changes have been made, such changes must be clearly indicated.
The author(s) must be appropriately credited and we ask that you include the end user license and a DOI link to the formal publication on ScienceDirect.
If any part of the material to be used (for example, figures) has appeared in our publication with credit or acknowledgement to another source it is the responsibility of the user to ensure their reuse complies with the terms and conditions determined by the rights holder.
Additional Terms & Conditions applicable to each Creative Commons user license:
CC BY: The CC-BY license allows users to copy, to create extracts, abstracts and new works from the Article, to alter and revise the Article and to make commercial use of the Article (including reuse and/or resale of the Article by commercial entities), provided the user gives appropriate credit (with a link to the formal publication through the relevant DOI), provides a link to the license, indicates if changes were made and the licensor is not represented as endorsing the use made of the work. The full details of the license are available at http://creativecommons.org/licenses/by/4.0.
CC BY NC SA: The CC BY-NC-SA license allows users to copy, to create extracts, abstracts and new works from the Article, to alter and revise the Article, provided this is not done for commercial purposes, and that the user gives appropriate credit (with a link to the formal publication through the relevant DOI), provides a link to the license, indicates if changes were made and the licensor is not represented as endorsing the use made of the work. Further, any new works must be made available on the same conditions. The full

Appendix E - Copyright Release for Electrochim. Acta

ELSEVIER LICENSE
TERMS AND CONDITIONS

Mar 02, 2017

This Agreement between Jeffrey G Bell ("You") and Elsevier ("Elsevier") consists of your license details and the terms and conditions provided by Elsevier and Copyright Clearance Center.

License Number	4037151494598
License date	
Licensed Content Publisher	Elsevier
Licensed Content Publication	Electrochimica Acta
Licensed Content Title	Nonlinear Instabilities during the Electrochemical Oxidation of Hydroxymethanesulfinate
Licensed Content Author	Jeffrey G. Bell,Jichang Wang
Licensed Content Date	20 December 2016
Licensed Content Volume	222
Licensed Content Issue	n/a
Licensed Content Pages	7
Start Page	678
End Page	684
Type of Use	reuse in a thesis/dissertation
Intended publisher of new work	other
Portion	full article
Format	both print and electronic
Are you the author of this Elsevier article?	Yes
Will you be translating?	No
Order reference number	
Title of your thesis/dissertation	Nonlinear Dynamical Behavior in Chemical and Electrochemical Systems
Expected completion date	Apr 2017
Estimated size (number of pages)	200
Elsevier VAT number	GB 494 6272 12
Requestor Location	

Total 0.00 CAD

Terms and Conditions

INTRODUCTION

1. The publisher for this copyrighted material is Elsevier. By clicking "accept" in connection with completing this licensing transaction, you agree that the following terms and conditions apply to this transaction (along with the Billing and Payment terms and conditions established by Copyright Clearance Center, Inc. ("CCC"), at the time that you opened your Rightslink account and that are available at any time at http://myaccount.copyright.com).

GENERAL TERMS

2. Elsevier hereby grants you permission to reproduce the aforementioned material subject to the terms and conditions indicated.

3. Acknowledgement: If any part of the material to be used (for example, figures) has appeared in our publication with credit or acknowledgement to another source, permission must also be sought from that source. If such permission is not obtained then that material may not be included in your publication/copies. Suitable acknowledgement to the source must be made, either as a footnote or in a reference list at the end of your publication, as follows:

"Reprinted from Publication title, Vol /edition number, Author(s), Title of article / title of chapter, Pages No., Copyright (Year), with permission from Elsevier [OR APPLICABLE SOCIETY COPYRIGHT OWNER]." Also Lancet special credit - "Reprinted from The Lancet, Vol. number, Author(s), Title of article, Pages No., Copyright (Year), with permission from Elsevier."

4. Reproduction of this material is confined to the purpose and/or media for which permission is hereby given.

5. Altering/Modifying Material: Not Permitted. However figures and illustrations may be altered/adapted minimally to serve your work. Any other abbreviations, additions, deletions and/or any other alterations shall be made only with prior written authorization of Elsevier Ltd. (Please contact Elsevier at permissions@elsevier.com). No modifications can be made to any Lancet figures/tables and they must be reproduced in full.

6. If the permission fee for the requested use of our material is waived in this instance, please be advised that your future requests for Elsevier materials may attract a fee.

7. Reservation of Rights: Publisher reserves all rights not specifically granted in the combination of (i) the license details provided by you and accepted in the course of this licensing transaction, (ii) these terms and conditions and (iii) CCC's Billing and Payment terms and conditions.

8. License Contingent Upon Payment: While you may exercise the rights licensed immediately upon issuance of the license at the end of the licensing process for the transaction, provided that you have disclosed complete and accurate details of your proposed use, no license is finally effective unless and until full payment is received from you (either by publisher or by CCC) as provided in CCC's Billing and Payment terms and conditions. If full payment is not received on a timely basis, then any license preliminarily granted shall be deemed automatically revoked and shall be void as if never granted. Further, in the event that you breach any of these terms and conditions or any of CCC's Billing and Payment terms and conditions, the license is automatically revoked and shall be void as if never granted. Use of materials as described in a revoked license, as well as any use of the materials beyond the scope of an unrevoked license, may constitute copyright infringement and publisher reserves the right to take any and all action to protect its copyright in the materials.

9. Warranties: Publisher makes no representations or warranties with respect to the licensed

material.
10. Indemnity: You hereby indemnify and agree to hold harmless publisher and CCC, and their respective officers, directors, employees and agents, from and against any and all claims arising out of your use of the licensed material other than as specifically authorized pursuant to this license.
11. No Transfer of License: This license is personal to you and may not be sublicensed, assigned, or transferred by you to any other person without publisher's written permission.
12. No Amendment Except in Writing: This license may not be amended except in a writing signed by both parties (or, in the case of publisher, by CCC on publisher's behalf).
13. Objection to Contrary Terms: Publisher hereby objects to any terms contained in any purchase order, acknowledgment, check endorsement or other writing prepared by you, which terms are inconsistent with these terms and conditions or CCC's Billing and Payment terms and conditions. These terms and conditions, together with CCC's Billing and Payment terms and conditions (which are incorporated herein), comprise the entire agreement between you and publisher (and CCC) concerning this licensing transaction. In the event of any conflict between your obligations established by these terms and conditions and those established by CCC's Billing and Payment terms and conditions, these terms and conditions shall control.
14. Revocation: Elsevier or Copyright Clearance Center may deny the permissions described in this License at their sole discretion, for any reason or no reason, with a full refund payable to you. Notice of such denial will be made using the contact information provided by you. Failure to receive such notice will not alter or invalidate the denial. In no event will Elsevier or Copyright Clearance Center be responsible or liable for any costs, expenses or damage incurred by you as a result of a denial of your permission request, other than a refund of the amount(s) paid by you to Elsevier and/or Copyright Clearance Center for denied permissions.

LIMITED LICENSE

The following terms and conditions apply only to specific license types:
15. **Translation**: This permission is granted for non-exclusive world **English** rights only unless your license was granted for translation rights. If you licensed translation rights you may only translate this content into the languages you requested. A professional translator must perform all translations and reproduce the content word for word preserving the integrity of the article.
16. **Posting licensed content on any Website**: The following terms and conditions apply as follows: Licensing material from an Elsevier journal: All content posted to the web site must maintain the copyright information line on the bottom of each image; A hyper-text must be included to the Homepage of the journal from which you are licensing at http://www.sciencedirect.com/science/journal/xxxxx or the Elsevier homepage for books at http://www.elsevier.com; Central Storage: This license does not include permission for a scanned version of the material to be stored in a central repository such as that provided by Heron/XanEdu.
Licensing material from an Elsevier book: A hyper-text link must be included to the Elsevier homepage at http://www.elsevier.com . All content posted to the web site must maintain the copyright information line on the bottom of each image.

Posting licensed content on Electronic reserve: In addition to the above the following clauses are applicable: The web site must be password-protected and made available only to bona fide students registered on a relevant course. This permission is granted for 1 year only. You may obtain a new license for future website posting.
17. **For journal authors:** the following clauses are applicable in addition to the above:
Preprints:

A preprint is an author's own write-up of research results and analysis, it has not been peer-reviewed, nor has it had any other value added to it by a publisher (such as formatting, copyright, technical enhancement etc.).
Authors can share their preprints anywhere at any time. Preprints should not be added to or enhanced in any way in order to appear more like, or to substitute for, the final versions of articles however authors can update their preprints on arXiv or RePEc with their Accepted Author Manuscript (see below).
If accepted for publication, we encourage authors to link from the preprint to their formal publication via its DOI. Millions of researchers have access to the formal publications on ScienceDirect, and so links will help users to find, access, cite and use the best available version. Please note that Cell Press, The Lancet and some society-owned have different preprint policies. Information on these policies is available on the journal homepage.
Accepted Author Manuscripts: An accepted author manuscript is the manuscript of an article that has been accepted for publication and which typically includes author-incorporated changes suggested during submission, peer review and editor-author communications.
Authors can share their accepted author manuscript:

- immediately
  - via their non-commercial person homepage or blog
  - by updating a preprint in arXiv or RePEc with the accepted manuscript
  - via their research institute or institutional repository for internal institutional uses or as part of an invitation-only research collaboration work-group
  - directly by providing copies to their students or to research collaborators for their personal use
  - for private scholarly sharing as part of an invitation-only work group on commercial sites with which Elsevier has an agreement
- after the embargo period
  - via non-commercial hosting platforms such as their institutional repository
  - via commercial sites with which Elsevier has an agreement

In all cases accepted manuscripts should:

- link to the formal publication via its DOI
- bear a CC-BY-NC-ND license - this is easy to do
- if aggregated with other manuscripts, for example in a repository or other site, be shared in alignment with our hosting policy not be added to or enhanced in any way to appear more like, or to substitute for, the published journal article.

Published journal article (JPA): A published journal article (PJA) is the definitive final record of published research that appears or will appear in the journal and embodies all value-adding publishing activities including peer review co-ordination, copy-editing, formatting, (if relevant) pagination and online enrichment.
Policies for sharing publishing journal articles differ for subscription and gold open access articles:
Subscription Articles: If you are an author, please share a link to your article rather than the full-text. Millions of researchers have access to the formal publications on ScienceDirect, and so links will help your users to find, access, cite, and use the best available version.
Theses and dissertations which contain embedded PJAs as part of the formal submission can be posted publicly by the awarding institution with DOI links back to the formal publications on ScienceDirect.

If you are affiliated with a library that subscribes to ScienceDirect you have additional private sharing rights for others' research accessed under that agreement. This includes use for classroom teaching and internal training at the institution (including use in course packs and courseware programs), and inclusion of the article for grant funding purposes.
Gold Open Access Articles: May be shared according to the author-selected end-user license and should contain a CrossMark logo, the end user license, and a DOI link to the formal publication on ScienceDirect.
Please refer to Elsevier's posting policy for further information.
18. **For book authors** the following clauses are applicable in addition to the above: Authors are permitted to place a brief summary of their work online only. You are not allowed to download and post the published electronic version of your chapter, nor may you scan the printed edition to create an electronic version. **Posting to a repository:** Authors are permitted to post a summary of their chapter only in their institution's repository.
19. **Thesis/Dissertation**: If your license is for use in a thesis/dissertation your thesis may be submitted to your institution in either print or electronic form. Should your thesis be published commercially, please reapply for permission. These requirements include permission for the Library and Archives of Canada to supply single copies, on demand, of the complete thesis and include permission for Proquest/UMI to supply single copies, on demand, of the complete thesis. Should your thesis be published commercially, please reapply for permission. Theses and dissertations which contain embedded PJAs as part of the formal submission can be posted publicly by the awarding institution with DOI links back to the formal publications on ScienceDirect.

Elsevier Open Access Terms and Conditions
You can publish open access with Elsevier in hundreds of open access journals or in nearly 2000 established subscription journals that support open access publishing. Permitted third party re-use of these open access articles is defined by the author's choice of Creative Commons user license. See our open access license policy for more information.
Terms & Conditions applicable to all Open Access articles published with Elsevier:
Any reuse of the article must not represent the author as endorsing the adaptation of the article nor should the article be modified in such a way as to damage the author's honour or reputation. If any changes have been made, such changes must be clearly indicated.
The author(s) must be appropriately credited and we ask that you include the end user license and a DOI link to the formal publication on ScienceDirect.
If any part of the material to be used (for example, figures) has appeared in our publication with credit or acknowledgement to another source it is the responsibility of the user to ensure their reuse complies with the terms and conditions determined by the rights holder.
Additional Terms & Conditions applicable to each Creative Commons user license:
CC BY: The CC-BY license allows users to copy, to create extracts, abstracts and new works from the Article, to alter and revise the Article and to make commercial use of the Article (including reuse and/or resale of the Article by commercial entities), provided the user gives appropriate credit (with a link to the formal publication through the relevant DOI), provides a link to the license, indicates if changes were made and the licensor is not represented as endorsing the use made of the work. The full details of the license are available at http://creativecommons.org/licenses/by/4.0.
CC BY NC SA: The CC BY-NC-SA license allows users to copy, to create extracts, abstracts and new works from the Article, to alter and revise the Article, provided this is not done for commercial purposes, and that the user gives appropriate credit (with a link to the formal publication through the relevant DOI), provides a link to the license, indicates if changes were made and the licensor is not represented as endorsing the use made of the work. Further, any new works must be made available on the same conditions. The full

VITA AUCTORIS

Jeffrey G. Bell was born in Windsor Ontario and attended Villanova Secondary School in LaSalle Ontario. He completed his B.Sc [Honours] in Chemistry in 2012. He is currently a PhD candidate in Physical Chemistry in the Chemistry and Biochemistry Department at the University of Windsor and is planning on graduating in June 2017.